Geotechnical, Geological and Earthquake Engineering

Rita Bento
Mario De Stefano
Dietlinde Köber
Zbigniew Zembaty *Editors*

Seismic Behaviour and Design of Irregular and Complex Civil Structures IV

Springer

Geotechnical, Geological and Earthquake Engineering

Volume 50

The book series entitled *Geotechnical, Geological and Earthquake Engineering* has been initiated to provide carefully selected and reviewed information from the most recent findings and observations in these engineering fields. Researchers as well as practitioners in these interdisciplinary fields will find valuable information in these book volumes, contributing to advancing the state-of-the-art and state-of-the-practice. This book series comprises monographs, edited volumes, handbooks as well as occasionally symposia and workshop proceedings volumes on the broad topics of geotechnical, geological and earthquake engineering. The topics covered are theoretical and applied soil mechanics, foundation engineering, geotechnical earthquake engineering, earthquake engineering, rock mechanics, engineering geology, engineering seismology, earthquake hazard, etc.

Prospective authors and/or editors should consult the **Series Editor Atilla Ansal** for more details. Any comments or suggestions for future volumes are welcomed.

EDITORS AND EDITORIAL BOARD MEMBERS IN THE GEOTECHNICAL, GEOLOGICAL AND EARTHQUAKE ENGINEERING BOOK SERIES:

Series Editor:

Atilla Ansal
Ozyegin University
School of Engineering
Alemdag Çekmeköy 34794, Istanbul, Turkey
Email: atilla.ansal@ozyegin.edu.tr

Advisory Board

Julian J. Bommer
Imperial College
Department of Civil & Environmental Engineering
Imperial College Road
London SW7 2AZ, United Kingdom
Email: j.bommer@imperial.ac.uk

Jonathan D. Bray
University of California, Berkeley
Department of Civil and Environmental Engineering
453 David Hall, Berkeley, CA 94720, USA
Email: jonbray@berkeley.edu

Kyriazis Pitilakis
Aristotle University Thessaloniki
Department of Civil Engineering
Laboratory of Soil Mechanics and Foundations
University Campus
54124 Thessaloniki, Greece
Email: pitilakis@civil.auth.gr

Susumu Yasuda
Tokyo Denki University
Department of Civil and Environmental Engineering
Hatoyama-Cho
Hiki-gun
Saitama 350-0394, Tokyo, Japan
Email: yasuda@g.dendai.ac.jp

More information about this series at https://link.springer.com/bookseries/6011

Rita Bento · Mario De Stefano · Dietlinde Köber ·
Zbigniew Zembaty
Editors

Seismic Behaviour and Design of Irregular and Complex Civil Structures IV

Springer

Editors
Rita Bento
Department of Civil Engineering,
Architecture, Georesources
Instituto Superior Técnico, University
of Lisbon
Lisbon, Portugal

Dietlinde Köber
Reinforced Concrete Buildings
Technical University of Civil Engineering
Bucharest
Bucharest, Romania

Mario De Stefano
Department of Architecture
Università degli Studi di Firenze
Florence, Italy

Zbigniew Zembaty
Opole University of Technology
Opole, Poland

ISSN 1573-6059 ISSN 1872-4671 (electronic)
Geotechnical, Geological and Earthquake Engineering
ISBN 978-3-030-83220-9 ISBN 978-3-030-83221-6 (eBook)
https://doi.org/10.1007/978-3-030-83221-6

This Springer imprint is published by the registered company Springer Nature Switzerland AG
The registered company address is: Gewerbestrasse 11, 6330 Cham, Switzerland

Introduction

This volume contains papers of the 9th European Workshop on the Seismic Behaviour of Irregular and Complex Structures (9EWICS) held in Lisbon, Portugal, in 2020. This workshop, organized at Instituto Superior Técnico, University of Lisbon, continued the successful three-annual series of workshops started back in 1996. Its organization had the sponsorship of Working Group 8 (Seismic Behaviour of Irregular and Complex Structures) of the European Association of Earthquake Engineering.

This international event provided a platform for discussion and exchange of ideas and unveiled new insights on the possibilities and challenges of irregular and complex structures under seismic actions. The topics addressed include criteria for regularity, seismic design of irregular structures, seismic assessment of irregular and complex structures, retrofit of irregular and complex structures, and soil-structure interaction for irregular and complex structures. Beyond an excellent number of interesting papers on these topics, this volume includes the papers of the two invited lectures—one devoted to irregularities in RC buildings, including perspectives in current seismic design codes, difficulties in their application and further research needs, and another one dedicated to the challenging and very up to date topic in the area of seismic response of masonry building aggregates in historical centers. This volume includes 26 contributions from authors of 11 countries, giving a complete and international view of the problem.

The holds particular interest for all the community involved in the challenging task of seismic design, assessment and/or retrofit of irregular and complex structures.

Contents

Irregularities in RC Buildings: Perspectives in Current Seismic Design Codes, Difficulties in Their Application and Further Research Needs

Humberto Varum, José Melo, André Furtado, and André Lima

1 Introduction

Observations on buildings' performance during strong earthquakes have served as a means of teaching builders and engineers on proper and improper construction of earthquake load resisting systems [1–3]. In regions that have long been inhabited and subjected to relatively frequent firm ground shaking, design procedures have evolved, resulting in relatively good performance of engineered structures. Although such design procedures are not universally applicable due to regional differences, structural engineers can learn much by studying those procedures in construction materials and techniques. Apart from that, the post-earthquake damage reconnaissance reports highlighted the importance of the infill walls in the RC building structures' seismic performance. Many authors pointed out that these elements, usually called "non-structural" elements, may play an essential role in the structural behaviour and are responsible for a significant part of the human, material and economic losses [4, 5].

The RC structures behaviour depends on the stiffness, strength, ductility and energy dissipation characteristics of the structural elements, among other factors. The structural strength is provided by each structural member and by the interaction and connection among them. Since the buildings are structures with a high degree of

H. Varum (✉) · J. Melo · A. Furtado
CONSTRUCT-LESE, Faculdade de Engenharia da, Universidade do Porto, Porto, Portugal
e-mail: hvarum@fe.up.pt

J. Melo
e-mail: josemelo@fe.up.pt

A. Furtado
e-mail: afurtado@fe.up.pt

A. Lima
Faculdade de Engenharia da, Universidade do Porto, Porto, Portugal
e-mail: up201505158@fe.up.pt

R. Bento et al. (eds.), *Seismic Behaviour and Design of Irregular and Complex Civil Structures IV*, Geotechnical, Geological and Earthquake Engineering 50,
https://doi.org/10.1007/978-3-030-83221-6_1

redundancy, their response is controlled by the loading redistribution capacity, which can fail some members, and/or by the possibility of those members not suitable to accommodate large deformation demands before failure. Some structural members' insufficient strength capacity can be due to the seismic actions significantly higher than the values considered during the design process and resulted in load demands higher than their capacity defined in the design stage [6].

The structures should be designed according to the seismic loading demands prescribed by the codes and ensuring that proper stiffness, strength and ductility is guaranteed and balanced between the elements. However, it is essential to mention that some structural design codes like Eurocode 8 [1] consider the infill panels as non-structural elements. Their contribution to the seismic structure response is disregarded, or its influence is considered with simplified procedures. Recent earthquakes evidenced that the infill walls often play an essential role in the RC structures' seismic response. They provide to the structure system higher stiffness, strength, and energy dissipation; however, depending on the infill walls characteristics, in-plan and in-elevation distribution, they can negatively affect the structure's global response. The infills reduce the deformation capacity and potentiate the development of failure mechanisms that the structural members were not designed to.

This research aims to provide a profound overview of the damages observed in recent earthquakes due to reinforced concrete buildings irregularities. The most common damages will be collected and discussed by comparing them with the code recommendations. After that, the results of numerical simulations carried out to assess the impact of the different disposition of the infill walls on a reinforced concrete structure's seismic behaviour will be presented. The vertical irregularity due to the infills' location, along with the building envelope, will be discussed. To finish, a review of the Eurocode 8 recommendations with practical applications/examples are presented.

2 Lessons Learned from Recent Earthquakes

2.1 Introduction

The Eurocode 8 [7] classifies the structural elements as structural or non-structural. Concerning the structural elements, they are subdivided as primary members (SP) or secondary members (SS). The primary members (SP) are considered part of the structural system that resists the seismic demands, which are modelled in the analysis for the seismic design situation and are fully designed and detailed for earthquake resistance. On the other hand, the secondary elements are not considered part of the seismic resisting system and whose strength and stiffness against seismic actions are neglected. They are not required to satisfy all Eurocode 8 [7] requirements but are designed and detailed to maintain the support of gravity loads when subjected to the displacements caused by the seismic actions. Lastly, the non-structural elements (NS)

comprise architectural, mechanical or electrical components, systems and components, which, whether due to lack of strength or the way they are connected to the structure, are not, considered in the seismic design as load-carrying elements. As mentioned before, the Eurocode 8 [7] recognizes that infill panels are included in this NS elements group.

The most common types of damage are listed bellow. The list was developed based on post-earthquake survey damage assessments in the major recent earthquakes done by different authors.

- Damage Type 1: Damages associated with stirrups and hoops (inadequate quantity and detailing, regarding the required ductility);
- Damage Type 2: Damages associated with longitudinal reinforcement detailing (bond, anchorage and lap-splices);
- Damage Type 3: Damages associated with the shear and flexural capacity of elements;
- Damage Type 4: Damages associated with the inadequate shear capacity of structural joints;
- Damage Type 5: Damages associated with strong-beam weak-column mechanism;
- Damage Type 6: Damages associated with short-column mechanism;
- Damage Type 7: Damages associated with structural irregularities (in plan and/or in elevation: torsion, "weak-storey" and "soft-storey");
- Damage Type 8: Damages associated with pounding;
- Damage Type 9: Damages in secondary elements (cantilevers, stairs, etc.);
- Damage Type 10: Damages in non-structural elements.

Even though Damage Type 1, 2 and 3 looks similar, they need to be distinguished based on after-earthquakes survey reports. Damage Type 1 is related to the poor detailing of the transverse reinforcement, e.g. absence of transverse reinforcement, hoops' poor detailing, large spacing between stirrups and insufficient transverse reinforcement. It is recommended that, along with the columns and beams, the concrete core should be adequately confined in the plastic hinge region to prevent strength degradation or fragile failure due to shear and flexural demands and ductility increase. This need for confinement is higher when the column is subjected to higher axial load levels and shear loadings. During an earthquake, the beams failure and the beam-column joints failure are usually related to the inadequate use of transverse reinforcement and confinement. These failures observed in the beams are commonly at a local level and could not result in the building structure's total collapse. A prevalent deficiency is the use of improper transverse reinforcement in the beams plastic hinge region.

If a proper and adequate design of the RC elements is carried out considering the seismic action, with appropriate transverse reinforcement and detailing, a ductile behaviour can be achieved. Without proper design and detailing of the transverse reinforcement, a fragile behaviour can occur during an earthquake, and the probability of occurring columns' failure is higher.

Damage Type 2 is dedicated to the longitudinal reinforcement detailing (bond, anchorage and lap splices). From the post-earthquake observations and experimental

studies, it was found a lower strength capacity of elements built with smooth bars. More substantial degradation of the bond conditions occurs along the longitudinal bars, which significantly exceeds and violates the plane sections theory. In most of the situations, their performance was characterized by a flexural behaviour followed by post-peak degradation, which was confirmed by the measurement of bar strains relatively lower than the steel yielding strain. This fact suggests that the code approach and the procedure to adopt in the seismic safety assessment to estimate the flexural strength capacity overestimate the RC elements' real flexural ability (when executed with smooth bars).

Damage type 3 is entirely related to the associated with shear and flexural capacity of RC elements. One of the most common failure modes observed over the last earthquakes is the structural elements' shear failure. The designers adopted global safety factors that reduce the seismic loadings, which affects the flexural forces (ductile behaviour), and the shear ones (fragile behaviour) equally. Subsequently, the shear strength capacity is reached before the yielding starts, and so, the energy dissipation is restrained. The shear strength and confinement problems are prevalent in corner columns, especially if the building structure has some eccentricity between the mass and stiffness centres. The corner columns should be designed with the highest confinement requirements.

From the list, the first eight damage types are related to the SP members, the ninth is related to SS members, and finally, the tenth is associated with the infill walls (NS elements). According to the post-earthquake damages survey assessment, it can be concluded that there is an interaction among the last five types of damage. Figures 1 and 2 show the schematic layout concerning the damages' typologies defined herein and the respective interaction. The damages observed in post-earthquake field trips highlighted that masonry infill walls, the central core of

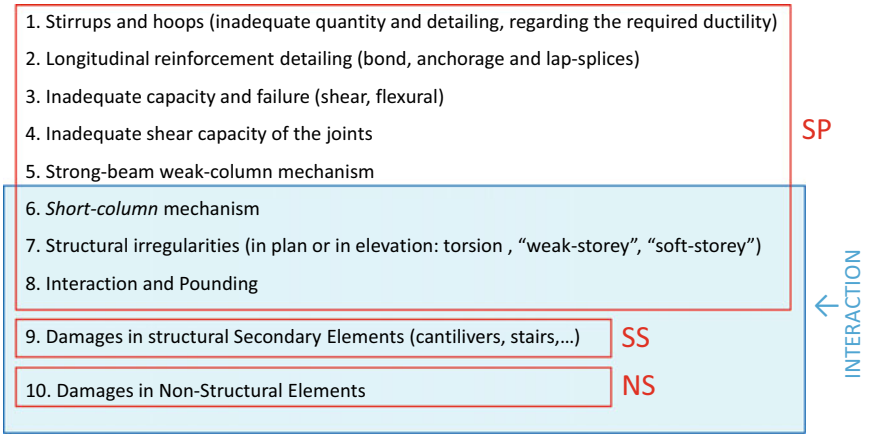

Fig. 1 Types of damages' definition for infilled RC frames due to earthquakes

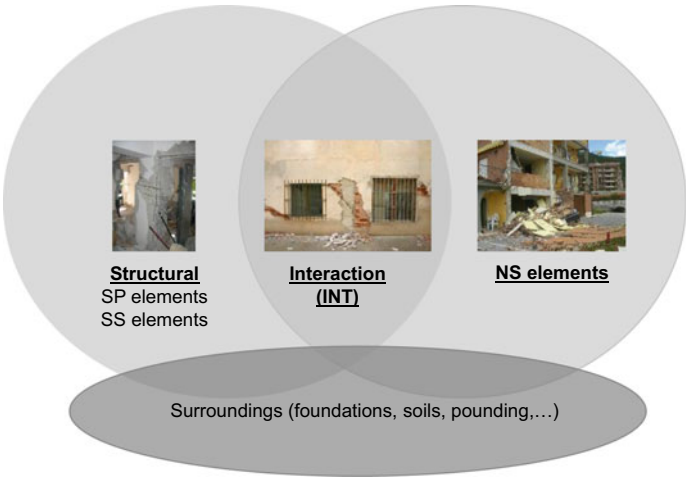

Fig. 2 Flowchart of the most common damages observed in RC structures due to earthquakes

this work, cannot be considered non-structural or secondary elements and disregarded from the building behaviour. The infill walls assume a more than secondary role since they can modify the global structural behaviour.

The next sub-section will detail the damage type 7 related to the in-plane and vertical irregularities based on observations and conclusions extracted from the post-earthquake damage reconnaissance missions.

2.2 Damages Associated with Structural Irregularities (in Plan and/or in Elevation: Torsion, "Weak-storey" and "Soft-storey")

A proper structural conception is essential to ensure a good performance against any loading demand, such as static or dynamic. Simple building structures, regular and with redundant resistant systems for horizontal loading demands tend to result in better behaviour. By contrast, complex structural systems, usually result in structures, in which the dimensions and detailing of structural elements show some deficiencies. Abrupt variations of stiffness, strength, mass and/or other elements' properties in one building, either in a plan or in elevation, can result in horizontal loading distributions and deformations much different from those that usually occur in regular structures.

A very common structural irregularity occurs in the bottom storey, due to the absence of the infill panels, for the location of commercial places, garages or only due to architectural reasons. This type of constructive solution may result in the deformation concentration in these storeys under an earthquake event, which triggers the soft-storey mechanism (Fig. 3) [8]. Typically, this failure mechanism is character-

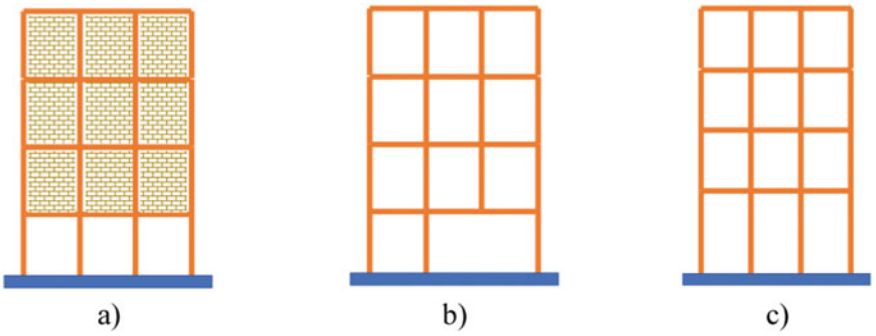

Fig. 3 Structural configurations vulnerable to trigger out soft-storey mechanisms: **a** stiffness difference between storeys, **b** columns discontinuity, and **c** height variations among the storeys

ized by the shear or bending failure of the columns and consequent collapse of the ground storey. In many situations, the soft-storeys' destruction was observed while the remaining ones were intact (or just with very slight damage).

Figure 4 shows two residential buildings that partially collapsed due to the soft-storey mechanism. Figure 4a shows the front view of a six-storey building that had a commercial storey at the ground-floor and, for this reason, a lower number of infill panels. Figure 4b shows a residential building, 4-storeys' high, with a garage on the ground floor that collapsed during the L'Aquila earthquake. This type of damage can be prevented by ensuring a uniform in elevation distribution of the infill panels and structural elements (columns and shear walls). Figure 4c is a 6-storey residential RC building in Nepal, that during the 12th May 2015 earthquake collapsed due to a soft-storey caused by the absence of masonry infill wall on the ground floor. The same occurred in the 5th storey building, presented in Fig. 4d, again due to the masonry infill walls' irregular vertical distribution.

In Portugal, particularly in Lisboa region, several infilled RC structures built in the 50's were designed with this structural configuration, inspired by the Le Corbusier, where the primary system is supported by *pilotis* to allow the circulation of the people, garage and commerce, as shown in Fig. 5. Residential buildings with vertical irregularities, located in Lisboa and Silves, are shown in Figs. 5a, 5b and 5c. Additionally, Fig. 5d presents a school situated in Sacavém, with the same structural irregularity.

Other examples of irregularities in-elevation at the upper-storeys were observed, which resulted in the collapse of those storeys, without leading to the building structure's total failure. Figure 6a and b show a 5-storey building severely damaged due to the significant aftershock following Gorkha (Nepal) earthquake in 2015. The third storey that collapsed corresponded in the past to the location of a restaurant with lower number of infill panels. This irregularity resulted in the deformation concentration and high shear demands, thus to the collapse of this level.

In 2017, the same phenomena were observed in an eight-storey building in Mexico, where the fourth storey's partial collapse (Fig. 6c).

Fig. 4 Examples of buildings collapsed due to soft-storey mechanism: **a** Sichuan, China, 2008, **b** L'Aquila, Italy, 2009, **c** and **d** Gorkha, Nepal, 2015

Another issue that can trigger this failure mechanism is the in-elevation reduction of the cross-section of the columns. Another common irregularity is modifying the position, between consecutive storeys, vertical structural elements, or/and non-structural elements. Different strategies can be adopted to prevent this failure mechanism by assuming an element by element retrofitting [9, 10] or global retrofitting scenarios [11].

Lisbon
a)

Lisbon
b)

Silves
c)

Sacavém
d)

Fig. 5 Examples of buildings with soft-storey configuration located in Portugal: **a** 11-storey building, **b** general view of 11-storey building structures, **c** 4-storey building and **d** school building

3 Importance of the in Fills Distribution in the Seismic Response of RC Structures

This section aims to assess the influence of the masonry infill walls vertical distribution on the buildings seismic behaviour. Two buildings with the same plan dimensions and different number of storeys (4 – PT4 and 8 – PT8) are studied in three different case scenarios: bare frame model (BF), with full infill model (INF) and without infill on the ground-floor (SS), as shown in Fig. 7. Each case scenario represents the possible distribution of the masonry infill walls along with the building height, aiming to study the effect of the infills vertical irregularity in the seismic response of the global structure.

3.1 Description of the Case Studies

The buildings have a plan dimensions of 20 m × 15 m, consisting of 4 × 5 m modules, with a storey height of 3 m. The building were designed by the Portuguese Laboratory of Earthquake and Civil Engineering (LNEC), according to the design code enforced

a) b)

Gorkha, Nepal, 2015

c)

Chiapas, Mexico, 2017

Fig. 6 Example of a partial collapse of the upper-storeys: **a** general view, **b** detail of the column shear failure, and **c** lateral view

in the 80's in Portugal [12]. The layout considered for the infill walls is illustrated in Fig. 1. The cross-section of the columns are: 30 × 60 cm (Storey 1 and 2); 30 × 50 cm (Storey 3 and 4); 40 × 30 cm (Storey 5 and 6) and 30 × 30 cm (Storey 7 and 8). The beam's cross-section is 30 × 60 cm with different reinforcement detailing according to the structure's storey and layout. The reinforcement detailing of all the structural elements can be found in [12]. Concerning the building's design, a global vertical load of 6.15kN/m^2 plus a variable load of 2.5 kN/m^2 was considered. 3D model were generated in the software OpenSees [13], assuming the layout shown in Fig. 7.

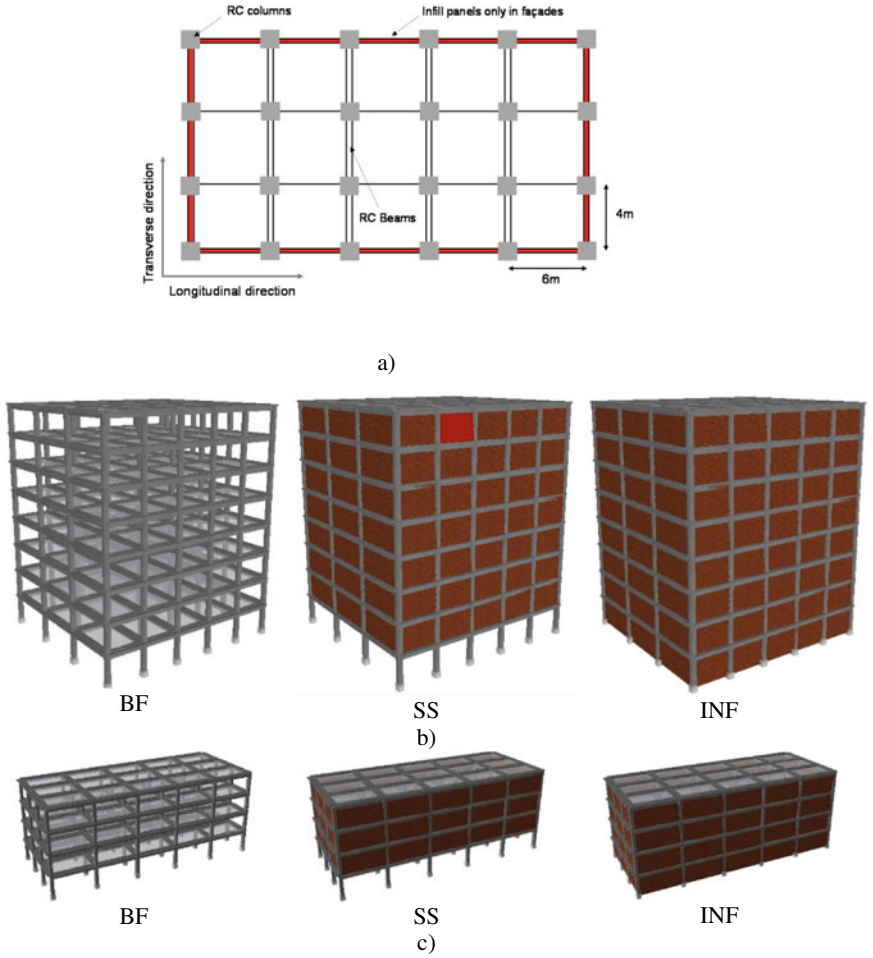

Fig. 7 Case studies: **a** plan layout, **b** PT8, **c** PT4

3.2 Numerical Modelling Strategies

The numerical models were built in the OpenSees [13] software based on the software library's materials models and elements. Concerning the modelling of the RC structural elements fibre discretization was adopted to simulate the behaviour at the section level, where each fibre is associated with a uniaxial stress–strain law. The sectional moment–curvature behaviour of the beam and column elements is then obtained by integrating the non-linear uniaxial stress–strain response of the individual fibres into which the section has been subdivided. The RC beams and columns were modelled using Force-Based BeamColumns elements, which is based on the

iterative force-based formulation. Each element's plastic hinge length was considered to be equal to half of their larger cross-section dimension. Figure 8a presents the numerical strategy adopted to simulate the infilled RC frames, and Fig. 8b is detailed the numerical approach to RC elements.

This decision was based on the reports provided by [15–17]. Concerning the uniaxial material models, it was adopted the model Concrete02, which is based in [18, 19]. The confined and unconfined concrete follow the cyclic rules, included in this model, as proposed by Martinez-Rueda and Elnashai [20]. The input properties considered were: concrete compressive strength f_c equal to 25 MPa, compressive strain at peak strength ε_c equal to 0.36‰, and a tensile strength f_t equal to 3.94 MPa. According to the Mander et al. [15] proposal, the confinement factor of each cross-section was determined[18]. The reinforcement steel bars' modelling adopted the

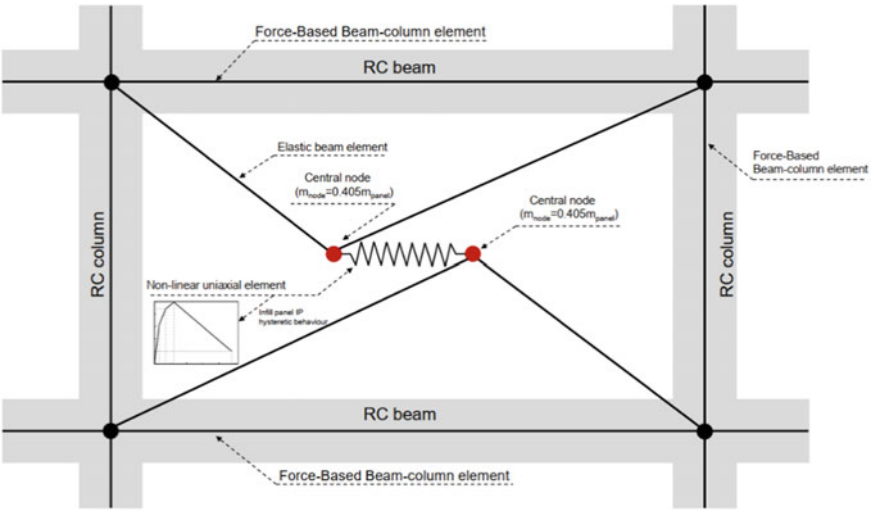

a)

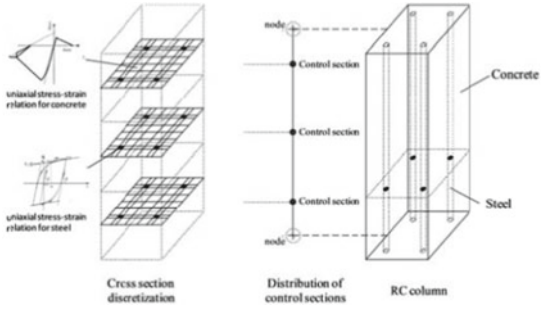

b)

Fig. 8 Numerical modelling strategy: **a** infilled RC frame, **b** RC elements (adapted from [14])

uniaxial material model Steel 02 proposed by [21], combined with the isotropic hardening rules proposed by Filippou et al.[22]. This material model considers the Bauschinger effect, which represents the columns' stiffness degradation under cyclic loading. The input properties adopted were: steel yield strength equal to 575.6 MPa, an elastic modulus equal to 194.7GPa, a strain-hardening ratio of 2.71%, a transition curve initial shape factor (R_o) of 20, and the transition curve shape parameters a_1 and a_2 of 18.5 and 0.15 respectively. Finally, the isotropic hardening parameters a_3 and a_4 the values 0.025 and 2 were assumed respectively.

Finally, the infill walls seismic behaviour were simulated by the Furtado et al. [23] proposal, which consists of an equivalent double-strut model where four diagonal struts simulate each masonry infill wall with rigid behaviour. A central element is included where the non-linearity hysteresis is concentrated, with the two central nodes having the panel mass lumped in. Each panel was simulated by four diagonals elastic beam elements and one central non-linear Beam column element. These values were selected based on the previous research works [24]. A Rayleigh damping proportional to the mass and stiffness matrix was considered, with coefficients calibrated to provide a 5% damping at first to third mode periods. In the non-linear models, the stiffness values used for computing damping coefficients and damping matrix are the initial and tangent ones.

3.3 Numerical Results

The numerical models were submitted to non-linear dynamic analysis, particularly to one artificial earthquake-generated medium/high-risk scenario in southern Europe [25] for different return periods. Hazard consistent time series of acceleration (with 15 s of duration) were artificially generated yielding a set of ten uniform hazard response spectra for increasing periods.

The maximum base shear results from the two case studies' dynamic analysis are shown in Fig. 9 for pga values ranging from 0.09 g to 0.63 g. It can be observed that the presence of the infills increases the strength of the buildings as expected. The base shear values of the 8-storey building are almost two times higher than the 4-storey building. It can be observed that the SS models values are very similar to the BF models, but with two times more initial stiffness.

The maximum drift observed in the structure is presented in Fig. 10. The maximum inter-storey drift was reached in both buildings by the scenario SS. The vertical irregularity introduced by the absence of infill walls in the ground-floor increased the deformation in this storey. For low pga demands until 0.35 g, it is possible to observe that the SS configuration followed the BF. For pga higher than 0.35 g, the SS model reached the highest inter-storey drifts about 10–30% higher than BF and 60% than INF model.

From these plots, it is possible to conclude that a global distribution of the infills can be protective to the structure. However, it depends of the RC structure (possible irregularity of cross-sections, shear walls, etc.).

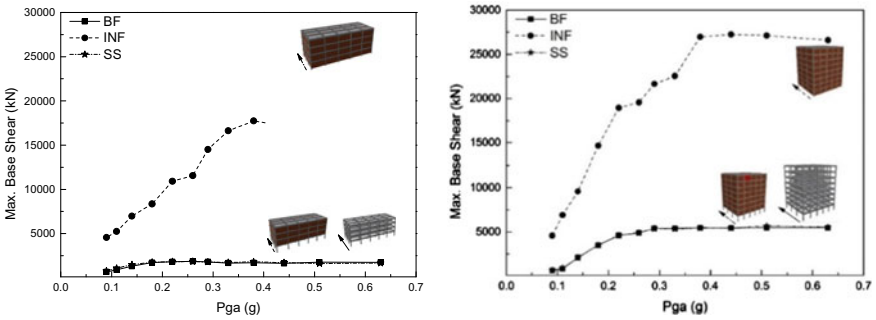

Fig. 9 Maximum base-shear results: **a** 4-storey buildings, **b** 8-storey buildings

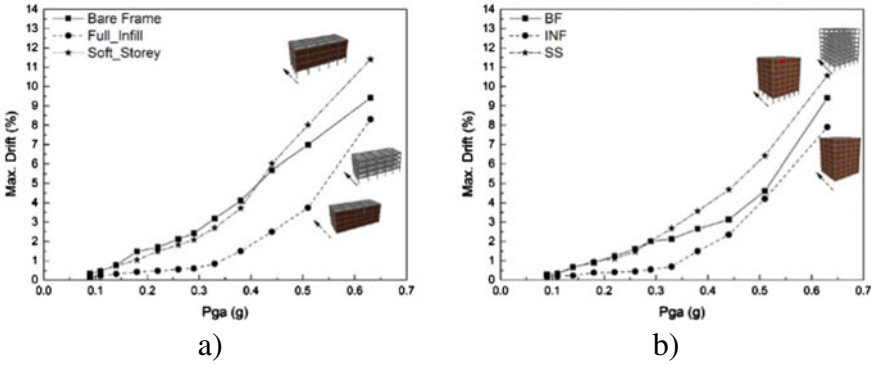

Fig. 10 Maximum inter-storey drift results: **a** 4-storey buildings, **b** 8-storey buildings

4 Structural Irregularities According to Codes

4.1 General Approach in International Codes

The criteria adopted in most national and international codes for the evaluation of the irregularities (in plan and in elevation) are, generally, based on simple qualitative and quantitative rules. Moreover, in most of the codes, the buildings irregularity limits the methods and models allowed in design. In force-based design approaches, the generality of the codes recommends a reduction of the q-factor (ranging between 10 and 30%), depending on the irregularity (in-plan, in elevation, or both) [26, 27].

4.2 Eurocode 8 Evolution

The Eurocode 8 [7] is actually under revision and a draft version was recently drawn [28]. For force based design, three ductility classes (DC1, DC2 and DC3) are considered in the draft version, but they are not totally aligned to the ductility classes in the actual version of the Eurocode 8 (DCL, DCM and DCH). With some minor adaptations, DC1 corresponds to DCL, DC3 to DCM, and a new ductitlity class (DC2) in proposed between DCL and DCM. DCH is dropped down. The structural types for concrete buildings are maintained, but the torsionally flexible system type is not formaly included. However, but the criteria to verify if a building is torsionally flexible are keeped. A new structural type is included corresponding to flat slab structures.

The criteria for regularity in plan are similar in both Eurocode 8 versions, except in the criteria that check the plan configuration. In the draft version, it is referred that for each set-back, the area corresponding to the difference between the convex polygonal line enveloping the floor and the area limited by the outline of the floor should not exceed 15% of the floor area, against the 5% prescrtibed in the actual version of the Eurocode 8 [7]. Regarding the regularity in elevation, the Eurocode 8 draft version introduced the changes presented in Table 1.

In the Eurocode 8 draft version [28], the requirements for consideration of infills are strongly linked with the concerns on the eventual irregular response of the building. According with the Eurocode 8 draft, interacting infills may be considered: a) with a model of the bare frame only (without modelling the infills); and b) with a model of the interaction between frame and infills. Infills with unsymmetrical arrangement in plan should be considered in the model (with spatial models). The recommendations for regularity in plan (Annex A) should be verified considering the influence of infills. The effects on the global response of a structure of the irregularity

Table 1 Regularity in elevation criteria

Criteria	EN 1998–1:2004	prEN 1998–1-2:2019.3 (*draft*)
Lateral stiffness and the mass of the individual storey variations	Constant or reduce gradually	No more than 20% relative to the storey below, without abrupt changes, from the base to at least one storey below the top storey
Ratio of the actual storey resistance to the resistance required by the analysis	In framed buildings the ratio of the actual storey resistance to the resistance required by the analysis should not vary disproportionately between adjacent storeys. Special aspects of masonry infilled frames are specified	The ratio of the actual storey resistance to the resistance required by the analysis does not vary by more than 30% between adjacent storeys. Special aspects of masonry infilled frames are specified
Setbacks	3 geometrical conditions	It was eliminated

in elevation due to interacting infills should be considered. With a reduction of more than 30% of infills in a storey, the design should consider the increase of the seismic action effects in the structure, adopting a magnification factor.

4.3 Case Studies

Eight case studies were analyzed, corresponding to buildings recently designed (between 2018 and 2020) in Portugal. Five buildings (E01-E04 and E06) were designed according to Eurocode 8 [7] and 3 (E05, E07 and E08) according to the Portuguese national code (RSA [29] – application accepted until November 2022). The buildings have 8 to 12 storeys (see Fig. 11), 4 are residential buildings with services in the ground-storey, 2 are office buildings and 2 are hotels. Only 2 buildings have constant inter-storey height and all buildings have structural systems composed of RC columns and walls with flat slabs. All buildings are classified as wall systems, in both directions, with a frame/total stiffness ratio lower than 5,7%. Seven structures are classified as torsionally flexible buildings, based on the disposition and stiffness of the vertical elements.

All studied buildings are classified as non-regular in plan, according to the criteria for regularity in plan presented in actual and in the draft versions of Eurocode 8 (see Table 2). Seven buildings are classified as non-regular in elevation, according to both Eurocode 8 versions (see Table 3).

Based on the results of the 8 buildings analyzed, presented in Tables 2 and 3, the Eurocode 8 draft tends to be slightly more permissive in the plan and elevation regularity regularity criteria.

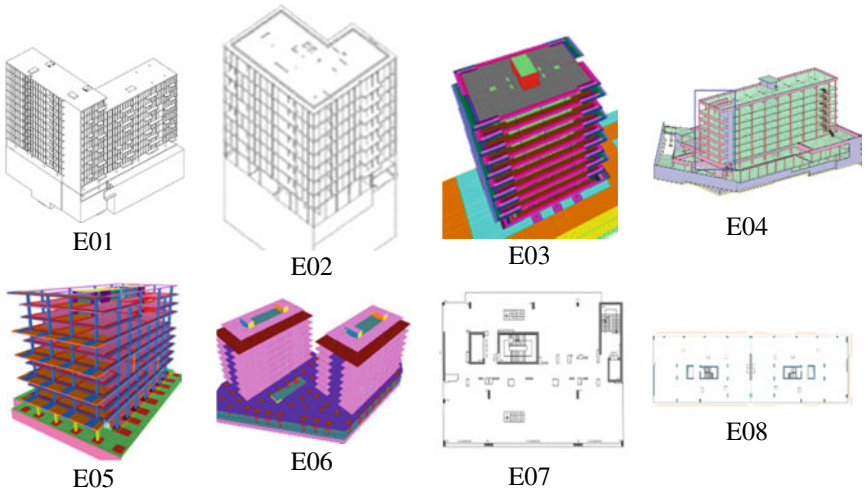

Fig. 11 General view of the 8 buildings studied [27]

Table 2 Regularity in plan criteria comparison [27]

Criteria		E01		E02		E03		E04		E05		E06		E07		E08		EC8 2004		*draft*	
		EC8 2004	*draft*	EC8 2004	*draft*	EC8 2004	*draft*	EC8 2004	*draft*	EC8 2004	*draft*	EC8 2004	*draft*	EC8 2004	*draft*	EC8 2004	*draft*	X %	✓ %	X %	✓ %
Lateral stiffness ~ symmetric	x	X	X	X	X	✓	✓	X	X	✓	✓	✓	X	X	X	X	X	75	25	75	25
	y	X	X	X	X	✓	✓	X	X	✓	✓	✓	✓	X	X	✓	✓	50	50	50	50
Mass distribution ~ symmetric	x	X	X	X	X	✓	✓	✓	✓	✓	✓	✓	✓	✓	✓	✓	✓	25	75	25	75
	y	X	X	✓	✓	✓	✓	X	X	✓	✓	✓	✓	X	X	✓	✓	37,5	62,5	37,5	62,5
Plan configuration compact		X	X	X	✓	✓	✓	X	X	✓	✓	✓	✓	✓	✓	X	✓	50	50	25	75
Rigid diaphragm condition	x	✓	✓	X	X	✓	✓	✓	✓	✓	✓	✓	✓	✓	✓	✓	✓	12,5	87,5	12,5	87,5
	y	X	X	X	X	✓	✓	X	X	✓	✓	✓	✓	✓	✓	✓	✓	37,5	62,5	37,5	62,5
Slenderness $\lambda = L\max/L\min$		✓	✓	✓	✓	✓	✓	X	✓	✓	✓	✓	✓	✓	✓	✓	✓	12,5	87,5	0	100
Eccentricity e_0 and the torsional radius r	x	X	X	X	X	X	X	X	X	X	X	X	X	X	X	X	X	100	0	100	0
	y	X	X	X	X	X	X	✓	✓	X	X	X	X	✓	✓	✓	✓	62,5	37,5	62,5	37,5

Table 3 Regularity in elevation criteria comparison [27]

Criteria		E01		E02		E03		E04		E05		E06		E07		E08		EC8 2004		*draft*	
		EC8 2004	*draft*	EC8 2004	*draft*	EC8 2004	*draft*	EC8 2004	*draft*	EC8 2004	*draft*	EC8 2004	*draft*	EC8 2004	*draft*	EC8 2004	*draft*	X %	✓ %	X %	✓ %
Vertical elements continuous up to the top		X	X	X	X	✓	✓	X	X	✓	✓	X	X	X	X	X	X	75	25	75	25
Lateral stiffness or gradual decrease	x	X	X	✓	✓	✓	✓	X	X	X	X	X	X	X	X	X	X	75	25	75	25
	y	X	X	X	X	✓	✓	X	X	X	X	X	X	X	X	X	X	87,5	12,5	87,5	12,5
Constant mass or gradual decrease		X	X	✓	✓	✓	✓	X	X	✓	✓	X	✓	✓	✓	✓	✓	37,5	62,5	25	75
Setbacks		X	-	✓	-	✓	-	X	-	✓	-	X	-	X	-	X	-	62,5	37,5	-	

5 Conclusions

Recent earthquakes keep showing that irregular response of buildings may have serious human and economic consequences. Many of our buildings tend to have irregular response. In the assessment of existing RC buildings, and in the design of new buildings, attention should be given to:

- irregularities in-elevation (as in the stiffness differences between the first and the upper storeys: storey height, dimensions and position of openings, distribution of the masonry infill walls);
- irregularities in-plan: torsion.

Considering the codes and design practice evolution, the tendency is that we are introducing more ductile structures, exploring important levels of damage and ductility demands in the structure. So, buildings regularity verification must be perfomed carefully. It is largely recognized that infill walls can change the seismic behaviour/response of the buildings drastically. So, they should be considered in the structural design, particularly for irregular distribution of infills (based on simple design rules/procedures).

Many international codes take into account the influence of the irregularities, reducing the q-factor (or other equivalent factor, in other codes than the Eurocode 8) in foce based design, and restricting the methods and models allowed in design. The new draft of the Eurocode 8, as the actual version, include different criteria to classify the structures in terms of their regularity in plan and in elevation. Based on the analyzed example, the actual version and tends to be more conservative in this regard. Further calibration and validation of the proposed rules in recent codes should be enforced (for different types of structural systems, type of irregularity, etc.), based on extensive numerical and experimental research.

Ackonwledgements This work was financially supported by: Base Funding–UIDB/04708/2020 and Programmatic Funding–UIDP/04708/2020 of the CONSTRUCT–Instituto de I&D em Estruturas e Construções–funded by national funds through the FCT/MCTES (PIDDAC).

References

1. Palermo M, Hernandez RR, Mazzoni S, Trombetti T (2014) On the seismic behavior of a reinforced concrete building with masonry infills collapsed during the 2009 L'aquila earthquake. Earthq Struct 6:45–69
2. Verderame GM, Luca F, Ricci P, Manfredi G (2011) Preliminary analysis of a soft-storey mechanism after the 2009 L'Aquila earthquake. Earthq Eng Struct Dyn vol. 40, 2011
3. Braga F, Manfredi V, Masi A, Salvatori A, Vona M (2011) Performance of non-structural elements in RC buildings during the L'Aquila, 2009 earthquake. Bull Earth Eng 9:307–324
4. Luca F, Verderame GM, Gómez-Martínez F, Pérez-García A (2014) The structural role played by masonry infills on RC building performances after the 2011 Lorca, Spain, earthquake. Bull Earthq Eng vol. 12, 2014
5. Hermanns L, Fraile A, Alarcón E, Álvarez R (2014) Performance of buildings with masonry infill walls during the 2011 Lorca earthquake. Bull Earthq Eng 12:1977–1997
6. Varum H (2003) Seismis assessment, strengthening and repair of existing buildings. Departamento de Engenharia Civil, Universidade de Aveiro, Aveiro, PhD
7. Eurocode 8, Design of structures for earthquake resistance–Part 1–1: General rules, seismic actions and rules for buildings, B. European Committee for Standardization, Belgium, 2005.
8. Varum H, Furtado A, Rodrigues H, Dias-Oliveira J, Vila-Pouca N, Arêde A (2017) Seismic performance of the infill masonry walls and ambient vibration tests after the Ghorka 2015, Nepal earthquake. Bull Earthq Eng 15:1185–1212
9. Rodrigues H, Arêde A, Furtado A, Rocha P (2015) Seismic rehabilitation of RC columns under biaxial loading: an experimental characterization. Struct 3:43–56, 1 Aug 2015
10. Rodrigues H, Furtado A, Arêde A (2017) Experimental evaluation of energy dissipation and viscous damping of repaired and strengthened RC columns with CFRP jacketing under biaxial load. Eng Struct 145:162–175, 8 Aug 2017
11. Rodrigues H, Furtado A, Vila-Pouca N, Varum H, Barbosa AR (2018) Seismic assessment of a school building in Nepal and analysis of retrofitting solutions. Int J Civ Eng 16:1573–1589
12. Carvalho E, Coelho E (1984) Análise Sísmica de estruturas de edifícios segundo a nova regulamentação - Análise Estrutural de um conjunto de 22 edifícios, vol II. Lisboa, Portugal
13. Mckenna F, Fenves G, Scott M, Jeremic B (2000) Open system for earthquake engineering simulation OpenSees (ed), Berkley, CA
14. Rodrigues H, Varum H, Arêde A, Costa A (2012) A comparative efficiency analysis of different non-linear modelling strategies to simulate the biaxial response of RC columns. Earthq Eng Eng Vib 11:553–566

15. Paulay T, Priestley MJN (1992) Seismic design of RC and masonry buildings. Wiley, ISBN 0–471–54915–0
16. Priestley MJN, Park R (1987) Strength and ductility of concrete bridge columns under seismic loading. ACI Struct J 84:61–76
17. Furtado A, Rodrigues H, Arêde A (2018) Load-path influence in the response of RC buildings subjected to biaxial horizontal loadings: numerical study. Int J Civ Eng 16:739–755
18. Mander JB, Priestley MJN, Park R (1988) Theoretical stress-strain model for confined concrete. J Struct Eng 114:1804–1826
19. Madas P, Elnashai AS (1992) A new passive confinement model for transient analysis of reinforced concrete structures. Earthquake Eng Struct Dynam 21:409–431
20. Martinez-Rueda JE, Elnashai AS (1997) Confined concrete model under cyclic load. Mater Struct 30:139–147
21. Menegotto M, Pinto PE (1973) Method of analysis for cyclically loaded R.C plane frames including changes in geometry and non-elastic behaviour of elements under combined normal force and bending. presented at the symposium on the resistance and ultimate deformability of structures acted on by well defined repeated loads, International association for bridge and structural engineering, Zurich, Switzerland
22. Filippou FC, Popov EP, Bertero VV (1983) Modelling of R/C joints under cyclic excitations. ASCE J Struct Eng 109:2666–2684
23. Furtado A, Rodrigues H, Arêde A, Varum H (2016) Simplified macro-model for infill masonry walls considering the out-of-plane behaviour. Earthquake Eng Struct Dynam 45:507–524
24. Mosalam K, Gunay S (2014) Progressive collapse analysis of RC frames with URM infill walls considering in-plane/out-of-plane interaction. Earthq Spectra 31:921–943
25. Varum H (2003) Seismic assessment, strengthening and repair of existing buildings. Universidade de Aveiro, Aveiro, Departamento de Engenharia Civil
26. Lima A (2020) Irregularidades estruturais no dimensionamento sísmico de edifícios de betão armado: discussão das exigências regulamentares e casos de estudo. Master Thesis, Civil Engineering, Faculdade de Engenharia da Universidade do Porto, Porto, Portugal
27. Lima A, Melo J, Varum H (2021) Irregularidades estruturais no dimensionamento sísmico de edifícios de betão armado: Discussão de exigências regulamentares e casos de estudo. Revista Portuguesa de Engenharia de Estruturas (RPEE), Série III, número 16, julho 2021
28. CEN (2019) prEN 1998–1–2:2019.3–draft of Eurocode 8: design of structures for earthquake resistance–Part 1–2: rules for new buildings (ed) European committee for standardization
29. RSA (1983) Regulamento de Segurança e Ações para Estruturas de Edifícios e Pontes. Decreto-Lei n.° 235/83, de 31 de Maio

Seismic Response of Masonry Building Aggregates in Historic Centres: Observations, Analyses and Tests

Andrea Penna, Annalisa Rosti, and Maria Rota

1 Introduction

A distinctive feature of many European cities is the presence of historical centres, with buildings in aggregate (Fig. 1). An aggregate is an assembly of buildings, adjacent one to the other, very often even sharing walls or other construction elements. This implies a very strong interaction among the different buildings within an aggregate, with an increased seismic vulnerability due to the very high level of irregularity, associated with the presence of buildings with different height, number of storeys, construction system and hence dynamic characteristics.

Being located in historical centres, aggregates are mainly constituted by old masonry buildings, with an intrinsically high seismic vulnerability. This vulnerability is further enhanced by the irregularity, in plan and in elevation, typical of building conglomerations. The seismic vulnerability of building aggregates has been pointed out during post-earthquake surveys following recent earthquakes, both in Italy and worldwide.

The main type of damage occurring to masonry aggregates in historical centres seems to be related with out-of-plane local collapse mechanisms (Fig. 2), which may consist of simple overturning, composite overturning, one-way bending or two-way

A. Penna (✉) · A. Rosti
Department of Civil Engineering and Architecture, University of Pavia, via Ferrata 3, 27100 Pavia, Italy
e-mail: andrea.penna@unipv.it

A. Rosti
e-mail: annalisa.rosti@unipv.it

M. Rota
EUCENTRE Foundation, via Ferrata 1, 27100 Pavia, Italy
e-mail: maria.rota@eucentre.it

R. Bento et al. (eds.), *Seismic Behaviour and Design of Irregular and Complex Civil Structures IV*, Geotechnical, Geological and Earthquake Engineering 50,
https://doi.org/10.1007/978-3-030-83221-6_2

Fig. 1 Examples of building aggregates in European cities **a** Camogli (Italy), **b** Barcelona

Fig. 2 Examples of local out-of-plane seismic damage to building aggregates, observed after the Central Italy sequence of 2016–2017 (Photos: A. Penna)

bending mechanisms. This is due, on the one hand, to the lack of appropriate connections between floors and walls and between perpendicular walls and, on the other hand, to the presence of a thick and redundant connection among the building units (and sometimes also between building aggregates). As discussed also in [1], local out-of-plane mechanisms are also favoured by the frequent presence of construction irregularities (e.g. walls not well clamped in the last built units, that obstructed the empty spaces) or geometric irregularities (e.g. different height between adjacent buildings). These significant irregularities in plan and/or in elevation can nevertheless also induce damage mechanisms associated to the in-plane response of masonry walls (Fig. 3).

Damages to masonry aggregates are often also related to interactions of adjacent buildings, due to the structural contiguity within the aggregates. This may induce in-plane and out-of-plane damages, often characterised by vertical cracks at the building interface, induced by non-synchronous motion, damage concentration at the emerging portion of the higher building, or in presence of misaligned floors. Example of damages due to interaction between adjacent buildings, observed after the L'Aquila (2009) earthquake, are shown in Fig. 4.

Fig. 3 Examples of global in-plane seismic damage to building aggregates, observed after the Central Italy sequence of 2016–2017 (Photos: A. Penna)

Fig. 4 Examples of damages observed after the L'Aquila (2009) event, due to interaction between adjacent buildings within an aggregate (Photos: A. Penna)

Seismic vulnerability assessment of building aggregates requires to be preceded and supported by a cognitive process, implying geometric survey and historical investigation, in-depth analysis of the architectural and technological features and critical survey and interpretation of the observed damage (e.g. [2, 3]).

Several literature studies assessed the global seismic response of URM building aggregates by nonlinear static analyses performed either through the equivalent frame method (e.g. [3–7]), implemented in the Tremuri software ([8–11]), or detailed finite elements models [12].

Given the significant vulnerability of URM building aggregates with respect to out-of-plane seismic actions (e.g. [13–16]), local mechanisms need to be opportunely considered when characterizing their seismic response. In this context, limit analysis represents a valuable tool for the analysis of local out-of-plane failures (e.g. [12]).

To overcome modelling issues, the seismic vulnerability of masonry aggregates can be estimated by using simplified approaches, for instance based on the vulnerability index formulation (e.g. [5, 7]) or on the Vulnus procedure [17], which allows to determine the in-plane and out-of-plane critical triggering accelerations, based on the analysis of possible mechanisms (e.g. [3, 7]).These procedures are useful in

case of large-scale seismic vulnerability applications, whereas they are inappropriate for the seismic evaluation of individual buildings, for which an accurate analysis is required.

2 Considerations from Statistical Processing of Post-Earthquake Damage Data

The effect of the building position on the empirical seismic vulnerability of URM buildings is investigated by statistically processing the L'Aquila (2009) post-earthquake damage data, available from the Da.D.O. platform [18]. The considered post-earthquake damage dataset counts about 28′000 masonry buildings, sited in municipalities with completeness ratio (i.e. number of inspected buildings over the total number of buildings from national building census [19]) exceeding 90%. The post-earthquake damage dataset is then integrated by undamaged buildings, sited in the Abruzzi non-surveyed and partially-surveyed (with completeness ratio < 10%) municipalities, to account for the negative evidence of damage in towns less affected by ground shaking [20]. The total number of masonry buildings, located in these municipalities and reasonably assumed to be undamaged (about 175′000 buildings), is retrieved from the national building census [19].

A global level of damage is assigned to each inspected building, by employing the Rota et al. [21] damage rule for converting the damage description of the post-earthquake survey form into discrete damage levels of the EMS-98 [22]. Once damage is evaluated individually on preselected building components, the overall damage classification is driven by the maximum level of damage. The ground motion severity is characterized by assigning a value of peak ground acceleration (PGA), estimated from the INGV shakemaps [23], to each building location (e.g. [24]).

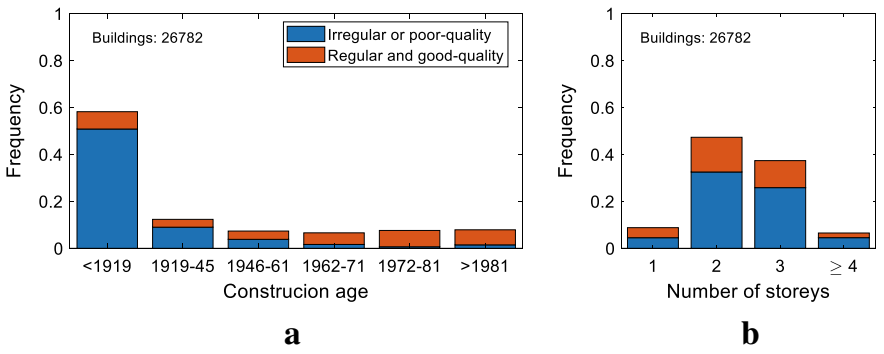

Fig. 5 Subdivision of URM buildings from the completely-surveyed municipalities based on construction age **a** and number of stories **b**

Figure 5 subdivides masonry buildings, from the completely-surveyed municipalities, based on the construction age and number of stories, respectively. In the figure, the different colours denote the quality and layout of the masonry fabric (i.e. irregular layout or poor-quality masonry and regular layout and good-quality masonry). About 67% of the considered sample is constituted by irregular layout or poor-quality masonry buildings, being the remaining 33% represented by URM buildings made of good-quality materials. About 60% of the URM buildings were constructed before year 1919 (Fig. 5a), whereas low-rise (1–2 stories) masonry buildings represent 56% of the available dataset (Fig. 5b).

Considering the information available from the post-earthquake survey form, each masonry building is then classified based on its position within the structural aggregate, namely corner, extreme, internal or isolated building (Fig. 6). About 15% of the considered dataset is constituted by corner URM buildings, 27% by extreme URM buildings, 33% by internal URM buildings, whereas 26% of the sample is represented by isolated URM buildings. Regardless the characteristics of the masonry fabric, the trend of the building position as a function of the construction age shows that structural units of building aggregates are predominant until period 1946–61. After year 1961, isolated buildings prevail.

Seismic vulnerability is quantified by empirical fragility curves, in terms of levels of physical damage and usability outcomes. In line with [25], the functional performance of a building is defined as one of three possible outcomes, i.e. usable (green tag), limited/restricted use (yellow tag) and unusable (red tag), allowing for a rough

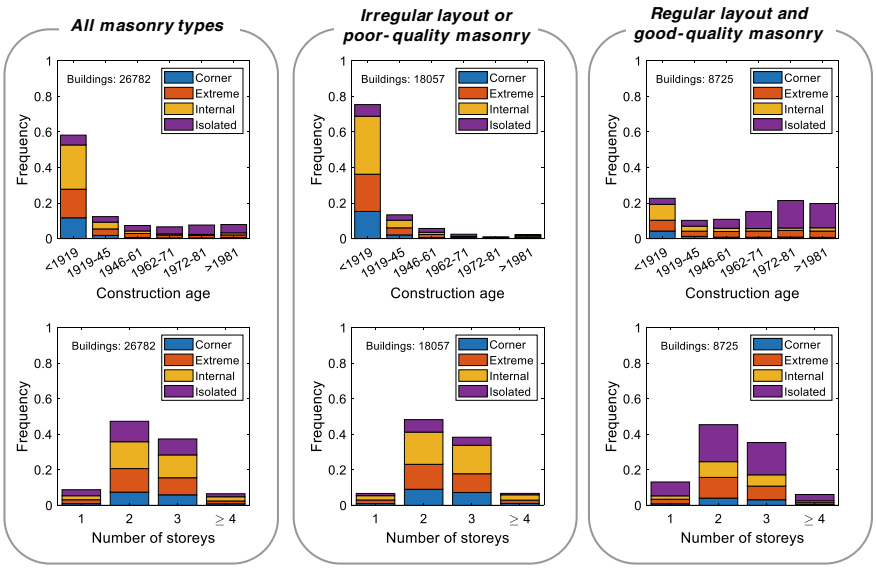

Fig. 6 Classification of masonry buildings from the completely-surveyed municipalities based on the masonry type, building position, construction age and number of stories

estimate of the building functional loss in the aftermath of an earthquake. Fragility curves are obtained by the statistical model and fitting technique described in [20]. The lognormal cumulative distribution is adopted to describe the probability of exceedance of the different damage levels/usability outcomes, whereas the subdivision of buildings in the different damage levels/usability outcomes is approximated by the multinomial distribution. A common dispersion is assumed for all damage levels/usability outcomes to impede intersecting fragility functions.

Figures 7 and 8 show empirically-derived fragility curves for URM buildings, accounting for building height (i.e. low-rise: 1–2 stories and mid-/high-rise: > 2 stories), and building position (i.e. corner, extreme, internal or isolated building). Fragility curves are derived in terms of damage levels (Fig. 7) and usability outcomes (Fig. 8). Seismic fragility results to be slightly affected by building position within the structural aggregate (i.e. corner/extreme/internal), whereas notable differences can be observed by comparing fragility functions for structural units of a building aggregate (i.e. corner/extreme/internal building) with those for isolated buildings. The reason of the higher vulnerability of building aggregates could be ascribed to the presence of structural and construction irregularities, such as different heights and lack of appropriate connections between adjacent buildings. Analogous considerations apply to usability outcomes (Fig. 8), where the building unusability is indeed more affected by the presence of structural irregularities rather than by the position of the building within the URM aggregate.

Based on the above considerations, fragility functions are derived by distinguishing structural units of building aggregates from isolated buildings (Figs. 9 and 10). Besides the number of stories, the layout and quality of masonry are also accounted for. Figure 9 shows that structural units of building aggregates are

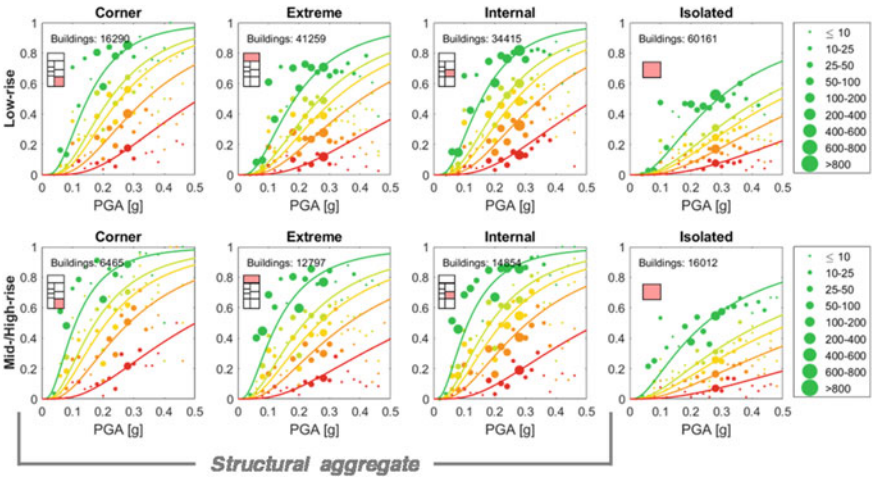

Fig. 7 Empirically-derived fragility curves in terms of physical damage levels for URM buildings, accounting for the building position: corner, extreme, internal and isolated buildings

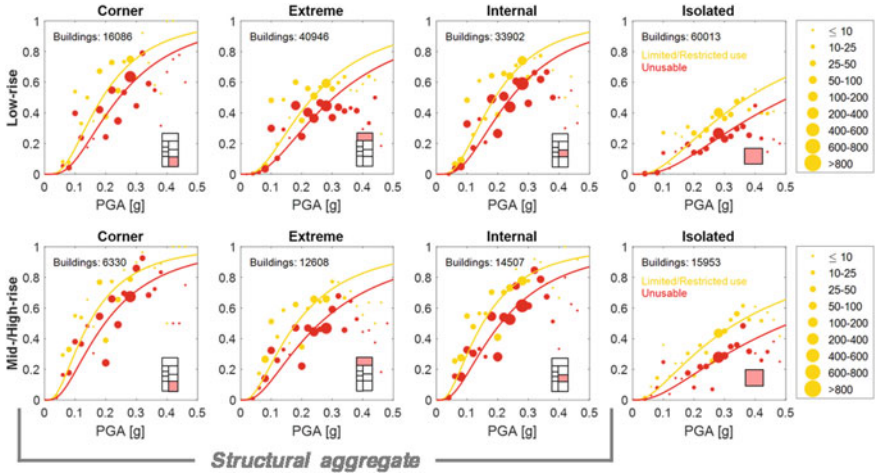

Fig. 8 Empirically-derived fragility curves in terms of usability outcomes for URM buildings, accounting for the building position: corner, extreme, internal and isolated buildings

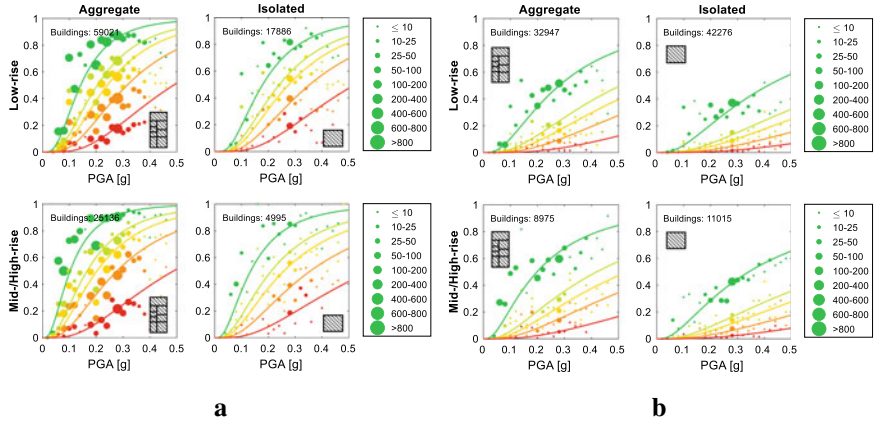

Fig. 9 Empirically-derived fragility curves in terms of physical damage levels for irregular layout or poor-quality **a** and regular layout and good-quality masonry buildings **b**: structural units of URM aggregates and isolated buildings

more vulnerable than isolated buildings. This aspect is more evident in case of regular layout and good-quality masonry (Fig. 9b), rather than in irregular layout and poor-quality masonry.

Indeed, the same use of poor-quality materials strongly impacts the seismic vulnerability, regardless the building position (Fig. 9a). Similarly, the presence of structural irregularities affects the building unusability, with larger impact in case of URM buildings made of good-quality materials.

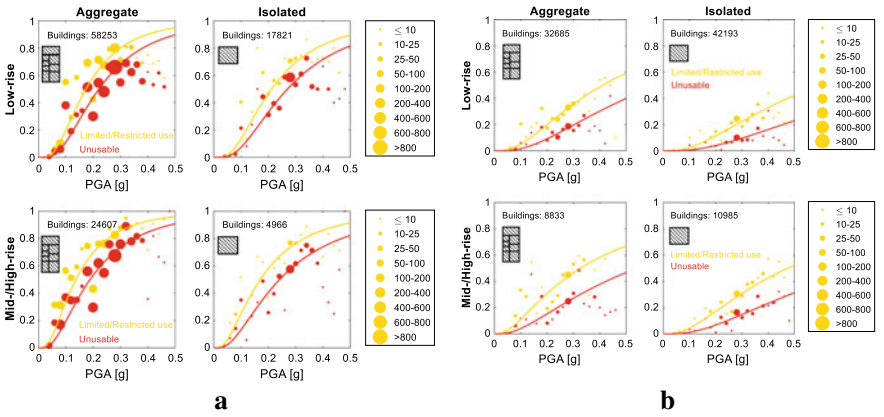

Fig. 10 Empirically-derived fragility curves in terms of usability outcomes for irregular layout or poor-quality **a** and regular layout and good-quality masonry buildings **b**: structural units of URM aggregates and isolated buildings

3 Seismic Assessment of URM Building Aggregates

The modelling and seismic assessment of masonry aggregates is a complex problem, as clear and reliable analytical tools have not been developed and codes only provide limited indications. The seismic response of these masonry buildings conglomerations can indeed be even significantly different from that of isolated buildings, due to the interconnection or contact of adjacent structural subsystems. The best option would ideally include the entire building aggregate in the numerical model. However, the relevant dimensions and irregularities of aggregates in historical centres make it often unfeasible, both for computational issues and for the impossibility of obtaining information on the structural units which are not directly the object of study. On the other hand, a model of the single building unit of analysis can be hardly meaningful, because isolating the structural unit of interest requires a proper simulation of the interactions with the adjacent buildings, by means of appropriate boundary conditions and/or contact elements.

The vulnerability of building aggregates is different from that of single buildings for several distinctive features, which can be summarised in a single concept: structural irregularity. This includes the presence of very common characteristics such as differences in height, misaligned floors, irregular soil morphology, structural transformations over time, poor connections between walls and floors and between adjacent buildings, pounding between adjacent buildings. Numerical models can easily show that the presence of buildings with different characteristics adjacent one to the other, with unilateral connections, may induce damage mechanisms which are different with respect to those of isolated buildings (Fig. 11).

The Italian Building Code [26] requires identifying the structural unit under investigation, indicating the actions that can be expected on the unit from contiguous ones.

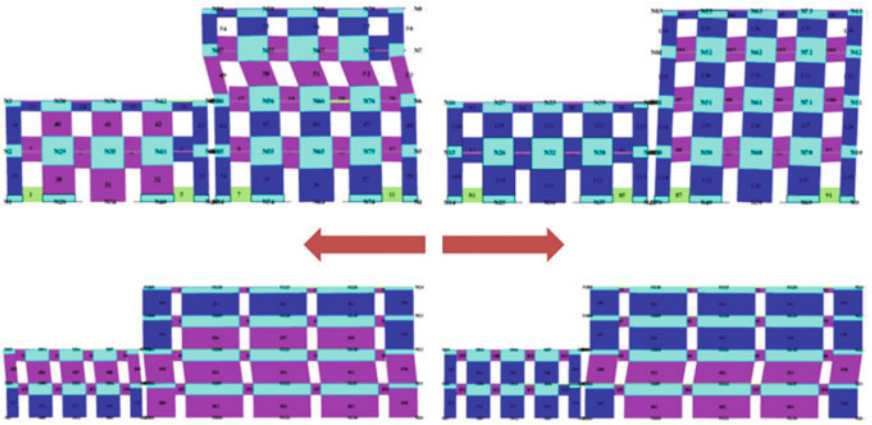

Fig. 11 Examples of in-plane pushover analysis of adjacent masonry façades with different characteristics and unilateral joints: different damage mechanisms occur in the aggregate depending on the direction of analysis

The structural unit is required to be defined from foundations to roof level and the seismic response of the different units should be reasonably identifiable and separable. In most practical cases, the extraction of a single unit is not straightforward and it requires evaluation of the effect of loads and thrusts on walls shared with adjacent units not counteracted due to staggering in height of floor levels, susceptibility to local mechanisms due to misaligned façades and differences in height or stiffness among units. In case of flexible diaphragms, it is possible to isolate single walls and carry out a pushover analysis of each of them, provided that tributary vertical loads and seismic actions are properly accounted for. The model should also account for the so-called flange effect, i.e. the contribution of collaborating portions of perpendicular walls, which should be introduced in the model, together with the corresponding tributary masses.

Although it would be generally better modelling the entire building aggregate, in some cases this is impractical, for several reasons, including the impossibility of inspecting all structural units, the significant uncertainties associated with the portions other than those investigated due to lack/scarcity of knowledge and the impossibility to make interventions on portions other than those investigated. An example is reported in Fig. 12, presenting a case in which it was possible to extract the building portion under study (red circle in Fig. 12a), accounting for the presence of the remaining portion by introducing appropriate constraints and/or deformable beams or springs.

The introduction of a unilateral constraint, working only when the different portions tend to compenetrate, induces a different response depending on the direction of analysis. In case of analysis in the longitudinal direction or in the positive transverse direction, the building tends to behave as an isolated structure (top and

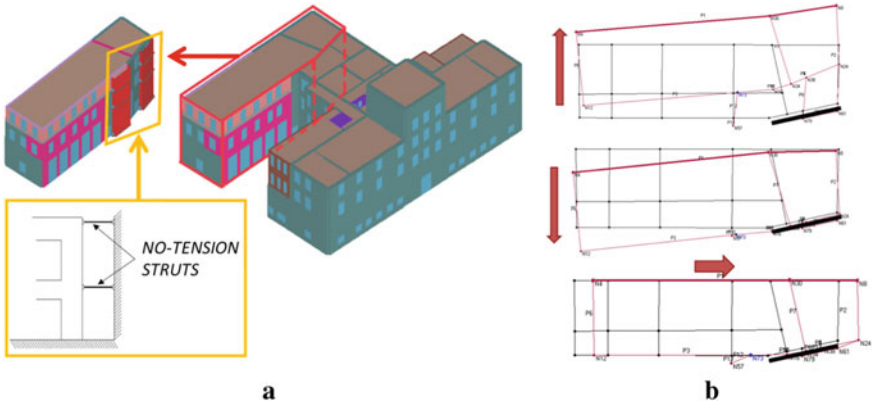

Fig. 12 **a** Example of a building aggregate, with identification of the portion of study; **b** effect of the presence of a unilateral eccentric constraint (thick black line) on the seismic response, depending on the direction of analysis (indicated by the red arrow)

bottom plot of Fig. 12b); if the analysis is carried out in the negative transverse direction, instead, there is interaction with the adjacent portions and the presence of the eccentric unilateral constraint induces a torsional response (central plot of Fig. 12b).

Frequently, in particular in historical centres, this modelling simplification is not possible and it is necessary to analyse the single unit under study. In some simpler cases, however, it would be useful to have criteria for accounting for the effect of position of the single unit within the aggregate. Senaldi et al. [27] studied the opportunity/possibility to "extract" the single structural unit to be analysed from the aggregate, by comparing its response with the response of the same unit when the dynamic behaviour of the entire aggregate is modelled. The results showed that the analysis of the single cell leads to conservative results in the longitudinal direction. The transversal response exhibited a higher in-plane distortion in end units of linear building conglomerations. The effect of the substitution of flexible diaphragms with rigid ones in one of the structural units was also investigated, showing a concentration of in-plane distortion in the structural units adjacent to the "retrofitted" one. This highlights the need for a careful assessment of the effect of interventions on single structural units within an aggregate.

4 Shaking Table Tests and Numerical Analyses on Masonry Building Aggregates

The literature presents several works reporting experimental and numerical results on the seismic behaviour of masonry building aggregates.

Guerrini et al. [28] and Senaldi et al. [29] present the results of shaking table tests carried out in Pavia on a half-scale natural stone masonry building aggregate

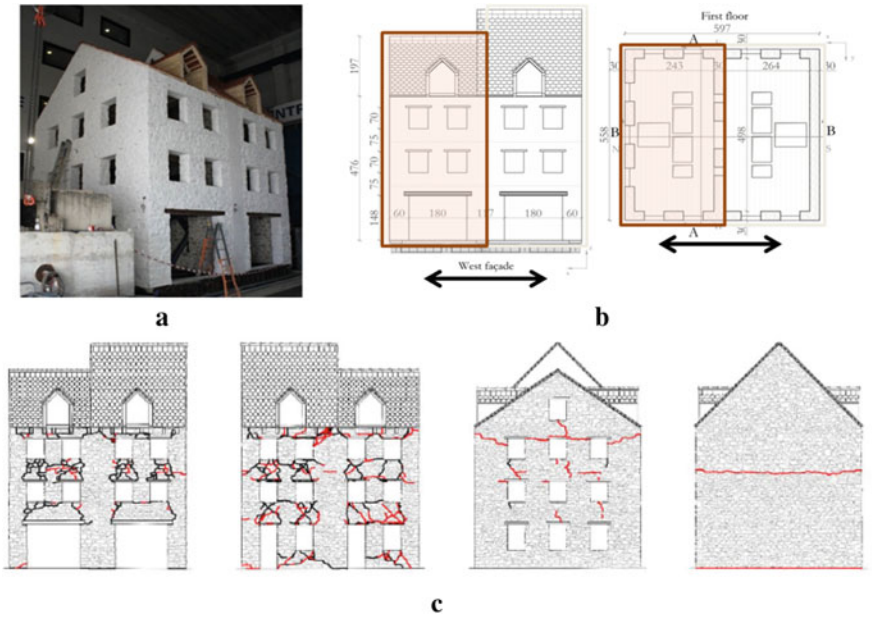

Fig. 13 **a, b** Building aggregate prototype analysed by Guerrini et al. [28] and Senaldi et al. [29], **c** damage pattern after tests at a PGA of 0.35 g, corresponding to a severe level of damage (adapted from [29]). Crack segments marked in red opened during the test at PGA = 0.35 g, crack segments marked in black were detected after previous tests on the specimen

(Fig. 13). The half-scale prototype was designed to reproduce the features of existing unreinforced stone masonry building aggregates, typical of the historical centres in many European cities, including the city of Basel, Switzerland. The prototype consisted of a three-storey-high aggregate, with two weakly connected structural units (through stones were provided only at opening edges and corners, although not in every masonry course), with double-leaf undressed stone masonry walls incorporating a small percentage of river pebbles. The specimen had flexible timber floor diaphragms and side-gabled timber roofs, with different heights above the two units. Material mechanical properties were scaled to satisfy similitude relationships without altering accelerations and material densities. Near-collapse conditions were reaching during the tests, using input ground motions selected to be compatible with realistic seismic scenarios for the region of Basel. Two retrofit solutions were then considered (i.e. improved wall-to-diaphragm connections and tie rods), initially pre-installed on the specimen and then activated after significant damage was reached testing the unstrengthened specimen.

Figure 13c reports a scheme of the cracks detected on the specimen after the test at a nominal PGA of 0.35 g. The specimen evidenced a severe damage condition, with widespread damage to spandrels (shear and flexural response) with cracks up to 3 mm, a rocking response of piers in the East and West façades, first activation of out-of-plane overturning mechanisms in the North and South façades, horizontal

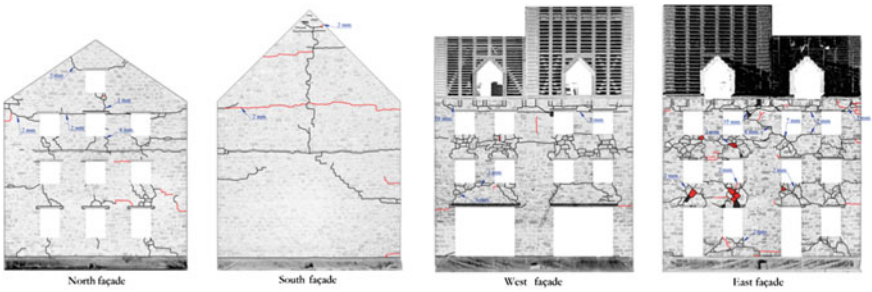

Fig. 14 Damage pattern of the strengthened building after test at a PGA of 0.64 g (adapted from in [28]). Crack segments marked in red opened during the test at PGA = 0.64 g, crack segments marked black were detected after previous tests on the specimen

cracks at the interface between foundation ring and perimeter walls and fall of pieces of plaster/mortar and small stones from East and West façades.

Because of the severe level of damage experienced by the specimen, the retrofit interventions previously installed were activated prior to reach near-collapse conditions, allowing continuation of the testing campaign. Fastening the wall-to-diaphragm connections and post-tensioning the tie rods resulted in almost complete recovery of residual displacements, floor joist slip, and residual cracks.

The activation of the strengthening interventions allowed to carry out tests until significantly higher levels of seismic input, with the strengthened specimen reaching near collapse conditions for the test with a PGA of 0.64 g. The damage pattern after this test is reported in Fig. 14, highlighting cracks with a residual thickness ranging between $2 \div 10$ mm, the evolution of out-of-plane overturning mechanisms in the North and South façades with identification of additional blocks, significant de-cohesion of stone blocks in all spandrels, opening of vertical cracks in correspondence of joint between the two structural units and significant residual displacement of timber lintels.

The experimental results of the unstrengthened specimen were then numerically simulated, using an equivalent frame approach accounting also for the out-of-plane contribution of masonry walls [30]. The model provided a satisfactory simulation of the experimental results, as evident from Fig. 15, reporting a comparison of the experimental and numerical force–displacement global response.

Within the SERA-AIMS Project–H2020 shaking table tests were recently carried out at LNEC on half-scale two-buildings aggregates with irregularity in height, realised with the same masonry typology but with dry connection between the two buildings (no-interlocking condition).

Another interesting experimental campaign was recently carried out at EUCENTRE (Pavia), with shaking table tests on a two-storey full scale unreinforced masonry building (Fig. 16a), meant to be the end-unit of a pre-1980 terraced house (Fig. 16b), built with cavity walls and without any particular seismic design or detailing [31]. The loadbearing masonry was composed of calcium silicate (CS) bricks, sustaining two reinforced concrete floors. A pitched timber roof was supported

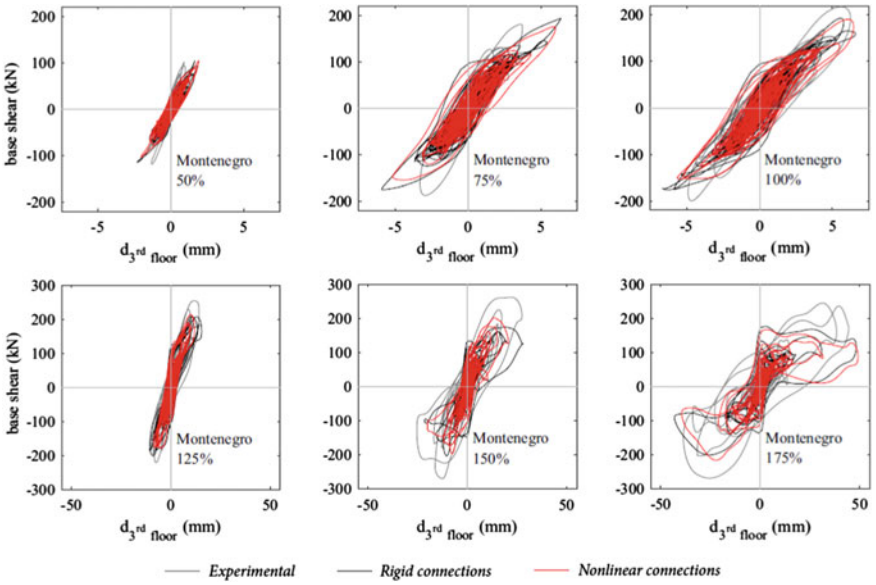

Fig. 15 Comparison of experimental and numerical force–displacement response of the building aggregate [30]. The different subplots correspond to different percentages of scaling of the input motion (Montenegro 1979)

by two gable walls. The veneer was made of clay bricks connected to the inner masonry by means of metallic ties, as seen in common construction practice.

The specimen was subjected to incremental dynamic tests, up to near-collapse conditions, which were reached for a PGA of 0.32 g, using input motions representative of the induced seismicity of the Groningen region of the Netherlands. The damage pattern observed after the final test showed shear cracks, mortar joint sliding and block separation in CS spandrels, cracks at base and at roof-beams support due to overturning in CS gables and diagonal cracks due to out-of-plane bending in CS transverse walls (Fig. 16c). The clay veneer piers experienced sliding at roof wall-plate interface, whereas shear and flexural cracks developed in clay veneer spandrels and a horizontal crack at the base due to overturning was noticed in the clay veneer gable (Fig. 16d).

These experimental results were numerically simulated by Kallioras et al. [32], with the aim of extending the utility of the tests for the seismic assessment of terraced houses in the Groningen region. Numerical models were developed in the Tremuri computer program, addressing the several issues related with the numerical simulation of the dynamic response of unreinforced cavity-wall systems in the context of an equivalent-frame modelling approach and also considering the effect of the nonlinear out-of-plane response of walls. The calibrated single-unit model was then enlarged to numerically assess the effects of human-induced earthquakes on an entire row of terraced houses. An extended numerical simulation was carried out, using a cloud

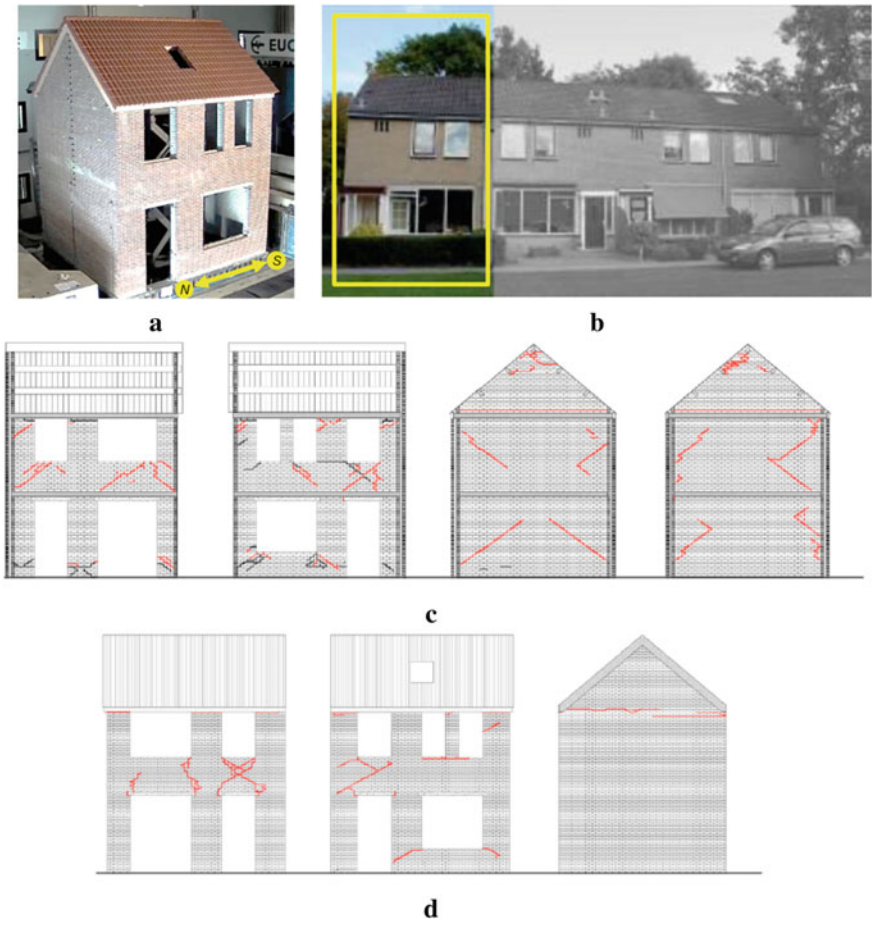

Fig. 16 **a, b** Building specimen subjected to incremental shaking table tests, representative of an end-unit of a Dutch terraced house [31], **c, d** damage pattern of the inner CS walls and outer clay walls, after tests at a PGA of 0.32 g, inducing a near collapse condition in the building [31]. Crack segments marked in red opened during the test at PGA = 0.64 g, crack segments marked in black were detected after previous tests on the specimen

method to establish the probabilistic relationship between ground-motion intensity and nonlinear structural response, using a large suite of records. The results were also used to derive fragility curves, allowing for a comparison of the seismic response of the single end-unit and the entire aggregate of the terraced house.

Figure 17 reports, as an example, the fragility curved derived in [32], in terms of PGA and modified Housner Intensity (defined as the integral between 0.1 s and 0.5 s of the pseudo-velocity, as in [33]), for 5 levels of damage. The comparison shows a rather limited difference between the curves for the single end-unit (continuous lines) and those for the extended terraced house (dashed lines), with the latter being slightly less

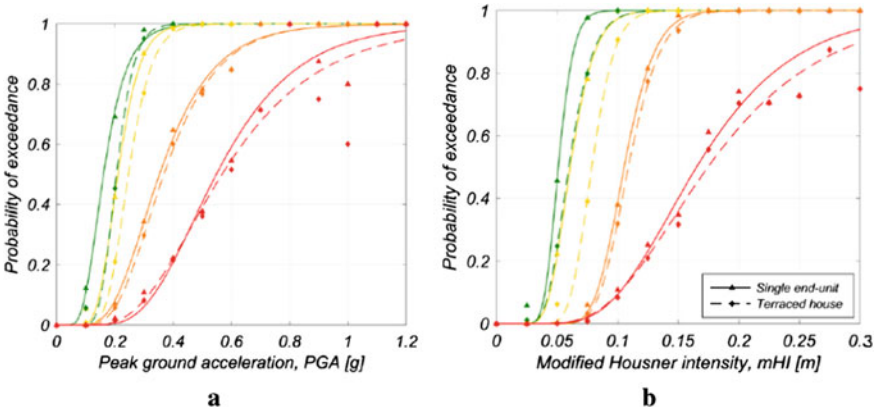

Fig. 17 Comparison of observed fractions of exceedance and fragility curves for a single end-unit and for the extended aggregate, in terms of PGA **a** and modified Housner Intensity **b** [32]

vulnerable. It should be noted that these fragility curves only account for record-to-record variability, neglecting other potential sources of variability, such as uncertainty on mechanical properties, correlations between the different parameters and between different structural components (e.g. [34, 35]) and modelling uncertainties [36].

5 Conclusions

The high seismic vulnerability of conglomerations of masonry buildings is well-known and evident from observations after seismic events. This is due in particular to the irregularity (in plan and in elevation) of these building aggregates, often due to their history and evolution, consisting of an aggregation of structural cells and units, with frequent transformations, enclosures, addition of storeys in buildings erected at different times and adjacent to already existing structures, with scarce or inexistent connection.

The structural assessment of URM building aggregates is inherently complex. The currently available numerical models can be used to analyse URM building aggregates, even in case of relatively large models, although it is often difficult to obtain a sufficient level of knowledge on the entire aggregate. In some cases, it is possible to extract a portion of the aggregate to be analysed as an isolated building, appropriately accounting for the interaction with adjacent units.

The availability of shaking table tests on building aggregates can help in understanding the seismic behaviour of these complex structures and validating more or less simplified numerical models, which can be calibrated on the experimental results and then used for modelling other and more complex cases. Parametric numerical studies could be useful also for deriving simplified approaches for «everyday» assessment

practice and to quantify the effect of different characteristics of building aggregates, to identify the most relevant parameters to be considered.

Also based on post-earthquake observations of damages, one would expect that building position within the aggregate could have a significant effect on seismic vulnerability. Actually, both the statistical treatment of post-earthquake damage data and numerical simulations seem to indicate that structural irregularity, characterising masonry aggregates with respect to isolated buildings, has a stronger effect on vulnerability than building position. A higher vulnerability of external structural units was observed in case of extremely regular and homogeneous aggregates, whereas in the much more frequent case of aggregates with structural units of different height and characteristics and with dry connections, damage concentration would occur at the interface between structural units with a different dynamic behaviour.

The spatial variability of seismic motion is another issue to be investigated, especially in very large aggregates and/or aggregates constructed on hill slopes (as often happens in historical centres).

References

1. Lagomarsino S, Magenes G (2009) Evaluation and reduction of the vulnerability of masonry buildings. In: Manfredi G, Dolce M (eds) the state of earthquake engineering research in Italy: the ReLUIS-DPC 2005–2008 Project, Doppiavoce, Napoli, Italy, 1–50
2. Carocci CF (2012) Small centres damaged by 2009 L'Aquila earthquake: on site analyses of historical masonry aggregates. Bull Earthq Eng 10:45–71
3. da Porto F, Munari M, Prota A, Modena C (2013) Analysis and repair of clustered buildings: case study of a block in the historic city centre of L'Aquila (central Italy). Constr Build Mater 38:1221–1237. https://doi.org/10.1016/j.conbuildmat.2012.09.108
4. Pujades LG, Barbat AH, Gonzales-Drigo R, Avila J, Lagomarsino S (2012) Seismic performance of a block of buildings representative of the typical construction in the example district in Barcelona (Spain). Bull Earthq Eng 10:331–349
5. Maio R, Vicente R, Formisano A, Varum H (2015) Seismic vulnerability of building aggregates through hybrid and indirect assessment techniques. Bull Earthq Eng 13:2995–3014
6. Fagundes C, Bento R, Cattari S (2017) On the seismic response of building in aggregate: analysis of a typical masonry building from Azores. Struct 10:184–196
7. Chieffo N, Formisano A (2019) Comparative seismic assessment methods for masonry building aggregates: a case study. Front Build Environ 5:123. https://doi.org/10.3389/fbuil.2019.00123
8. Lagomarsino L, Penna A, Galasco A, Cattari S (2013) TREMURI program: an equivalent frame model for the nonlinear seismic analysis of masonry buildings. Eng Struct 56:1787–1799. https ://doi.org/https://doi.org/10.1016/j.engst ruct.2013.08.002
9. Penna A, Lagomarsino L, Galasco A (2014) A nonlinear macroelement model for the seismic analysis of masonry buildings. Earthq Eng Struct Dyn 43(2):159–179. https ://doi.org/https://doi.org/10.1002/eqe.2335.
10. Bracchi S, Galasco A, Penna A (2021) A novel macroelement model for the nonlinear analysis of masonry buildings. part 1: axial and flexural behaviour. Earthq Eng Struct Dyn, doi: https://doi.org/10.1002/eqe.3445.
11. Bracchi S, Penna A (2021) A novel macroelement model for the nonlinear analysis of masonry buildings. part 2: shear behaviour. Earthq Eng Struct Dyn. doi: https://doi.org/10.1002/eqe.3444.

12. Grillanda N, Valente M, Milani G, Chiozzi A, Tralli A (2020) Advanced numerical strategies for seismic assessment of historical masonry. Eng Struct 212: 110441
13. D'Ayala DF, Paganoni S (2011) Assessment and analysis of damage in L'Aquila historic city centre after 6th April 2009. Bull Earthq Eng 9:81–104
14. Fragomeli A, Galasco A, Graziotti F, Guerrini G, Kallioras S, Magenes G, Malomo D, Mandirola M, Manzini CF, Marchesi B, Milanesi RR, Morandi P, Penna A, Rossi A, Rosti A, Rota M, Senaldi IE, Tomassetti U, Cattari S, da Porto F, Sorrentino L (2017) Performance of masonry buildings in the seismic sequence of central Italy 2016–Part 1: Overview. Progett Sismica 8(2):49–77
15. Fiorentino G, Forte A, Pagano E, Sabetta F, Baggio C, Lavorato D, Nuti C, Santini S (2018) Damage patterns in the town of Amatrice after aug 24th 2016 Central Italy earthquakes. Bull Earthq Eng 16(3):1399–1423
16. Sorrentino L, Cattari S, da Porto F, Magenes G, Penna A (2019) Seismic behaviour of ordinary masonry buildings during the 2016 Central Italy earthquakes. Bull Earthq Eng 17:5583–5607
17. Bernardini A, Gori R, Modena C (1989) An application of coupled analytical models and experimental knowledge for seismic vulnerability analyses of masonry buildings. In: Koridze A (ed) Engineering aspects of earthquake phenomena 3:161–180
18. Dolce M, Speranza E, Giordano F, Borzi B, Bocchi F, Conte C, Di Meo A, Faravelli M, Pascale V (2019) Observed damage database of past Italian earthquakes: the DaDO WebGIS. Bollettino di Geofisica Teorica e Applicata 60(2):141–164
19. Census Data (2001) http://dawinci.istat.it/jsp/MD/dawinciMD.jsp
20. Rosti A, Rota M, Penna A (2020) Empirical fragility curves for Italian URM buildings. Bull Earthq Eng. https://doi.org/10.1007/s10518-020-00845-9
21. Rota M, Penna A, Strobbia CL (2008) Processing Italian damage data to derive typological fragility curves. Soil DynEarthq Eng 28(10):933–947
22. Grünthal G (ed), Musson RMW, Schwarz J, Stucchi M (1998) European macroseismic scale. cahiers du centre Européen de géodynamique et de séismologie. Vol 15-European Macroseismic Scale 1998. European centre for geodynamics and seismology, Luxembourg
23. Michelini A, Faenza L, Lanzano G, Lauciani V, Jozinovic D, Puglia R, Luzi L (2020) The new shakemap in Italy: progress and advances in the last 10 Yr. Seismol Res Lett 91(1):317–333. https://doi.org/10.1785/0220190130
24. Rosti A, Rota M, Penna A (2020) Influence of seismic input characterisation on empirical damage probability matrices for the 2009 L'Aquila event Soil Dyn Earthq Eng 128:105870 https://doi.org/10.1016/j.soildyn.2019.105870
25. Rosti A, Rota M, Penna A (2018) Damage classification and derivation of damage probability matrices from L'Aquila (2009) post-earthquake survey data. Bull Earthq Eng 16(9):3687–3720. https://doi.org/10.1007/s10518-018-0352-6
26. NTC (2018) Decreto ministeriale 17 gennaio 2018: aggiornamento delle "Norme tecniche per le costruzioni". ministero delle infrastrutture e dei trasporti. SO. n.8 alla G.U. del 2 Feb 2018, No 42 (in Italian)
27. Senaldi I, Magenes G, Penna A (2010) Numerical investigations on the seismic response of masonry building aggregates. Advanced materials research, 133–134.715 720. https://doi.org/10.4028/www.scientific.net/AMR.133-134.715
28. Guerrini G, Senaldi I, Graziotti F, Magenes G, Beyer K, Penna A (2019) Shake-table test of a strengthened stone masonry building aggregate with flexible diaphragms. Int J Arch Herit 13(7):1078–1097. https://doi.org/10.1080/15583058.2019.1635661
29. Senaldi IE, Guerrini G, Comini P, Graziotti F, Penna A, Beyer K, Magenes G (2020) Experimental seismic performance of a half-scale stone masonry building aggregate. Bull Earthq Eng 18:609–643. https://doi.org/10.1007/s10518-019-00631-2
30. Vanin F, Penna A, Beyer K (2020) Equivalent-frame modelling of two shaking table tests of masonry buildings accounting for their out-of-plane response. Front Built Environ 6:42. https://doi.org/10.3389/fbuil.2020.00042
31. Graziotti F, Tomassetti U, Kallioras S, Penna A, Magenes G (2017) Shaking table test on a full scale URM cavity wall building. Bull Earthq Eng 15:5329–5364. https://doi.org/10.1007/s10518-017-0185-8

32. Kallioras S, Graziotti F, Penna A (2019) Numerical assessment of the dynamic response of a URM terraced house exposed to induced seismicity. Bull Earthq Eng 17:1521–1552. https://doi.org/10.1007/s10518-018-0495-5
33. Mouyiannou A, Penna A, Rota M, Graziotti F, Magenes G (2014) Implications of cumulated seismic damage on the seismic performance of unreinforced masonry buildings. Bull N Z Soc Earthq Eng 47(2):157–170. https://doi.org/10.5459/bnzsee.47.2.157-170
34. Bracchi S, Rota M, Magenes G, Penna A (2016) Seismic assessment of masonry buildings accounting for limited knowledge on materials by Bayesian updating. Bull Earthq Eng 14(8):2273–2297. https://doi.org/10.1007/s10518-016-9905-8
35. Franchin P, Ragni L, Rota M, Zona A (2018) Modelling uncertainties of Italian code-conforming structures for the purpose of seismic response analysis. J Earthquake Eng 22(S2):28–53. https://doi.org/10.1080/13632469.2018.1527262
36. Bracchi S, Rota M, Penna A, Magenes G (2015) Consideration of modelling uncertainties in the seismic assessment of masonry buildings by equivalent-frame approach. Bull Earthq Eng 13(11):3423–3448. https://doi.org/10.1007/s10518-015-9760-z

Seismic Enforced Displacement-Based Pushover Analysis on Irregular In-Plan R/C Multi-storey Buildings

Triantafyllos K. Makarios and Athanasios P. Bakalis

1 Introduction

As it is well known, the major limitation of nonlinear static (pushover) analysis on asymmetric multi-storey buildings proposed by contemporary seismic codes, such as Eurocode EN 1998 [1, 2], is its inability to rationally estimate the coupled torsional/translational oscillations of the floor-diaphragms as well as the higher mode effects within the linear and nonlinear area of response. Additionally, superposition of nonlinear analysis results is proposed to consider the spatial seismic action, a fact that is mathematically forbidden in general in the nonlinear area. Further, it is not clear which is the appropriate principal reference system in the nonlinear area for the documented application of the pushover method and in order to verify the torsional sensitivity of the building. These weaknesses have already been recognized in single-storey buildings [3–5] and multi-storey ones [6, 7]. Because of the above mentioned, but also others such as P-Delta effects, the application of the pushover method on irregular in-plan multi-storey buildings often leads to an uncertain estimation of the seismic floor inelastic angular deformations (also known as inter-storey drift ratios). Also, the seismic floor inelastic displacements are often underestimated, especially as regards the stiff sides of torsionally flexible buildings.

To improve the effectiveness of the pushover method, various pushover procedures (Forced-Based and Displacement-Based) have been proposed in the last two decades that use (a) an invariable static loading vector, combined or not with some dynamic spectrum analysis [8–11], (b) a variable loading vector, in combination or not with dynamic spectrum analysis [12–15], and (c) elastic or inelastic dynamic

T. K. Makarios (✉) · A. P. Bakalis
Aristotle University of Thessaloniki, Thessaloniki, Greece
e-mail: makariostr@civil.auth.gr

A. P. Bakalis
e-mail: abakalis@civil.auth.gr

R. Bento et al. (eds.), *Seismic Behaviour and Design of Irregular and Complex Civil Structures IV*, Geotechnical, Geological and Earthquake Engineering 50,
https://doi.org/10.1007/978-3-030-83221-6_3

eccentricities for the application of the floor lateral static forces [3–5, 16]. A major disadvantage of some of the abovementioned pushover procedures is the complexity of their application that makes them unclear and difficult to apply.

To rationally estimate the seismic demands on irregular in-plan, multi-storey, reinforced concrete (r/c) buildings, the current work proposes a Displacement-based pushover procedure that uses drift-based enforced-displacements on each floor as the action [6]. The latter derive from a large parametric analysis in the framework of the second author's doctoral dissertation and have been calibrated to directly cause the state of Near Collapse (NC) of the building. The enforced-displacements refer to an ideal inelastic principal system at NC, called as the "Capable Near Collapse Principal System ($CR_{sec}(III_{sec})$, I_{sec}, II_{sec})" of the building [3–6]. Therefore, three enforced-displacements must be applied on each floor at the location of the vertical axis III_{sec}, two enforced-translations along the horizontal axes I_{sec} and II_{sec} and an enforced-rotation about the vertical axis III_{sec}. Moreover, the three enforced-displacements of each floor are suitably combined and the spatial seismic action is fully considered by a total of sixteen separate pushover analyses, the envelope of which provides accurate estimates of the seismic demand. The proposed procedure is simple and supervisory having as main objective to fully control the distribution in elevation of the seismic inelastic angular deformations of the building floors developed at NC. In addition, it predicts with safety the seismic inelastic displacements of all floors. The proposed procedure is suitable to be applied on all irregular in-plan multi-storey r/c buildings whether or not having torsional sensitivity or high asymmetry and on all multi-storey plane r/c frames, provided that all of them have the required regularity in elevation according to the seismic codes and are designed to exclude the possibility of forming a floor plastic mechanism.

2 Methodology

To implement the proposed pushover methodology by applying the enforced-displacements on each floor, the basic steps are the following:

(a) All structural members of the nonlinear model of the multi-storey r/c building are provided with their secant stiffness at yield, EI_{sec}, to simulate the extreme capable Near Collapse state [3–5]. The secant stiffness EI_{sec} at yield of an r/c end-section is calculated as suggested in Eurocode EN 1998–3 [2] using Eq. 1:

$$EI_{sec} = M_y \cdot L_v / 3\theta_y \tag{1}$$

where, M_y is the yield moment, θ_y is the yield chord rotation and L_v is the shear span of the examined member end-section.

(b) The "inelastic centre of stiffness" of the building which corresponds to this ideal Near Collapse state, is calculated by linear analysis. This is the well-known "Capable Near Collapse Centre of Stiffness,CR_{sec}" recently defined in single-storey r/c buildings, as well as the horizontal "Capable Near Collapse Principal Axes, (I_{sec}, II_{sec})" and the corresponding "Capable Near Collapse Torsional Radii, ($r_{I,sec}$, $r_{II,sec}$)" [3–5]. The relevant concepts in multi-storey r/c buildings can be defined in an approximate and optimum way using the well-known methodology for the identification of the vertical fictitious elastic axis (torsional optimum axis) of the multi-storey building [6, 17, 18]. According to [17, 18], a total of five temporary elastic analyses are performed to find the in-plan location of CR_{sec} (trace of the vertical ideal principal axis III_{sec} on the building level that is closest to $0.8H_n$ from the base of the building), the orientation of the horizontal ideal principal axes I_{sec}, II_{sec} and the values of the ideal torsional radii $r_{II,sec}$, $r_{I,sec}$ of the multi-storey building. Thus, the above methodology approximately defines an ideal 3D "inelastic principal" reference system $CR_{sec}(I_{sec}, II_{sec}, III_{sec})$ at NC state. Moreover, the torsional sensitivity of the multi-storey building is verified at the NC state with Eq. 2:

$$r_{I,sec} \text{ or } r_{II,sec} \leq 1.10 \cdot r_m \tag{2}$$

where, the limit value (1.10) that separates the torsionally flexible from the torsionally stiff buildings is increased in the nonlinear area for safety reasons [3] and $r_m = \sqrt{J_m/m}$ is the radius of gyration of the diaphragm closest to the $0.8H_n$ level (H_n is the total building height), where J_m is the mass moment of inertia of this diaphragm about a vertical axis passing through its geometric centre and m is its mass.

(c) In the framework of the proposed pushover procedure, the floor enforced-displacements are applied at the in-plan location of the vertical ideal principal axis III_{sec}. The translational components of the action vector, $\psi_{Isec,i}$ and $\psi_{IIsec,i}$, on each i-floor, along the horizontal ideal principal axes I_{sec} and II_{sec}, are calculated by proposed distributions in elevation of the (mean) floor angular deformation demands $\gamma_{CRsec,i}$ of the building. The latter were obtained as a result of an extensive parametric analysis aiming directly at the NC state and are shown in Fig. 1 (initial values) [6]. For this purpose, N-LRHA with pairs of accelerograms was performed on different structural types of multi-storey r/c buildings using the FEM analysis program SAP2000 [19], each time considering different orientations of the excitation (per ten degrees) as well as all four sign combinations of the two accelerograms. P-Delta effects were always included in N-LRHA. All the multi-story r/c buildings under investigation were regular in elevation and designed as ductile ones according to EN 1998–1. The structural types that examined were: (i) pure frame buildings without walls, (ii) pure wall buildings, (iii) coupled (via beams) wall buildings, (iv) dual buildings consisting of frames and walls, equivalent to frame type or to wall type, according to EN 1998–1. The examined buildings were 15-storey, 10-storey, 5-storey and 2-storey asymmetric buildings with varying magnitude of static eccentricity and torsional sensitivity. Additionally, the proposed distributions in elevation

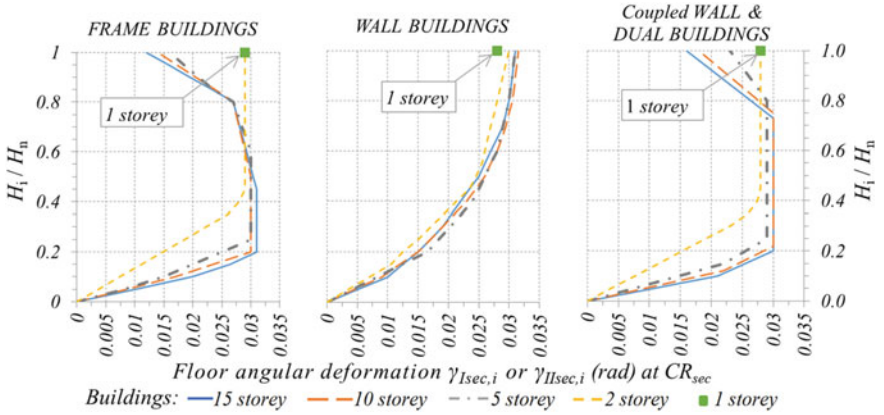

Fig. 1 Proposed distribution in elevation of the floor inelastic angular deformations $\gamma_{\text{Isec;IIsec,i}}$ at the NC state, on the vertical ideal axis III_{sec} and along the horizontal I_{sec} or II_{sec} axis, for all cases of inelastic static eccentricity and torsional sensitivity of various types of multi-storey r/c buildings

of the (mean) floor enforced-rotations $\psi_{\text{R,IIIsec,i}}$ about the vertical III_{sec} axis obtained from the extended parametric analysis (by N-LRHA) are shown in Fig. 2. In both Figs. 1 and 2, the proposed values are given relative to the height ratio H_i/H_n of the examined i-level from the building base. Moreover, Figs. 1 and 2 present values

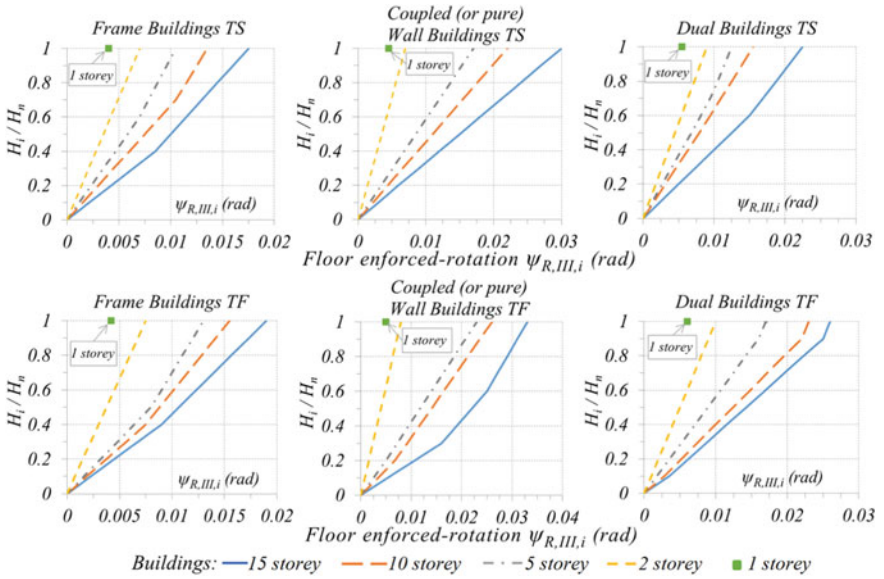

Fig. 2 Proposed distribution in elevation of the (total) floor inelastic enforced-rotations $\psi_{\text{R,IIIsec,i}}$ (rad) about the vertical axis III_{sec} at the NC state, for various structural types of torsionally flexible (TF) and torsionally stiff (TS) multi-storey r/c buildings and all cases of static eccentricity

for single-storey buildings compatible with the corresponding parametric analysis [3–5]. It is noted that for the use of Figs. 1 and 2, the structural type of the building is examined separately along each horizontal ideal principal direction I_{sec} and II_{sec}. In case of different building types per principal direction, the total floor rotation is obtained from Fig. 2 as the average of the proposed values for each building type.

(d) To consider the specific characteristics (stiffness/strength/ductility) of the examined building, the final proposed floor angular deformations $\gamma_{\text{CRsec,i}}$ come as a result of an envelope from three sources. The first source is the extensive parametric (by N-LRHA) analysis, i.e. the proposed (initial) inelastic values of step (c) (Fig. 1). The second source is a set of temporary pushover analyses with floor lateral forces applied at the in-plan location of the vertical axis III_{sec} following the uncoupled modal translational distribution in elevation along each horizontal axis I_{sec} and II_{sec}. The third source is another set of temporary pushover analyses, but this time the uncoupled modal translational distribution in elevation of the floor lateral forces along the I_{sec} and II_{sec} axes is determined for 80% of the base shear and the remaining 20% of the base shear is applied as an additional floor force at the building top (i.e. at the intersection of the vertical III_{sec} axis with the top floor). Considering the two signs (±) of action of the floor lateral forces, a total of eight (8) temporary pushover analyses are performed, which also include P-Delta effects. The target-displacement on the top of the III_{sec} axis is calculated through Table 1, which gives the seismic (target) angular deformation $\gamma_{\text{t,top}}$ of the building, from the base directly to its top, derived from the parametric analysis of the current work. Alternatively, the target displacement can be calculated from Annex B of EN 1998–1. Therefore, the enforced-translations $\psi_{\text{I;II,sec,i}}$ of the i-floors in elevation of the building are calculated by Eq. 3, starting from the first level towards the top of the building:

$$\psi_{\text{Isec,i}} = \psi_{\text{Isec},i-1} + \gamma_{\text{I,CRsec,i}} * h_{\text{i}} \; ; \; \psi_{\text{IIsec,i}} = \psi_{\text{IIsec},i-1} + \gamma_{\text{II,CRsec,i}} * h_{\text{i}} \qquad (3)$$

where, h_{i} is the height of the i-floor, $\gamma_{\text{I;II,CRsec,i}}$ is the final proposed value of the angular deformation of the i-floor along the I_{sec} or II_{sec} axis and $\psi_{\text{I;II,sec},i-1} = 0$ in the first floor of the building (i=1). It is noted that, if the multi-storey r/c building under consideration shows insufficient ductility capacity under the application of the temporary pushover analyses, then the proposed target displacement of Table 1 as well as the proposed values $\gamma_{\text{CRsec,i}}$ of Fig. 1 are scaled-down, correspondingly.

Table 1 Seismic (mean) target angular deformation $\gamma_{\text{t,top}}$ of the building top (III_{sec}) at the NC state along the horizontal axes I_{sec} and II_{sec}, in the framework of the eight (8) temporary pushovers

Number of Storeys	1	2	5	10	15
Pure frame buildings without walls	0.0300	0.0295	0.0235	0.0205	0.0195
Pure wall buildings without frames	0.0280	0.0290	0.0260	0.0240	0.0230

* For intermediate structural types of dual systems (frames and walls) or coupled (via beams) wall systems, as well as for various number of stories, linear interpolation is performed

(e) To consider the spatial action of the seismic components, we obtain each floor enforced-translation in one horizontal ideal principal direction and a simultaneous floor enforced-translation equal to 30% of its full value in the other horizontal ideal principal direction. Moreover, we consider also the (total) floor enforced-rotation about the vertical III_{sec} axis. Considering the ($\pm$) signs of action, a total of sixteen (16) possible combinations may be obtained, eight (8) for each horizontal ideal principal direction I_{sec} and II_{sec} (Table 2). The seismic target-displacement to be reached in the last step of the (16) enforced-displacement pushover analyses is equal to the enforced-translation of the top level of the building calculated by Eq. 3.

(f) The displacements along the axes I_{sec} and II_{sec} resulting from the envelope of the sixteen (16) pushover analyses of step (e) are usually higher compared with the corresponding seismic demand ones resulting from a typical set of N-LRHA. However, this is expected to happen since the proposed distributions in elevation of the floor angular deformations $\gamma_{CRsec,i}$ of Fig. 1 derive from the extended parametric analysis (mean values), showing maximized values in various floors. For this reason, it is proposed that the displacement response resulting from the application of the proposed pushover analysis must be scaled down by 10 to15%.

(g) For the verification of the Damage Limitation (DL) performance level, it is suggested to supply all the structural members of the nonlinear model with the effective bending stiffness $EI_{eff} = 2EI_{sec}$ (and not less than $0.25EI_g$ and also not greater than $0.5EI_g$, where I_g is the moment of inertia of the geometric section). Next, the proposed pushover procedure is performed using floor enforced-translations that equal to the combined by the SRSS rule results of two separate dynamic spectral analyses along each horizontal ideal principal axis I_{sec} and II_{sec}. Finally, we can work similarly at the seismic performance level of Significant Damage (SD), provided that the floor enforced-displacements appropriate for the NC state must be reduced by 25%, while the effective bending stiffness of each structural member is suggested to be the average of those used in the above two states (NC and DL).

Table 2 Earthquake spatial action of simultaneous floor enforced-displacements (16 combinations)

Eight (8) enforced-displacement combinations of nonlinear static analysis where the displacement along axis I_{sec} is maximized		Eight (8) enforced-displacement combinations of nonlinear static analysis where the displacement along axis II_{sec} is maximized	
$+\psi_{I,i}+0.3\psi_{II,i}+\psi_{R,III,i}$	$+\psi_{I,i}+0.3\psi_{II,i}-\psi_{R,III,i}$	$+0.3\psi_{I,i}+\psi_{II,i}+\psi_{R,III,i}$	$+0.3\psi_{I,i}+\psi_{II,i}-\psi_{R,III,i}$
$+\psi_{I,i}-0.3\psi_{II,i}+\psi_{R,III,i}$	$+\psi_{I,i}-0.3\psi_{II,i}-\psi_{R,III,i}$	$+0.3\psi_{I,i}-\psi_{II,i}+\psi_{R,III,i}$	$+0.3\psi_{I,i}-\psi_{II,i}-\psi_{R,III,i}$
$-\psi_{I,i}+0.3\psi_{II,i}+\psi_{R,III,i}$	$-\psi_{I,i}+0.3\psi_{II,i}-\psi_{R,III,i}$	$-0.3\psi_{I,i}+\psi_{II,i}+\psi_{R,III,i}$	$-0.3\psi_{I,i}+\psi_{II,i}-\psi_{R,III,i}$
$-\psi_{I,i}-0.3\psi_{II,i}+\psi_{R,III,i}$	$-\psi_{I,i}-0.3\psi_{II,i}-\psi_{R,III,i}$	$-0.3\psi_{I,i}-\psi_{II,i}+\psi_{R,III,i}$	$-0.3\psi_{I,i}-\psi_{II,i}-\psi_{R,III,i}$

3 Numerical Example

For verification purposes, a five-storey, double asymmetric, torsionally flexible r/c building (Fig. 3) will be assessed by the proposed enforced-displacement pushover procedure. It is a dual building, equivalent to wall-buildings according to EN 1998–1, with construction materials C30/37 for the concrete and B500c for the steel reinforcement of average strengths $f_{cm} = 38$Mpa and $f_{ym} = 550$Mpa. The total building height is 20 m, having five levels of 4 m height each. A rigid diaphragm of thickness 0.20 m extends outwards of the building perimeter forming a 2 m cantilever. The mass of each floor is equal to 160 Tn and is located on their geometric centres that lie in the same vertical line. The mass moment of inertia of each floor is 9000 Tn · m^2. The building was designed as a ductile one (DCH) according to the provisions of EN 1998–1. All structural members of the nonlinear model of the building are supplied with their secant stiffness EI_{sec} at yield to simulate the NC state. Both the ratios r_{Isec}/r_m and r_{IIsec}/r_m are less than 1.10 (Eq. 2) and therefore the building is characterized as torsionally flexible. The first 3 uncoupled periods $T_{R,IIIsec}$, T_{Isec}, T_{IIsec} of the building are 2.05, 1.63 and 1.57 s, respectively.

Initially, N-LRHA is carried out with three pairs of artificial accelerograms (methodology (c)), in which the Peak Ground Acceleration (PGA) was set at the value $a_g = 0.4$g, leading the building to the NC state. The envelope of the results of N-LRHA represents the seismic demand. Next, the two sets of temporary pushover analyses are performed (methodology (d), 4 analyses for each case along the $\pm I_{sec}$ & II_{sec} axis) with NC target displacement on the top of the vertical III_{sec} axis calculated

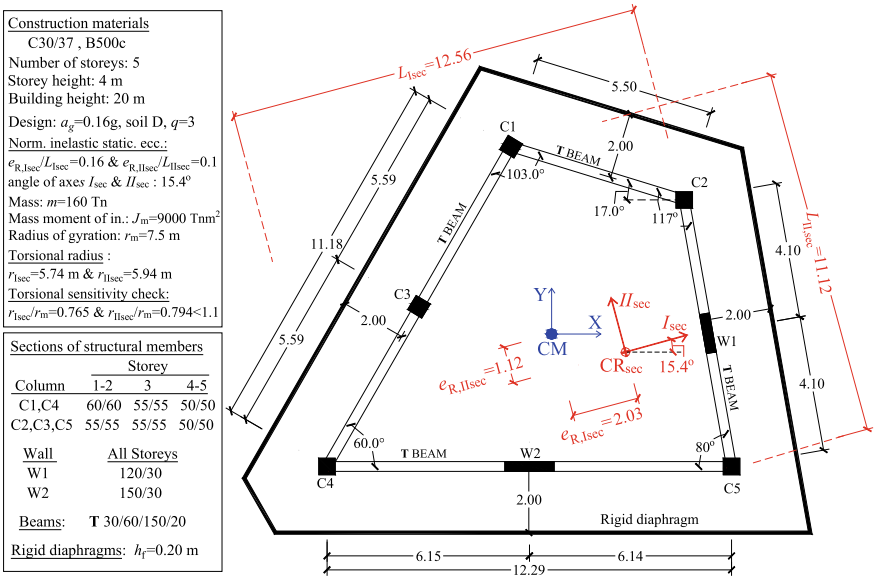

Fig. 3 Plan view of the 5-storey asymmetric building with Dual system of frames and walls

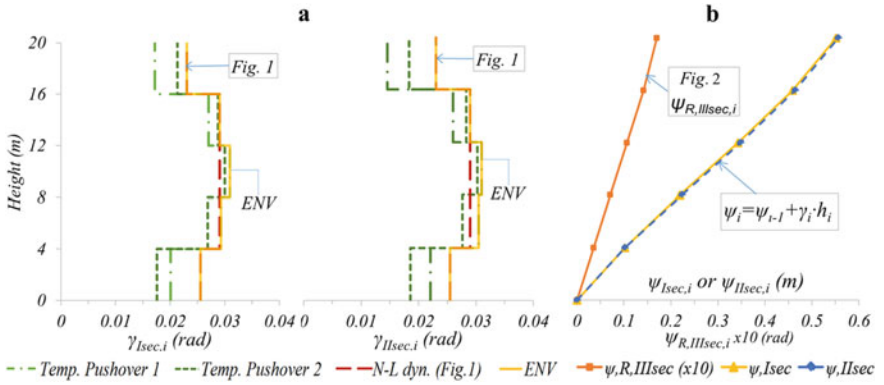

Fig. 4 **a** Proposed floor angular deformations on the vertical axis III_{sec}, along the horizontal axes I_{sec} and II_{sec}, from the envelope of two cases of temporary pushover analyses and the proposed inelastic values of Fig. 1, **b** floor enforced-displacements of the proposed pushover procedure

by Table 1 (linear interpolation between 5-storey frame and wall buildings):

$$u_{\text{t}} = \gamma_{\text{t,top}} \cdot H_{\text{n}} = \left(\frac{0.0235 + 0.0260}{2} \right) \cdot 20.00 = 0.0247 \cdot 20.00 = 0.494\text{m}$$

which is close enough to the corresponding N-LRHA results of 0.45 and 0.47 m along I_{sec} and II_{sec} axes, respectively. The floor angular deformations at the location of III_{sec} axis resulted from the envelope of each set of temporary pushover analyses together with the corresponding proposed values of Fig. 1 (for five-storey dual buildings) are shown in Fig. 4a. Their final envelope, which is also shown in Fig. 4a as *ENV*, is used for the calculation of the floor enforced-translations (Eq. 3) which are shown in Fig. 4b together with the proposed values of floor-enforced rotations from Fig. 2 (for torsionally flexible 5-storey dual buildings).

Next, we perform the sixteen (16) separate proposed nonlinear static analyses of Table 2, in multiple steps, with seismic target-displacement equal to the enforced-translation of the top building level. From the envelope of the sixteen (16) nonlinear static analyses, we can plot the inelastic plan displacement profiles (Fig. 5), which are scaled-down by 12% according to (f) of methodology, as well as the distribution in elevation of the floor angular deformations into two vertical bending planes (Fig. 6) and compare them with the seismic demand (N-LRHA). We observe that the proposed nonlinear static procedure provides in general safe estimates for the seismic behavior at the NC state in terms of floor angular deformations and displacements, along both the horizontal ideal principal directions. Only the flexible side of the building along the II_{sec} axis, at the second and third storey, shows floor angular deformation values just below the seismic demand by 6% on average. Conservative results of floor angular deformations are found on average by 30% in the first and top floors and by 10% in the intermediate floors.

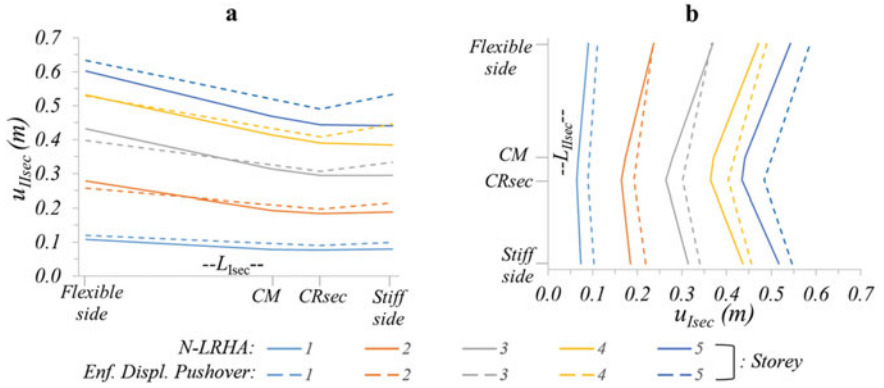

Fig. 5 Inelastic plan displacement profiles: **a** u_{IIsec}, along axis II_{sec}, **b** u_{Isec}, along axis I_{sec}

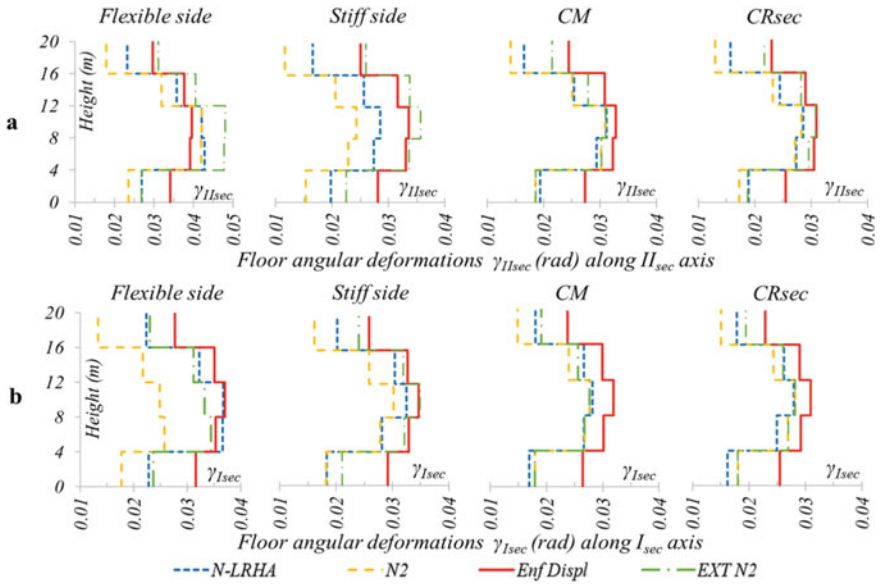

Fig. 6 Comparison of floor angular deformations: **a** γ_{IIsec}, along axis II_{sec}, **b** γ_{Isec}, along axis I_{sec}. Enforced displacement pushover procedure vs N-LRHA and N2 & Extended N2 pushovers

The plastic chord rotations of the beam end-sections are also calculated conservatively on all floors and the plastic mechanism image of the building resulted from the proposed pushover procedure is close enough to the corresponding image derived from N-LRHA. Figure 6 also presents a comparison of the floor angular deformations results from the proposed, the N2 (EN 1998–1) and the Extended N2 [10] procedures of pushover analysis. We observe that both the proposed pushover procedure and the Ext N2 pushover procedure predict better the floor angular deformations at

the stiff and flexible sides as well as at the two upper floors of the building than the N2 pushover procedure, which seriously underestimates them, especially at the stiff side along II_{sec} axis and at the flexible side along I_{sec} axis.

4 Conclusions

A new Displacement-based procedure of nonlinear static (pushover) analysis on multi-storey r/c buildings is proposed by this paper. According to the proposed procedure, a loading vector of drift-based enforced-displacements is applied at each floor with respect to the "Capable Near Collapse Principal System $CR_{sec}(I_{sec}, II_{sec}, III_{sec})$" of the building. This action vector consists of two floor enforced-translations along the horizontal I_{sec} and II_{sec} axes and a floor enforced-rotation about the vertical III_{sec} axis that are properly calibrated to cause the near collapse state (NC) of the building. The three enforced-displacements of each floor are suitably combined and the spatial seismic action is fully considered by a total of sixteen separate pushover analyses, the envelope of which provides accurate estimates of the seismic demand. The proposed pushover procedure can be applied on any ductile asymmetric multi-storey r/c building, torsionally sensitive or not, provided that the possibility of a floor plastic mechanism formation has been excluded and the building has the required regularity in elevation by the seismic codes.

The effectiveness of the proposed pushover procedure is verified on a 5-storey, double asymmetric, torsionally flexible r/c building in terms of floor angular deformations and in-plan displacements. The comparison with the results of N-LRHA shows that the new pushover procedure provides safe estimates of the seismic demand and a conservative view of the plastic mechanism developed throughout the building at the NC state.

Therefore, the new proposed enforced-displacement pushover procedure on asymmetric multi-story r/c buildings is a simple and efficient method to predict with safety the (real) coupling between the torsional and translational response as well as the higher-mode effects.

References

1. CEN EN 1998–1: Eurocode 8 (2004) Design of structures for earthquake resistance—Part 1: general rules, seismic actions and rules for buildings. Authority: The European Union Per Regulation 305/2011, Directive 98/34/EC, Directive 2004/18/EC, Brussels
2. CEN EN 1998–3. Eurocode 8 (2005) Design of structures for earthquake resistance—Part 3: assessment and retrofitting of buildings. Authority: The European Union Per Regulation 305/2011, Directive 98/34/EC, Directive 2004/18/EC, Brussels
3. Bakalis A, Makarios T (2018) Dynamic eccentricities and the "capable near collapse centre of stiffness" of reinforced concrete single-storey buildings in pushover analysis. Eng Struct 166:62–78. https://doi.org/10.1016/j.engstruct.2018.03.056

4. Bakalis A, Makarios T (2019) Seismic assessment of asymmetric single-story RC buildings by modified pushover analysis using the "capable near collapse centre of stiffness": Validation of the method. J Earthq Eng https://doi.org/10.1080/13632469.2019.1698477
5. Bakalis A, Makarios T (2020) Dynamic eccentricities in pushover analysis of asymmetric single-storey buildings. In: Chapter 24 of Book "seismic behaviour and design of irregular and complex civil structures III". Geotechnical, geological and earthquake engineering, Springer Publishing House
6. Bakalis A, Makarios T (2021) Seismic enforced-displacement pushover procedure on multi-srorey R/C buildings. Eng. Struct. 229.https://doi.org/10.1016/j.engstruct.2020.111631
7. Bakalis A, Makarios T (2020) Seismic enforced displacement-based pushover analysis on irregular in-plan R/C multi-storey buildings. In: Proceedings of ninth European workshop on the seismic behaviour of irregular and complex structures, Lisbon, Portugal, 15–16 December 2020
8. Chopra AK, Goel RK (2004) A modal pushover analysis procedure to estimate seismic demands for unsymmetric-plan buildings. Earthquake Engng Struct Dyn 33(8):903–927. https://doi.org/10.1002/eqe.380
9. Belejo A, Bento R (2016) Improved modal pushover analysis in seismic assessment of asymmetric plan buildings under the influence of one and two horizontal components of ground motions. Soil Dyn Earthq Eng 87:1–15
10. Kreslin M, Fajfar P (2012) The extended N2 method considering higher mode effects in both plan and elevation. Bull Earthquake Eng 10:695–715. https://doi.org/10.1007/s10518-011-9319-6
11. Rofooei FR, Mirjalili MR (2018) Dynamic-based pushover analysis for one-way plan-asymmetric buildings. Eng Struct 163:332–346
12. Antoniou S, Pinho R (2004) Development and verification of a displacement-based adaptive pushover procedure. J Earthquake Eng 8(5):643–661
13. Bhatt C, Bento R (2014) The extended adaptive capacity spectrum method for the seismic assessment of plan-asymmetric buildings. Earthq Spectra 30(2):683–703
14. Abbasnia R, Davoudi AT, Maddah MM (2014) An improved displacement-based adaptive pushover procedure for the analysis of frame buildings. J Earthquake Eng 18(7):987–1008. https://doi.org/10.1080/13632469.2014.919242
15. Shakeri K, Tarbali K, Mohebbi M (2012) An adaptive modal pushover procedure for asymmetric-plan buildings. Eng Struct 36:160–172. https://doi.org/10.1016/j.engstruct.2011.11.03
16. Bosco M, Ghersi A, Marino EM, Rossi PP (2017) Generalized corrective eccentricities for nonlinear static analysis of buildings with framed or braced structure. Bull Earthq Eng. https://doi.org/10.1007/s10518-017-0159-x
17. Makarios T, Anastassiadis K (1998) Real and fictitious elastic axis of multi-storey buildings: theory. Struct Design Tall Build 7(1):33–55
18. Makarios T (2008) Practical calculation of the torsional stiffness radius of multistorey tall buildings. J Struct Design Tall Spec Build 17(1):39–65
19. CSI, SAP2000 (2013) Three dimensional static and dynamic finite element analysis and design of structures V16.0.2. Computers and Structures Inc. Berkeley, CA, USA

Design Approach for an Irregular Hospital Building in Bucharest

Dietlinde Köber, Paul Semrau, and Felix Weber

1 Introduction

Large areas of the Romanian Plane, situated mostly in the Southern part of the country are passed by rivers which have accumulated in time alluvial deposits. This soil stratigraphy leads to rather high corner period values (up to $T_c = 1{,}6$ s) in the response spectrum of the Romanian Seismic Design Code P100-1 [1]. Supplementary, the Vrancea seismic source which affects the entire South-Eastern part of the country, produces pulse-type ground acceleration records. In return, the design of earthquake resistant structures in this area needs to cover large displacement demands, of up to 40 cm.

Under these special soil conditions (rather unique in the world, [2] the efficiency of base isolation as an alternative to capacity design [3–5] is investigated. Base isolation for civil structures is still emerging in Romania (less than 10 base isolated structures for now), due on one hand to the special seismic conditions and on the other hand to the conservative design preferences of structural engineers. This study was thought to help Romanian design engineers to gain confidence in the advantages that base isolation as alternative to stiffening may offer for civil structures built in high-corner period areas.

A plan irregular hospital building has been designed according to both approaches because, especial for hospitals, no-damage requirements need to be satisfied. In other seismic countries (like Turkey) base isolation is mandatory as design solution for new

D. Köber (✉)
Technical University of Bucharest, B-dul Lacul Tei no. 122-124, 020396 Bucharest, Romania

P. Semrau
MAURER SE, Munich, Germany

F. Weber
Maurer Switzerland GmbH, Pfaffhausen, Switzerland

R. Bento et al. (eds.), *Seismic Behaviour and Design of Irregular and Complex Civil Structures IV*, Geotechnical, Geological and Earthquake Engineering 50,
https://doi.org/10.1007/978-3-030-83221-6_4

hospital buildings (because hospitals should remain operational after an important seismic demand and structural damage may alter also cost-intensive equipment).

2 Description of the Analysed Structure

The analysed frame structure has plan dimensions of approximately 12 × 28 m. The underground level, the ground level and the last level have a height of approximately 3,5 m whereas overground levels 1 to 3 have a height of 3,2 m. The overall building height above ground is 16,55 m. The underground level and the ground floor have an extension along the X-axis between 2,4 m and 3,6 m. This setback of 20% to 30% of the plan dimension of the building in X direction indicates elevation irregularity according to P100-1/2013. Due to the fact that the setback affects only one of the overground floors, the structure was considered elevation regular during the design process and no reduction of the behaviour factor value was performed. This choice was confirmed by the push-over analysis conducted for the structure. The building is part of a state hospital ensemble in Bucharest. Its plan layout at underground and ground floor is shown in Fig. 1.

The structure is plan irregular. Due to the position of the vertical circulation wall assembly, for earthquake in X-direction, a displacement amplification of 37% is registered (maximum displacement along the structural perimeter versus mean floor displacement, P100-1/2013).

A 3D view of the overground structure is shown in Fig. 2.

The hospital building has a RC structure and was designed according to the former version (2006) of the Romanian Seismic Design Code, P100-1/2013, considering the capacity design method. Following structural element dimensions were settled: current beams 40 × 50 cm and 40 × 60 cm; most columns 60 × 60 cm; 20 cm wall thickness; 15 cm slab thickness.

As an alternative to capacity design, base isolation was considered in order to outline the structural advantages that may arise from this alternative. Base shear, structural displacements and structural accelerations are compared for both design approaches. Especially for long corner period areas ($T_c = 1{,}6$ s for Bucharest) and pulse-type accelerograms limited research on base isolation has been performed so far, [2] and practical engineers are not comfortable with the design choice of base isolation.

Therefore the same building layout was designed also as receiving an isolated base. Following structural element dimensions were settled: current beams 25 × 50 cm and 25 × 60 cm; most columns 50 × 50 cm; 20 cm wall thickness; 15 cm slab thickness. Sliding isolators with double curvature were considered in order to reduce the dimensions of the isolators and to optimize the structural design. The isolator design was performed in order to obtain a minimum response spectrum ordinate for a chosen Eigen period of the isolated structure equal to 4,4 s. According to P100-1/2013 the design earthquake has 225 years return period. The maximum expected earthquake was considered according to EN 1998–1 [7], having a return

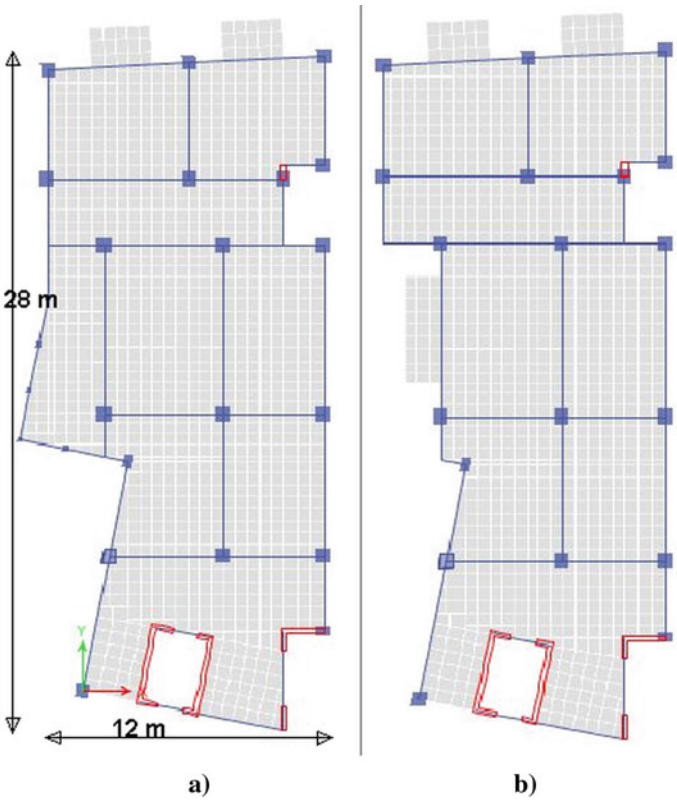

Fig. 1 Plan layout (CSI [6]): **a** underground and ground level; **b** current level

period of 475 years (in order to offer the opportunity of direct comparison to the isolator device design in other European countries, EN 15,129:2010–06) [8]. An isolator displacement capacity of 64,2 cm was designed.

The structure is supported by a foundation slab in both design versions. Between the isolators, which are placed at the bottom of the underground level, and the structure, a foundation beam girder is provided. This structural solution came out as being more cost efficient than a double foundation slab. The seismic input has been considered at the superstructure base.

3 Seismic Particularities and Methods of Analysis

The hospital building presented in this paper is built in Bucharest (maximum expected ground acceleration of 0.30 g), a region characterized by large corner period values ($Tc = 1.6$ s). The seismic design spectrum according to the Romanian Seismic Design

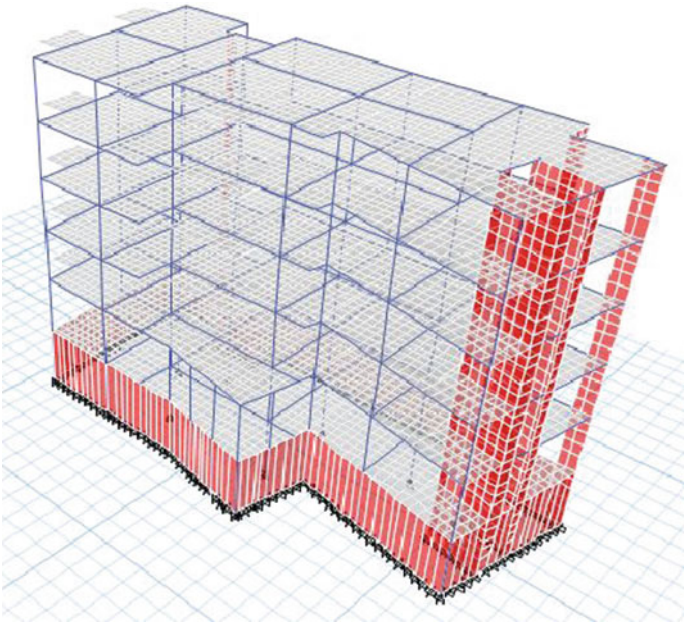

Fig. 2 3D structural view, (CSI [6])

Code is shown in Fig. 3, where $\beta(T)$ is the ratio between the response acceleration and the peak ground acceleration.

Capacity design was performed by modal analysis, (CSI [6]). The structural performance was checked by static and dynamic nonlinear analysis, (CSI [9]).

For static nonlinear analysis a triangular distribution of forces was considered. For dynamic analysis three original records and three spectrum compatible accelerograms were applied. Horizontal components as well as vertical accelerations were defined for dynamic analysis, although the influence of the vertical component of

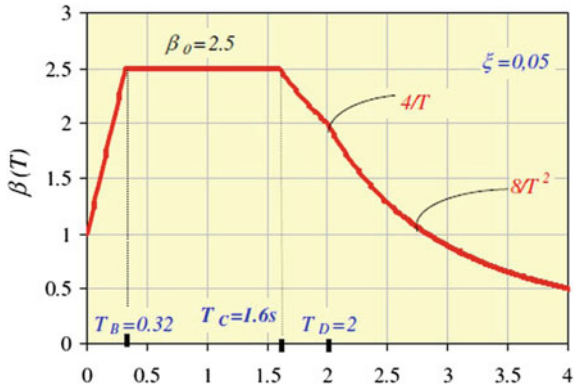

Fig. 3 Seismic design spectrum for Bucharest, [P100-1/2013]

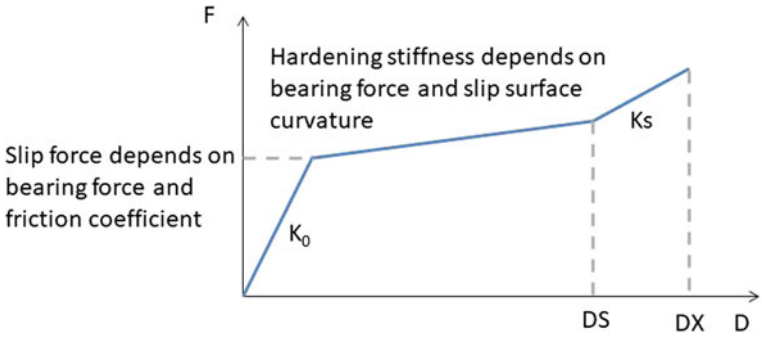

Fig. 4 Sliding isolator definition, (CSI [9]): D_S-displacement capacity, D_X-higher displacement value needed for convergence, F-lateral force, K_0-initial stiffness, K_S-restoring stiffness

the ground movement turned out to have a negligible influence on the structural behaviour and at isolation level.

Plastic hinges in beams and columns were modelled as point hinges [EN1998-3] and structural walls as fibre sections with nonlinear material behaviour for bending.

The sliding isolators were modelled by defining force – displacement curves as shown in Fig. 4.

The design of the structure was performed according to modal analysis results and considering a behaviour factor value of 6.75 (high ductility class, frame structure and multiple frames in plan and elevation, P100-1/2013). No reduction of 20% of the behaviour factor was applied according to code regulations for elevation irregular structures. This choice was confirmed by push-over analysis (see Chap. 4).

In order to check for vertical loading, damping and stiffness characteristics, ambient vibration measurements were performed and results were used to calibrate the finite element model. Although a model with consideration of serviceability limit state requirements and structural as well as non-structural elements was evaluated, useful information on modelling assumptions could be gathered, [10].

4 Observations Regarding the Structural Behaviour

4.1 Modal Analysis

For modal analysis, vertical load transfer and calibration with the ambient vibration measurements the ETABS software was used, (CSI [6]). The first three Eigen-modes for the building designed according to the capacity method are shown in Table 1.

For modal analysis a 50% reduced bending stiffness for beams, columns and walls and a 80% reduced torsional stiffness for beams and columns were considered, (P100-1/2013).

Table 1 Modal information for the non-isolated structure

Eigen-mode	Eigen-period T [s]	Direction
1	0.571	66% translation X
		17% torsion
2	0.492	65% translation Y
		13% torsion
3	0.436	torsion

As expected, due to the position of the elevator shaft, translation in X direction and torsion are coupled in the first Eigen-mode. Due to the rectangular plan layout also translation in Y direction and torsion are coupled in the second Eigen-mode.

4.2 Push-Over Curve

The nonlinear structural behaviour was investigated by the help of the Perform software, (CSI [9]). Push-over analysis was performed mostly in order to check the choice of the behaviour factor considered during the design and to establish the overall structural safety offered by the capacity method design approach.

Due to the fact that the X-direction is the weak direction of the structure (smaller overall plan dimension is X-direction and first Eigen mode shows translation in X-direction) and that for earthquake input along X-direction important torsional displacement amplification is registered, the structural investigation concentrates on the X-direction.

Figure 5 shows the push-over curve for the X-direction, considering a triangular lateral force distribution. The link between the base shear force at overground level and the deformation at the last floor (displacement or rotation) is represented for the non-isolated structure.

The green line in Fig. 5a indicates the design situation. Reported to design, the push-over analysis along X-direction showed a rather high over strength, equal to

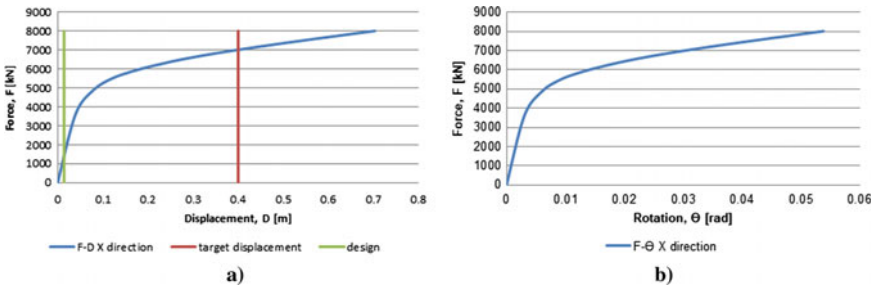

Fig. 5 Structural results: **a** base shear force-top displacement; **b** base shear force-top rotation

3. Therefor the target displacement is not an important parameter for the structural behaviour and is not reachable as limited ductility demand is requested from the plastic hinges.

The ratio α_u/α_1 (lateral force at which the structure becomes a plastic mechanism per lateral force at which the first plastic hinge becomes active) emerged from the force–displacement curve shown in Fig. 5a is almost 3 times larger than the value considered for design. So the choice of the behaviour factor has been confirmed.

4.3 Dynamic Nonlinear Analysis

For dynamic nonlinear analysis full horizontal earthquake input along one main structural direction and 30% horizontal earthquake input in the other main structural direction were considered, according to the combination rules for plan irregular structures, P100 -1/ 2013.

According to the design rules for base isolated structures, also the vertical earthquake component has been applied. Results showed no important influence of the vertical earthquake component on the structural behavior and on the isolator behavior, as no lift-up appears.

Results are shown consequently for the weak structural direction, the X-direction.

Due to the structural softening and to the supplementary damping provided by base isolation, a 7 times base shear force reduction was possible.

Figure 6 shows structural rotations registered at the upper floor, for the isolated as well as for the non-isolated structure, considering a spectrum compatible seismic input.

The base-isolated structure experiences 3.5 times larger structural rotations for the considered earthquake input. Movement appears at the isolation level and does not affect the structure above the isolation level. The torsional movement is more smooth (peaks are more rare) for the base isolated structure, the peaks are delayed compared to the non-isolated structure and the amplitude drops more rapid after the main peak.

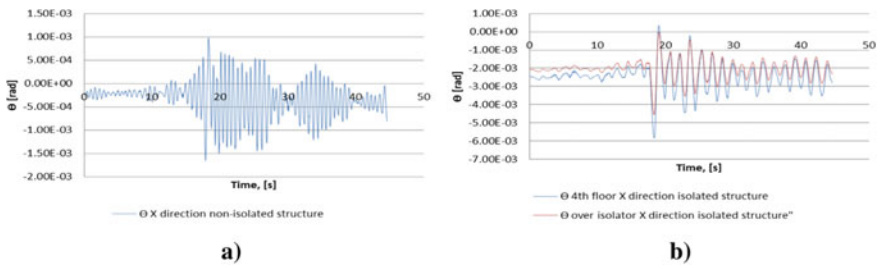

Fig. 6 Structural rotation at top level/isolation level for a spectrum compatible input: **a** non-isolated structure; **b** base isolated structure

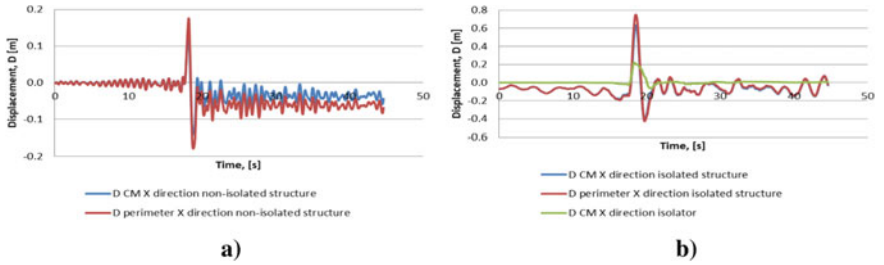

Fig. 7 Structural X—displacement in CM and along the perimeter, at top level/isolation level for a spectrum compatible input: **a** non-isolated structure; **b** base isolated structure

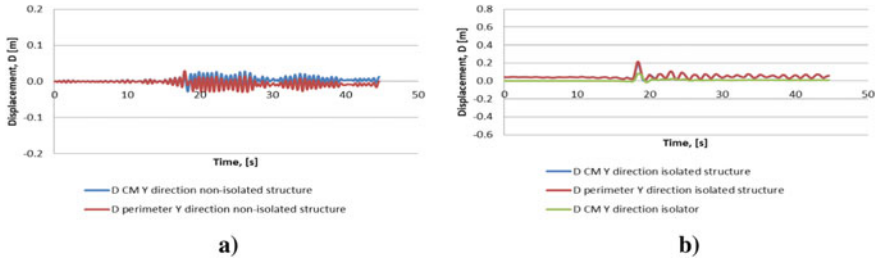

Fig. 8 Structural Y—displacement in CM and along the perimeter, at top level/isolation level for a spectrum compatible input: **a** non-isolated structure; **b** base isolated structure

For the same seismic input Figs. 7 and 8 show structural displacements at the top floor in the mass centre (CM) and at a point along the perimeter. For comparison, displacements of the isolation level are also shown. Figure 7 indicates displacements along X direction for earthquake input in X direction. Figure 8 indicates displacements in Y direction for earthquake input in X direction, in order to catch the torsional displacement amplification.

For the non-isolated structure displacements along the seismic input (X-direction) are 20% higher along the perimeter than in CM. Displacements perpendicular to the seismic input, are 5% higher along the perimeter than in CM. Both values are registered at the flexible side of the structure (opposite with respect to the elevator shaft).

For the isolated structure those percentages drop to 15% for X direction and rise to 10% for the Y direction. The maximum displacement amplifications are registered at the stiff side of the structure. 35% of the observed displacement in X direction and 40% in Y direction takes place at isolation level. The rest is due to a rigid body movement of the structure on the isolation level.

The isolated structure has 3 to 5 times larger displacements in X-direction and smaller displacements in Y-direction (probably due to high damping of the sliding surface) than the non-isolated structure. Those displacements are concentrated at the isolation level and peaks are more smooth.

5 Conclusions

In the context of large corner periods ($T_c = 1{,}6$ s) and pulse-type ground acceleration records base isolation turns out to be a valuable alternative to capacity design.

Base isolation doesn't correct plan irregularity, but it neutralizes its structural effects by concentrating deformations at isolation level (displacement time histories in the mass centre and along the perimeter of the plan layout are alike, see Figs. 7 and 8).

By base isolation (higher damping and larger Eigen-period) a base shear force reduction of about 7 (quite the same as in capacity design due to the behaviour factor q) is achieved. But base isolation means no plastic hinge formation so no damage, whereas capacity design is based on large plastic deformations.

The lack of reduction of the behaviour factor due to the setback from the first overground floor up has been confirmed by push-over analysis.

The non-isolated structure, although plan irregular, for which capacity design has been applied, turned out to have an over strength equal to 3.

Supplementary to the structural comparison between the isolated and the non-isolated structure, an economical study is planned to be performed.

Acknowledgements D. Köber wishes to acknowledge the help of her colleagues from SC Consild SRL for their valuable contribution to the design of the structure presented in this paper.

References

1. P100 -1/ 2013. Cod de proiectare seismică. Prevederi de proiectare pentru clădiri, 32–61
2. Pavel F, Popa V, Văcăreanu R (2018) Impact of long-period ground motions on structural design: a case study for Bucharest. Springer, Romania
3. Moehle J (2014) Seismic design of reinforced concrete buildings. McGraw-Hill Education, ISBN 978–0–07–183944–0
4. Derecho AT, Kianoush MR (2001) Seismic design of reinforced concrete structures. In: Naeim F (eds) The seismic design handbook. Springer, Boston, MA. https://doi.org/10.1007/978-1-4615-1693-4_10
5. Fajfar P (2018) Analysis in seismic provisions for buildings: past, present and future. In: Pitilakis K (eds) Recent advances in earthquake engineering in Europe. ECEE 2018. Geotechnical, Geological and Earthquake Engineering, vol 46. Springer. https://doi.org/10.1007/978-3-319-75741-4_1
6. CSI analysis reference manual (2013) ETABS integrated building design software. Computers and Structures Inc., Berkeley, California
7. EN 1998–3: 2005. Design of structures for earthquake resistance. Assessment and retrofitting of buildings, 35–42
8. EN 15129:2010–06. Anti-seismic devices
9. CSI Perform-3D User Guide (2006) Nonlinear analysis and performance assessment for 3D structures, Version 4
10. Köber D, Aldea A, Enache R, Weber F, Semrau P (2019). Measured and computed dynamic characteristics of a hospital building in Bucharest. Proceedings of 5th international conference on smart monitoring, assessment and rehabilitation of civil structures, Potsdam, Germany

Seismic Capacity of EC8 Compliant RC Frames with Irregular Vertical Distribution of Stiffness

Francesca Barbagallo, Melina Bosco, Aurelio Ghersi, Edoardo M. Marino, and Pier Paolo Rossi

1 Introduction

The awareness that structural regularity deeply affects the seismic response of structures dates back to the beginning of the XX century. However, the first studies on the effects of the so called "set-backs" in structures appeared only in the second part of the past century. The main goal of those studies was to evaluate if the seismic response of irregular structures could be predicted accurately by lateral force method of analysis. Due to the limited computation capacity at that time, the structural models were quite simple and used mainly shear-type frames [1]. Such an approach is not coherent with the present design criteria that aim at avoiding soft story mechanisms and is ineffective for evaluating collapse mechanism and ductility demand of a structure. The first criteria for the evaluation of the vertical regularity of structures were developed at the end of the XX century and seemed to be based more on "common sense" rather than on rigorous analyses.

The knowledge acquired in the earlier studies reflected on both Uniform Building Code [2] and International Building Code [3], which provided the definition of

F. Barbagallo · M. Bosco · A. Ghersi · E. M. Marino (✉) · P. P. Rossi
Department of Civil Engineering and Architecture, University of Catania, Via Santa Sofia 64, 95125 Catania, Italy
e-mail: emarino@dica.unict.it

F. Barbagallo
e-mail: fbarbaga@dica.unict.it

M. Bosco
e-mail: mbosco@dica.unict.it

A. Ghersi
e-mail: aghersi@dica.unict.it

P. P. Rossi
e-mail: prossi@dica.unict.it

R. Bento et al. (eds.), *Seismic Behaviour and Design of Irregular and Complex Civil Structures IV*, Geotechnical, Geological and Earthquake Engineering 50,
https://doi.org/10.1007/978-3-030-83221-6_5

vertical regularity/irregularity. Eurocode 8 [4] introduced similar criteria to judge whether a structure was regular in elevation or not. These criteria were also used to reduce the value of the behavior factor q adopted in the structural design, even though this provision was not supported by specific scientific studies.

In the first two decades of the XXI century, scientific research devoted increasing efforts to the topic of vertical irregularity [5, 6]. These new studies mainly aimed at judging the effectiveness of nonlinear static procedures in evaluating the seismic response of irregular structures [7]. Due to the higher computational capacity, the adopted structural models became more realistic. Nonetheless, the vertical irregularity is obtained by varying stiffness and/or strength without a specific correlation between them. Furthermore, the structural performance is still evaluated in terms of interstory drifts, even though this response parameter becomes less significant in the case of global collapse mechanisms. Only few studies available in literature aims at analyzing the seismic performance instead of the effectiveness of the nonlinear procedures [8, 9], while the study by Athanassiadou and Bervanakis [10] shows that capacity design criteria are able to lead to a global collapse mechanism even in the case of irregular structures.

Most of the current seismic codes define a structure as regular in elevation based on the vertical distribution of mass, lateral stiffness and strength and introduce penalties for irregular structures. However, the parameters adopted to classify structures as regular or irregular vary according to the different seismic codes. This paper is focused on lateral stiffness distribution, which has been determined as the ratio of the story shear to the interstory drift.

Eurocode 8 classifies a structure as vertically regular when the lateral stiffness is constant in elevation or, at most, reduces gradually without abrupt reductions from the base to the top. Note that, even if the stiffness of a story is slightly larger than that of the story below the structure is considered as vertically irregular. The Italian seismic code NTC2018 [11] requires that lateral stiffness of regular structures be constant along the height or vary gradually, without abrupt changes. It quantifies the limits of the increase/reduction of lateral stiffness in elevation, specifying that lateral stiffness of the lower story must not be lower than 30% or larger than 10% of the stiffness of the upper story. In the case of irregular structures, both the European and Italian code prescribes 20% reduction of the behavior factor.

This research focuses on the prescriptions provided by seismic codes for the definition of vertically regular Vs. irregular structures. Indeed, criteria given by the European and the Italian codes lead to classify a large number of new buildings as irregular. This has been confirmed by an extended survey, conducted by one of the authors (Ghersi), that showed that the interviewed engineers classified 75% of their designed buildings as irregular in elevation, mainly due to the change of stiffness between two consecutive stories. This tendency may diminish the motivation and the efforts devoted by professional engineers in designing actual regular structures. This paper examines the seismic response of RC framed structures designed in compliance with code prescriptions, i.e. structures are designed according to the capacity design approach and structural members have good local ductility. The investigated structures were designed assuming the same value of the behavior factor q, but differed

because of the level of variation of lateral stiffness along the height: vertically regular structures, wherein the value of lateral stiffness is constant or gradually changes in elevation; vertically irregular structures, wherein the value of lateral stiffness drastically varies and this change occurs in a few stories. The goal is to investigate (i) if the variation along the height of the lateral stiffness affects the seismic response of structures and (ii) whether the reduction of the behavior factor imposed by seismic codes for irregular structures can be considered appropriate or too conservative.

2 Description of Case Study Frames

The set of case study frames aimed to be representative of a wide range of real structures. To this end, 54 frames were designed to include the typical features of RC framed structures (presence of flat beam and deep beam, columns orientated along their strong axis or weak axis). Furthermore, 27 frames were 4-story high and the other 27 were 7-story high. Figure 1 shows the part of plan layout weighing on the designed frame and the vertical configuration of the 7-story frame. The 54 case study frames were all designed to be regular according to the NTC2018 and differ because of the following aspects:

– Beam span: three lengths of beam spans were considered (4.00 m, 5.00 m, 6.00 m) to have a different amount of bending moment due to gravity loads on beams.
– Ratio of the size of cross sections of columns and beams: the depth of cross sections of deep beams was assumed equal or reduced of 10–20 cm with respect to that of columns.

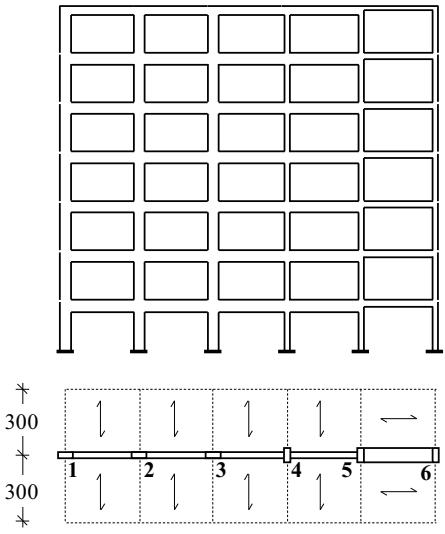

Fig. 1 Vertical view and plan layout of the analysed frame

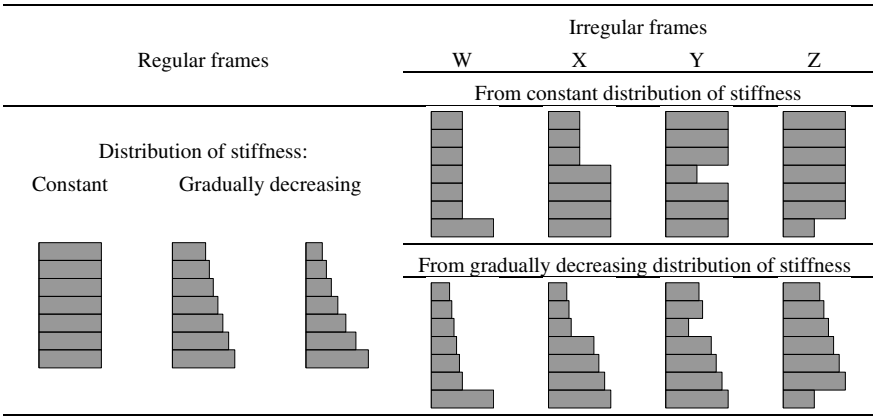

Fig. 2 Distribution of lateral stiffness along the height of case study frames

– Stiffness of columns: three distributions of story lateral stiffness were considered, as shown in Fig. 2. First, the stiffness of columns was set constant along the height; second, it was assumed to reduce from the bottom to the top by 10% at each story; third, it was assumed to reduce from the bottom to the top by 20% at each story.

To design structures that could be classified as (rigorously) regular, the first inter-story height was increased compared to other stories. This approach permitted to mitigate the increase of stiffness of the first story due the rigid restraint at column base that simulates the foundation. The regular 4-story frames and 7-story frames have fundamental period of vibration equal to 0.50 s and 0.85 s, respectively.

The set of case study frames was extended to include also irregular structures. The irregular frames were derived from the regular ones by reducing/increasing the lateral stiffness. The elastic modulus of all members was slightly scaled in order to maintain the same fundamental period of vibration. The following cases of irregularity were considered:

W- Decrease of the lateral stiffness from the first to the second story, that considers the stiffening effect of foundation.

X- Decrease of the lateral stiffness from the bottom part of the frame to the top part (reduced stiffness from third story for 4-story frames and fifth story for 7-story frames). Indeed, the lower part of the structure is usually stiffer than the upper one due to the design practice that tends to reduce the cross sections of structural members at higher stories.

Y- Abrupt decrease of the lateral stiffness at a single intermediate story (second story for 4-story frames and fourth story for 7-story frames). This configuration is less usual but could be caused by a specific need related to the destination of use of the relevant story.

Z- Abrupt increase of stiffness from the first to the second story. This configuration simulates the lack of infill panels that characterises buildings with *pilotis*.

Figure 2 shows the considered distributions of stiffness for the irregular structures. The variation of stiffness Δk between two consecutive stories was evaluated as follows:

$$\Delta k = \frac{k_{\text{inf}} - k_{\text{sup}}}{k_{\text{inf}}} \tag{1}$$

where k_{inf} and k_{sup} are the lateral stiffnesses of the lower and upper stories, respectively.

This parameter was assumed as the reference to evaluate the regularity/irregularity of structures and it was increased in step of 0.1. The value of stiffness was modified by changing both the dimensions (depth and width) of the cross sections of deep beams and columns. The rate of variation to be applied to the dimensions of the cross sections was determined according to a preliminary estimation of the stiffness. Then, the obtained stiffness was analytically evaluated by lateral force method of analysis and resulted to be close enough to the predicted one.

The set of regular frames included 27 frames with 4 stories and 27 frames with 7 stories. Each set of 27 frames generated 378 irregular frames, having up to 80% variation of stiffness between consecutive stories: 405 (27 + 378) 4-story frames and 405 7-story frames.

3 Research Methodology

To design the case study frames (regular or irregular), the internal forces are determined by a modal response spectrum analysis and for each of the 405 + 405 frames four values of behavior factor q were considered:

- $q = 5.85$, that is the maximum value allowed by the Italian seismic code for high ductility structures (ductility class A);
- $q = 4.68$ (5.85×0.8), that is the previous value of q reduced by the coefficient $K_R = 0.8$;
- $q = 3.90$, that is the maximum value allowed for low ductility structures (ductility class B);
- $q = 3.12$ (3.90×0.8), that is the previous value of q reduced by the coefficient $K_R = 0.8$.

Hence, all the 405 frames with four stories and the 405 frames with 7 stories, having a stiffness distribution of type A, B, C and W, were designed four times assuming the four aforementioned values of q. All the case studies were supposed to be located in Messina (peak ground acceleration $a_g = 0.250$ g, $F_o = 2.410$, $T_C{}^* = 0.360$) on soil type C.

A member-by-member modelling with beam elements is adopted for beams and columns. The intersection between column and beam is modelled separately from

the rest of the element and assumed to remain elastic. Hence, plastic hinge develops at the external face of the column. The same cross section and the same moment of inertia is assigned to the two parts of beam elements (internal and external to the node). The moment of inertia is assumed equal to its nominal value because the stiffness reduction caused by the cracking of the concrete may be assumed as included in the considered variation of stiffness.

The case study frames are designed using concrete C25/30 and steel B450C, following the capacity design principles of the Italian seismic code. Rebars are sized based on the results of the modal response spectrum analyses. The amount of rebars of beams is assumed exactly equal to that calculated to resist the bending moment at the external face of the column, or equal to the minimum value required by the code. The stirrups are determined to sustain a shear force determined by equilibrium conditions and assuming that at both the ends of the beam the bending moment is equal to the flexural plastic resistance, increased by the coefficient γ_{Rd}. The longitudinal rebars of columns are designed so that in each node the summation of the resisting bending moment of columns equals the summation of the resisting bending moment of beams increased by $\gamma_{Rd} = 1.3$. The minimum longitudinal reinforcement area is set equal to 0.25% on each side of the cross section. The stirrups of columns are determined based on the shear resistance of columns, following the modifications introduced by NTC2018. The reinforcement of the nodes is not specifically determined, but it is assumed sufficient to avoid shear failure. Each value of the behavior factor q leads to a structure with a different lateral resistance.

The seismic response of each designed frame is evaluated by nonlinear static analysis. The numerical model uses beam elements with concentrated elastic perfectly plastic hinges, which can develop only outside the beam-column node. According to the prescriptions of seismic codes for the seismic assessment of existing structures, the resisting bending moment of columns and beams should be evaluated considering the average value of the material strength. For this research, it was considered more adequate to determine the resisting bending moment of columns and beams using the characteristic values of the material strength, i.e. cylinder strength $f_c = 25$ MPa for concrete and yielding strength $f_y = 450$ MPa for steel. In particular, the resisting bending moment of columns was determined assuming the value of axial force equal to that calculated considering gravity loads acting in seismic combination. The shear resistance of both columns and beams was evaluated considering the partial safety coefficients γ_c e γ_s.

The nonlinear static analysis was performed assuming a distribution of lateral forces proportional to the first mode of vibration. The displacement demand of each step of the pushover analyses was associated with the corresponding value of a_g according to the procedure suggested by the Italian seismic code. This analysis allowed the assessment of the seismic response of each structure subjected to seismic inputs with increasing magnitude, i.e. increasing values of a_g. A preliminary evaluation of the seismic behavior and collapse mechanism of the case study frames was conducted by observing the distribution of plastic hinges in structural members.

However, the seismic assessment of structures must be based on numerical evidences, i.e. the development of shear failure or the attainment of the ultimate

value of plastic rotation. The nonlinear static analyses showed that none of the case study frame developed shear failures, which means that the capacity design approach was effective in avoiding brittle behavior of buildings. Hence, in the following, only the plastic rotation of members will be observed.

Both the Italian seismic code [11] and the European seismic code (EC8—part 3 [4]) determine the value of the chord rotation corresponding to the attainment of Near Collapse limit state $\theta_{u,NC}$ according to the equation provided by Panagiotakos e Fardis [12]. The value of the chord rotation at the attainment of the Significant Damage limit state (SD) $\theta_{u,SD}$ is derived from that of $\theta_{u,NC}$. The numerical model with concentrated plastic hinges allowed the determination of the plastic rotation demand φ. The limit value of the plastic rotation corresponding to the SD limit state $\varphi_{u,SD}$ was determined subtracting the elastic part of the rotation from $\theta_{u,SD}$:

$$\varphi_{u,SD} = \theta_{u,SD} - \frac{V\ L_V^2}{3\ E\ I} \tag{2}$$

where V is the shear force corresponding to the attainment of the limit value of the chord rotation, L_v is the shear length and EI is the stiffness of the section. For each cross section where plastic hinge develops, the damage is estimated as the ratio D of the plastic rotation to the plastic rotation corresponding to the DL limit state:

$$D = \frac{\varphi}{\varphi_{u,SD}} \tag{3}$$

The value of peak ground acceleration $a_{g(D=1)}$ corresponding to $D = 1$, i.e. the attainment of the SD, was evaluated for both columns and beams of each structure. In addition, the damage index D corresponding to the reference value of $a_g = 0.25$ g, i.e. the peak ground acceleration corresponding to the SD limit state, was evaluated and the average value $D_{av,SD}$ of D was calculated for columns and beams. These response parameters are used to assess the seismic response of each case study frame and to compare the seismic performances of regular and irregular structures.

4 Results of the Numerical Analysis

4.1 Case A: Stiffness Reduction from First to Second Story

Figure 3a, b show, for increasing values of the rate of stiffness variation Δk, the average damage $D_{av,SD}$ corresponding to the SD limit state and the peak ground acceleration a_g leading to the attainment of the SD limit state, respectively. The results refer to the frames with seven stories designed by $q = 5.85$. The damage is mainly concentrated in beams (black diamond), as required by the capacity design approach, and it is not significantly related to the stiffness variation. The continuous

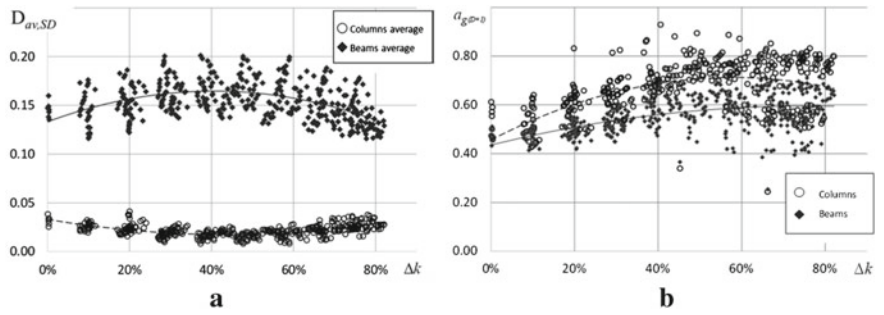

Fig. 3 Case A, 7-story frames, $q = 5.85$: **a** Average damage at SD limit state, **b** PGA corresponding to the SD limit state

line and the dashed line represent the trend equation of the average damage for beams and columns, respectively. The trend line shows that for values of Δk lower than 40%, the average damage of columns slightly decreases with Δk, while the average damage tends to increase if Δk is larger than 40%. However, the damage attained for structures with strong irregularities (large values of Δk) does not differ significantly from that occurred in regular structures ($\Delta k = 0$). Figure 3b shows that almost all case study frames attains the SD limit state for peak ground accelerations that are larger than the value used to design the frames (0.25 g). The values of a_g leading to D = 1 in columns (white circles in the Figure) are generally larger than those leading to D = 1 in beams. The values of $a_{g(D=1)}$ of beams are more scattered compared to columns. However, they increase for larger irregularity, with a slight reduction in case of Δk larger than 60%. Even if not shown in figure, the results obtained for frames with 4 stories are analogous to those of frames with 7 stories.

The trend lines in Fig. 4 show for increasing values of irregularity the values of $a_{g(D=1)}$, determined as the minimum of the two values of peak ground acceleration corresponding to the attainment of SD limit state in columns and beams. Each line refers to a different value of q and shows a seismic response almost independent of

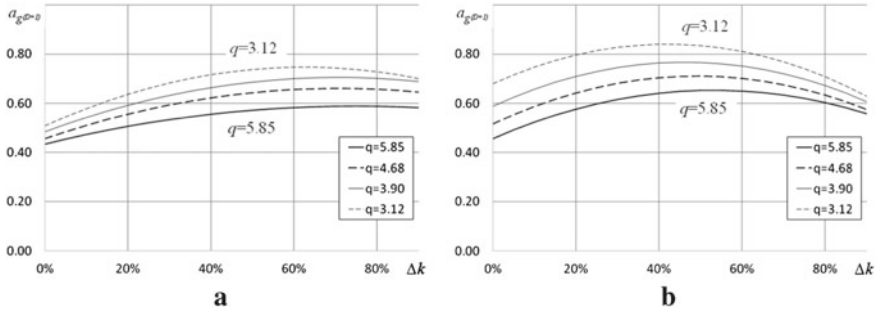

Fig. 4 Values of a_g corresponding to the SD limit states for increasing values of Δk and different values of q: **a** Case A, 7 stories, **b** Case A, 4 stories

the value of Δk. Lower values of q reduce the damage in beams and the structural collapse is attained for significantly larger peak ground accelerations.

It can be observed that large values of Δk lead the structures to the SD limit state for lower values of peak ground accelerations. However, the value of a_g at the SD limit state is still larger than, or at least comparable, to that of regular frames.

4.2 *Case B: Stiffness Reduction from the Lower to the Upper Part of the Frame*

The stiffness variation considered as Case B corresponds to structures where the cross sections of columns and beams is drastically reduced in the upper part of the building. Figure 5a shows the average damage experienced by structural members of 7-story frames designed by $q = 5.85$, at the SD limit state. In these cases, the value of Δk quantifies the difference of stiffness between the fourth and fifth story. The results are close to those obtained for case A: the damage mainly occurs in beams, as result of the capacity design, and it is not significantly affected by the increase of irregularity. The value of $a_g$corresponding to the SD limit state of columns and beams is reported in Fig. 5b. The majority of the case study frames collapse for a peak ground acceleration larger than that used in design (0.25 g) and the capacity of structural members is not influenced by Δk.

The design of frames belonging to Case B was conducted assuming different values of q. Figure 6a, b show the trend lines of a_g at the SD limit state for increasing values of Δk, for different values of q, for 7-story frames and 4-story frames, respectively. The trend lines show results similar to those of Case A, that is the value of the $a_{g,D=1}$ is not affected by the increase of Δk.

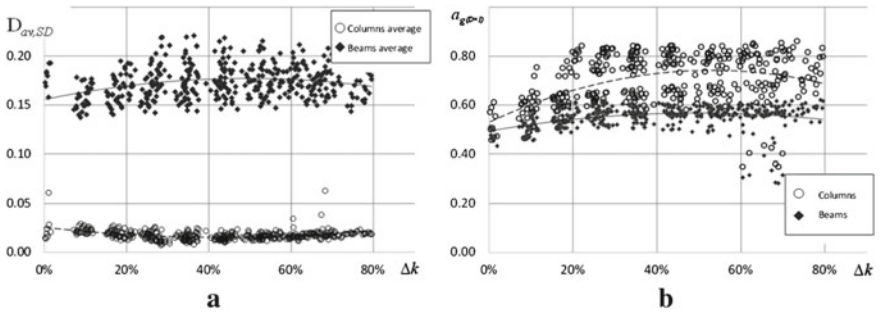

Fig. 5 Case B, 7-story frames, $q = 5.85$: **a** Average damage at SD limit state, **b** PGA corresponding to the SD limit state

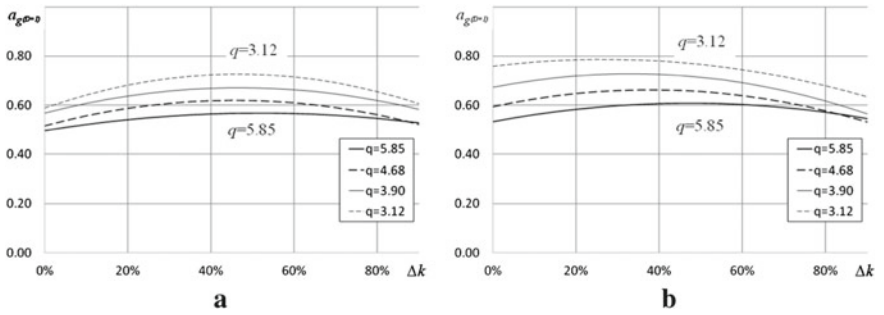

Fig. 6 Values of a_g corresponding to the SD limit states for increasing values of Δk and different values of q: **a** Case B, 7 stories, **b** Case B, 4 stories

4.3 Case C: Stiffness Reduction in an Intermediate Story

The abrupt reduction of lateral stiffness at an intermediate story (Case C) could be representative of real buildings where one of the stories is dedicated to a different destination of use and requires an interstory height larger than in other stories.

The average damage cumulated at the SD limit state in columns and beams of 7-story frames designed by $q = 5.85$ is displayed in Fig. 7a. In this case, the parameter Δk is determined as the difference of lateral stiffness between the third and fourth story, that is followed by an increase of stiffness between the fourth and the fifth story. The results are close to those obtained for Case A or B. In fact, the damage mainly occurs in beams. However, it can be noted that, in case of strong irregularity (large values Δk), the damage in columns has a non-negligible increase. Nevertheless, for all the case study frames, the peak ground acceleration corresponding to the SD limit state is larger than the reference value (0.25 g) (Fig. 7b). However, compared to Case A and B, the values of $a_{g,D=1}$ of columns are more scattered and show a more significant dependency from Δk.

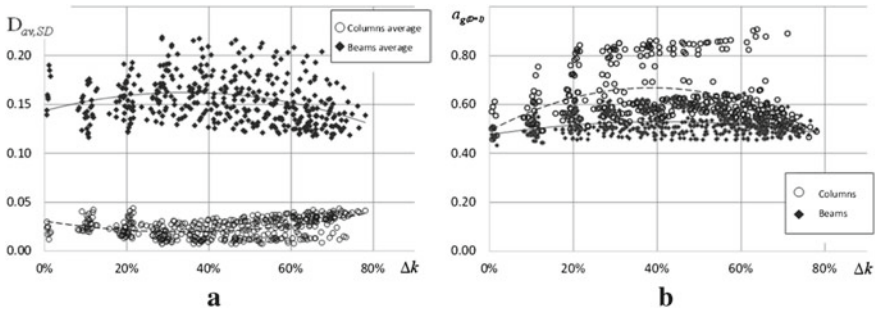

Fig. 7 Case C, 7-story frames, $q = 5.85$: **a** Average damage at SD limit state, **b** PGA corresponding to the SD limit state

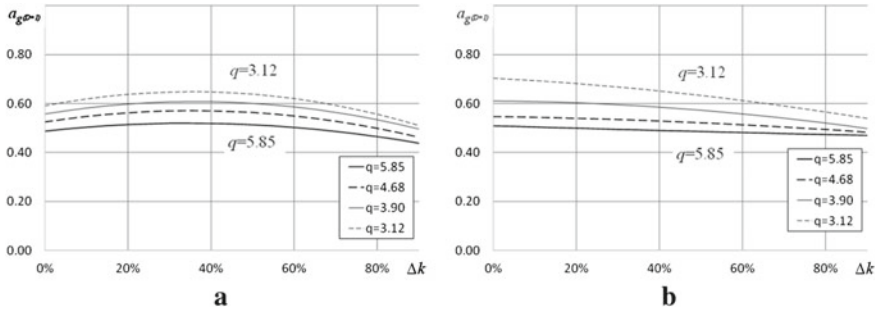

Fig. 8 Values of a_g corresponding to the SD limit states for increasing values of Δk and different values of q, **a** Case C, 7 stories, **b** Case C, 4 stories

Although different values of q were adopted for the design, the seismic capacity 7-story frames resulted to be almost independent from the entity of vertical irregularity, as shown in Fig. 8a. On the contrary, the seismic capacity of 4-story frames was affected by Δk. Indeed, the value of a_g leading these frames to the SD limit state tends to decrease with Δk, as shown in Fig. 8b.

4.4 *Case W: Stiffness Increase from the First to the Second Story*

The increase of lateral stiffness from the first to the second story, named Case W, can be found in case of buildings having the first interstory height larger than other stories, or in case of the presence of a *pilotis*.

The average damage of structural members at SD limit state is showed in Fig. 9a for 7-story frames designed by $q = 5.85$. Note that, in this case, the parameter Δk defined by Eq. 1 assumes negative values. However, the absolute value of Δk is

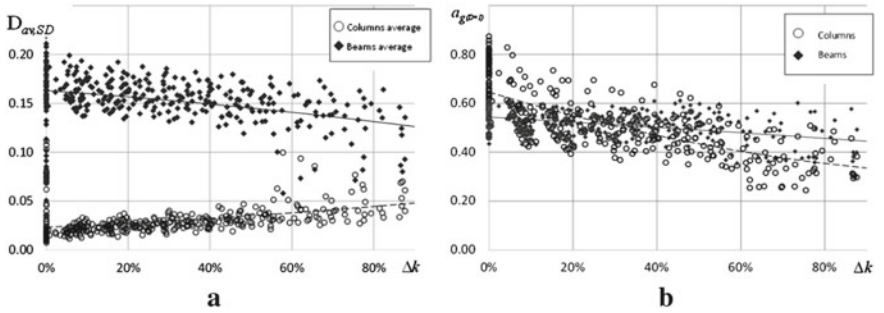

Fig. 9 Case W, 7-story frames, $q = 5.85$: **a** Average damage at SD limit state, **b** PGA corresponding to the SD limit state

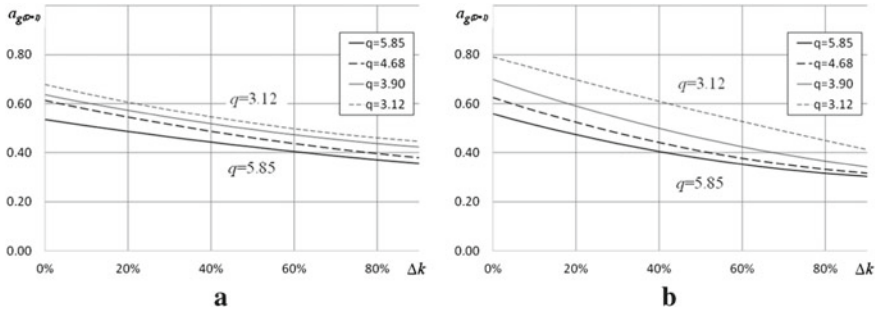

Fig. 10 Values of a_g corresponding to the SD limit states for increasing values of Δk and different values of q: **a** Case W, 7 stories, **b** Case W, 4 stories

reported in Fig. 9. The results obtained for structures belonging to Case W are in line with the previous cases. In fact, damage is mainly concentrated in beams. However, differently from Case A, B or C, the damage in columns increases almost linearly with the parameter Δk, while that in beams tends to decrease. As a consequence (Fig. 9b), for larger values of Δk, the plastic rotation capacity is attained in columns and the peak ground acceleration corresponding to the SD limit state decreases almost linearly with increasing structural irregularity. This result is confirmed by the trend lines reported in Fig. 10 for both the 7-story and 4-story frames.

It is noteworthy that in this case the presence of vertical irregularity strongly affects the seismic capacity of structures. Hence, a proper reduction of the behavior factor q is necessary to ensure that the seismic capacity of irregular structures is not penalized by the variation of stiffness. In fact, a value of the reductive coefficient $K_R = 0.8$, suggested by code for $\Delta k > 0.1$, appeared to be insufficient. Based on the obtained results, the value of K_R should be determined as function of Δk:

$$K_R = 1 + 0.6\ \Delta k \tag{4}$$

where Δk is determined by Eq. 1 considering its sign, and $K_R = 1$ for $|\Delta k| < 0.1$.

5 Conclusions

The seismic response of case study frames belonging to category A, B or C was basically independent of the variation of stiffness along the height, even in the case of significant values of stiffness reduction. These results show that the design criteria stipulated by seismic codes provide the structures with a good seismic capacity and guarantee a satisfying seismic performance even in the case of significant reduction of lateral stiffness. Hence, it is too restrictive to classify the structures with stiffness

reduction as irregular, even though avoiding abrupt reduction of lateral stiffness along the height remains a valid design indication.

Differently, the increase of lateral stiffness along the height showed a significant impact on the seismic response of structures. Increasing values of the rate of variation of stiffness Δk from the first to the second story led to a larger concentration of damage at first story and lower values of the peak ground acceleration a_g corresponding to the attainment of the SD limit state. In particular, large values of the rate of stiffness variation almost nullify the effect of the parameter $K_R = 0.8$ that Italian and European seismic codes introduce to reduce the behavior factor q in the case of irregular structures. Based on the obtained results, it seems reasonable that the reduction of the behavior factor should be evaluated as a function of the rate of stiffness Δk, as proposed by Eq. 4. The values of q so reduced should provide irregular structures with a suitable seismic response. Note that, this study has to be intended as a preliminary investigation. Further investigations are of interest and studies with more realistic numerical models with distributed plasticity members and nonlinear dynamic analysis are in progress. The goal is to verify whether and the extent to which the results presented in this paper are confirmed or not.

References

1. Valmundsson E, Nau JM (1997) Seismic response of building frames with vertical structural irregularities. J Struct Eng 123(1):30–41
2. ICBO (1997) Uniform building code, Whittier, California
3. ICC (2000) International building code
4. CEN Eurocode 8 (2004) Design of structures for earthquake resistance. Part 1: general rules, seismic actions and rules for buildings. EN 1998–1:2004. Brussels, Belgium
5. De Stefano M, Pintucchi B (2008) A review of research on seismic behaviour of irregular building structures since 2002. Bull Earthq Eng 6:285–308
6. Magliulo G, Ramasco R, Realfonzo R (2001) Sul comportamento sismico di telai piani in c.a. caratterizzati da irregolarità in elevazione. Proceedings of 10° Convegno Nazionale "L'ingegneria Sismica in Italia", Potenza-Matera, 9–13 September 2001
7. Chintanapakdee C, Chopra AK (2004) Seismic response of vertically irregular frames—response history and modal pushover analyses. J Struct Eng 130(8):1177–1185
8. Bhosale AS, Davis R, Sarkar P (2017) Vertical irregularity of buildings: regularity index versus seismic risk. ASCE-ASME J Risk Uncert Eng Syst Part A: Civil Eng 3(3)
9. Dya AFC, Oretaa AWC (2015) Seismic vulnerability assessment of soft story irregular buildings using pushover analysis. Procedia Engineering 125:925–932
10. Athanassiadou C, Bervanakis S (2005) Seismic behaviour of R/C buildings with setbacks designed to EC8. Proceedings of the 4th European workshop on the seismic behaviour of irregular and complex structures. CD ROM. Thessaloniki, August 2005
11. D.M. 17/1/2018, 2018. Aggiornamento delle "Norme Tecniche per le Costruzioni"
12. Panagiotakos TB, Fardis MN (2001) Deformations of reinforced concrete members at yielding and ultimate. ACI Struct J 98(2):135–148

The Effect of the Number and Height of Adjacent Buildings on the Seismic Response of Structures

Behroozeh Sharifi and Gholamreza Nouri

1 Introduction

As in cities and urban areas, the building structures are built near to each other, because of interference of the structural responses through the soil, the soil-structure problem evolves to a cross-interaction problem between multiple structures [1, 2]. Under such circumstances, the dynamic interaction and dynamic coupling of adjacent buildings via the underlying soil should not be ignored [3]. However, available evidences show that the interaction of adjacent structures has not been paid comprehensive attention.

In addition, most researches in this field are subjected to simulate superstructures as lumped mass with a single degree of freedom [3–6]. Also, two-dimensional models with plain strain behavior [7] are applied. Soil is simulated by spring, mass, and damper, or an equivalent impedance function [8] or assumption as a homogeneous, isotropic and linear elastic half-space [9]. Because of this excessive simplification, the complex geometry of the cross-section, the wrapping and secondary torsion in complicated and massive structures, are disregarded [1]. This would be led to obtaining reliable seismic results rather than 3D models, therefore 2D simplification has a high risk in the seismic analysis of soil-structure interaction (SSI) [10].

The result of researches in this field have shown that the structure-soil-structure interaction (SSSI) effects are very dependent on adjacent structures height in two structures, three structures and a group of structures on shallow foundations or deep foundations [4, 5, 11, 12].

B. Sharifi (✉)
Civil Engineering, Faculty of Engineering, Kharazmi University, Tehran, Iran

G. Nouri
Faculty of Engineering, Kharazmi University, Tehran, Iran
e-mail: r.nouri@khu.ac.ir

R. Bento et al. (eds.), *Seismic Behaviour and Design of Irregular and Complex Civil Structures IV*, Geotechnical, Geological and Earthquake Engineering 50,
https://doi.org/10.1007/978-3-030-83221-6_6

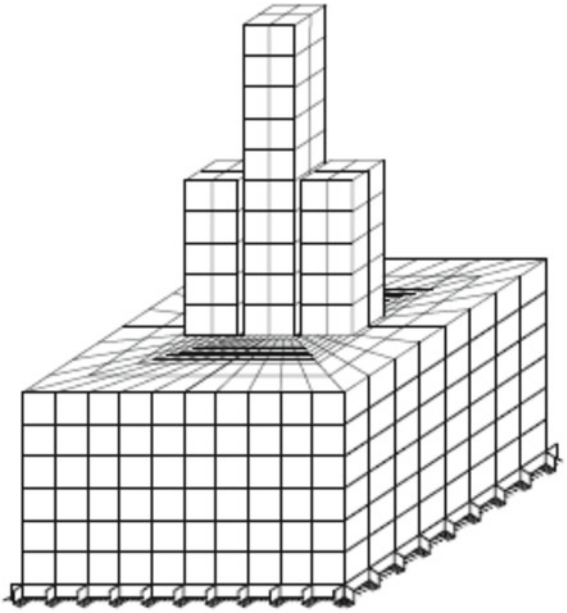

Fig. 1 Modelling of structure-soil-structure interaction for a group of three structures by direct method

The purpose of this study is to investigate the effect of the number and height of adjacent buildings (according to Fig. 1, as a sample of models) on the seismic performance of structures, which has been investigated by nonlinear dynamic analysis and three-dimensional modeling in OpenSees software.

2 Structure-Soil-Structure System

2.1 Super Structure Model

In this study, in order to use a 3D model of a group of structures, five-, ten-, fifteen-story RC frame structures, two (5 m) spans in the X direction and two (4 m) spans in the Y direction with shallow foundations were employed. Design of each structure without any effects of SSI or SSSI according to Iranian seismic design code [13] using ETABS software, were conducted.

In this paper, 3D finite element analysis was applied using the OpenSees package [14]. The details of the finite element modeling of the concrete frame and foundation are as follows: beam and columns were modeled as nonlinear force-based beam-column elements with distributed plasticity along the length of elements. Concrete behavior was modeled by a uniaxial material object with tensile strength and linear tension softening (Concrete02) [15]. Steel behavior was represented by a uniaxial Giuffre-Menegotto-Pinto model (Steel02).

Table 1 Properties of soft clay (Vs = 270 m/s) [16]

Model parameters	Value	Model parameters	Value
ρ = massdensity ($\frac{kg}{m^3}$)	1.595	K = bulkmodulus (kpa)	9.37×10^4
G = shearmodulus (kpa)	15.9×10^3	ν = Poisson's ratio	0.42
E = elasticmodulus (kpa)	4.5×10^4	c = cohesionintercept (kpa)	90
φ = frictionangle (deg)	24	c_{sb} = interfacecohesion (kpa)	50
k_n = normalstiffness ($\frac{kpa}{m}$)	7.6×10^4	k_s = shearstiffness ($\frac{kpa}{m}$)	8×10^2

Foundations were modeled as shallow foundations made of eight-node mixed volume/pressure brick elements, which use trilinear isotropic formulation, and the material formulations for the elastic isotropic objects are three-dimensional, plane strain, plane stress, axisymmetric and plate fiber.

2.2 Substructure Model

Semi-infinite soil was modeled based on the direct method and applying 3D OpenSees software in conjunction with a group of building structures, as shown in Fig. 1. Table 1, shows the dynamic properties of the soil [16] which categorized as type III according to the Iranian seismic design code, with 30 (m) depth of soil and shear wave velocity of 270 (m/s^2), that includes eight-node brick elements, with three translational degrees of freedom along X, Y and Z coordinates and elastic–plastic behavior. In order to the numerous values of soil elements and to prevent excessive computation time, the element's size varied from 1 m in each dimension around the buildings as well as near the surface in the soil to 5 m far from the structures. Boundary conditions comprise fixed boundaries at the lowest level of the soil, to model the bedrock and absorbent viscous boundaries, to avoid reflective waves that produced by lateral soil boundaries. Absorbent boundaries are made of a uniaxial and viscous material with non-linear elastic behavior located as lateral boundaries in horizontal directions at a distance of 5 times the structure width [16].

2.3 Interface Elements

The interfaces between the foundation and soil were modeled as linear spring-slider systems and zero-length contact 3D elements (Fig. 2) in the 3D OpenSees model, while interface shear strength is defined by the Mohr–Coulomb failure criterion. The relative interface movement is controlled by interface stiffness values in the normal (kn) and tangential (ks) directions, based on recommended rule-of-thumb estimates for maximum interface stiffness values given by Itasca Consulting Group (2005) [17]

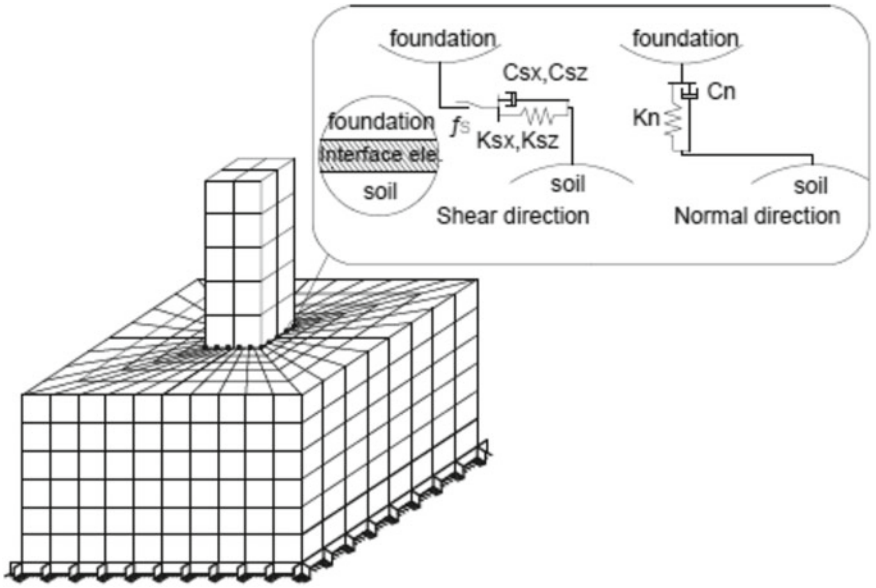

Fig. 2 Interface elements in SSI or SSSI models

and refining the magnitude of kn and ks is, to avoid intrusion of adjacent zones and to prevent excessive computation time.

3 Dynamic Analysis of SSSI and SSI Interaction

Fully nonlinear dynamic time history analysis was applied by 3D OpenSees software under the influence of three different ground motions records as shown in Table 2. All ground motions were recorded on high rigid soil that complies with the rigidity of soil type I [13]. The displacement time history of the scaled records were used as bedrock excitation.

Table 2 Earthquake records for the parametric analysis obtained from the Pacific Earthquake Engineering Research (PEER) Centre Database

Peak ground displacement (m)	Magnitude (Mw)	Soil shear velocity (m/s)	Year	Station	Earthquake
0.043	6.90	655.45	2008	Minse YuZawa	Iwait
0.051	6.93	663.31	1989	Gilroy Array#6	Loma Prieta
0.067	7.30	671.52	1986	SMART1 E02	Taiwan SMART1(45)

using the direct method, horizontal components of the three different ground motion records have been applied in three different models; (i) a 10-story structure as a SSI model. (ii) The 10-story structure flanked by one (shorter, taller and the same) adjacent building structure as a SSSI model with two structures. (iii) The 10-story building structure flanked by two (shorter, taller and the same) adjacent building structures as a SSSI model with three structures.

4 Results and Discussions

The SSI and SSSI systems are analyzed with horizontal component ground motions from three earthquake records, and the maximum responses of relative acceleration, displacement, drift and shear force of stories of the 10-story structure, have been considered when the 10-story structure as SSI model is (i) alone, (ii) in a group of two structures, flanked by one shorter, taller and the same adjacent structure or (iii) in a group of three structures flanked by two shorter, taller and the same adjacent structures.

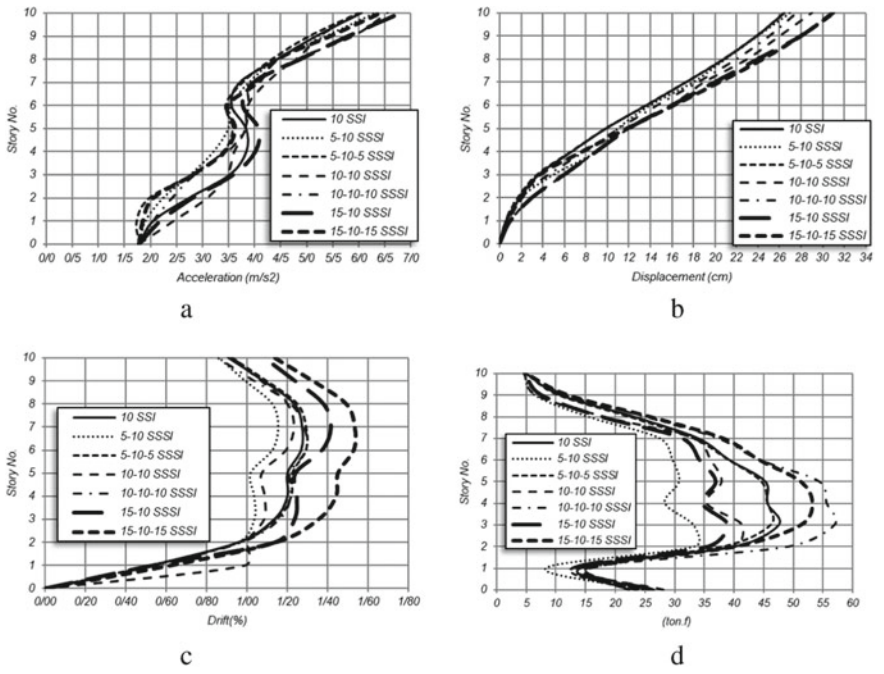

Fig. 3 **a** Maximum responses of relative acceleration, **b** displacement, **c** drift and **d** shear force of the 10-story structure when it is alone in SSI model or adjacent with one or two other structures in SSSI models

Results of the relative acceleration have been showed in Fig. 3a. Comparing the SSSI with SSI response, the 10-story structure appears to be significantly affected, attenuated relative acceleration responses, −21% and −28%, by the presence of one and two 50% shorter structures respectively. While 12% amplified acceleration response is shown, by a 50% taller structure and 25% attenuated response by two 50% taller structures.

In Fig. 3b, the10-story structure's displacement amplifies up to 48% when adjoined by a 50% shorter structure and attenuates up to 11% when adjoined by two 50% shorter structures. 64% and 20% amplifications are seen when one and two 50% taller structure respectively are present in adjacency.

Responses of the drift are shown in Fig. 3c, 17% attenuation is seen when one 50% shorter structure is in adjacency; while adjoining with two 50% shorter structures has no significant attenuation or amplification in drift responses. Presence of one and two 50% taller structures, amplify drift responses up to16% and 20% respectively.

Responses of the shear force in Fig. 3d, indicate that, up to 68% and 9% attenuation of responses are occurred in adjacency with one and two 50% shorter structures respectively. Response attenuates up to 30% in adjacency with a 50% taller structure and amplifies up to 16%, when the10-story structure is adjacent by two 50% taller structures. Although adjacency with one identical building structure can attenuate response of shear force up to 39%. Two identical building structures can amplify response up to 22%.

Study of the response of relative acceleration, displacement, drift and shear force in the stories of the 10-story structure, indicate that effects of SSSI can be more prominent when there are more than one building structure interacting that depend on the number and height of adjacent structures, dynamic characteristics of buildings, and frequency content of seismic data. The results show that considering different adjacent structures lead to increase or decrease about 10 times of percent of responses.

5 Conclusions

As previously discussed, this study focuses on the seismic response of adjacent structures. In urban areas, we are faced with structures with several neighborhoods, while the analysis and design of the structures are still based on the patterns of the single structure analysis, which according to the results do not meet the design needs of structural elements; in other words, it may be over-designed or high risk, in some cases. For this purpose, this paper examined the effects of the 5, 10 and 15-story adjacent structures on a 10-story structure while this SSSI system is conjunction with the soft soil.

As a general conclusion, adjacency with a shorter structure leads to reduction in responses, even two adjacent shorter structures have greater reduction effects, in such cases, lighter sections can be used. Instant, adjacency with a taller structure leads to increases in the responses and also the two adjacent taller structures have greater incremental effects; that there are weaknesses in the current analysis.

References

1. Lou M, Wang H, Chen X, and Zhai Y (2011) Structure-soil-structure interaction: literature review. Soil Dyn Earthq Eng
2. Sharifi B, Nouri G, Ghanbari A (2020) Structure-soil-structure interaction in a group of buildings using 3D nonlinear analyses. Earthq Struct, 667–675
3. Vicencio F, Alexander NA (2018) Dynamic interaction between adjacent buildings through nonlinear soil. Soil Dyn Earthq Eng, 130–141
4. Alexander NA, Ibraim E, Aldaikh H (2013) A simple discrete model for interaction of adjacent buildings during earthquakes. Comput Struct, 1–10
5. Aldaikh H, Alexander NA, Ibraim E, Oddbjornsson O (2015) Two dimensional numerical and experimental models for study of structure-soil-structure interaction involving three buildings. Comput Struct, 79–91
6. Vicencio F, Alexander NA (2018) Higher mode seismic structure-soil-structure interaction between adjacent building during earthquakes. Eng Struct 174:322–337
7. Behnamfar F, Sugimura Y (1999) Dynamic response of adjacent structures under spatially variable seismic waves. Probab Eng Mech 14(1/2):33–44
8. Wolf JP (1994) Foundation vibration analysis using simple physical models. Englewood Cliffs: PTR Prentice Hall
9. Mulliken JS, Karabalis Dl (1998) Discrit model for dynamic through-the-soil coupling of 3-D foundations and structures. Earthq Eng Struct Dyn 27(7):687–710
10. Lianga J, Han B, Fu J, Liu A (2018) Influence of site dynamic characteristics on dynamic soil-structure. Soil Dyn Earthq Eng, 79–95
11. Chen Z, Hutchinson TC, Trombetta NW (2010) Seismic performance assessment in dense urban environments. In Recent advances in geothechnical earthquake engineering and soil dynamics, San Diego, California
12. Padron LA, Aznarez JJ, Maeso O (2009) Dynamic structure-soil-structure interaction between nearby pield buildings under seismic excitation by BEM-FEM model. Soil Dyn Earthq Eng, 1084–1096
13. B. a. H. R. C. (BHRC) (2014) Iranian code of practice for seismic resistant design of buildings. Standard no. 2800, 4th ed
14. McKenna F, Fenves GL, Jeremic B, Scott MH (2007) Open System for earthquake engineering simulation
15. Mohd Yassin MH (1994) Nonlinear Analysis of prestressed concrete structures under monotonic and cycling loads. PhD dissertation, University of california, Berkeley
16. Rayhani MH, El naggar MH (2008) Numerical modeling of seismic response of rigid foundation on soft soil. Int J Geomech 8(6): 336–346
17. Itasca Consulting Group, Inc. (Itasca) (2005) "FLAC3D: Fast lagrangian analysis of continuma in 3 dimensions, version 3.0," User's manual, Minneapolis.

Evaluation of Torsional Parameters in Seismic Code Provisions for Multi-story Unsymmetric-Plan Buildings

Luis Ardila, Juan C. Reyes, and Maria P. Moreno

1 Introduction

Seismic design provisions specify that the torsional effects in buildings need to be included by applying static equivalent lateral forces at a distance e_d from the center of rigidity, which induce an increased story torque and shear demand on the structure. Both the American standards (ASCE 7–16 and ASCE 41–17) [1, 2], as well as the Eurocode 8 [3] specify that the earthquake forces need to be applied at every story shifted by $\pm 0.05b$, where b corresponds to the in-plan building dimension perpendicular to the seismic excitation. The total design eccentricity e_d is calculated as the sum of $\pm 0.05b$ and the static eccentricity e_s defined as the distance between the in-plan story center of mass and center of rigidity of the structure.

The static eccentricity e_s accounts for the in-plan torsional response of the building, by considering the asymmetries at every floor of the structure. The $\pm 0.05b$ term, often known as the accidental eccentricity, considers sources of uncertainty in the dynamic properties of the structure, such as mass and stiffness, assumed in the modeling and design phase, and those of the real structure at the time of an earthquake. In-plan symmetric buildings, where the center of mass and rigidity coincide, will only require the evaluation of accidental torsion by applying the lateral loads at the center of mass shifted by $\pm 0.05b$ [4].

Recent research [5–8] suggests that the current seismic provisions to evaluate torsional effects on buildings are not sufficiently accurate because they are based

L. Ardila (✉)
University of Toronto, Toronto, ON, Canada
e-mail: l.ardila@mail.utoronto.ca

J. C. Reyes
Universidad de Los Andes, Bogotá, Colombia

M. P. Moreno
Choate Construction, Atlanta, GA, USA

R. Bento et al. (eds.), *Seismic Behaviour and Design of Irregular and Complex Civil Structures IV*, Geotechnical, Geological and Earthquake Engineering 50,
https://doi.org/10.1007/978-3-030-83221-6_7

on linear spectrum analysis, and therefore, do not consider the inelastic response of the structure, and the potential redistribution of the center of rigidity at every floor as the structure undergoes large inelastic deformations [8]. In order to assess the torsional effects in asymmetric structures and determine an adequate earthquake design procedure, it is necessary to evaluate properly the level of in-plan irregularity [8]. This paper evaluates a torsional parameter that is based on linear spectrum analysis, by studying the inelastic earthquake response of an irregular structure. Torsion seismic design provisions are then evaluated, and some design recommendations are outlined.

2 Torsional Parameters in Seismic Code Provisions

2.1 ASCE 7–16 and ASCE 41–17

The standard ASCE 7 defines three levels of torsional irregularity according to the following index:

$$\alpha = \frac{\Delta_{max}}{\Delta_{average}} \tag{1}$$

where Δ_{max} is the maximum story drift corresponding to the maximum value between Δ_1 and Δ_2, and $\Delta_{average}$ is the average between Δ_1 and Δ_2 as describe in Fig. 1. Torsional irregularity is defined as follows: (i) not torsional irregularity if $\alpha < 1.2$; (ii) torsional irregularity for $1.2 \leq \alpha \leq 1.4$ and (iii) extreme torsional irregularity for $\alpha > 1.4$. Accidental torsion needs to be considered by shifting the center of mass of every floor by 5% of the in-plane building dimension perpendicular to the seismic excitation. In addition, if the building has extreme torsional irregularity, the moments resulting from the accidental torsion of the building need to be amplified by a factor A_x (Eq. 2).

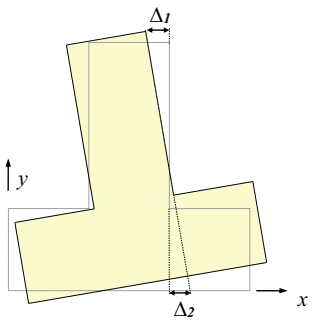

Fig. 1 Structural drifts used to calculate α to define in plan irregularity

$$A_x = \frac{\Delta_{\max}}{1.2\Delta_{prom}}, \ldots 1.0 < A_x \leq 3.0 \quad (2)$$

The torsional ratio considered in the ASCE 41–17 is analogous to the ratio α shown previously. Additional torsional requirements are introduced for the evaluation of existing buildings in Sect. 7.2.3.2.2 [2].

2.2 Eurocode 8

There are not structural regulations for torsional irregularity in the Eurocode 8 [3], and the standard lacks of parameters to classify in-plan, or in-height irregularity for un-symmetric buildings. Nonetheless, the European standard specifies that irregular buildings need to have adequate torsional stiffness and considers accidental torsion similarly to the ASCE 7–16 (by shifting 5% the center of mass of the structure). In addition, it is suggested that structures with high levels of in-plan irregularities should not be designed for seismic prone areas, and if the structure needs to be irregular, the structural engineer of record will need to adequately select the method for seismic analysis and design.

The ASCE 7 standard provides a simple approach to determine the level of torsional irregularity of asymmetric buildings by calculating the ratio α introduced in Eq. 1. However, this ratio is based on linear spectrum analysis, without accounting for the potential structural changes that the building will undergo when subject to large inelastic demands. This study evaluates the robustness and consistency of α by considering buildings with different levels of torsional irregularity, and a broad variety of near field earthquake ground motions. In addition, a full three-dimensional non-linear model was considered to investigate the variability of this parameter upon different levels of inelastic demands.

3 Structural Systems Selected

This study was conducted in two phases. In the first phase, we initially considered nine un-symmetric buildings designed in accordance to the 2009 International Building Code [9] to be located in Los Angeles, California. Torsional parameters for in-plan irregularity were calculated from bi-directional linear response spectrum analysis. The structural system for these structures consists of special moment resistant frame (SMRFs), and the seismic design spectrum was reduced by a response modification factor of $R = 8$. The structural floor plans were selected to define three ranges of torsional irregularity as per ASCE 7: low, moderate and severe. Structures in this study are labeled with the letters “R”, “L” and “T” to reflect their in-plan structural shape as presented in Fig. 2, followed by their number of stories: 5, 10 and 15. For example, R10 will be a regular shape structure with 10 stories. Figure 2. also shows

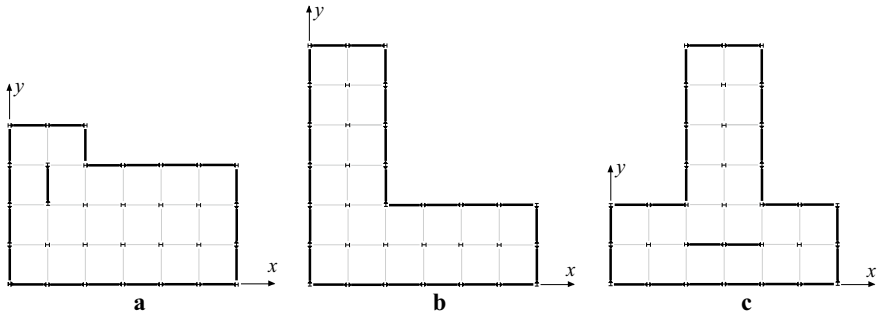

Fig. 2 Structural plan views for **a** regular, **b** L shape, and **c** T shape structures selected [10]

the moment frames along the principal axes of these buildings. Figure 3. shows the mass participation ratios for these buildings for their first three modes of vibration in the direction of the orthogonal axes x and y as presented in Fig. 2 More details about the dynamic properties of these buildings can be found in [10]. α values for each of these buildings were calculated and are presented in Table 1, as per ASCE

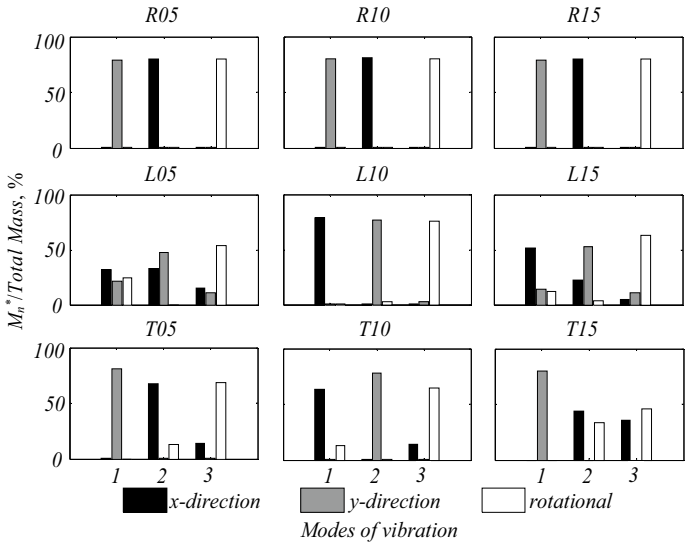

Fig. 3 Effective modal masses $M_n{}^*$ of structures selected. Taken from [10]

Table 1 Torsional irregularity ratios. Taken from [10]

Building	R05	R15	R10	L10	L15	T15	L05	T10	T05
α	1.00	1.10	1.13	1.20	1.26	1.30	1.35	1.41	1.43

7–16 considering the maximum drift from each of the orthogonal axes of earthquake analysis x and y as denoted in Fig. 2. (Eq. 1).

In the second phase, Building T10 was selected in this study to evaluate the robustness and consistency of the torsional ratio α for different levels of seismic inelastic demands. Non linear time history analysis was conducted in PERFORM-3D [11], considering the following non-linear features: (i) floor diaphragms were assumed as rigid; (ii) girders were modeled using lumped plastic hinges at their ends; (iii) columns considered moment-axial load interaction based on plasticity theory; (iv) panel zones were modeled with four rigid links hinged at the corners and coupled by a rotational spring that represented the stiffness and strength of the connection using the formulations by Krawinkler [12]; (iv) columns of gravity frames were assumed as hinged at their based, while columns in moment frames were considered fixed at their based, and (v) nonlinear geometry effects were estimated using standard P-Δ formulation for the entire structure.

4 Ground Motions Selected

This study considered thirty ground motion records from seven shallow crustal earthquakes with fault distances (R_{JB}) ranging from 20 to 30 km, with moment magnitude $M_w = 6.7 \pm 0.20$ and soil classification corresponding to very dense soil (Type C) and stiff soil (Type D). These ground motions were obtained from the PEER (Pacific Earthquake Engineering Research Center) and are listed in Table 2. The ground motions were selected to represent a level of compatibility with the design spectrum, and scaled to simulate three different earthquake intensity levels. Figure 4 presents the geometric mean of the 5% damped response spectra for the fault normal (FN) and fault parallel (FP) components of the ground motions, with three scale factors, and

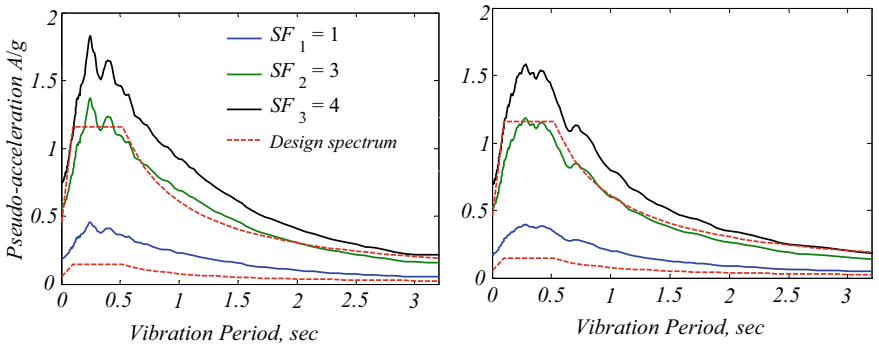

Fig. 4 Geometric-mean pseudo-acceleration response spectra, **a** fault normal (x-direction) and **b** fault parallel component (y-direction) of the selected ground motions

the design spectrum reduced by a response modification factor of $R = 8$ and $R = 1$. The three scale factors considered intent to simulate the following dynamic response for the T10 structure: (i) for scaling factor $SF = 1$, it is expected that the structural response will be characterized by low nonlinear behavior; (ii) $SF = 3$ is close to the design spectrum with $R = 1$, thus a moderate inelastic behavior is expected and (iii) $SF = 4$ is far beyond the design spectrum representing a high level of nonlinear deformations.

5 Evaluation of the ASCE 7–16 Torsional Parameter α

Building T10 was selected to evaluate the consistency of the torsional parameter α for various levels of seismic intensities. According to the ASCE 7–16, building T10 is classified as having extreme torsional irregularity with $\alpha_{Design} = 1.41$ (Table 2). Bi-directional nonlinear time history analyses were conducted using the suite of ground motions presented in the previous section and using a three-dimensional structural model built in PERFORM 3D for building T10. The torsional ratio α was calculated in each direction of excitation using the following equations:

$$\alpha_x = \frac{2|\max(\Delta_{1x}, \Delta_{2x})|}{|\Delta_{1x} + \Delta_{2x}|} \tag{3}$$

$$\alpha_y = \frac{2\left|\max(\Delta_{1y}, \Delta_{2y})\right|}{\left|\Delta_{1y} + \Delta_{2y}\right|} \tag{4}$$

$$\alpha = \max(\alpha_x, \alpha_y) \tag{5}$$

Δ_1 is the corner drift, and Δ_2 is the drift considered in the opposite corner along the axis of reference, as presented in Fig. 5.

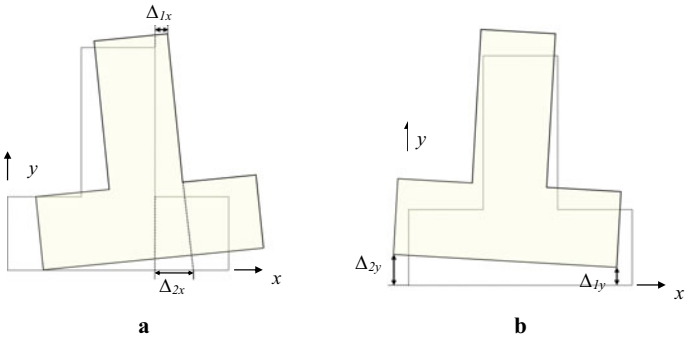

Fig. 5 Story drifts used to calculate the torsional factor α in, **a** x-direction, **b** y-direction

Table 2 List of 30 selected ground motions records

ID	Earthquake name	Year	Station name	M_w	R_{JB} km	NEHRP site class
1	San Fernando	1971	LA—Hollywood Stor FF	6.6	22.8	D
2	San Fernando	1971	Santa Felita Dam (Outlet)	6.6	24.7	C
3	Imperial Valley-06	1979	Calipatria Fire Station	6.5	23.2	D
4	Imperial Valley-06	1979	Delta	6.5	22.0	D
5	Imperial Valley-06	1979	El Centro Array #1	6.5	19.8	D
6	Imperial Valley-06	1979	El Centro Array #13	6.5	22.0	D
7	Imperial Valley-06	1979	Superstition Mtn Camera	6.5	24.6	C
8	Irpinia, Italy-01	1980	Brienza	6.9	22.5	C
9	Superstition Hills-02	1987	Wildlife Liquef. Array	6.5	23.9	D
10	Loma Prieta	1989	Agnews State Hospital	6.9	24.3	D
11	Loma Prieta	1989	Anderson Dam (Downstream)	6.9	19.9	C
12	Loma Prieta	1989	Anderson Dam (L Abut)	6.9	19.9	C
13	Loma Prieta	1989	Coyote Lake Dam (Downst)	6.9	20.4	D
14	Loma Prieta	1989	Coyote Lake Dam (SW Abut)	6.9	20.0	C
15	Loma Prieta	1989	Gilroy Array #7	6.9	22.4	D
16	Loma Prieta	1989	Hollister—SAGO Vault	6.9	29.5	C
17	Northridge-01	1994	Castaic—Old Ridge Route	6.7	20.1	C
18	Northridge-01	1994	Glendale—Las Palmas	6.7	21.6	C
19	Northridge-01	1994	LA—Baldwin Hills	6.7	23.5	D
20	Northridge-01	1994	LA—Centinela St	6.7	20.4	D
21	Northridge-01	1994	LA—Cypress Ave	6.7	29.0	C
22	Northridge-01	1994	LA—Fletcher Dr	6.7	25.7	C

(continued)

Table 2 (continued)

ID	Earthquake name	Year	Station name	M_w	R_{JB} km	NEHRP site class
23	Northridge-01	1994	LA—N Westmoreland	6.7	23.4	D
24	Northridge-01	1994	LA—Pico & Sentous	6.7	27.8	D
25	Kobe, Japan	1995	Abeno	6.9	24.9	D
26	Kobe, Japan	1995	Kakogawa	6.9	22.5	D
27	Kobe, Japan	1995	Morigawachi	6.9	24.8	D
28	Kobe, Japan	1995	OSAJ	6.9	21.4	D
29	Kobe, Japan	1995	Sakai	6.9	28.1	D
30	Kobe, Japan	1995	Yae	6.9	27.8	D

Figure 6 shows the variation of the torsional parameter α for each axis of excitation as a function of the earthquake records considered. For reference, this figure also shows horizontal lines at $\alpha = 1.4$ and 1.1 in the x and y direction, respectively; these values correspond to the linear parameters calculated using response spectrum analysis. Results indicate that α is in most cases above the reference design value suggesting low dependency with the level of nonlinearity developed by the structure. Figure 7 shows the variability of α with respect to the maximum drift achieved at each level of seismic intensity for each earthquake record. It can be inferred from the results that there is a low record-to-record variability, and even though there is a higher inelastic demand with corresponding drift ratios of about 3%–5%, α shows a constant behavior around the reference design value.

High torsional irregularity can also be related with the fundamental mode mass participation ratio of a structure. Figure 8 shows the relationship between α and the

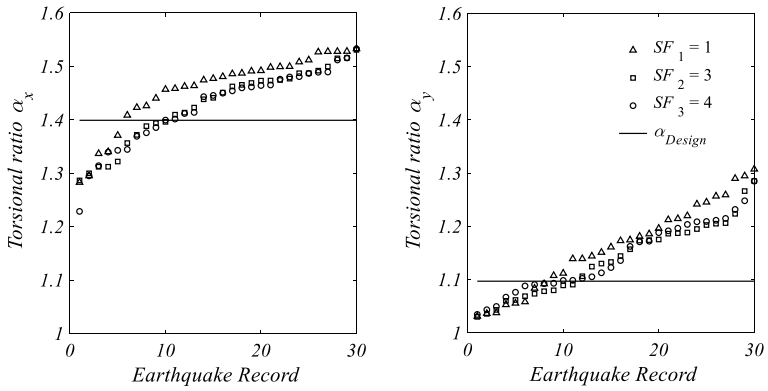

Fig. 6 Torsional ratios for different levels of seismic intensities earthquake record

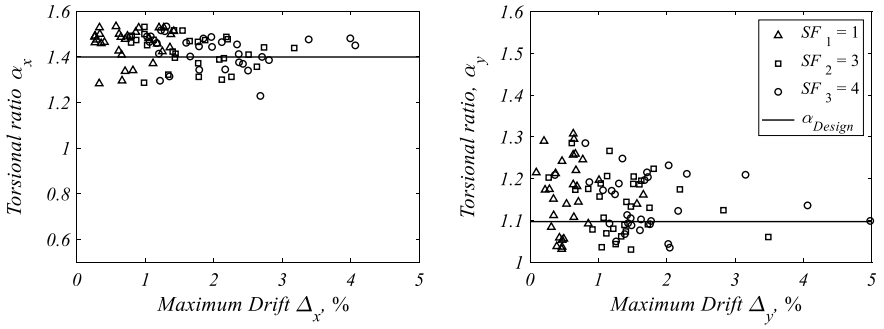

Fig. 7 Relationship between the torsional ratio α and the maximum drift obtained from RHAs

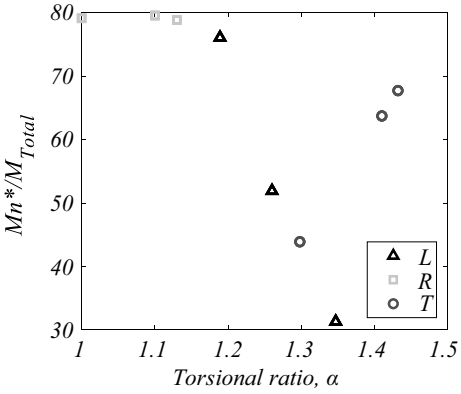

Fig. 8 Relationship between the fundamental mode mass participation ratio and the torsional ratio α

first-mode mass participation ratio (M_n^*/M_{total}) for the nine structures considered in this study. For R and L structures, mass participation decreases with increasing α values; in general, for $\alpha > 1.2$, the mass participation ratio is lower than 70%. This figure confirms that higher mode effects are more significant for structures with larger α values.

6 Conclusions

This study evaluates the adequacy of the ASCE 7–16 torsional index α (as described in this paper) to identify plan irregularity of buildings. Results from linear models of nine multi-story buildings with different levels of plan irregularity, alongside a nonlinear 3D model of building T10 (classified as having extreme torsional irregularity) has led to the following conclusions:

(1) Results from the nonlinear RHAs conducted for building T10 indicate that the torsional ratio α has small variations with respect to seismic intensity levels and shows low record-to-record variability.
(2) The torsional ratio α might be adequate to identify plan irregularity of multi-story buildings, and can provide significant information to determine if higher-mode effects should be considered in the design of unsymmetric-plan buildings. Nevertheless, non-linear RHAs from other structures, such as L05 and T05, with coupled lateral and torsional modal response (Fig. 3) are needed to extend and complete the validation of the torsional ratio α.

References

1. American Society of Civil Engineers (ASCE) Minimum design loads and associated criteria for buildings and other structures. ASCE/SEI 7–16. 2016, Reston, VA
2. American Society of Civil Engineers (ASCE) Seismic evaluation and retrofit of existing buildings. ASCE/SEI 41–17. 2017, Reston, VA
3. EC8-Part 1: Eurocode 8 (2005) Design provisions for earthquake resistance of structures. Part 1–1: General Rules—seismic actions and general requirements for structures. ENV 1998–1, CEN: Brussels
4. Chopra AK, De la Llera JC (1994) Accidental and natural torsion in earthquake response and design of buildings. Report No. UCB/EERC-94/07
5. Chopra AK, Goel K (1991) Evaluation of torsional provisions in seismic codes. J Struct Eng 117:3762–3782
6. Wen-Hsiung L, Chopra AK, De La Llera JC (2001) (2001) Accidental torsion in buildings: analysis versus earthquake motions. J Struct Eng 127:475–481
7. Saffari H, Tabatabaei R (2011) Evaluation of the torsional response of multistory buildings using equivalent static eccentricity. J Struct Eng 137:862–868
8. Köber D, Zamfirescu D (2012) Issues concerning general torsion in code provisions. Proceedings of the 9th World conference in earthquake engineering. Lisboa, Portugal
9. International Code Council—ICC (2009) International building code. Country Club Hills, IL
10. Reyes JC, Riano AC, Kalkan E, Arango C (2015) Extending modal pushover-based scaling procedure for nonlinear response history analysis of multi-story Unsymmetric-plan buildings. Eng Struct 88:125–137
11. Computers and Structures (CSI), Inc. (2006) PERFORM 3D, user guide v4, non-linear analysis and performance assessment for 3D structures. Berkeley, CA: Computers and Structures, Inc
12. Krawinkler H (1978) Shear in Beam-column joints in seismic design of frames. Eng J 15(3):82–91

Multiobjective Optimization of Long Irregular RC Bridges' Piers Subjected to Strong Motions and Definition of Classification Tree Surrogate Models

Vitor Camacho, Nuno Horta, and Mário Lopes

1 Introduction

Seismic design of long irregular bridges is inherently complex. Long and irregular bridges, in terms of pier height along the bridge, especially ones where relatively short piers are located away from the edges (abutments) of the bridge, can have transverse horizontal displacement profiles (THDP) that differ significantly from a parabolic shape usually associated to a bridge's first vibration mode. In such bridges, the displacement demand of each pier is not easy to define without the use of nonlinear dynamic analysis (NDA), according to Kappos et al. [1]. Furthermore, the THDP of the bridge may vary during the seismic action, with the loss of stiffness of certain elements, and subsequent change in fundamental vibration mode. This makes employing traditional static pushover analysis not ideal, in terms of quality of results. The need for NDAs, which are usually computationally expensive, plus the fact that more than one earthquake record needs to be employed due to the stochastic nature of strong motions, makes these bridges particularly complex to design. For that reason, design firms usually design these structures resorting to approximate methods, trial and error and/or experience gained from past designs. After finding a possible feasible solution they check its feasibility through NDAs, hopefully not

V. Camacho (✉) · M. Lopes
CERIS, Instituto Superior Técnico, University of Lisbon, Av. Rovisco Pais, 1049-001 Lisbon, Portugal
e-mail: vitorteixeiracamacho@tecnico.ulisboa.pt

M. Lopes
e-mail: mlopes@civil.ist.utl.pt

N. Horta
IT, Instituto Superior Técnico, University of Lisbon, Av. Rovisco Pais, 1049-001 Lisbon, Portugal
e-mail: nuno.horta@lx.it.pt

R. Bento et al. (eds.), *Seismic Behaviour and Design of Irregular and Complex Civil Structures IV*, Geotechnical, Geological and Earthquake Engineering 50,
https://doi.org/10.1007/978-3-030-83221-6_8

needing more than one or two iterations in the design process. The resulting solutions are not optimized and may also have a less than ideal distribution of resistance among piers. This study shows how multi-objective optimization techniques may be employed, particularly genetic algorithms (GA) [2] such as the NSGA-II [3], not only for the optimization of long irregular bridges, but also with the goal of identifying critical variables and variable sets that correlate with better seismic performances. Through the identification of critical variables and variable sets or schemata, better design rules may be formulated.

Structural optimization is complex and not easy to perform with traditional optimization methods, such as gradient descent methods. The reason is that such methods have several drawbacks, such as inability to work well with discrete variables and non-convex problems, which are usual characteristics of real-world structural optimization problems. Furthermore, the fact that GAs are population-based methods means that the output of multi-objective optimization problems (MOP) is a set of solutions rather than a single solution. Consequently, the output provides a trade-off between objectives, which is further advantageous by providing many "good" solutions from which a final solution may be chosen.

In this study, a modified NSGA-II algorithm, which was introduced in [4], is used for the optimization of a long irregular bridge with short central piers. The seismic action is applied only in the transverse direction. The results for different solutions are compared in terms of performance, stiffness distribution, total cost, etc. Afterwards, classification trees are employed to define critical variables and to create a surrogate model. The critical variables are those that provide larger information gain, regarding the instances' classification, by knowing their value. These techniques are applied to the entire set of solutions that were generated and analyzed during the GA runs.

2 Objectives, MOP Definition and Classification Tree

2.1 Objectives

The design of RC bridges for earthquake resistance essentially focuses on the RC bridge's infrastructure, piers and abutments. The design of RC piers compounds several variables from (1) pier-deck connections, to the piers' design variables, which are (2) flexural steel reinforcement (longitudinal reinforcement) (3) cross-section shape and dimensions, and (4) transverse steel reinforcement, including confinement. These variables all have complex interdependences and strongly influence bridge dynamic behavior. For instance, the variation of (1)–(3) modify, simultaneously, the piers' stiffness, ductility and strength.

Hence, the objective of this paper is to apply a multi-objective evolutionary algorithm (MOEA), a modified NSGA-II [4], to optimize the seismic design of a long irregular bridge, considering most variables associated to pier design (1–3), and using different standardization criteria. The results obtained from the application of the

MOEA show trade-off solutions for cost and performance objectives, showing how the design variables vary between solutions inside the optimal Pareto set. Furthermore, the subsequent application of a classification tree that processes over the entire population of solutions classifying them into feasible and infeasible solutions, returns a ranking on the relative importance of each variable, and generates the shortest path towards classification, which is to say, returns the set of variables that matter the most in terms of the bridge's seismic performance.

2.2 MOP Definition

As mentioned in the introductory section, this study applies the same MOP framework introduced in a previous work by the authors [4]. The inner workings of the MOEA, including its operators, are outside the scope of this study, and will not be further explained.

The MOP concerning seismic design of RC bridges is presented herein. The case-study to which it will be applied is shown in Sect. 3. The characteristics of the MOP, which are essential to the understanding of its performance, are: the optimization objectives and corresponding fitness functions, the constraint functions, and the decision variables. A brief description is given, on each one, without going into much detail. For a more in-depth explanation, the previous work by the authors [4] should be checked.

The objective functions, as mentioned previously, concern cost and performance. The cost is computed only from the amount of material, steel and concrete, present in the piers. The assumed material cost for concrete (C30/37) was 100 €/m^3 and for steel (A500NR) was 0.82 €/kg, which are relatively standard prices.

The constraint functions are somewhat complex, and for a thorough comprehension, the previous work by the authors [4] should be checked.

Regarding the decision variables there are three: (1) pier-deck connections, (2) flexural steel reinforcement and (3) cross-section size (only circular piers were considered). The fourth variable mentioned in the introduction as (4) (pier confinement), here is taken as a constant approximately equal to the minimum confinement for ductile bridges in EC8-2 [5]. As for the three variables, the following are their limit values between which they were sampled:

- Pier-deck connections: [1-monolithic, 2-pinned]-connection
- Flexural reinforcement steel: [0.6, 3.5] %
- Pier Diameter: [1.0, 2.5] m

All the piers, in each bridge solution, are modelled with the same pier diameter. Regarding the other two variables, their value in each pier depends on the adopted standardization criteria (pier groups).

2.3 Classification Tree

The classification tree algorithm employed is the REPTree learner from the Weka software suite version 3.8 [6], which is a variation of the well-known C4.5 classification tree [7]. The REPTree is a fast decision tree learner which can be applied for both classification and regression problems. It is built using information gain/variance and reduced error pruning with back-fitting.

3 Case-Study and Earthquake Definition

3.1 Earthquake Definition

In the FE step, NDAs with multiple strong motions are applied. The strong motions used herein were selected from among a set of earthquake records that provide a good match to EC8's response spectrum [8], in terms of frequency content. The initial set of selected strong motions is composed by 9 strong-motion pairs, and from this set, a subset was defined with 4 strong-motion pairs. The 4-pair subset is employed for the FE in the MOEA. At the end of the optimization procedure, the final output is validated by using the 9-pair set. Further details about the earthquake action employed can be found in [4].

3.2 FEM Analysis

The seismic analyses were performed resorting to OpenSEES software [9], more specifically OpenSEESMP for the conduction of the seismic analysis in parallel processes. Since the population evaluation in a MOEA is a fully parallelizable process, this allowed a significant reduction of the total run-time by a factor of around 20, due to the utilization of 32 parallel processors. The population size of the MOP, in each generation, is 64.

3.3 Case-Study Definition

The case-study selected for analysis is an irregular bridge with relatively short central piers, and with a total length of 480 m. An illustration of the type of irregularity is given in Fig. 1.

In addition, the length of each pier and the pier groups defined for the analysis are presented in Table 1. The bridge has a total of 15 piers and the chosen standardization criteria assembles the piers into four groups. In Table 1, on the left-hand side the

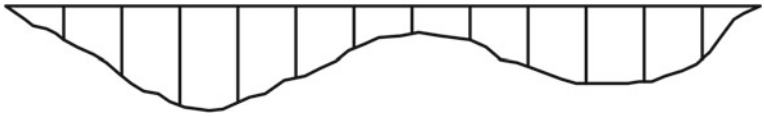

Fig. 1 Irregularity layout of case-study bridge

Table 1 Case-study pier lengths and pier variable groupings used in the optimization procedure. The bridge has 15 piers in total, numbered 1 through 15

Pier lengths (m)	Pier groups (pier position)
11 11 14 14 11 11 7 7 7 11 11 14 14 11 11	(1 2 14 15) (3 4 12 13) (5 6 10 11) (7 8 9)

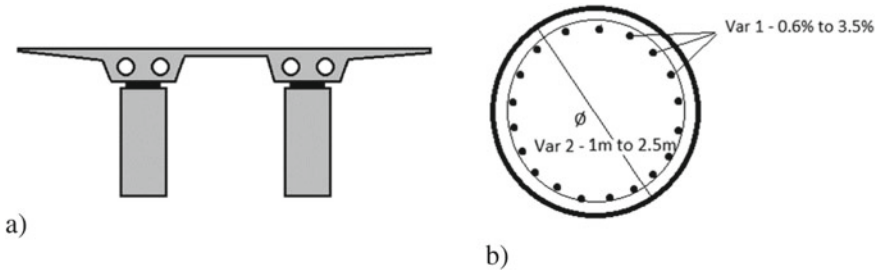

Fig. 2 Cross-sections of **a** the deck and **b** the piers

pier lengths along the bridge and on the right-hand side the pier groups, where the numbers (1–15) correspond to the position of the pier regarding the left abutment. For example, group 1 is represented by (1, 2, 14, 15), which means the two piers closest to the left abutment (1 and 2) and the two piers closest to the right abutment (14 and 15).

The cross-sections of both the piers and the deck are presented in Fig. 2. In the case of the piers, the corresponding design variables associated to the pier's cross-section are highlighted.

4 Result Analysis and Discussion

In this section results are presented pertaining to both the optimization procedure with the MOEA and the application of the classification tree algorithm.

4.1 MOEA Results

The optimization results are presented in the objective space in Fig. 3. There, the solutions are divided into three groups: feasible solutions, which are solutions that were able to sustain the seismic action; infeasible solutions, so defined by failing any constraint, particularly the seismic action; and Pareto-optimal solutions, which are defined by being non-dominated solutions, simultaneously for both objectives, by any other solution in the entire population set.

The Pareto-optimal front (POF) is the set of all Pareto-optimal solutions, represented by the blue dots, in the objective space. It is clear from the POF that there exists a knee-region located between x-axis values of 30,000 and 60,000. The knee-region in terms of multi-objective optimization is a region before and after which a small gain in one objective implies a large loss in the other. It is therefore an ideal region for choosing a smaller set of solutions from the POF. It is also clear, from the figure, that solutions with costs in the knee-region range vary significantly in terms of performance, that is, the solutions costing close to 30,000 have performance values ranging from 0.010 to −0.020. It is, therefore, crucial to be able to understand the factors that influence that variance in performance for solutions with equal costs. The performance, ec-ecu, corresponds to the difference between the concrete's maximum compressive strain at the critical sections of the piers (ec) and the concrete's ultimate compressive strain (ecu), for a given bridge solution. Positive values of performance correspond to having a larger absolute value of ecu compared to ec, which means that the ultimate compressive strain was not reached in the critical sections of any pier. Conversely, a negative value means that the value of ecu was reached at least

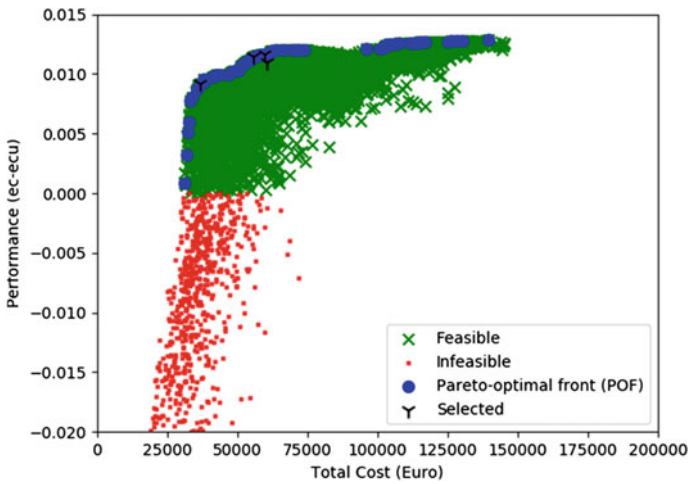

Fig. 3 Cost versus Performance objectives. All analyzed solutions in the objective-space identified as feasible or infeasible, with POF solutions highlighted

in one of the piers' critical sections at a given instant of the analysis, thus rendering the solution infeasible.

From the knee region, three solutions are chosen to illustrate the results in the decision-space, i.e., in the space of the design variables. A fourth solution, which is sub-optimal, i.e. does not belong to the POF, is also presented. This fourth solution has similar performance to the three optimal solutions and is presented because it takes different variable values and significantly different dynamic behavior. The four solutions are presented in Table 2 and Fig. 4.

The POF solutions (A, B and C) have pinned connections for piers in Group 1 and monolithic connections for the other pier groups. Furthermore, the pier groups closer to the center of the bridge (Groups 3 and 4) have substantially more flexural steel than Groups 1 and 3. The design of solutions A, B and C is done with stiffer piers closer to the center of the bridge and more flexible piers closer to the abutments. This is the opposite of solution D, which has monolithic connections for Groups 1, 2 and 3 and pinned connections for Group 4. Additionally, in the case of solution D, Group 4 piers (central piers) have very low flexural steel, which together with the pinned connections make very flexible piers. Conversely, Group 3 piers are very stiff, with 3.2% of flexural steel. The reason for both design schemes is that both promote different bridge behavior. Solutions A to C, increase stiffness of central piers (Groups 3 and 4) and the result is a THDP closer to a third vibration mode, with little displacement at the center of the bridge and large displacement at the ¼ and ¾ positions. Therefore, the stiffer short piers have less displacement demand even though they also have smaller ultimate displacements. For solution D, on the other hand, the design increases the stiffness of long piers and decreases the stiffness of short piers. The resulting THDP is close to a first mode and the short central piers, due to the low flexural steel and pinned connections have large ultimate displacement. At the same time, the large stiffness of Group 3 piers controls the amplitude of the THDP, thus limiting the displacement demand to the flexible central piers (Group 4).

4.2 Classification Tree Results

The behavior of the bridge is distinctively non-linear, with the design of each pier not only influencing its own displacement demand, but also the displacement demand of other piers and the global dynamic behavior of the bridge. This non-linear behavior makes the design of the bridge somewhat difficult. The optimization procedure in the previous section not only provides a series of possible solutions, but is also an efficient sampling tool, obtaining solutions with a high likelihood of being feasible solutions, as the algorithm's search progresses. The entire population of analyzed solutions obtained during the optimization can be used afterwards to define which variables are more important to obtain solutions with good seismic behavior. To that end, the use of classification trees, coupled with variable selection algorithms can be used to create a surrogate model, which can be used as a first approach to obtain a feasible solution.

Table 2 Variables from four solutions, where solutions A to C are from the knee-region of the POF, and solution D is a sub-optimal solution with good performance

	Pier-deck connections				Flex. steel (%)						
Id	Gr.1	Gr.2	Gr.3	Gr.4	Gr.1	Gr.2	Gr.3	Gr.4	Diam. (m)	Cost (euros)	Performance (ecu-ec)
A	2	1	1	1	0.60	1.15	1.55	2.90	1.525	55,844	0.0114
B	2	1	1	1	0.60	1.80	2.50	2.45	1.475	59,761	0.0117
C	2	1	1	1	0.65	0.85	1.10	2.30	1.3	36,588	0.0092
D	1	1	1	2	0.65	1.30	3.20	0.75	1.525	60,292	0.0110

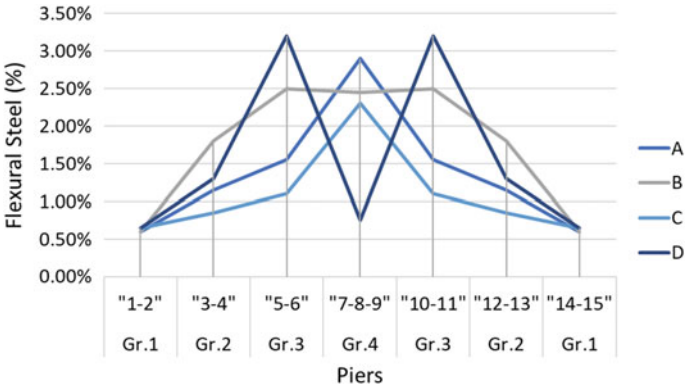

Fig. 4 Flexural steel distribution along the bridge for each pier group and regarding the four chosen solutions

In addition to the design variables or decision space, a few indicators have been added such as effective stiffness of the piers in sections of the bridge, sum of the piers' effective stiffness divided by length of the bridge and normalized axial force in the piers.

A classification tree groups all the instances in a data set according to predetermined classes. In this case, two classes were defined as "FAIL" and "OK", characterizing instances that failed to sustain the earthquake action and instances that resisted the earthquake action, respectively. The classification tree chooses the variables to perform each split according to information gain, i.e., at each branch the variable that best separates the data set is chosen, until reaching the leaf node, which classifies the instance according to one of the predefined classes. The obtained classification tree is shown in Fig. 5. The attributes that best divide the instances are, above all others, Kt/L and Nnorm. The first is total pier effective stiffness per bridge length, and the second one is normalized axial force in the piers. The resulting tree was obtained through a tenfold cross validation process with the 6894 instances in the data set. A tenfold cross-validation process consists in the data set being divided into 10 equal-sized sub-sets which are used to train and test the tree in 10 iterations. At each iteration a different subset is used to test the tree that was generated with the other 9 subsets. The final tree is the result of all ten iterations. The tree is concise, with only 4 levels and 13 nodes, and has high accuracy, with 96.03% correctly classified instances, as seen in Table 3a. In Table 3b the tree's confusion matrix is given, where correctly and incorrectly classified instances per class are displayed.

The tree provides an intuitive guide for design. Starting from the root node, the tree divides solutions based on the Kt/L (total pier effective stiffness per bridge length), which is the feature that best separates the two classes, "OK" and "FAIL". At the root node, solutions with a ratio Kt/L larger or equal to 723.5 kN/m^2 belong to the right-hand side of the tree where most solutions belong to the "OK" class, that is, are feasible (except for some solutions where the short central piers have monolithic connections, Conn4 < 1.5). On the other hand, solutions with Kt/L lower

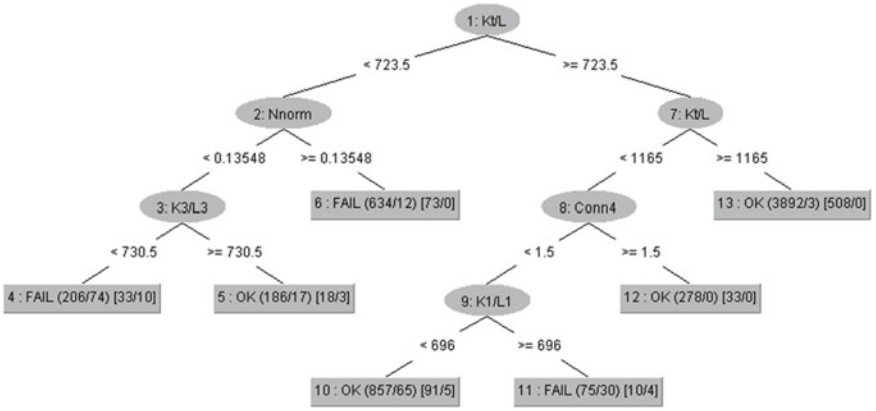

Fig. 5 Classification tree after pruning and attribute selection. Kt/L-total pier effective stiffness divided by total bridge length; Nnorm—Normalized axial force; K3/L3—effective stiffness of Group 3 piers normalized by length of Group 3; Conn4—Pier/deck connections for Group 4 piers

Table 3 Classification tree's **a** accuracy and **b** confusion matrix

Correctly classified instances	6620	96.03%
Incorrectly classified instances	274	3.97%

a)

a	b	←classified as
838	156	a = Fail
118	5782	b = OK

b)

than 723.5 kN/m^2 are on the left-hand side of the tree, which mean they are more likely to be unfeasible, except if the normalized axial force (Nnorm) is under 13.5% and the normalized effective stiffness of the group 3 piers (K3/L3) is above a certain threshold (730.5 kN/m^2). The tree shows that the design engineer should focus on total effective stiffness, and then consider checking normalized axial force and the connection of the Group 4 piers (short central piers), since these seem to be the features with larger importance, which makes sense intuitively.

5 Conclusions

Irregular structures are both difficult to analyze and design, especially if they are prone to having very non-linear behavior. This is the case with long irregular bridges. In this work, a methodology is presented composed by two procedures performed by machine learning algorithms, genetic algorithms and classification trees, applied to the case study of a long irregular bridge. The first algorithm performs an optimization of the pier design variables for earthquake resistance, while the second makes use of

all analyzed solutions, generated in the first procedure, as input to create a surrogate model that defines important variables and classifies the solutions according to their ability to resist the earthquake. The obtained results are very useful in defining strategies to design irregular bridges and allow to focus on specific characteristics of the structure to assess whether a design solution is good or not, without having to perform a full NDA analysis. The application of this methodology to many different case-studies can produce an ensemble of classification trees that can be used as surrogate models in preliminary design stages. The possibilities and applications are numerous and make sense in any situation where the non-linear and complex nature of the problem hinders the ability to easily analyze or design a solution. Furthermore, these methodologies can be used to confirm or even find new design rules that are usually employed and are associated with engineering design experience.

5.1 Future Works

In the next studies, the idea is to apply these methodologies to several case-studies, concerning bridges with different typologies and irregularities, and seeing the classification accuracy of trees on bridges with different typologies. Also, analyzing the viability of using kriging models or regression trees instead of nonlinear analysis during the optimization procedure.

Acknowledgements We acknowledge CERIS/DECivil from IST for all the support.

References

1. Kappos AJ, Saiidi MS, Aydinoglu MN, Isakovic T (2012) Seismic design and assessment of bridges, inelastic methods of analysis and case studies. In: Geotechnical, geological and earthquake engineering, vol 21. Springer, New York
2. Deb K (2001) Multi-objective optimization using evolutionary Algorithms. Wiley, New York
3. Deb K, Pratap A, Agarwal S, Meyarivan T (2002) A fast and elitist multiobjective genetic algorithm: NSGA-II. IEEE Trans Evol Comput 6(2):182–197
4. Camacho VT, Horta N, Lopes M, Oliveira CS (2020) Optimizing earthquake design of reinforced concrete bridge infrastructures based on evolutionary computation techniques. Struct Multidisc Optim 61:1087–1105. https://doi.org/10.1007/s00158-019-02407-3
5. CEN (2005) EN 1998–2: Eurocode 8: Design of structures for earthquake resistance—Part 2: Bridges. CEN—European Committee for Standardisation
6. Frank E, Hall MA, Witten IH (2016) The WEKA Workbench. Online Appendix for "Data Mining: Practical Machine Learning Tools and Techniques". Morgan Kaufmann
7. Rokach L, Maimon O (2014) Data mining with decision trees. Theory and applications. World Scientific

8. CEN (2005) EN1998–1: Eurocode 8: Design of structures for earthquake resistance—Part 1: General rules, seismic actions and rules for buildings. CEN—European Committee for Standardisation
9. McKenna F, Fenves G (1999) OpenSEES—open system for earthquake engineering simulation. The Regents of the University of California, Berkeley, CA

The Slenderness of Buildings in Plan as a Structural Regularity Criterion

Grigorios E. Manoukas and Asimina Athanatopoulou

1 Introduction

According to modern seismic codes all buildings are categorized into being regular or irregular in plan and in elevation. This distinction influences crucial aspects of the seismic design such as the structural modelling, the selection of analysis method and the value of the behavior factor. One of the criteria for regularity in plan adopted by some codes (e.g. [1, 2]) prescribes an upper limit of the slenderness of buildings in plan, namely the ratio L_{max}/L_{min}, where L_{max} and L_{min} are the larger and smaller in plan dimension respectively. Obviously, this criterion, along with others, aims to ensure that the floor slabs behave as rigid diaphragms and are able to transmit and distribute the lateral loads to the vertical structural elements. Furthermore, such a behavior permits the simplification of the structural model of the buildings and leads to the reduction of the computational effort.

The in-plane function of floor slabs has been investigated in the past by many researchers (e.g. [3–7]). All these investigations concluded that the deformability of floor slabs depends on several parameters such as the slenderness, the slab thickness and shape, the configuration of the lateral load resisting system, the relative stiffness of the vertical elements to the in-plane floor stiffness and the size and distribution of openings. As a consequence, it is very difficult to define efficient quantitative criteria in order to identify whether the rigid diaphragm assumption is reliable or not. Thus, the seismic codes use simplified criteria which take into account only some of the aforementioned parameters.

G. E. Manoukas (✉) · A. Athanatopoulou
Aristotle University, Thessaloniki, Greece
e-mail: grman@civil.auth.gr

A. Athanatopoulou
e-mail: minak@civil.auth.gr

R. Bento et al. (eds.), *Seismic Behaviour and Design of Irregular and Complex Civil Structures IV*, Geotechnical, Geological and Earthquake Engineering 50,
https://doi.org/10.1007/978-3-030-83221-6_9

In particular, Eurocode 8 [1] adopts (among others) the following criterion: "the slenderness $\lambda = L_{max}/L_{min}$ of the building in plan shall be not higher than 4, where L_{max} and L_{min} are respectively the larger and smaller in plan dimension of the building, measured in orthogonal directions". Furthermore, draft 3 of the revised version of the code [8] specifies that "this rule does not pertain where the number of lines of primary seismic structures perpendicular to the long side of a building is $>0.5\lambda$".

The objective of the present study is the evaluation of the aforementioned structural regularity criterion in both its original and its revised form. For this purpose, a series of reinforced concrete buildings with various in plan slenderness values are analyzed by means of response spectrum analysis using two alternative models for the in-plane stiffness of floor slabs: (i) rigid diaphragm and (ii) shell elements which is considered as the 'exact' model. The relative values of the horizontal displacements of selected points resulting from the two models are used as a measure of the reliability of the rigid diaphragm assumption and of the adequacy of the slenderness limit specified by the code. Besides, the influence of other parameters such as the number of storeys, the relative stiffness of the structural elements and the number of primary structural elements perpendicular to the long side of the buildings is examined. The whole study leads to the derivation of interesting conclusions concerning the efficiency of the slenderness criterion and designates the directions of possible modifications.

2 Structural Modelling and Analysis

A total of 36 reinforced concrete buildings with various floor plans, number of storeys and structural configurations is examined. These buildings are not intended to represent any specific kind of real structures. They are selected in order to be suitable for the objectives of the present study. Each building is characterized by a string symbol comprising one letter and two numbers separated by a dash. The meaning of the symbols is as follows:

- The letter (A to F) indicates the floor plan of each building (Fig. 1). The slenderness $\lambda = L_{max}/L_{min}$ of floor slabs is 2.5 (A), 4 (B) or 5.5 (C, D, E, F).
- The first number (2 or 4) indicates the number of storeys.
- The second number (1, 2 or 10) is a modification factor used for the amplification of stiffness of selected vertical structural components (C1, C2, W1 in Fig. 1).

For example, the symbol B4-2 corresponds to a four storey building with the floor plan B shown in Fig. 1, in which the actual stiffness of components C1, C2 and W1 is multiplied by 2.

All storey heights are 3 m. The slab thickness is equal to 15 cm which is the usual dimension in common buildings in Greece. All beams have a height of 60 cm and a thickness of 25 cm. The columns are square shaped with dimension of 30 cm. The length of the walls is equal to 1 m (W1–W7) or 1.5 m (W4) and their thickness is equal to 25 cm. All the vertical resisting elements are fixed at base. The mass of each floor is taken equal to 1.5 t/m^2.

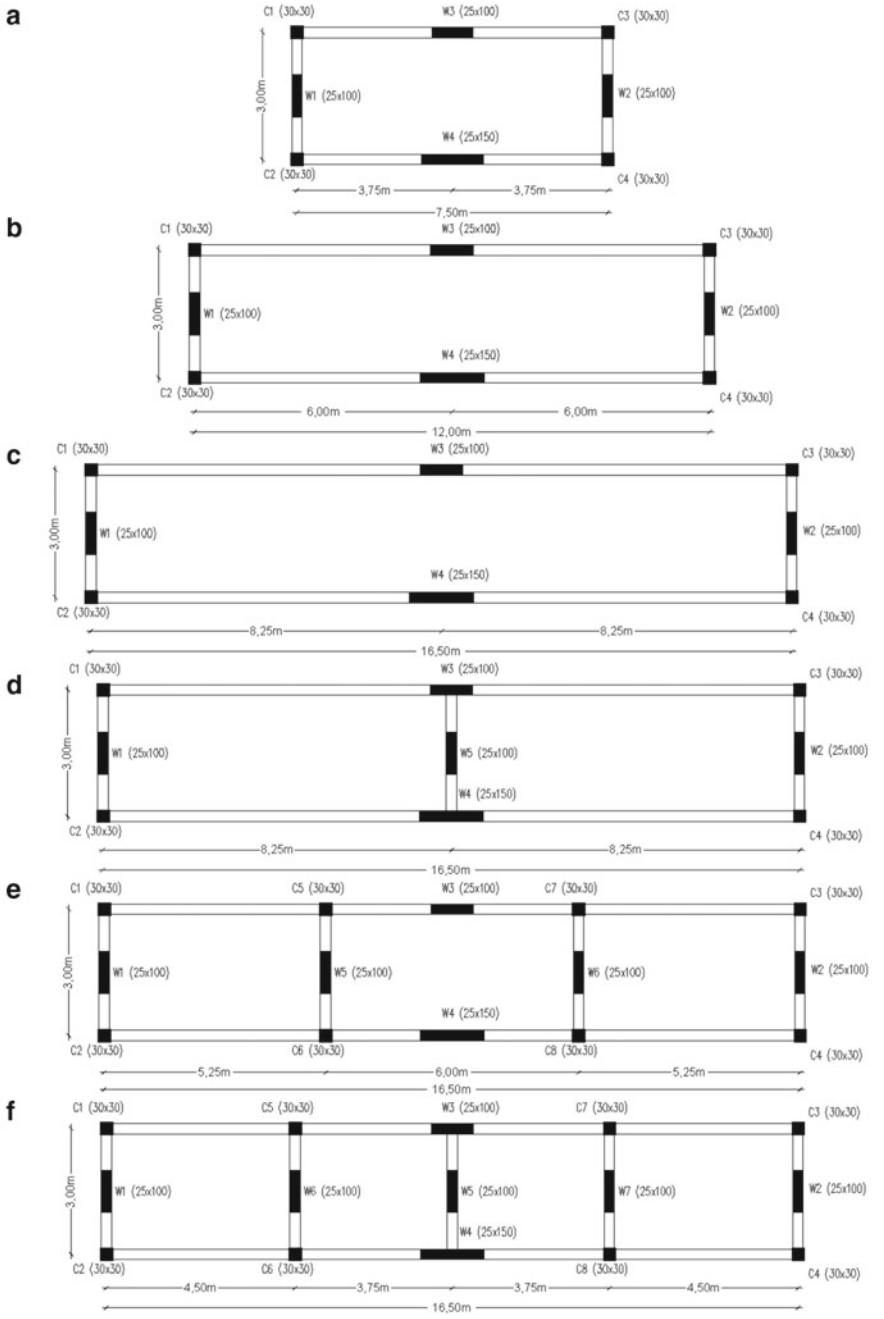

Fig. 1 Floor plans of the analyzed buildings

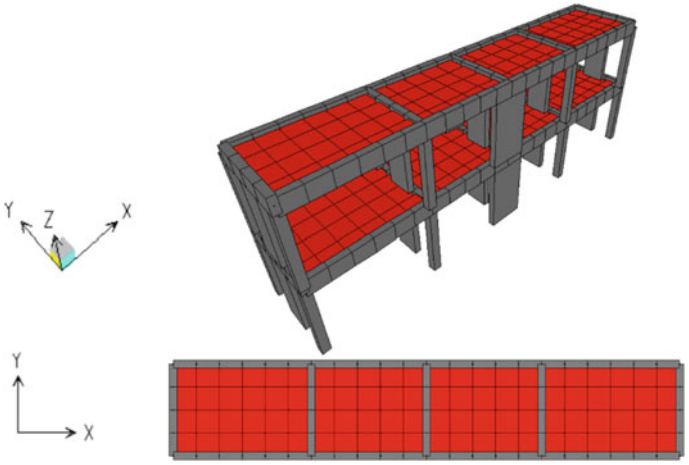

Fig. 2 Model of building F2-1 with shell elements

For each building two alternative options for the simulation of in-plane stiffness of floor slabs are adopted:

- Rigid diaphragms, utilizing the relevant feature available in the software used. The storey masses along horizontal axes as well as the storey mass moments of inertia around vertical axis are concentrated in the geometrical center of the plan.
- 4-node shell elements, which is considered as the 'exact' model. The storey masses are uniformly distributed on the slabs (masses along vertical axis included). The dimensions of shell elements are 75 × 75 cm, although a coarser discretization mesh would be adequate for the estimation of horizontal displacements [7, 9]. This choice ensures that the nodes of the discretization mesh include all connection points of vertical structural elements with the diaphragms. Indicatively the model of building F2-1 in the structural analysis program SAP 2000 is shown in Fig. 2.

The natural periods resulting from the two alternative options nearly coincide to each other. The periods T_y of the modes which dominate the response for seismic excitation along the short side of the plan are tabulated in Table 1.

All buildings are analyzed by means of response spectrum analysis and the displacements of selected points resulting from the two alternative models are estimated. In order to identify whether the rigid diaphragm assumption is reliable, the following criterion adopted by Eurocode 8 [1] is applied: 'The diaphragm is taken as being rigid, if, when it is modelled with its actual in-plane flexibility, its horizontal displacements nowhere exceed those resulting from the rigid diaphragm assumption by more than 10% of the corresponding absolute horizontal displacements in the seismic design situation'. For the application of this criterion, the percentages of displacements exceedance (p_i) for each point i of a diaphragm are calculated from the following relation:

Table 1 Natural periods T_y (s)

Building	Natural period T_y		Building	Natural period T_y		Building	Natural period T_y	
	Shell Elements	Rigid diaphragm		Shell elements	Rigid diaphragm		Shell elements	Rigid diaphragm
A2-1	0.118	0.120	A2-2	0.111	0.112	A2-10	0.103	0.104
A4-1	0.268	0.277	A4-2	0.256	0.265	A4-10	0.235	0.241
B2-1	0.153	0.153	B2-2	0.144	0.143	B2-10	0.132	0.130
B4-1	0.348	0.361	B4-2	0.334	0.346	B4-10	0.310	0.319
C2-1	0.185	0.179	C2-2	0.175	0.168	C2-10	0.162	0.154
C4-1	0.412	0.427	C4-2	0.397	0.409	C4-10	0.368	0.377
D2-1	0.141	0.140	D2-2	0.136	0.134	D2-10	0.132	0.129
D4-1	0.310	0.313	D4-2	0.304	0.306	D4-10	0.294	0.296
E2-1	0.126	0.126	E2-2	0.123	0.123	E2-10	0.119	0.118
E4-1	0.286	0.292	E4-2	0.281	0.286	E4-10	0.272	0.276
F2-1	0.110	0.111	F2-2	0.108	0.108	F2-10	0.106	0.106
F4-1	0.250	0.252	F4-2	0.247	0.249	F4-10	0.243	0.244

$$p_i(\%) = 100\,\frac{u_{yi,se} - u_{yi,rd}}{u_{yi,rd}} \tag{1}$$

where $u_{yi,se}$, $u_{yi,rd}$ are the maximum absolute displacement of point i along the short side of the buildings (direction y) resulting from the shell elements and the rigid diaphragm model respectively. The maximum value of p_i ($maxp_i$) for all points of a diaphragm is compared to the limit (10%) prescribed by Eurocode 8. Negative value of $maxp_i$ means that the rigid diaphragm assumption is conservative. Positive value of $maxp_i$ below or above the limit of 10% means that the rigid diaphragm assumption is acceptable or unacceptable respectively.

Given that according to the aforementioned criterion only the relative values of displacements resulting from the two alternative models are important, the use of a typical 'code' response spectrum is not necessary. Hence, in the framework of the present study, a simple response spectrum with a constant value of spectral pseudo-acceleration equal to 10 m/s^2 is applied. The seismic excitation is considered to act concurrently along two orthogonal directions and the directional combination is conducted using the Square Root of the Sum of the Squares (SRSS) rule. For rigid diaphragm models all vibration modes (6 or 12) are taken into account, while for shell elements models the first 12 modes. In all cases the modal superposition is conducted using the Complete Quadratic Combination (CQC) rule.

3 Results and Discussion

In Table 2 the points where the maximum p_i occurs along with the relevant value $maxp_i$ for all diaphragms are tabulated. Table 2 leads to the derivation of interesting conclusions which become more apparent with the aid of Figs. 3, 4, 5, 6 and 7.

In Figs. 3 and 4 the maximum values of p_i ($maxp_i$) for all diaphragms of all buildings are shown. From these Figs. two main observations can be made: (i) $maxp_i$ decrease from the lower to the higher floors of each building and (ii) $maxp_i$ of 4-storey buildings are always below the limit of 10% specified by Eurocode 8, regardless of the slenderness ratio and any other parameter influencing the behavior of the diaphragms. The latter observation indicates that probably the slenderness criterion specified by Eurocode 8 should not pertain for buildings where the number of storeys exceeds a limit.

Concerning the influence of the slenderness ratio, as it is expected, the values of $maxp_i$ increase with increasing λ. This becomes clear from Fig. 5, where each curve illustrates the variation of $maxp_i$ with respect to λ, while the other parameters (number of storeys, number and relative stiffness of vertical structural elements) remain constant. For example, the curve entitled "2-storey, mf = 1" corresponds to 2-storey buildings in which the stiffness of components C1, C2, W1 is multiplied by a modification factor (mf) equal to 1, namely to buildings A2-1, B2-1 and C2-1. It is worth noticing that compliance with the upper limit of slenderness ratio ($\lambda \leq 4$) prescribed by Eurocode 8 does not ensure the diaphragmatic behavior of the slabs, since $maxp_i$ can exceed the limit of 10% in case of major difference between the stiffness of vertical structural elements ("2-storey, mf = 10" curve).

The importance of the relative stiffness of vertical elements is highlighted in Fig. 6, where each curve illustrates the variation of $maxp_i$ with respect to the modification factor applied for the amplification of components C1, C2 and W1 stiffness, while the other parameters (slenderness ratio, number of storeys, number of vertical structural elements) remain constant. For example, the curve entitled "2-storey, $\lambda = 2.5$" corresponds to 2-storey buildings with slenderness ratio (λ) equal to 2.5, namely to buildings A2-1, A2-2 and A2-10. It is obvious that $maxp_i$ increases with increasing value of the stiffness modification factor used.

In Fig. 7 the influence of the number of dual frames (nf) perpendicular to the long side of the buildings is examined. Each curve illustrates the variation of $maxp_i$ with respect to nf, while the other parameters (number of storeys, stiffness modification factor, slenderness ratio equal to 5.5) remain constant. For example, the curve entitled "2-storey, mf = 1" corresponds to 2-storey buildings with slenderness ratio (λ) equal to 5.5 and stiffness modification factor equal to 1, namely to buildings C2-1, D2-1, E2-1 and F2-1. In general, for 2-storey buildings $maxp_i$ decreases with increasing number of frames, while for 4-storey buildings no specific trend is observed. According to draft 3 of the revised version of Eurocode 8 the slenderness criterion "does not pertain where the number of lines of primary seismic structures perpendicular to the long side of a building is greater than 0.5λ", namely $0.5 \cdot 5.5 = 2.75$ for the case examined here. Given the results shown in Fig. 7, this provision is not justified.

Table 2 Points with $maxp_i$ and relevant values (%)

Building	Floor	Point	$maxp_i$	Building	Floor	Point	$maxp_i$	Building	Floor	Point	$maxp_i$
A2-1	1	W3, W4	−0, 5	A2-2	1	W3, W4	0, 6	A2-10	1	W3, W4	1, 6
	2	W3, W4	−1, 8		2	W3, W4	−1, 1		2	W3, W4	0, 7
A4-1	1	W3, W4	−4, 0	A4-2	1	W3, W4	−3, 7	A4-10	1	C3, C4	−3, 7
	2	W3, W4	−5, 3		2	W3, W4	−5, 1		2	W3, W4	−4, 3
	3	W3, W4	−6, 1		3	W3, W4	−5, 8		3	W3, W4	−4, 9
	4	W3, W4	−6, 8		4	W3, W4	−6, 5		4	W3, W4	−5, 4
B2-1	1	W3, W4	4, 6	B2-2	1	W3, W4	6, 6	B2-10	1	W3, W4	10, 3
	2	W3, W4	3, 1		2	W3, W4	4, 6		2	W3, W4	8, 5
B4-1	1	W3, W4	−3,7	B4-2	1	W3, W4	−3, 2	B4-10	1	W3, W4	−2, 3
	2	W3, W4	−5, 1		2	W3, W4	−4, 8		2	W3, W4	−3, 6
	3	W3, W4	−6, 2		3	W3, W4	−5, 8		3	W3, W4	−4, 5
	4	W3, W4	−7, 3		4	W3, W4	−6, 8		4	W3, W4	−5, 4
C2-1	1	W3, W4	14, 5	C2-2	1	W3, W4	19, 3	C2-10	1	W3, W4	27, 9
	2	W3, W4	12, 9		2	W3, W4	16, 3		2	W3, W4	24, 4
C4-1	1	W3, W4	−1, 8	C4-2	1	W3, W4	−0, 8	C4-10	1	W3, W4	1, 0
	2	W3, W4	−3, 2		2	W3, W4	−2, 6		2	W3, W4	−0, 7
	3	W3, W4	−4, 5		3	W3, W4	−3, 9		3	W3, W4	−1, 9
	4	W3, W4	−6, 1		4	W3, W4	−5, 5		4	W3, W4	−3, 5
D2-1	1	W3, W4	7, 6	D2-2	1	W3, W4	11, 9	D2-10	1	W3, W4	17,2
	2	W3, W4	3, 0		2	W3, W4	5, 4		2	W3, W4	10, 0
D4-1	1	W3, W4	2, 4	D4-2	1	W3, W4	4, 5	D4-10	1	W3, W4	6, 8

(continued)

Table 2 (continued)

Building	Floor	Point	$maxp_i$	Building	Floor	Point	$maxp_i$	Building	Floor	Point	$maxp_i$
	2	W3, W4	−0, 5		2	W3, W4	0, 4		2	W3, W4	2, 1
	3	W3, W4	−1, 3		3	W3, W4	−0, 7		3	W3, W4	0, 7
	4	W3, W4	−2, 2		4	C1, C2	−1, 9		4	C1, C2	−0, 4
E2-1	1	C5, C6, C7, C8	2,2	E2-2	1	C5, C6	7, 1	E2-10	1	C5, C6	18, 0
	2	C5, C6, C7, C8	0,6		2	C5, C6	4, 0		2	C5, C6	12, 0
E4-1	1	C5, C6, C7, C8	−1,8	E4-2	1	C5, C6	0, 2	E4-10	1	C5, C6	3, 7
	2	C5, C6, C7, C8	−2,9		2	C5, C6	−2, 1		2	C5, C6	0, 4
	3	C5, C6, C7, C8	−3,5		3	C5, C6	−3, 0		3	C5, C6	−1, 0
	4	C5, C6, C7, C8	−4,1		4	C5, C6	−3, 8		4	C5, C6	−2, 5
F2-1	1	W3, W4	2,8	F2-2	1	W3, W4	6, 2	F2-10	1	C5, C6	14, 8
	2	W3, W4	0,3		2	W3, W4	2, 0		2	C5, C6	7, 7
F4-1	1	W3, W4	0,5	F4-2	1	W3, W4	2, 2	F4-10	1	C5, C6	5, 7
	2	W3, W4	−1,5		2	W3, W4	−0, 6		2	C5, C6	1, 8
	3	W3, W4	−1,9		3	C5, C6	−1, 3		3	C5, C6	0, 7
	4	C5, C6, C7, C8	−2,0		4	C1, C2	−1, 3		4	C5, C6	−0, 2

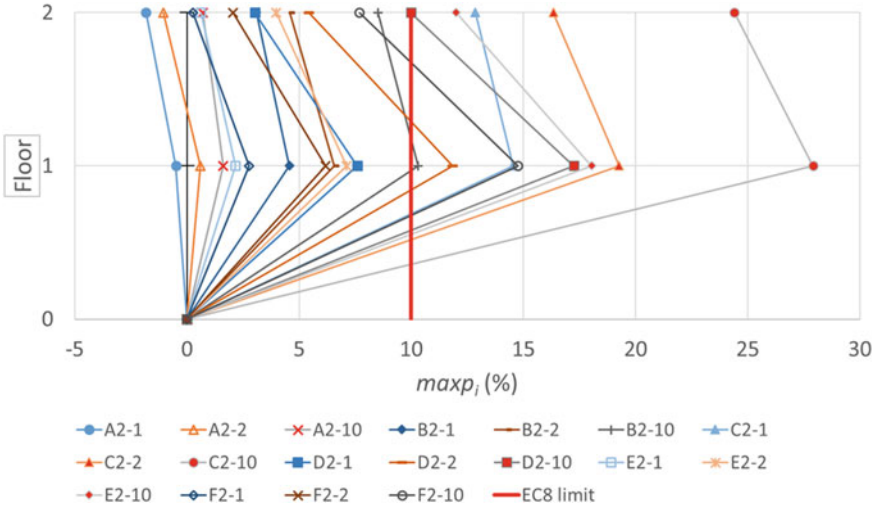

Fig. 3 *maxp$_i$* for all diaphragms (%)—2-storey buildings

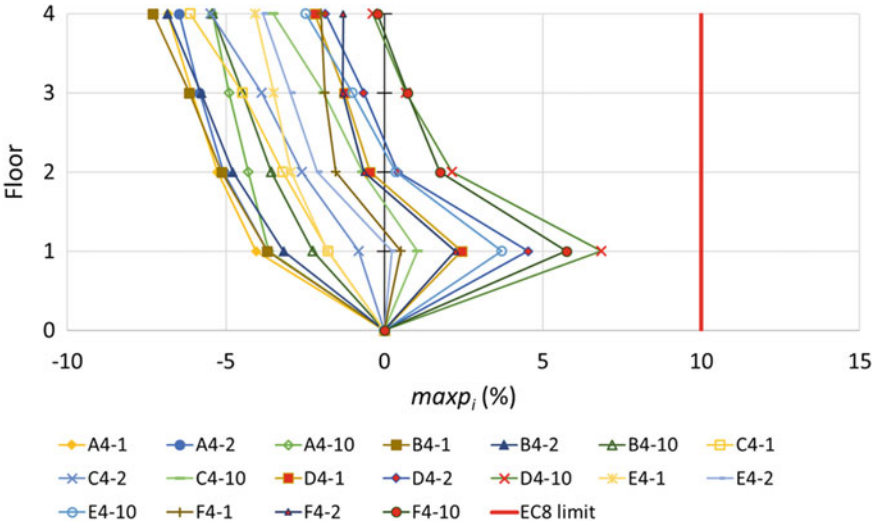

Fig. 4 *maxp$_i$* for all diaphragms (%)—4-storey buildings

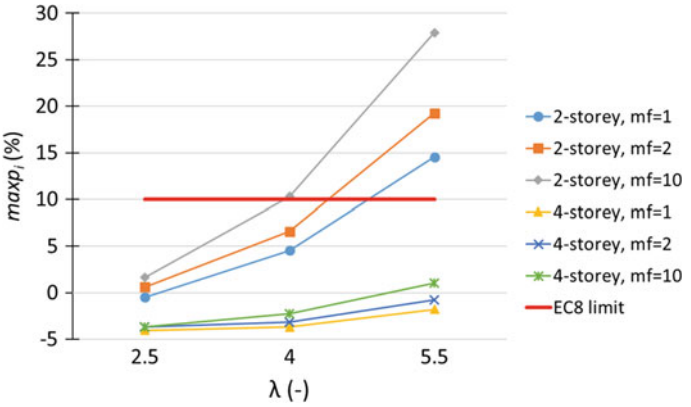

Fig. 5 Influence of slenderness ratio λ on $maxp_i$

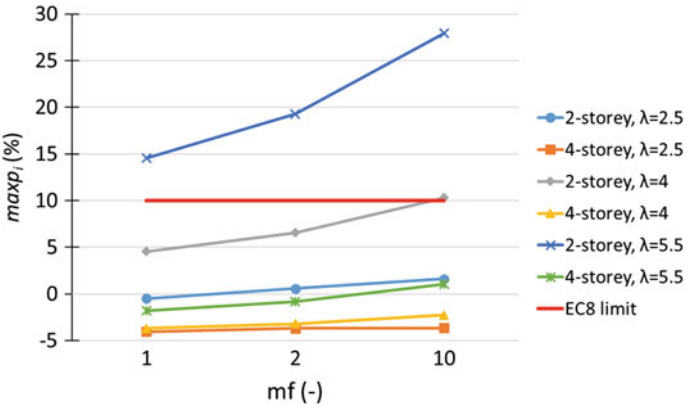

Fig. 6 Influence of relative stiffness of vertical structural elements on $maxp_i$

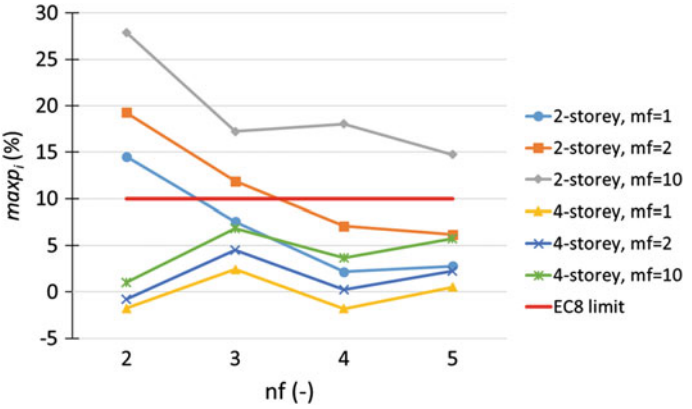

Fig. 7 Influence of number of vertical structural elements on $maxp_i$

4 Conclusions

The whole study leads to the following conclusions:

- Apart from the slenderness ratio, the in-plane behavior of slabs depends also on many other parameters such as the number of storeys, the number and the relative stiffness of vertical structural elements and others not examined here.
- The rigid diaphragm assumption tends to provide more conservative results for the higher floors of each building than for the lower ones.
- It seems that the rigid diaphragm assumption is conservative for buildings with medium and high number of storeys regardless of the slenderness ratio. Hence, the relevant regularity criterion probably should not pertain for such buildings.
- The compliance with the upper limit of slenderness ratio ($\lambda \leq 4$) prescribed by Eurocode 8 does not ensure the diaphragmatic behavior of the slabs in case of major difference between the stiffness of vertical elements. This indicates that a possible revision of this limit should be examined.
- The provision of draft 3 of the revised version of Eurocode 8 which specifies that the slenderness criterion "does not pertain where the number of lines of primary seismic structures perpendicular to the long side of a building is greater than 0.5λ", is not justified by the present study. Hence a possible elimination of this provision should be examined.

References

1. EC8-Part 1: Eurocode 8 (2005) Design provisions for earthquake resistance of structures. Part 1-1: General rules—seismic actions and general requirements for structures. ENV 1998-1. CEN, Brussels
2. Greek Seismic Code: EAK (2003) Earthquake resistant design of structures. In: Earthquake Planning and Protection Organization, Athens, Greece
3. Athanatopoulou AM (1991) A parametric study of the influence of the diaphragm flexibility in the static and dynamic analysis of multi-storey buildings. PhD Dissertation, Aristotle University of Thessaloniki
4. Kunnanth S, Panahshahi N, Reinhorn A (1991) Seismic response of RC buildings with inelastic floor diaphragms. J Struct Eng ASCE 117:1218–1237
5. Saffarini H, Qudaimat M (1992) In-plane floor deformations in RC structures. J Struct Eng ASCE 118:3089–3102
6. Ju SH, Lin MC (1999) Comparison of building analyses assuming rigid or flexible floors. J Struct Eng ASCE 125:25–39
7. Doudoumis IN, Athanatopoulou AM (2001) Code provisions and analytical modelling for the in-plane flexibility of floor diaphragms in building structures. J Earthq Eng 5(4):565–594
8. EC8-Part 1: Eurocode 8 (2019) Design of structures for earthquake resistance. Part 1-1: General rules—seismic actions and general requirements for structures. Draft 3, ENV 1998-1-1. CEN, Brussels
9. Doudoumis IN, Agouridakis I, Diamandopoulos V, Athanatopoulou AM (1996) Modelling the in-plane floor flexibility of buildings with simplified models of finite elements. In: Proceedings of 12th hellenic concrete conference, Limassol, Cyprus

Evaluation of the Effectiveness of Accidental Eccentricity in Capturing the Effects of Irregular Masonry Infills

Konstantinos Kostinakis and Asimina Athanatopoulou

1 Introduction

Reinforced Concrete (R/C) buildings with unreinforced masonry infills is a very common construction strategy in many regions characterized by high seismicity throughout the world. Nevertheless, due to the uncertainties related with the appropriate modeling of the infill panels, their effect on the R/C structural elements and, consequently their impact on the seismic behavior of the buildings is often not taken into account. Thus, the infills are usually accounted for as non-structural elements and are neglected in the process of the buildings' analytical modelling. The above approximation has been adopted by current seismic code provisions, which give only few general guidelines for the proper deal of the non-structural elements, being often insufficient, incomplete and not adequately clarified. Nevertheless, a large number of experimental and numerical researches, as well as the observation of post-earthquake damages, have shown that the masonry walls in many cases tend to interact with the surrounding structural elements when seismic loads are applied to the buildings, resulting in significant modification of the structural behavior [e.g. 1–4]. Some of the seismic codes recognize this fact, for example according to the New Zealand Society for Earthquake Engineering one of the major problems associated with the analyses of moment resisting frames is the uncertain behavior of the structure as a result of the presence of nonstructural elements, typically infill walls, which can significantly alter the structural behavior of the frame [5].

The non-uniform placement of the masonry infills is usually made for functional reasons, causing to the R/C buildings significant irregularities. Such irregularities

K. Kostinakis (✉) · A. Athanatopoulou
Aristotle University of Thessaloniki, Thessaloniki, Greece
e-mail: kkostina@civil.auth.gr

A. Athanatopoulou
e-mail: minak@civil.auth.gr

R. Bento et al. (eds.), *Seismic Behaviour and Design of Irregular and Complex Civil Structures IV*, Geotechnical, Geological and Earthquake Engineering 50,
https://doi.org/10.1007/978-3-030-83221-6_10

(in-elevation or in-plan) may cause important increase of the seismic vulnerability, or even in some cases disproportionate structural damage or collapse. This is the reason why a lot of research investigations in recent years have focused on the seismic assessment of buildings with irregular placement of masonry infills [e.g. 6–13]. Note that the EC8-1 [14] states that "strongly irregular, unsymmetrical or non-uniform arrangements of infills in plan should be avoided" (par. 4.3.4.3.1). Moreover, the same code suggests that in case of "masonry infills irregularly distributed, these irregularities may be taken into account by increasing by a factor of 2.0 the effects of the accidental eccentricity".

In the present paper the need to increase accidental torsion in nonlinear seismic analyses as a parameter to capture the effects of the infills' irregularities is further investigated through the evaluation of a 3D R/C building with masonry infills placed irregularly. The building is subjected to Nonlinear Pushover Analysis according to the EC8-1 provisions. Structural models which take into account the masonry infills as diagonal struts are analyzed. Moreover, structural models which ignore the infills, but increase the accidental eccentricity by a factor of 2.0, are considered. Finally, a comparative evaluation between the aforementioned models is carried out in order to derive useful conclusions.

2 Examined Building

2.1 Description

For the analyses conducted in the present paper a R/C building consisting of five storeys and a basement is considered. The building is located in the city of Thessaloniki (Greece) and was constructed in 1960 without following modern seismic code provisions. The plan-view of the building's storeys, as well as the dimensions and the longitudinal reinforcement of the structural elements, are shown in Figs. 1 and 2. The main load bearing structure consists of beams, columns, as well as a reinforced concrete corewall, which comprises of five wall sections with a width of 20 cm. The core's web has a transverse reinforcement of Ø8/250 and the longitudinal reinforcement of the boundary elements is 4Ø12. The longitudinal reinforcement of the beams and the columns are shown in Fig. 1, whereas the shear reinforcement of both beams and columns is stirrups Ø6/200 within both critical and non-critical regions. The slabs have a thickness of 10 cm with reinforcement of Ø10/150 along the two horizontal axes. The foundation of the building consists of individual footings and connecting beams with dimensions of 25×40 (cm), longitudinal reinforcement 4Ø14 and shear reinforcement Ø6/200. The concrete belongs to the category of B160 and the reinforcing steel to the category of S220. Analytical description of the material properties is given in Table 1. The vertical loads of the slabs are: dead load $g = 1.55$ kN/m^2 and live load $q = 2.00$ kN/m^2. The internal masonry infills have a width of 10 cm, while the perimeter ones have a width of 20 cm.

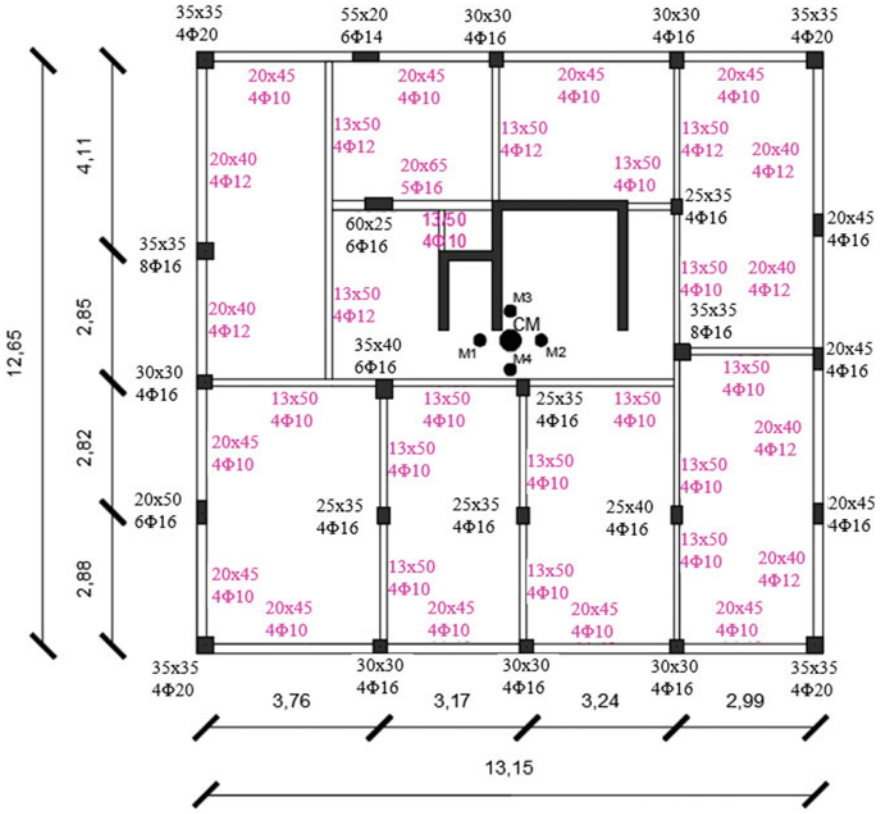

Fig. 1 Plan view of the typical storey and properties of the structural elements. CM: Centre of Mass, M1–M4: the four positions of mass according to the accidental eccentricity given by EC8-1

2.2 Elastic and Inelastic Modelling

The building presented in Sect. 2.1 was modelled in the professional program for R/C building analysis and design RA.F. [15] in order to conduct *N*onlinear *P*ushover *A*nalyses (NPA). For the modelling of the building all basic recommendations of EC8-1 [14] (e.g. diaphragmatic behavior of the slabs, rigid zones in the joint regions of beams/columns and beams/walls) were taken into account. The building was analyzed by means of NPA, as defined in EC8 [14, 16]. In order to model the nonlinear behavior of the structural elements lumped plastic hinges were placed at the column and beam ends, as well as at the base of the walls. The properties of the plastic hinges (e.g. material models, bilinear moment-rotation diagrams, post-yield stiffness) were defined according to the code provisions of EC8 [14, 16] and the Greek Code of Interventions KAN.EPE. [17].

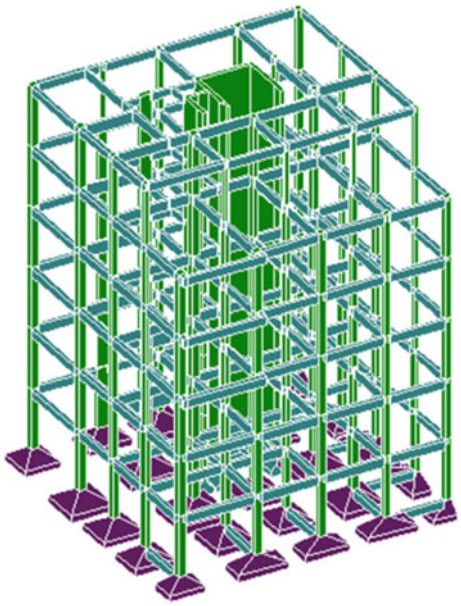

Fig. 2 Structural model of the building

Table 1 Properties of the materials

Concrete B160		Steel S220	
Modulus of elasticity (GPa)	27	Modulus of elasticity (GPa)	200
Weight (kN/m^2)	25	Weight (kN/m^2)	78.5
f_{ck} (MPa)	12	f_{yk} (MPa)	240
f_{cd} (MPa)	8	f_{yd} (MPa)	209
f_{cm} (MPa)	20	f_{ym} (MPa)	280
f_{ctm} (MPa)	1.6	ε_{ys} (‰)	1.04
ε_{c2} (‰)	−2.0	ε_{yu} (‰)	20.0
ε_{cu2} (‰)	−3.5		

2.3 Modelling of the Unreinforced Masonry Infills

The masonry infills were modelled according to the provisions of the Greek Code of Interventions KAN.EPE. [17]. More specifically, each infill was modelled as an equivalent hinged diagonal strut in compression with a given width b. It must be noted that the influence of the infills' openings on the properties of the diagonal struts was not taken into account, since their impact on the results was rather small. The nonlinear behavior of the infills was accounted for according to KAN.EPE. (par. 7.4.1) [17]. The mechanical properties of the infills were estimated using the mechanical properties of the bricks and mortar, taking appropriately into consideration the

method of masonry construction. The geometrical properties (thickness t and width b) of each strut were determined using the relative code provisions of KAN.EPE (par. 7.4.1) [17]. Moreover, The mean compressive strength of the infill walls along the direction of the diagonal $f_{wc,s}$ was estimated taking into consideration both the mean compressive strength along the vertical direction, as well as its reduction due to horizontal tensile stresses [17].

3 Analyses

3.1 Description of the Analyses Conducted

The building presented in Sect. 2 was assessed using the *N*onlinear *P*ushover *A*nalysis (NPA) according to the EC8-1 [14] provisions. The following different structural models were investigated:

- a model without taking into account the infills and using the value of the accidental eccentricity proposed by the most seismic codes (including EC8-1) $e_a = 0.05L$, where L is the floor dimension perpendicular to the direction of the seismic action
- a model without taking into account the infills, but increasing by a factor of 2.0 the accidental eccentricity (i.e. $e_a = 0.10L$), as EC8-1 proposes in par. 4.3.6.3.1
- two models with masonry infills distributed irregularly in-plan in such a way that asymmetry along X-axis is caused and taking into account the infills' effect as diagonal struts according to the modelling procedure presented in Sect. 2.3 (the models possess different degrees of asymmetry in the infills placement and more specifically the values of the mean e_{ox} over all the storeys (EC8-1-par. 4.2.3.2) are 0.15 and 0.25 respectively (Fig. 3). For these models the accidental eccentricity

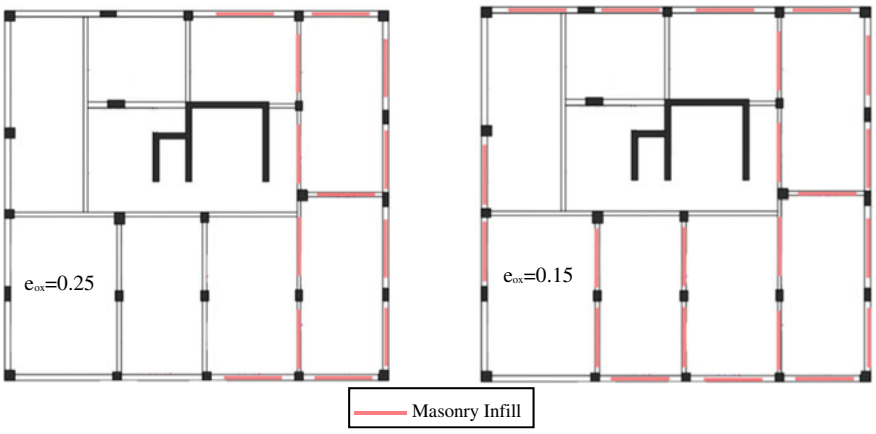

Fig. 3 Distribution of masonry infills for models with mean $e_{ox} = 0.15$ and $e_{ox} = 0.25$

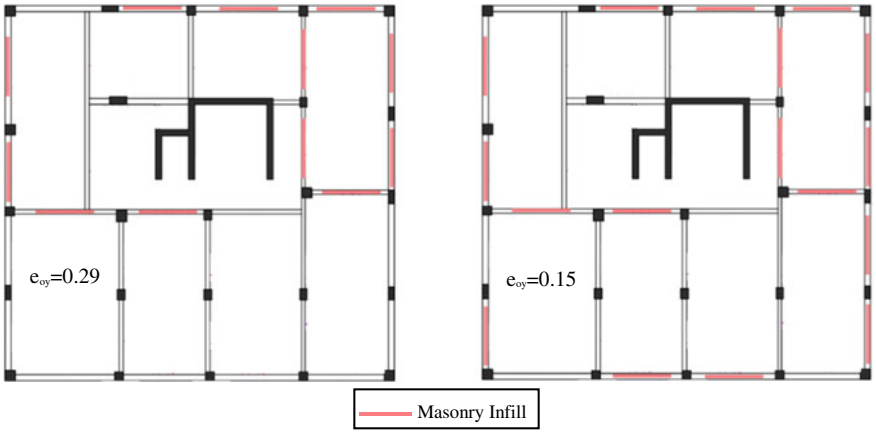

Fig. 4 Distribution of masonry infills for models with mean $e_{oy} = 0.15$ and $e_{oy} = 0.29$

proposed by the most seismic codes (including EC8-1) $e_a = 0.05L$ is taken into account.

- two models with masonry infills distributed irregularly in-plan in such a way that asymmetry along Y-axis is caused and taking into account the infills' effect as diagonal struts according to the modelling procedure presented in Sect. 2.3 (the models possess different degrees of asymmetry in the infills placement and more specifically the values of the mean e_{oy} over all the storeys (EC8-1-par. 4.2.3.2) are 0.15 and 0.29 respectively (Fig. 4). For these models the accidental eccentricity proposed by the most seismic codes (including EC8-1) $e_a = 0.05L$ is taken into account.

The above structural models were subjected to NPA and all the structural elements of each model were assessed for bending and shear according to the provisions of EC8-1 [14] and EC8-3 [16]. For the NPA the following assumptions were made:

- Limit State of Significant Damage.
- Knowledge Level of Normal Knowledge (KL2).
- Horizontal elastic spectrum as defined in EC8-1 for $\alpha_g = 0.24$ g, viscous damping 5%, ground type C.
- Two different lateral load patters: a uniform and a modal one.
- Target displacement according to the Annex B of EC8-1.
- Assessment of the capacity of each structural element according to the Annex A of EC8-3 [16].
- Combination of the effects of the seismic action's components according to the Greek Code of Interventions KAN.EPE (par. 5.4.9) [17].

3.2 Results

The following figures illustrate the results of the analyses in terms of percentages of failures, i.e. the ratios of the number of critical cross sections that fail to the whole number of the building's critical cross sections. Note that due to space restrictions only the following results are presented, which are the ones with the more pronounced results:

- Figsures 5, 6, 7 and 8 present the results for models with $e_a = 0.05L$ and $e_a = 0.10L$ and with infills distributed irregularly in-plan in such a way that asymmetry along Y-axis, under seismic actions X + 0.3Y (KAN.EPE, par. 5.4.9) for masses in positions M3 and M4 (Fig. 1) under both uniform and modal lateral loads.
- Figures 9, 10, 11 and 12 present the results for models with $e_a = 0.05L$ and $e_a = 0.10L$ and with infills distributed irregularly in-plan in such a way that asymmetry along X-axis is produced, under seismic actions Y + 0.3X (KAN.EPE, par. 5.4.9)

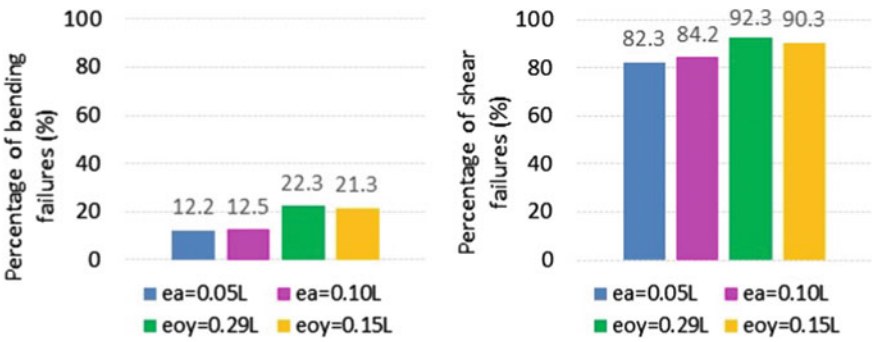

Fig. 5 Percentages of failure in case of seismic action along X-axis—Uniform load pattern—Mass position M3

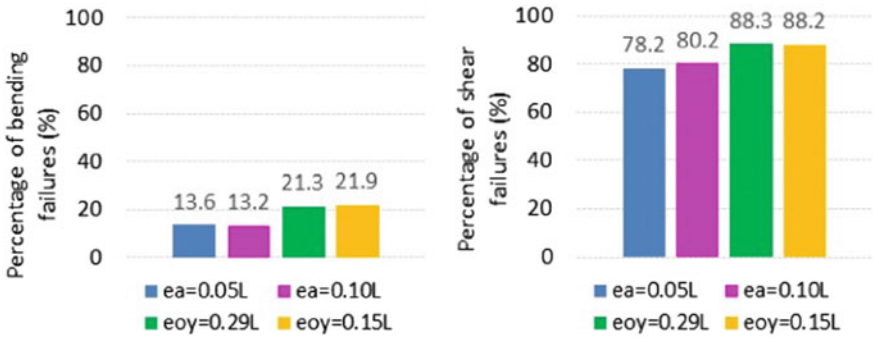

Fig. 6 Percentages of failure in case of seismic action along X-axis—Uniform load pattern—Mass position M4

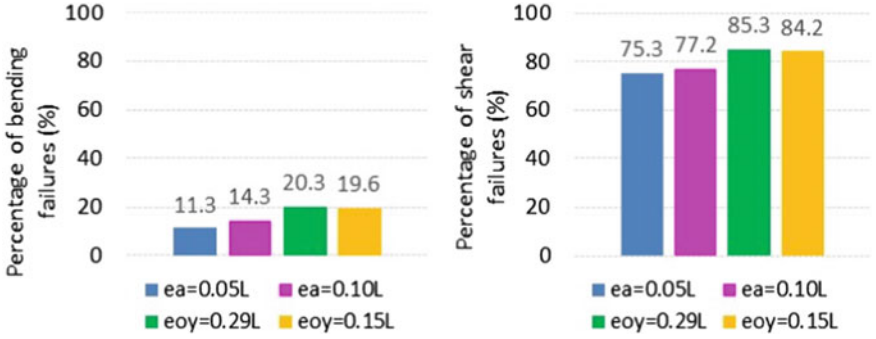

Fig. 7 Percentages of failure in case of seismic action along X-axis—Modal load pattern—Mass position M3

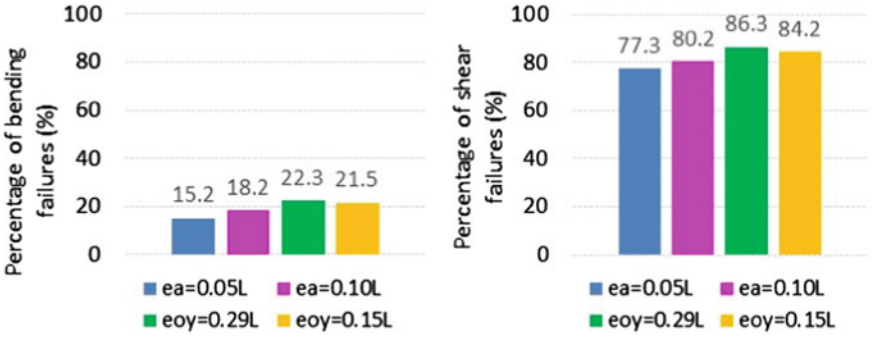

Fig. 8 Percentages of failure in case of seismic action along X-axis—Modal load pattern—Mass position M4

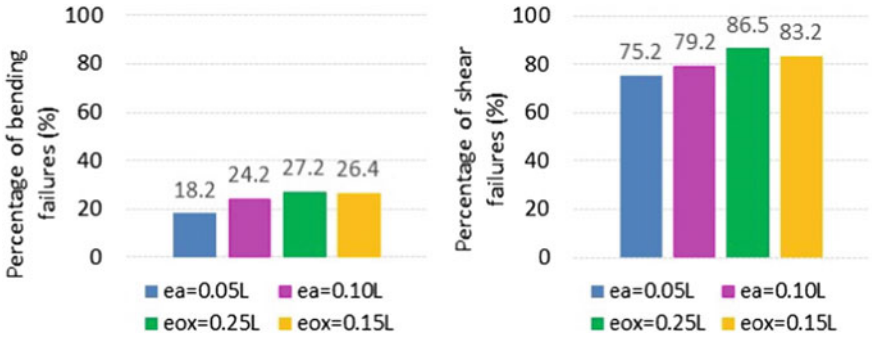

Fig. 9 Percentages of failure in case of seismic action along Y-axis—Uniform load pattern—Mass position M1

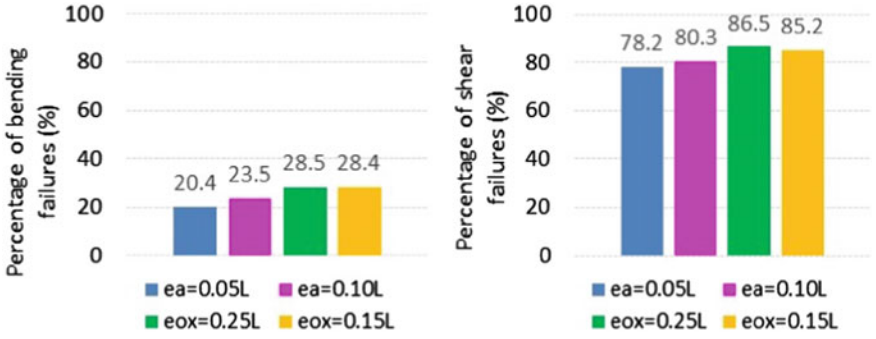

Fig. 10 Percentages of failure in case of seismic action along Y-axis—Uniform load pattern—Mass position M2

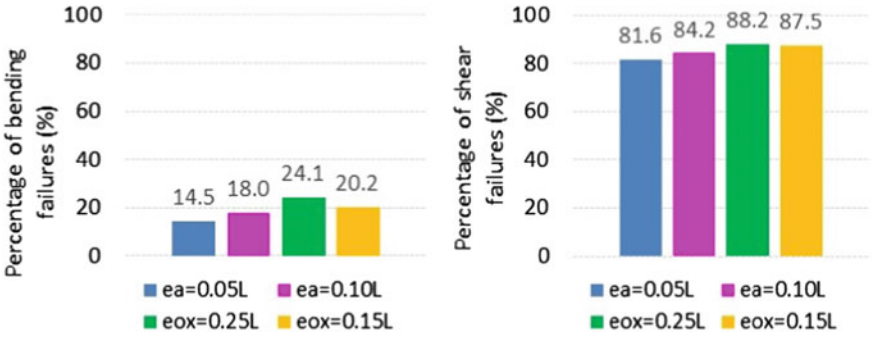

Fig. 11 Percentages of failure in case of seismic action along Y-axis—Modal load pattern—Mass position M1

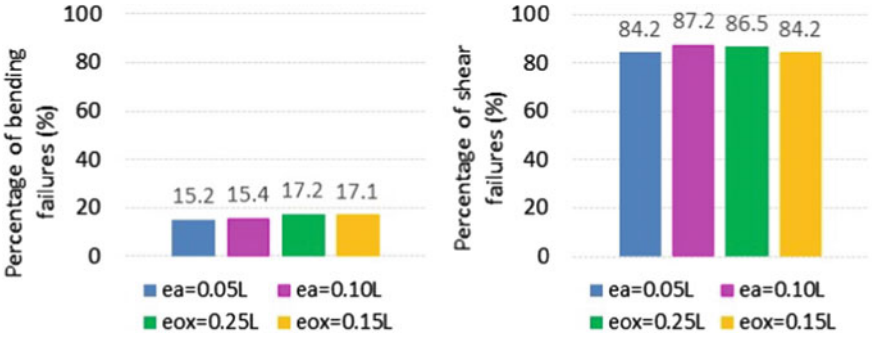

Fig. 12 Percentages of failure in case of seismic action along Y-axis—Modal load pattern—Mass position M2

for masses in positions M1 and M2 (Fig. 1) under both uniform and modal lateral loads.

From the above figures we can see that in most cases the consideration of the masonry infills in the structure's modeling leads to larger number of bending and shear failures. The analyses revealed that the number of shear failures is much larger than the one of bending failures, something which was expected since the investigated building was constructed according to old codes without seismic provisions and capacity design. Moreover, practically no difference has been noticed between the models with small and large infills' irregularities.

Considering the comparison between the models with $e_a = 0.05L$ and $e_a = 010L$, it can be seen that when the accidental eccentricity is multiplied by a factor of 2.0, as EC8 proposes, the damage is more severe (larger number of failures in the critical elements' sections). However, the difference between the two models is rather small. See for example that in case of the building under seismic action along Y-axis (modal load pattern and mass position M1) (Fig. 11) 14.5 and 81.6% of the critical frame sections have failed in bending and shear respectively when the accidental eccentricity is $e_a = 0.05L$, whereas the respective percentages in case of $e_a = 0.10L$ are 18.0 and 84.2%. This observation leads to the conclusion that the provision of EC8 which suggests increase of the accidental eccentricity in order to account for the irregular placement of the infills was proved to be effective up to a point, since it failed to capture adequately the effects of the irregularities in the infills' distribution. The adequacy of this provision depends on the analysis (direction of the seismic action, load pattern, mass position). See for example that in case of the building under seismic action along Y-axis (uniform load pattern and mass position M1) (Fig. 9) the increase of the accidental eccentricity by a factor of 2.0 led to 79.2% of shear failures compared to 75.2% for $e_a = 0.05L$, whereas when the masonry infills were taken into consideration in the model the shear failures were 86.5 and 83.2% for large and small irregularities respectively.

4 Conclusions

In the present paper the need to increase accidental torsion in nonlinear seismic analyses as a parameter to capture the effects of the infills' irregularities is investigated through the evaluation of a multi-storey 3-dimensional R/C building with irregularly placed masonry infills. The seismic assessment of the building is carried out using the Nonlinear Pushover Analysis according to the EC8-1 provisions. Based on the results of the study, the following general conclusions can be drawn:

- In most cases the consideration of the irregularly distributed masonry infills in the structure's modeling leads to larger number of bending and shear failures than the models without infill walls. However, the increase is rather small. Moreover, practically no difference has been noticed between the models with small and large infills' irregularities.

- The increase of the accidental eccentricity by a factor of 2.0, as EC8-1 proposes, leads to more severe damage for the studied buildings than the damage when the accidental eccentricity of $e_a = 0.05L$ is considered. However, this provision of EC8-1 was proved to be effective up to a level of irregular infill walls distribution, since it failed to capture adequately the effects of the irregularities in the infills' distribution for the investigated buildings.

References

1. Dolsek M, Fajfar P (2001) The effect of masonry infills on the seismic response of a four storey reinforced concrete frame—a deterministc assessment. Eng Struct 30:1991–2001
2. Fiore A, Porco F, Raffaele D, Uva G (2012) About the influence of the infill panel over the collapse mechanisms actived under pushover analyses: two case studies. Soil Dyn Earthq Eng 39:11–22
3. Ricci P, De Ricci MT, Verderame GM, Manfredi G (2013) Influence of infill distribution and design typology on seismic performance of low-and mid-rise RC buildings. Bull Earthq Eng 11:1585–1616
4. Ricci P, De Luca F, Verderame GM (2010) 6th April 2009 L' Aquila earthquake, Italy: reinforced concrete building performance. Bull Earthq Eng 9(1):285–305
5. Assessment and Improvement of the Structural Performance of Buildings in Earthquakes (2017) New Zealand Society for Earthquake Engineering, New Zealand
6. Das S, Nau JM (2003) Seismic design aspects of vertically irregular reinforced concrete buildings. Earthq Spectra 19(3):455–477
7. Manfredi G, Ricci P and Verderame GM (2012) Influence of infill panels and their distribution on seismic behavior of existing reinforced concrete buildings. Open Const Build Technol J 6 (Suppl 1-M15):236–253
8. Mondal G, Tesfamariam S (2014) Effects of vertical irregularity and thickness of unreinforced masonry infill on the robustness of RC framed buildings. Earthq Eng Struct Dynam 43:205–223
9. Morfidis K, Kostinakis K (2017) The role of masonry infills on the damage response of R/C buildings subjected to seismic sequences. Eng Struct 131:459–476
10. Barnaure M (2017) Structural irregularities in RC frame structures due to masonry enclosure walls. In: Proceedings of the 8th European workshop on the seismic behaviour of irregular and complex structures, Bucharest, Romania
11. Kostinakis K (2018) Impact of the masonry infills on the correlation between seismic intensity measures and damage of R/C buildings. Earthq Struct 14(1):55–71
12. Kostinakis K, Vasileiadis V and Athanatopoulou A (2018) Incremental dynamic analysis of R/C buildings with various ditributions of masonry infills. In: Proceedings of the 16th European conference on earthquake engineering, Thessaloniki, Greece, paper No. 10631
13. Kostinakis K and Athanatopoulou A (2020) Effects of in-plan irregularities caused by masonry infills on the seismic behavior of R/C buildings. Soil Dyn Earthq Eng 129:105598
14. EC8-Part 1: Eurocode 8 (2005) Design provisions for earthquake resistance of structures. Part 1-1: General rules—Seismic actions and general requirements for structures. ENV 1998-1. CEN, Brussels
15. TOL-Engineering Software House (2020) RAF Version 7.1.0.2: Structural analysis and design software, Iraklion, Crete, Greece.
16. EC8-Part 3: Eurocode 8 (2005) design provisions for earthquake resistance of structures. Part 3: Assessment and retrofitting of buildings. EN 1998-3. CEN, Brussels
17. Code of interventions (KAN.EPE.) (2013) Athens, Greece

Design of Irregular Frames with Fluid Viscous Dampers Using Optimization

Ohad Idels and Oren Lavan

1 Introduction

Energy dissipation devices are proved as an efficient design strategy to control structural responses. They absorb some of the seismic input energy, and by that reduce the displacements, floor accelerations, and plastic deformations. Buildings with elevation irregularity may be vulnerable in the region of irregularity, because of the drastic changes in the strength, stiffness and/or mass in this area. In particular, large inter-story drifts are expected at these specific stories. The use of supplemental damping devices in such irregular buildings may be the answer for these large inter-story drifts. There is a wide variety of damping devices, among them the very popular Fluid Viscous Dampers (FVDs). FVDs have been successfully utilized for the retrofitting of existing structures and new buildings where high-performance level were desired. One of the main advantages the FVDs hold is the out-of-phase effect, in which the peak forces developed in the force-resisting and damping systems are not acting at the same time. This effect may play a key role in the design of irregular steel Moment-Resisting Frames (MRFs) with FVDs, due to the large forces developed in the elements and FVDs in the region of irregularly. As mentioned above, irregular buildings may be exposed to large deformations under seismic excitation. Moreover, evaluation of their dynamic response is quite a challenge. Therefore, the design of these structures is far from being straightforward or intuitive, and it may result in over design of the MRF and FVDs properties.

O. Idels · O. Lavan (✉)
Faculty of Civil and Environmental Engineering, Technion—Israel Institute of Technology, Technion City, Haifa, Israel
e-mail: lavan@technion.ac.il

O. Idels
e-mail: ohadidels@campus.technion.ac.il

R. Bento et al. (eds.), *Seismic Behaviour and Design of Irregular and Complex Civil Structures IV*, Geotechnical, Geological and Earthquake Engineering 50,
https://doi.org/10.1007/978-3-030-83221-6_11

The optimal design of MRFs with FVDs has been widely investigated to avoid over design. However, most works focused on the optimal retrofitting of an existing structure with given parameters be adding FVDs (e.g., [1–5]). In particular, Lavan and Levy [6, 7] tackled the optimal design of irregular frames. All of these studies tackled the retrofitting problem where the structural elements are known a-priori. In this case, the design variables represent only the FVDs properties as locations and damping coefficients.

The optimal design of steel MRFs without any supplemental damping devices has also been studied. Among these works, some adopted a nonlinear static procedure, the pushover analysis (e.g., [8, 9]), while others preferred to utilize a more precise analysis tool, as the Nonlinear Response History Analysis (NRHA) (e.g., [10, 11]). In the problem of the optimal design of MRFs without dampers, the design variables represent the cross-sections properties only.

A small number of works considered the design of MRFs and FVDs parameters simultaneously. Viti et al. [12], utilized the pushover analysis and the Monte Carlo simulation for the hospital retrofitting problem. Takewaki [13] and Cimellaro [14], minimized the sum of amplitudes of the transfer function to optimize both the stiffness and damping in shear frames. Lavan et al. [15] presented a procedure for the optimal design of nonlinear structures using optimal control theory. A more practical design process was suggested by Lavan [16], where the design procedure relies only on analysis tools.

The works mentioned above indeed present an important step towards the optimal design of MRFs with FVDs. Nevertheless, a formal optimization approach that considers the MRF and FVDs parameters as design variables, while accounting for the nonlinear behavior of the MRF and FVDs using NRHA, has not been implemented yet.

In this work, the optimization of the design of new MRFs with FVDs is presented. The structural analysis is carried out using NRHA, and as a result, it can capture the seismic response of complex and irregular buildings. A model of spread plasticity beam element is adopted for the MRF members, and the Maxwell model is utilized to evaluate the response of the nonlinear FVDs and their bracing systems. The optimization problem is formulated to attain a minimum cost design, accounting for both the members and FVDs cost. Several code requirements, such as “strong column weak beam” and a limit on the stability coefficient, are considered, in addition to performance constraints. For the optimization process, the well-known Genetic Algorithm (GA) is utilized. A numerical example of a five-story with elevation irregularity is presented, in which the cross-section and FVDs properties are being optimized simultaneously.

2 Problem Formulation

This section presents the formulation of the optimization problem. The optimization aims to minimize the combined cost of the MRF elements and the FVDs. Several code requirements are considered as constraints in addition to inter-story drift limitations. The design variables represent the cross-section properties of the elements, as well as the locations and damping coefficients of the FVDs. In addition, to achieve a practical design, the cross-section properties are to be selected out of standard steel tables (e.g., IPB, IPE). While the dampers are also formulated to attain practical design, that relies on two types of dampers. The dynamic response is evaluated using a NRHA, accounting for the nonlinear behavior of the MRF members and the dampers.

2.1 NRHA

To evaluate the structural response and account for the nonlinear behavior, a NRHA is utilized to solve the equations of motion (Eq. 1) numerically. The Newmark-beta integration scheme is adopted along with the Newton–Raphson algorithm. $P-\Delta$ effects are considered using a geometrical stiffness matrix [17].

$$\mathbf{M}\ddot{\mathbf{u}}(t) + \mathbf{C}_s\dot{\mathbf{u}}(t) + \mathbf{f}_s(t) + \mathbf{f}_d(t) = -\mathbf{M}\mathbf{e}\mathrm{a}_g(t) \tag{1}$$

where $\mathbf{M}$ is the mass matrix; $\mathbf{C}_s$ is the inherent damping matrix; $\mathbf{u}$ is the displacement of the degree of freedom relative to the ground; $\mathbf{e}$ is the influence vector; a_g is the ground acceleration; $\mathbf{f}_s$ is a vector of the nonlinear resisting forces of the structural elements, assessed using a spread plasticity beam element [18]; $\mathbf{f}_d$ is the vector of resisting forces of the FVDs, based on a Maxwell model and evaluated over time using the 4-order Runge–Kutta method.

2.2 Design Variables

As mention above, the design variables represent both the member and damper properties. The cross-section parameters of the members are represented by the plastic modulus (W), that is the one to be optimized. To ensure a practical design is obtained the plastic modulus is optimally selected out of a predefined standard set (Eq. 2a). The dampers are also formulated to achieve a practical design that relies on just two size groups of dampers within the structure (Eq. 2b).

$$W_i \in \{W_1; W_2; W_3; W_4; \ldots\} \tag{2a}$$

$$c_{d,j} \in \left\{0; \overline{C}_d \cdot y_1; \overline{C}_d \cdot y_2\right\} \tag{2b}$$

where W_i is the plastic modulus of the ith element, and W_1, W_2, etc., represent the plastic modulus of potential sections from standard steel tables. $c_{d,j}$ is the damping coefficient of the jth damper that can receive the following values: 0—no damper; $\overline{C}_d \cdot y_1$damper from group one; $\overline{C}_d \cdot y_2$—damper from group two. Where $\overline{C}_d$ is the maximum considered damping coefficients, and y_1, y_2 are continuous design variables that scale the damping coefficient of each group, respectively.

2.3 Objective Function and Constrains

Objective function: Keeping in mind the goal of minimum cost design, two cost components are considered, the total cost of steel in the frame (J_{str}) and the total cost of the FVDs (J_{damp}). J_{str} is correlative to the total volume of steel. J_{damp} is correlative to the square root of the peak forces developed in the most loaded damper from each group and the number of dampers in the same group. The mathematical representation of the cost of steel and dampers is presented in Eqs. (3a) and (3b), respectively.

$$J_{str} = \beta_s \sum_{i=1}^{N_{ele}} A_i \cdot L_i \tag{3a}$$

$$J_{damp} = \beta_d \cdot \left[N_d^{g1} \cdot \sqrt{\max\left|\hat{\mathrm{f}}_d^{g1}\right|} + N_d^{g2} \cdot \sqrt{\max\left|\hat{\mathrm{f}}_d^{g2}\right|} \right] \tag{3b}$$

where β_s and β_d are parameters that scale the cost of the steel and the dampers, respectively; A_i and L_i are the length and the cross-section area of the ith member; N_d^{g1} and N_d^{g2} are the number of dampers in groups one and two, respectively, and $\hat{\mathrm{f}}_d^{g1}$ and $\hat{\mathrm{f}}_d^{g2}$ are the maximum of the peak forces developed in all dampers from groups one and two, respectively (i.e. in each group, the maximum peak force from all dampers).

Constrains: As mentioned, a number of code requirements are set as constraints. Among them are the "strong column weak beam", stability coefficient, minimum base shear capacity and gravity load combination. In addition, performance constraints on the peak inter-story drifts are considered.

First, the performance constraints are presented, where the peak inter-story drift of each story is limited to an allowable value (Eq. 4a). Also, the "strong column weak beam" is considered by Eq. (4b). This constraint, that appears in many codes and guidelines, reduces the chance of plastic hinges in the columns and in turn of a soft story mechanism. In some cases, the stability of the structure may be a governing

criterion. This may be true in particular for flexible structures such as steel MRFs. Therefore, the stability coefficient is also limited to a maximum value, as suggested in many codes. The stability coefficient is evaluated through the eigenvalue problem (Eq. 4c) [19]. In addition, the structure is checked against two design cases, the Equivalent Lateral Load (ELF) procedure and the gravity load combination, as given in Eqs. (4d) and (4e), respectively. The ELF analysis is performed to evaluate the capacity of the force-resisting system and, in particular, the base shear capacity of the MRF. In addition, the gravity design load is considered. In both load combinations, the demand is that all elements should remain elastic.

$$d_{c,k} = \max_t \left(\left| \frac{d_k(t)}{d_{all}} \right| \right) \leq 1 \qquad \forall k = 1 \ldots N_{drift} \tag{4a}$$

$$\sum M_{y,c} \geq \gamma \cdot \sum M_{y,g} \qquad \forall k = 1 \ldots N_{joints} \tag{4b}$$

$$\theta = \frac{\boldsymbol{\phi}_{s,1}^T \mathbf{K}_G \boldsymbol{\phi}_{s,1}}{\boldsymbol{\phi}_{s,1}^T \mathbf{K} \boldsymbol{\phi}_{s,1}} \leq \theta_{max} \tag{4c}$$

$$M_y \geq M_d^{ELF} \qquad \forall j = 1 \ldots N_{sec} \tag{4d}$$

$$M_y \geq M_d^{gr} \qquad \forall j = 1 \ldots N_{sec} \tag{4e}$$

where $d_{c,k}$ is the normalized peak inter-story drift of the k-th story, assessed based on the peak inter-story drift in time divided by the allowable inter-story drift. $\sum M_c$ and $\sum M_g$ are the sums of the yielding moments of all the columns and beams connected to the same joint, respectively and γ is the beam overstrength factor (e.g., 1.2). $\mathbf{K}$ and $\mathbf{K_G}$ are the stiffness and geometrical stiffness matrices, respectively, $\boldsymbol{\phi}_{s,1}$ is the first eigenvector and θ_{max} is the maximum allowable value for the stability coefficient (e.g., 0.1). M_d^{ELF} and M_d^{gr} are the design moments at each control section, under the ELF and gravity load combinations, respectively, and M_y is the yield moment of the relevant member.

2.4 Formal Mixed-Integer Solution Scheme

Summarizing the equations given above, the mixed-integer optimization problem is given as follows:

$$\min_{W, c_d, y_1, y_2} \quad J = J_{str} + J_{damp}$$

$$s.t.:$$

$$
\begin{aligned}
& d_{c,k} = \max_{t}\left(\left|\frac{d_k(t)}{d_{all}}\right|\right) \leq 1.0 \;\forall\; k = 1 \;\ldots\; N_{drift} \\
& M_y \geq M_d^{ELE} \qquad\qquad \forall\; j = 1 \;\ldots\; N_{sec} \\
& M_y \geq M_d^{gr} \qquad\qquad \forall\; j = 1 \;\ldots\; N_{sec} \\
& \sum_{\substack{\theta \leq \theta_{max} \\ y_2 \geq y_1}} M_c \geq \gamma \cdot \sum M_g \qquad \forall\; k = 1 \;\ldots\; N_{joints}
\end{aligned}
\tag{Prob. 1}
$$

With:

$$
\begin{aligned}
& \mathbf{MR(t)} + \mathbf{C}_s\dot{\mathbf{u}}(\mathbf{t}) + \mathbf{f}_s(\mathbf{t}) + \mathbf{f}_d(t) = -\mathbf{M}\mathbf{e}a_g(t) \\
& \mathbf{u}(0) = \mathbf{u}_{\text{static}},\ \dot{\mathbf{u}}(0) = \mathbf{0},\ \ \mathbf{f}_s(0) = \mathbf{f}_{s,\text{static}},\ \mathbf{f}_d(0) = \mathbf{0} \\
& [\mathbf{K} - \boldsymbol{\lambda}_s\mathbf{K}_G]\boldsymbol{\phi}_s = \mathbf{0} \\
& \mathbf{KU} = \boldsymbol{F}_{ELE} \\
& \mathbf{KU} = \boldsymbol{F}_{\text{gravity}} \\
& \mathrm{W}_i \in \{\mathrm{W}_1, \mathrm{W}_2, \mathrm{W}_3, \ \ldots\} \\
& c_{d,j} \in \{0, \overline{C}_d \cdot y_1, \ \overline{C}_d \cdot y_2\}.
\end{aligned}
\tag{Prob. 1 Cont.}
$$

3 Numerical Example

In this section, Prob. 1 is solved using a zero-order optimization tool, the Genetic Algorithm (GA). The irregular five-story frame structure shown in Fig. 1 is to be optimized. The geometrical properties of the MRF and all the possible locations for the FVDs are shown also in Fig. 1. The frame is subjected to the LA02 ground record from the LA 10%@50 years ensemble. The Rayleigh inherent damping matrix based on 5% of critical damping for the first and the third modes is considered. The sections of the columns and beams are selected out of the IPB and IPE steel tables,

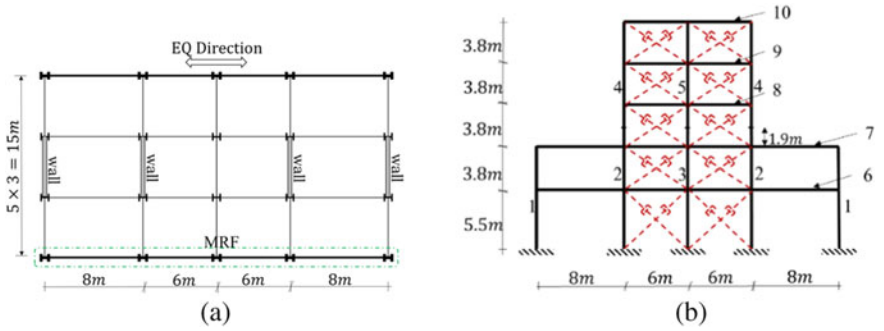

Fig. 1 **a** Plan view; **b** Elevation view

respectively. A dead load of $D = 3\left[\frac{kN}{m^2}\right]$, live load of $L = 5\left[\frac{kN}{m^2}\right]$ and combination coefficient for the quasi-permanent ($\psi = 0.3$) were considered. The yield stresses of the column and beam elements are 345 Mpa and 248 Mpa, respectively. The ground structure considered in this example is shown in Fig. 1b. In which ten types of elements (five columns and five beams) and twenty possible locations for the FVDs (two at each bay) are all to be optimized, along with the size of damping in each size group. Each element is selected out of seven options (IPB 260–400 for the columns and IPE 300–550 for the beams). The dampers maximum considered coefficient set to $\overline{C}_d = 80\left[\text{kN}\left(\frac{\text{s}}{\text{mm}}\right)^{\alpha}\right]$, and nonlinear dampers with an exponent of $\alpha = 0.5$ are considered. The objective function is evaluated based on $\beta_s = 39,250\left(\frac{\$}{\text{m}^3}\right)$ which corresponds with $5000\left(\frac{\$}{\text{ton}}\right)$ for the steel price. For the dampers price the parameter β_d is set to $358\left(\frac{\$}{\sqrt{\text{kN}}}\right)$, based on the practical price of 8,000$ for a damper defined by a peak force of 500 kN. The maximum allowed value for the stability coefficient is $\theta_{max} = 0.1$. The force-resisting system is designed for a minimum base shear of $V_{min} = 517\,\text{kN}$ and the overstrength factor for the "strong column weak beam" constraint is set to $\gamma = 1.2$. The allowable drift limited to 1% of the story height.

The optimization process is carried out using the MATLAB built-in Genetic Algorithm function. A number of stopping criteria are set. Among the criteria: maximum number of generations, if the average relative change in the best fitness function value over "MaxStallGenerations" is less than or equal to "FunctionTolerance". For numerical experiments a parallel-processor MATLAB code was executed on Tamnun, a computer cluster hosted and maintained by the Division for Computing and Information System at the Technion–Israel Institute of Technology.

Figure 2 shows the optimal structure obtained using GA, as well as the normalized peak inter-story drifts of the various stories. It can be seen that the drifts of the first four stories are quite uniformly distributed and close to the allowable drift. The design relies on two different types of FVDs, with damping coefficients of 17.9 $\left[\text{kN}\left(\frac{\text{s}}{\text{mm}}\right)^{\alpha}\right]$

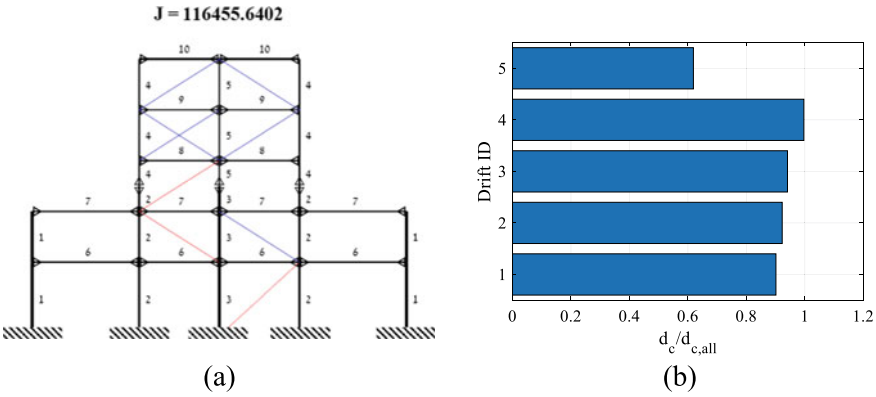

Fig. 2 **a** Optimized layout of the MRF; **b** Normalized inter-story drifts

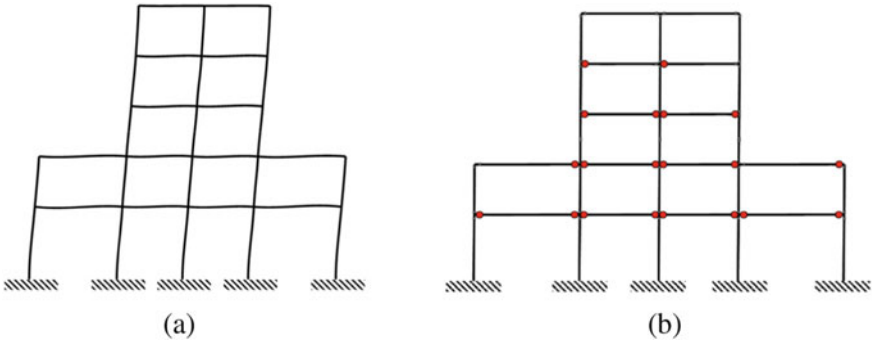

Fig. 3 **a** The first mode of the optimal structure; **b** Locations of plastic hinges

(in red) and 4.2 $\left[\text{kN}\left(\frac{\text{s}}{\text{mm}}\right)^{\alpha}\right]$(in blue). The optimal locations of the FVDs are also given in Fig. 2a. The total cost of the structure is 116,456 [$], where the cost of steel and FVDs are 78,651 [$] and 37,805 [$], respectively.

The natural period of the optimized structure is 1.3647 s, and the first mode is shown in Fig. 3a. Figure 3b shows the locations of the plastic hinges. As can be seen, the plastic hinges developed at the beams' ends and not at the columns, as demanded. Moreover, except of the top floor beams, the other beams developed plastic deformation and pretty uniform distribution of damage is attained. Such a design has been found to be an efficient design strategy and has been targeted in the past [19].

To examine the efficiency of the proposed methodology and the advantages of using FVDs in steel MRFs in general, the same MRF was designed conventionally without any supplemental damping. The conventional MRF was designed to the same performance level in terms of inter-story drift (1% of the story height). However, the steel elements required to achieve this target drift were much heavier compared to the MRF with FVDs, and the MRF characterized by a short natural period of 0.5125 s. Furthermore, the total cost was found to be higher by 52% (178,991 [$]). Besides the efficiency from an economic point of view, the damped MRF behave much better in terms of floor accelerations and shear forces. The shear forces in all stories are given in Fig. 4, where the peak shear forces developed in the frame elements, FVDs, and total forces in the damped and conventional MRF, respectively, are presented. The base shear of the undamped MRF is higher by 380% than the optimal damped MRF. Although it has not been considered within the optimization, the peak base shear has a significant impact on the cost of foundations.

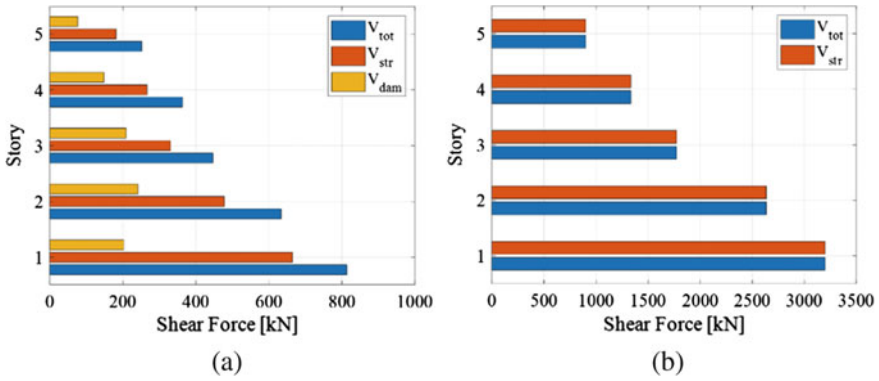

Fig. 4 **a** Shear forces, optimized structure; **b** Conventional structure

4 Conclusions

This paper presented a methodology for the seismic design of irregular MRFs with FVDs. The goal of the optimization is to achieve a minimum cost design while satisfying several code requirements in addition to performance constraints on inter-story drifts. Moreover, the approach relies on NRHA, considering both the nonlinear behavior of the MRF members and FVDs.

The numerical example shows the robustness of the formulation and the GA, where an optimized design is attained. The design achieved by the GA is characterized by an efficient distribution of damage and inter-story drifts. Furthermore, the efficiency of utilizing FVDs in new irregular steel MRF is exposed. The design that utilizes FVDs results in a cheaper structure compared to a conventional MRF design. Also, it is essential to point out the significant base shear reduction achieved by the optimal damped MRF compared to the conventional design.

As mentioned above, the optimized design heavily relies on FVDs; however, it should be noted that the solution may be sensitive to the input parameters. Such as the ratio between the cost of steel and dampers and the allowable inter-story drift. Any change in these parameters may affect the optimized design properties as the topology of FVDs and the natural period.

Acknowledgements This research was supported by the Israeli Ministry of Housing and Construction through the National Building Research Institute grant # 2028281. The authors are grateful for this support.

References

1. Gluck N, Reinhorn AM, Gluck J, Levy R (1996) Design of supplemental dampers for control of structures. J Struct Eng 122(12):1394–1399. https://doi.org/10.1061/(ASCE)0733-9445(1996)122:12(1394)
2. Lopez Garcia D, Soong TT (2002) Efficiency of a simple approach to damper allocation in MDOF structures. J Struct Control 9(1):19–30. https://doi.org/10.1002/stc.3
3. Singh MP, Moreschi LM (2002) Optimal placement of dampers for passive response control. Earthq Eng Struct Dyn 31(4):955–976. https://doi.org/10.1002/eqe.132
4. Pollini N, Lavan O, Amir O (2017) Minimum-cost optimization of nonlinear fluid viscous dampers and their supporting members for seismic retrofitting Nicolò. Earthq Eng Struct Dyn 46(12):1941–1961. https://doi.org/10.1002/eqe
5. Takewaki I (1997) Optimal damper placement for minimum transfer functions. Earthq Eng Struct Dynam 26(11):1113–1124
6. Lavan O, Levy R (2005) Optimal design of supplemental viscous dampers for irregular shear-frames in the presence of yielding. Earthq Eng Struct Dyn 34(8):889–907. https://doi.org/10.1002/eqe.458
7. Lavan O, Levy R (2006) Optimal peripheral drift control of 3d irregular framed structures using supplemental viscous dampers. J Earthq Eng 10(6):903–923. https://doi.org/10.1080/13632460609350623
8. Ganzerli S, Pantelides CP, Reaveley LD (2000) Performance-based design using structural optimization. Earthq Eng Struct Dyn 29(11):1677–1690. https://doi.org/10.1002/1096-9845(200011)29:11%3c1677::AID-EQE986%3e3.0.CO;2-N
9. Chan CM, Zou XK (2004) Elastic and inelastic drift performance optimization for reinforced concrete buildings under earthquake loads. Earthq Eng Struct Dyn 33(8):929–950. https://doi.org/10.1002/eqe.385
10. Fragiadakis M, Papadrakakis M (2008) Performance-based optimum seismic design of reinforced concrete structures. Earthq Eng Struct Dyn 37(6):825–844. https://doi.org/10.1002/eqe.786
11. Lavan O, Wilkinson PJ (2016) Efficient seismic design of 3D asymmetric and setback RC frame buildings for drift and strain limitation. J Struct Eng 04016205. https://doi.org/10.1061/(ASCE)ST.1943-541X.0001689
12. Viti S, Cimellaro GP, Reinhorn AM (2006) Retrofit of a hospital through strength reduction and enhanced damping. Smart Struct Syst 2(4):339–355. https://doi.org/10.12989/sss.2006.2.4.339
13. Takewaki I (1999) Displacement-acceleration control via stiffness-damping collaboration. Earthq Eng Struct Dyn 28(12):1567–1585. https://doi.org/10.1002/(SICI)1096-9845(199912)28:12%3c1567::AID-EQE882%3e3.0.CO;2-1
14. Cimellaro GP (2007) Simultaneous stiffness-damping optimization of structures with respect to acceleration, displacement and base shear. Eng Struct 29(11):2853–2870. https://doi.org/10.1016/j.engstruct.2007.01.001
15. Lavan O, Cimellaro GP, Reinhorn AM (2008) Noniterative optimization procedure for seismic weakening and damping of inelastic structures. Pacific Earthq Eng Res Cent 9445(November):2004–2008. https://doi.org/10.1061/(ASCE)0733-9445(2008)134
16. Lavan O (2015) A methodology for the integrated seismic design of nonlinear buildings with supplemental damping. Struct Control Heal Monit 19(1):88–106. https://doi.org/10.1002/stc
17. Rutenberg A (1981) A direct p-delta analysis using standard plane frame computer programs. Comput Struct 14(I):97–102
18. Spacone E, La R, Filippou FC (1992) A beam element for seismic damage analysis, no. August 19921–110
19. Levy R, Lavan O (2006) Fully stressed design of passive controllers in framed structures for seismic loadings. Struct Multidiscip Optim 32(6):485–498. https://doi.org/10.1007/s00158-005-0558-5

Stiffening Solution of Façade Frames for Reducing the Eccentricity in Plan-Irregular Buildings

Gabriel Moyano and Jesús-Miguel Bairán

1 Introduction

In the design process of a building, the structural configuration should be compatible with architectural and functionality requirements. Sometimes, this may condition the regularity of the structures from the earthquake-resistant point of view. In particular, in the case of Peruvian cities, there are two unfavourable aspects to consider. On one hand, the current local regulations are rather exigent in relation to inter-storey drifts and plan torsion limits. In the EC-8 inelastic interstory drifts are limited to 0.0075 h/v, with a recommended value of $v = 0.4$ for importance categories I and II, and $v = 0.5$ for categories III and IV. Torsional irregularities are required to be checked but have no upper limit, and if found the reference behaviour factor is not reduced. In comparision, the Peruvian design code limits the drifts to 0.007 h in all concrete structures. In the irregularity check ratio of max/average drift is limited to 130% for importance category I and II structures and 150% for importance category III structures. The reference behaviour factor must be reduced by multiplying the base value by 0.75. Hence, this commonly requires the use of structural walls to achieve enough stiffness. On the other hand, the typical long geometry of urban land lots, with the street façade in the short dimension, frequently makes impracticable to arrange the structural elements on a bidirectional regular configuration, due to space limitations. This generates plans with important eccentricities between the centres of mass and stiffness, see Fig. 1; thus, significant torsional behaviour will occur under lateral loading.

G. Moyano · J.-M. Bairán (✉)
Department of Civil and Environmental Engineering, Universitat Politècnica de Catalunya, C. Jordi Girona, 1-3, 08034 Barcelona, Spain
e-mail: jesus.miguel.bairan@upc.edu

R. Bento et al. (eds.), *Seismic Behaviour and Design of Irregular and Complex Civil Structures IV*, Geotechnical, Geological and Earthquake Engineering 50,
https://doi.org/10.1007/978-3-030-83221-6_12

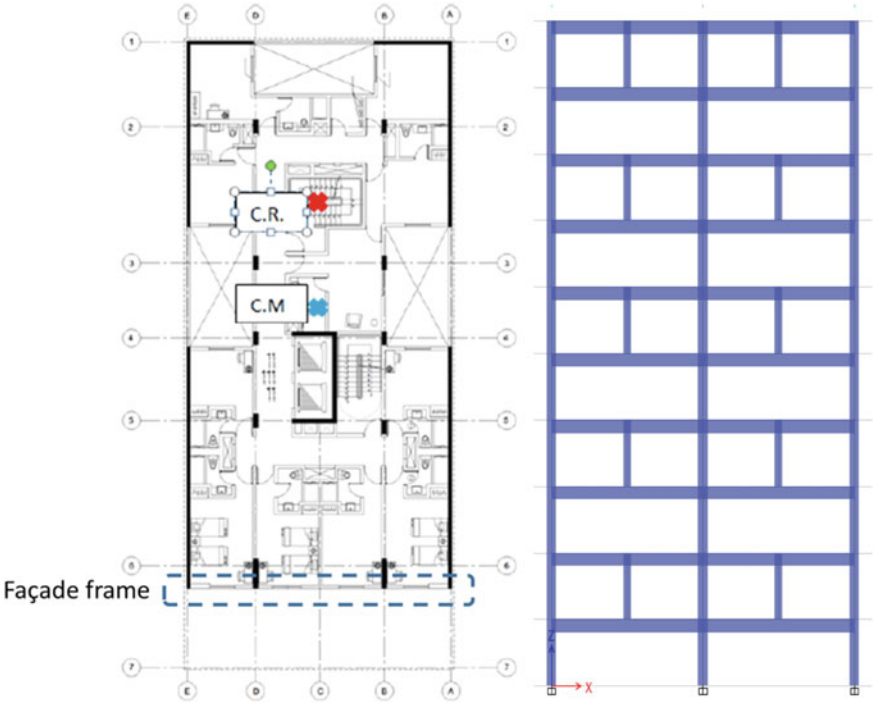

Fig. 1 Example building configuration with walls and façade frame. **a** Plan-irregular configuration with eccentricity between centres of mass stiffness. **b** Proposed stiffened Vierendeel-frame

This paper presents and investigates the feasibility of a structural design concept to reduce in-plan irregularities consisting of the use of a *Vierendeel-frame* system to stiffen the façade against lateral actions.

2 Methodology

Following the Eurocode requirements [1, 2], two 2D moment resisting concrete frames are designed for ductility class high (DCH). Both frames are 10 storeys. The first structure, taken as reference, consists in a regular frame, while the second one is stiffened using the proposed Vierendeel system, see Fig. 4. Both are analysed using multimodal response spectrum and pushover analyses, in order to assess their performance. Based on the observations, additional design procedures for capacity design are proposed and validated.

The non-linear performance is assessed using the commercial software Etabs 16 [3]. The performance of the solution is verified using pushover analysis, and an additional capacity design requirement is proposed to avoid local failure modes.

Finally, the benefits are investigated on a 3D case-study building, comparing the use of the traditional frame and the novel stiffened frame in the façade.

3 Conceptual Behaviour of the Vierendeel-Type Frame

In a traditional Vierendeel truss, the webs are rigidly connected to the chords [4]. The beam slope is opposed by the stiffness of the web, generating moment and shear distribution in this element, which is transferred to the top and bottom chords as axial forces (Fig. 2). The pair of forces generated in the top and bottom chords balance the bending moment in the cross-section.

The Vierendeel-type frame here proposed has one single web at centre span of intermittent stories. Therefore, under gravity loads the stresses on the web will be negligible, as the beam slope in that point is close to zero (Fig. 3a). Similarly, because of the intermittent story arrangement, the axial force in the web is almost null. Therefore, it is independent of the main gravity resisting system. Conversely, under lateral

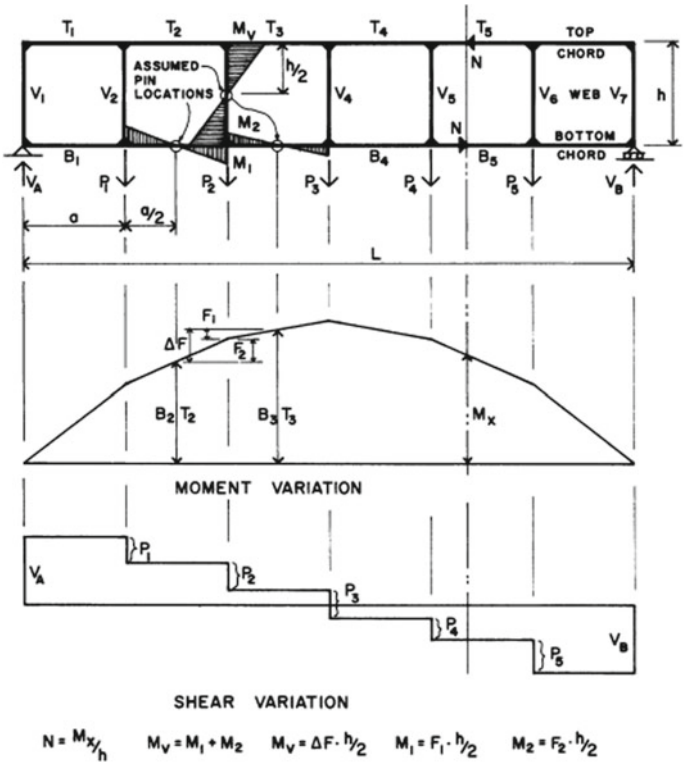

Fig. 2 Behaviour of a traditional Vierendeel truss [4]

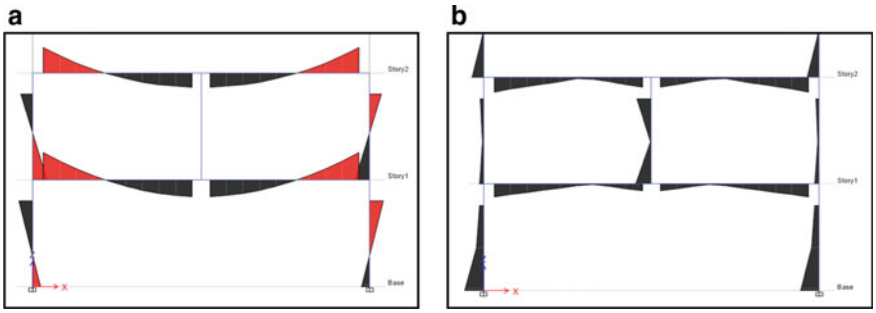

Fig. 3 Behaviour of Vierendeel-type frame. **a** Bending moments under gravity loads. **b** Bending moments under lateral loads

loads, the frame web will develop important stresses, effectively cutting the length of the beams, and greatly stiffening the structure under horizontal displacements (Fig. 3b).

Capacity design may be used to enable the plastic hinges at the top and bottom of the web, in addition to those the base of the structure and at both ends of the beams. This provides one additional plastic hinge per bay per level; therefore, energy dissipation and damage control are expected to improve.

4 Initial Assessment

An isolated 2D frame is designed according to Eurocode [1, 2], for importance class II and soil type B. A similar frame is also designed using a metal web to stiffen the structure. The stiffened web may consist of either concrete of metal elements. In this first analysis, a steel stiffening web is considered, without loss of generality. The steel component has potential advantages in repairing and retrofitting. It is easily replaceable after an earthquake, because it is not part of the gravity resisting system it can be removed and replaced after the earthquake if needed. The behaviour of the alternative concrete stiffener is demonstrated on the same frame in Sect. 5.

Each story is loaded with a distributed load of 60 kN/m on the beams. Both structures are also designed under a horizontal acceleration of $a_{gh} = 0.4$ g and a vertical acceleration $a_{gv} = 0.36$ g. Table 1 shows the elements geometry. Both structures have span of 9.5 m, and ten stories of 3 m inter-storey height.

Table 1 Element properties for initial verification

Element	Section	Material
Column	400 mm × 600 mm	Concrete C30/37
Beam	300 mm × 600 mm	Concrete C30/37
Web stiffener	HEB 340	Steel S235

4.1 Response-Spectrum Analysis

Under seismic loads, the stiffened frame exhibits noticeable rotation restriction on the concrete beams produced by the metallic web. Bending moments appear at the centre of the beam, and the shear increases significantly, similarly to shorter span beams. The period (T) of the first mode of vibration reduces in 0.173 s (11%), compared to the standard frame. Table 2 summarizes the results of the first three vibration modes.

The increment of mass provided by the additional web is negligible, while the stiffness of the traditional structure is 20.9% less than in the stiffened frame.

Table 3 shows the maximum displacement and drifts in all the stories based on the response spectrum analysis. The maximum deformation of the structure is reduced by 38.9% and its maximum drift is reduced by 35.6%.

Table 2 Modal results

Mode	Traditional structure		Stiffened structure	
	T (s)	% Mass (%)	T (s)	% Mass (%)
1	1.566	79.09	1.393	79.98
2	0.492	10.52	0.449	10.93
3	0.265	4.12	0.252	3.91

Table 3 Displacement results of according to multi-modal response spectrum analysis

Story	Traditional structure		Stiffened structure	
	Max. lateral displacement (mm)	Max. drift (%)	Max. lateral displacement (mm)	Max. drift (%)
10	448	0.80	274	0.44
9	428	1.09	262	0.72
8	401	1.37	244	0.80
7	365	1.60	223	1.03
6	322	1.79	196	1.00
5	272	1.95	168	1.22
4	215	2.08	133	1.14
3	154	2.12	100	1.37
2	91	1.94	59	1.14
1	33	1.10	25	0.83

Table 4 Performance point results—rectangular load case

	Rectangular pattern		Mode 1 pattern	
	Traditional	Stiffened	Traditional	Stiffened
Displacement	303 mm	279 mm	342 mm	310 mm
Base shear	404.5 kN	759.3 kN	337.5 kN	669.9 kN
Ductility	6.9	4.0	7.0	4.2
Hinges IO	4	3	10	2
Hinges LS	6	6	3	7
Hinges CP	4	4	5	5
Collapsed hinges	0	0	0	0

4.2 Pushover Analysis

Two lateral load patterns are used for the non-linear static analysis (pushover), according to [1], i.e. constant lateral force and consistent with the first vibration mode. Both cases are referred below as "Rectangular" and "Mode 1", respectively. The results of the analyses are summarized in Table 4.

Figure 4 shows the capacity curves for each structure. The performance points for the demands of return period 100 and 475 years are indicated with cross and circle marks, respectively. It is evidenced that the stiffened structure has a significantly better performance for return periods up to 475 years, which corresponds to the demand used in design. However, for return periods slightly higher than 475 years, the stiffened structure rapidly loses strength and collapses.

Figure 5 revels that the cause of this premature failure is the formation of a plastic hinge at the centre of the beam, which triggers a local collapse mechanism. The demand in which the first plastic hinge occurs in the centre span is shown in Fig. 4 with the diamond marker.

5 Proposed Design Method

As shown in the previous section, the behaviour of the stiffened structure designed using the provisions for standard frames is not adequate for seismic performance, as the possible failure mechanism with hinges at the centre of the beam rapidly reduces the capacity of the structure. A capacity-design criterion is developed below to avoid this local failure mode.

The target outcome is that the plastic hinge forms in the web stiffener instead of the main girder. Therefore, the moment capacity at the centre of the beam (M_{Cb}) should be bigger than the sum of the moments due to gravity load in an isostatic configuration (M_{iso}) plus the plastic moments that appear at both ends of the beam ($M_{beam,left}$ and $M_{beam,right}$) and at the web stiffener (Fig. 7). Equation (1) shows the

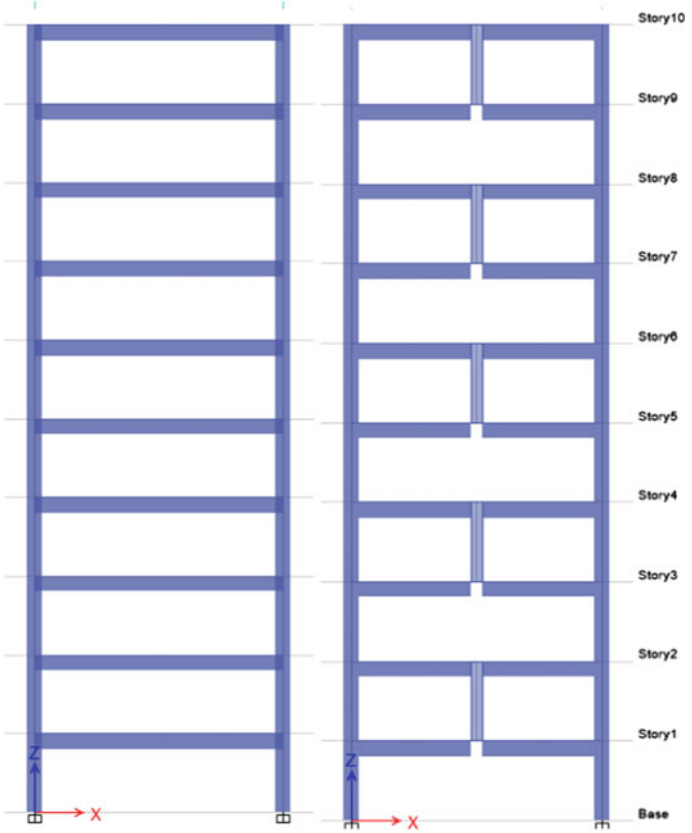

Fig. 4 Alternative façade frames. **a** Designed traditional frame. **b** Designed stiffened frame

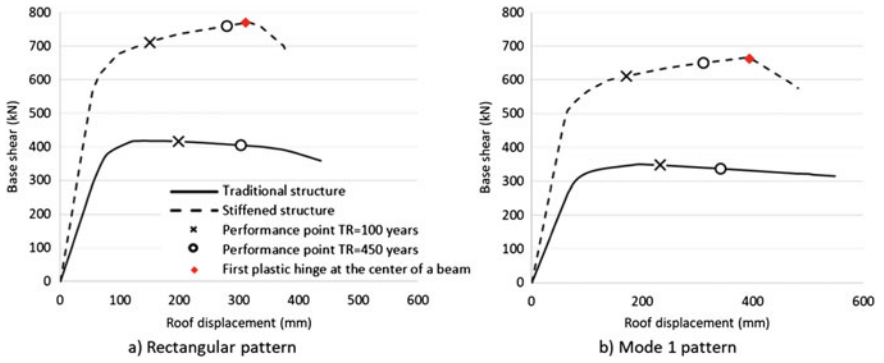

Fig. 5 Capacity curves for the traditional and stiffened frames. **a** Rectangular load pattern, **b** mode 1 load pattern

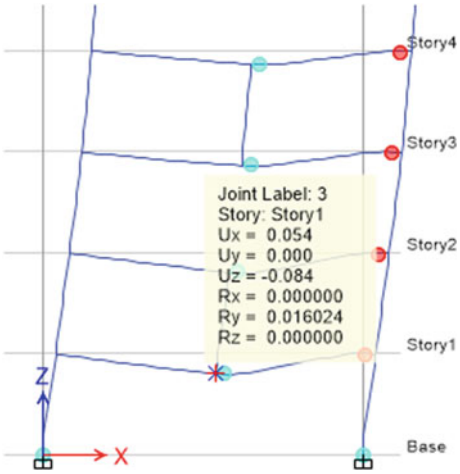

Fig. 6 Possible local failure mechanism

local design condition. The estimation of the shear demand in the beam must account for this bending distribution. Equation (2) can be used to estimate the shear demand.

$$M_{Cb} > M_{iso} + \frac{M_{web}}{2} + \frac{M_{beam\ left}}{2} + \frac{M_{beam\ right}}{2} \tag{1}$$

$$V_d > max\left[2\frac{\left(M_{Cb}^{+} + M_{beam}^{-}\right)}{L}, 2\frac{\left(M_{Cb}^{-} + M_{beam}^{+}\right)}{L}\right] + \frac{gL}{2} \tag{2}$$

In order to verify the effectiveness of the proposed capacity-design, the method is applied to the design of the structures of the previous section, by stiffening it with a 500 mm × 300 mm concrete web. In this case, a concrete web was considered in order to also show the adequate response of the concrete alternative. Nevertheless, as mentioned in Sect. 4, a metal web has some advantages, as it would be easier to replace after an eventual damage. In addition, using the concrete element in the following analysis allows varying the resistance of the element by changing the longitudinal reinforcement. This is convenient for carrying out a sensitivity analysis of the value of the over-strength factor. On the other hand, in the case of a steel element, a modification of profile is required, with a greater effect in the elastic stiffness.

The design moments of the elements of the structure are shown in Table 5. From the application of Eq. (1), the minimum design strength of the beam at the centre is the span is computed in Eq. (3).

$$\begin{aligned} M_{Cb} &> 720\ \text{kNm} + \frac{590\ \text{kNm}}{2} + \frac{500\ \text{kNm}}{2} - \frac{900\ \text{kNm}}{2} \\ &= 815\ \text{kNm} \end{aligned} \tag{3}$$

Table 5 Plastic moments considered for capacity design

Description	Moment kN-m
Beam left	500
Beam right	−900
Web stiffener	590
Isostatic moment	720
Isostatic moment	720

To investigate the benefits the of the above criterion, a number of pushover analyses were performed on six different structures, with different ratios of the resisting moment in the centre span of the beam to the capacity-design criterion value of Eq. (1), M_{Rd}/M_{Cb}. The geometry of the design frames are similar to those of Sect. 4, although the stiffener is made of concrete. Figure 7 shows the response of the modelled structures using a lateral load distribution with a rectangular pattern. As the ratio of M_{Rd}/M_{Cb} approaches 100%, the local failure mode produced by the plastic hinge at the centre of the beam disappears; hence, the displacement capacity increases significantly. Similarly, Fig. 8 shows the response using a lateral load shape coincides with the first vibration mode. In both load patterns studied, the structure with $M_{Rd}/M_{Cb} = 100\%$ is the only one capable of resisting the intensity demand of 2500 years return period (MCE).

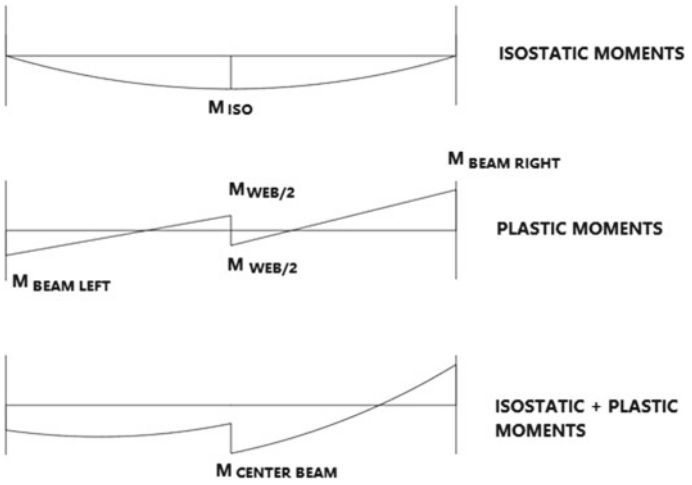

Fig. 7 Bending moment diagrams local plastic mechanism

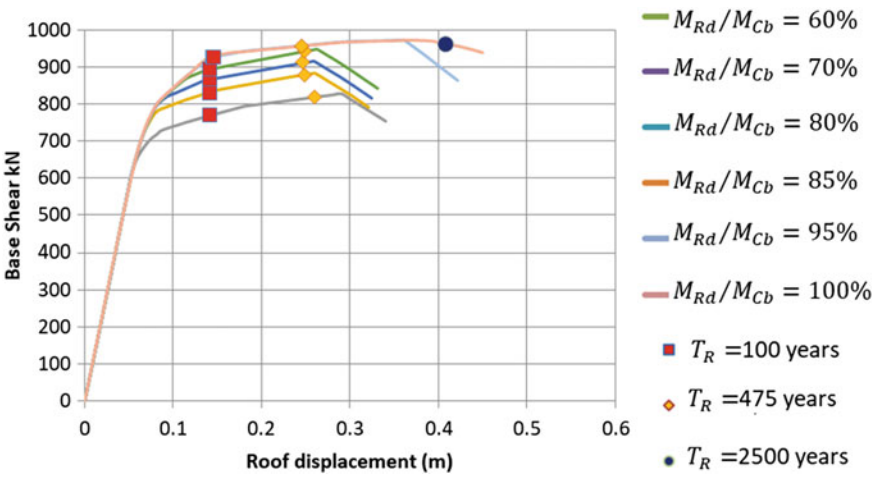

Fig. 8 Comparison of capacity curves of stiffened structure with different M_{Rd}/M_{Cb} ratios under rectangular load pattern. Markers indicate the performance-points for return periods of 100, 475 and 2500 years

6 Practical Application on 3d Building

To verify the benefits of the stiffened frames in a complete structure, a 10-stories building with torsional irregularity was analysed via response spectrum analysis, using the Eurocode standards [1, 2], for the same seismic demand described in Sect. 4. Two structures were designed, one using a standard frame in the façade and the other using the stiffened frame. Table 6 summarizes the properties of the resisting elements. Figure 9 shows the general geometry of the unstiffened and stiffened models (Fig. 10).

The position of the centre of mass and stiffness were computed for both models. Table 7 shows the position of the centre of mass and stiffness, the position of both points are shown in Fig. 9, for the two designed cases. The eccentricity between the centre of mass and rigidity is reduced in 57.8%, from 5.85 to 2.47 m.

Tables 8 and 9 show the main results of the first 6 vibration modes of the unstiffened and stiffened models, respectively. Using the stiffened façade frame reduced the first mode period from 1.282 to 1.098 s. Neglecting the difference of mass due to the stiffeners, this variation on the vibration period represents an increase of the structure stiffness of 36.3%.

Table 6 Element properties of 3D model

Element	Section	Material
Column	600 mm × 600 mm	Concrete C30/37
Beam	300 mm × 600 mm	Concrete C30/37
Shear walls	300 mm × Variable	Concrete C30/37
Web stiffener	IPE 500	Steel S235

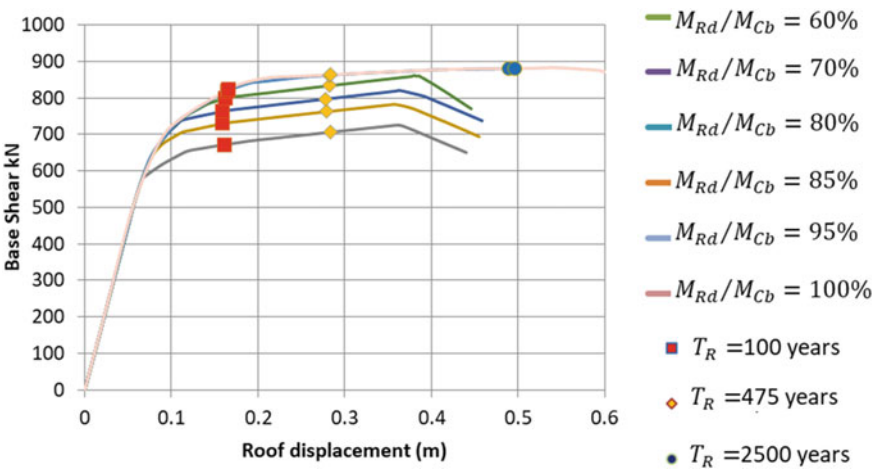

Fig. 9 Comparison of capacity curves of stiffened structure with different M_{Rd}/M_{Cb} ratios under load pattern according to mode 1. Markers indicate the performance-points for return periods of 100, 475 and 2500 years

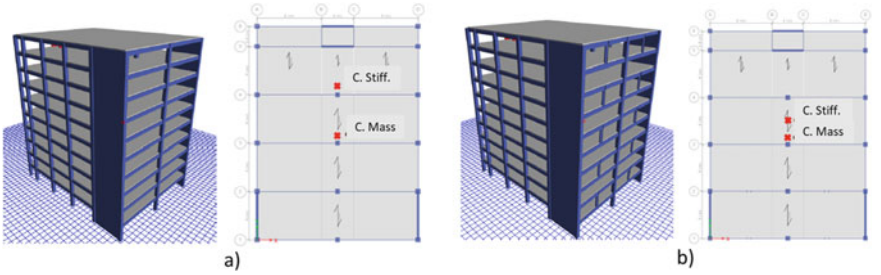

Fig. 10 Geometry and position of centres of mass and stiffness. **a** Unstiffened façade frame. **b** Stiffened façade model

Table 7 Distance from façade to centre of mass and rigidity

	Distance from façade	
	Unstiffened structure (m)	Stiffened structure (m)
Centre of mass	12.66	12.66
Centre of rigidity	18.51	15.15

Both displacements and inter-storey drifts, obtained from the response spectrum analysis, are significantly reduced in the stiffened structure. Table 10 shows the maximum and average inter-storey drift in each level. The maximum drifts are reduced up to 35.2%, while the maximum displacements are reduced up to 21.4%.

Table 8 Modal results from unstiffened structure

Mode	Period (s)	% Mass X (%)	% Mass Y (%)	% Mass Rz (%)
1	1.282	66.8	0	5.3
2	0.755	0	68.4	0
3	0.727	4.9	0	64.1
4	0.342	13.7	0	1.1
5	0.169	0	0	17.1
6	0.167	0	19.7	0

Table 9 Modal results from stiffened structure

Mode	Period (s)	% Mass X (%)	% Mass Y (%)	% Mass Rz (%)
1	1.098	71.4	0	2.2
2	0.752	0	68.5	0
3	0.706	1.6	0	67.9
4	0.308	13.1	0	0.5
5	0.168	0	0	17.3
6	0.166	0	19.7	0

Table 10 Inter-storey drifts

Level	Unstiffened		Stiffened	
	Max. drift (%)	Avg. drift (%)	Max. drift (%)	Avg. drift (%)
Storey10	1.13	0.88	0.73	0.66
Storey9	1.25	0.96	0.88	0.77
Storey8	1.34	1.03%	0.96	0.84
Storey7	1.41	1.09	1.09	0.94
Storey6	1.45	1.13	1.12	0.97
Storey5	1.44	1.12	1.20	1.01
Storey4	1.37	1.07	1.13	0.96
Storey3	1.22	0.94	1.08	0.89
Storey2	0.94	0.72	0.83	0.67
Storey1	0.48	0.35	0.45	0.34

7 Conclusions

A conceptual design solution for stiffening the façade frames through the formation of a Vierendeel-effect was proposed. The concept consists on the addition of a vertical element in the façade frame in the centre of the spans of the beams in intermittent storey, which can be either metallic or made of concrete. The addition of the stiffener

has negligible influence on the modal mass, while the effects in the frame stiffness is relevant. This application is particularly interesting in long buildings using structural walls, but with a functionality constraint enforcing diaphanous portal frame the street façade (e.g. parking accessibility, commercial use, etc.). The solution allows the open space in the ground storey and stiffens the portal frame, reducing eccentricity between centres of mass and stiffness.

The maximum displacements and drift in the stiffened structure were reduced in 39% and 36%, respectively, in comparison to the standard frame.

From the non-linear performance assessment, it was identified that a potential inadequate local failure mechanism in the stiffened frame. The mechanism develops when a plastic hinge takes place in the centre span of the storey beams, in addition to the expected hinges in the connection with the columns. When this mechanism forms, softening in the capacity curve begins. In the studied structure, such mechanism did not took place for the design spectrum, with return period of 475 years. However, it was observed for demands lower than the MCE of 2500 years return period, so it may compromise the near collapse performance levels.

To avoid the previous failure mode, a new capacity-design condition was developed, specific for the Vierendeel-stiffened frames. According to this condition, a minimum resistance for the beams in the centre span region is needed. The shear capacity of the beam should be designed in consequence to this moment capacity.

The additional capacity design condition effectively avoided the local failure mechanism for demands exceeding return periods of 2500 years (MCE). Therefore, following these design recommendations allows adequate use of stiffened frame with a no-collapse performance at rare events, while effectively controlling damage in more frequent events.

The benefits of the use of the frame was demonstrated through its application on a 10-storey 3D structure showing plan irregularity. The performance of the 3D building, assessed via response spectrum analysis, improved significantly by reducing the maximum displacements up to 25% and the inter-storey drift in 35%. Similarly, the difference ratio between the maximum and average drift of individual storey and the torsional irregularity were reduced. It is expected that in both pushover and time history analysis maximum displacements would be reduced in a similar manner and the plastic hinge at the centre of the beam would be avoided. The direct application of a response spectrum analysis for the design and the 3D performance through explicit non-linear time history analysis will be considered in future research.

Acknowledgements The authors acknowledge support of the Spanish State Research Agency and the European Funds for Regional Development, through the research project RTI2018-097314-BC21.

References

1. EC8-Part 1: Eurocode 8 (2005) Design provisions for earthquake resistance of structures. Part 1-1: General rules—seismic actions and general requirements for structures. ENV 1998-1. CEN, Brussels
2. EC2-Part 1-1: Eurocode 2 (2004) Design of concrete structures. Part 1-1: General rules and rules for buildings. ENV 1992-1-1. CEN, Brussels
3. CSI (2016) ETABS 16, User's guide. Computers and structures, Berkeley
4. Wickersheimer DJ (2018) The Vierendeel. University of California Press on Behalf of the Society of Architectural Historians S 35(1):54–60

Retrofitting of Irregular Structures for Seismic Loads Using Rocking Walls

Ameer Marzok and Oren Lavan

1 Introduction

Steel Moment Resisting Frames (SMRFs) are widely used for the seismic protection of steel structures. This is due to their high ductility and their efficient mass-to-stiffness ratio [1]. However, large ISDs could develop in these systems. This may become more significant when the structure has an irregular elevation or setback. This is due to the concentration of shear forces and flexural moments in these areas [2].

SMRFs are usually expected to develop large rotations in the structural elements in order to achieve a ductile behaviour [3, 4]. This provides a large amount of energy dissipation due to plastic behaviour. However, it has been shown that this large plasticity is accompanied by large deformations and ISDs [5]. This may cause stability issues to the structure. In addition, when large plastic deformations are present, the residual displacements are expected to be large. Repairing a building that has undergone large permanent deformations is challenging and often is not possible [6].

Adding a shear wall or a stiff spine system to an SMRF is expected to significantly reduce the ISDs [7]. This is due to its high stiffness which causes a first mode dominant displacements profile along with the wall's height. Different types of shear walls can be added to an SMRF to regulate the ISDs. This includes traditional reinforced concrete walls [8], pinned walls or dissipative towers [7], and Self-centring rocking walls. The behaviour of the latter as a retrofit system for SMRF has not been examined.

Self-centring rocking walls have shown the ability to withstand large deformations with small amount of residual displacements [9–11]. In these systems, a rocking

A. Marzok (✉) · O. Lavan
Technion Israel Institute of Technology, Haifa, Israel
e-mail: ameerm@campus.technion.ac.il

O. Lavan
e-mail: lavan@technion.ac.il

R. Bento et al. (eds.), *Seismic Behaviour and Design of Irregular and Complex Civil Structures IV*, Geotechnical, Geological and Earthquake Engineering 50,
https://doi.org/10.1007/978-3-030-83221-6_13

section is usually designed at the wall's base, causing a free rotational movement of the wall at this section. In addition, the energy dissipation is concentrated in dedicated elements rather than yielding of the primary structural elements. This leads to reduced economic losses after a seismic event compared to traditional systems.

Post Tensioned (PT) cables are usually provided to produce a flexural moment which causes the structure to return to its initial configuration when the external load is removed. This is usually referred to as a self-centring behaviour. In addition, Energy Dissipation (ED) material is usually added at the rocking section which provides the system the ability to absorb the seismic energy. Different types of energy dissipating materials have been examined. This includes metallic yield energy dissipators [9], fluid viscous dampers [10], shear fuses [12], etc. Adding nonlinear metallic dampers with the post tensioned cables at the rocking section produces a flag-shaped behaviour [13].

Adding walls to irregular moment resisting frames are expected to be beneficial. This is due to their high stiffness which regulates the displacements and prevent soft story mechanism. However, large forces could develop with the height of the wall due to the irregularity and the higher vibration modes effect [14]. To reduce these forces multiple rocking solutions can be designed.

Multiple rocking systems have been proposed for vertical spine systems [14, 15]. In these systems, an additional rocking section is designed at higher level of the wall. This rocking section is usually designed at the locations where the flexural moment due to the higher vibration modes is expected to be large [15, 16]. It has been shown that this design could significantly reduce the flexural moments and shear forces that are attributed to the higher mode effects in high-rise buildings. Studies on this system were limited for buildings in which the lateral load resisting system is based only on rocking walls. Furthermore, the design and the location of the top rocking section in these systems are less intuitive than in regular spine systems.

In this paper, an SMRF with irregular elevation will be retrofitted with a rocking wall with two rocking sections. The moment demands and shear forces received when using this system will be examined for various rocking levels and decomposition moments.

2 Mitigation of Higher Mode Effects

The addition of a stiff wall to an SMRF could regulate the ISDs and prevent soft story mechanisms. However, large flexural moment demands could develop throughout the height of the wall due to the higher vibration modes effect and the irregularity of the structure. To reduce these demands an additional rocking section is added at higher levels of the wall system.

The location of this rocking section may affect the moment, shear force, displacements and the ISDs demands. Moreover, the designed decomposition moment (the moment needed to initiate the rocking behaviour) could also affect these demands. Design methods have been proposed for systems with multiple rocking systems.

However, these methods are limited for regular structures in which a first vibration mode shape is expected. In addition, the behaviour of a rocking wall system with a nonlinear SMRF has not been examined.

Due to the lack of design methods, which are suitable for the examined system, a parametric study is conducted. In this study, the effect of the location of the higher rocking section and its design moment will be examined. These parameters were selected due to their significant effect on the behaviour of the system.

An SMRF with a setback will be studied. First, a nonlinear time history analysis will be conducted to calculate the behaviour of the bare frame system, which will be the reference system in this study. Later, this SMRF will be retrofitted with a rocking wall with a traditional base rocking section. Lastly, the effect of adding a rocking section at various levels and its design moment will be examined. The results are compared to the behaviour of the system with a base rocking section. The main target of the additional rocking section is to reduce the moment and shear force demands in the wall while preserving an acceptable level of displacements and ISDs.

3 Analytical Model

Nonlinear Time History Analyses (NTHA) were performed in the finite element platform OpenSEES [17]. The frame was modelled using nonlinear beam elements which were modelled using fiber elements. Four integration points were set along the length of the beam and the column elements as shown in Fig. 1a. At each integration point, the section is divided into fibers which have uniaxial material properties.

The rocking wall was modelled using a simplified model for this parametric study. Local phenomena such as concrete crashing and the change of the location of the rotation point at the rocking section were neglected. The simplified model is described in Fig. 1b. The nonlinear behaviour is assumed to be concentrated in the ED elements located at the rocking sections; this leads to damage-free behaviour. This should be ensured at the design process [18]. Therefore, to reduce the computational effort these walls were represented by elastic Timoshenko beam elements with sectional properties of the concrete walls.

Each rocking section was presented by stiff beams representing the width of the rocking walls. These beams were connected using compression only gap elements. Additional nodes were provided to add the metallic energy dissipators (EDs). These elements were assumed to have an elastic perfectly plastic behaviour and they were modelled as nonlinear truss elements. Stiff linear truss elements were added to describe the true elongation of these elements at the rocking section by connecting the top stiff beam with the additional nodes. The cable elements were modelled using elastic truss elements with pre-stressed material. Shear links were provided to connect between the two adjacent surfaces of the rocking section.

The frame was connected to the wall using horizontal stiff truss elements as shown in Fig. 2. These elements transfer only the horizontal forces from the MRF to the rocking wall. The masses were concentrated at the nodes of the frame. They include

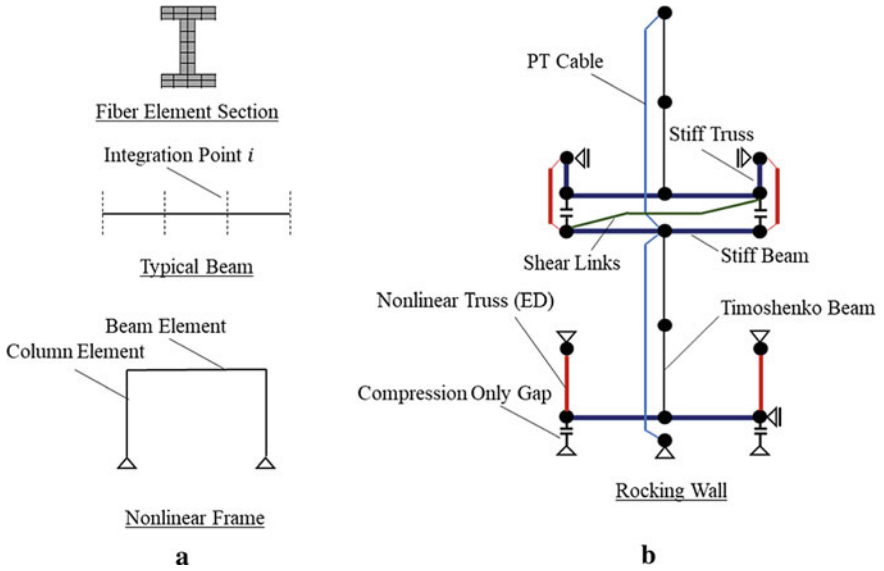

Fig. 1 **a** Numerical model for nonlinear MRF. **b** Numerical model for rocking wall with multiple rocking sections

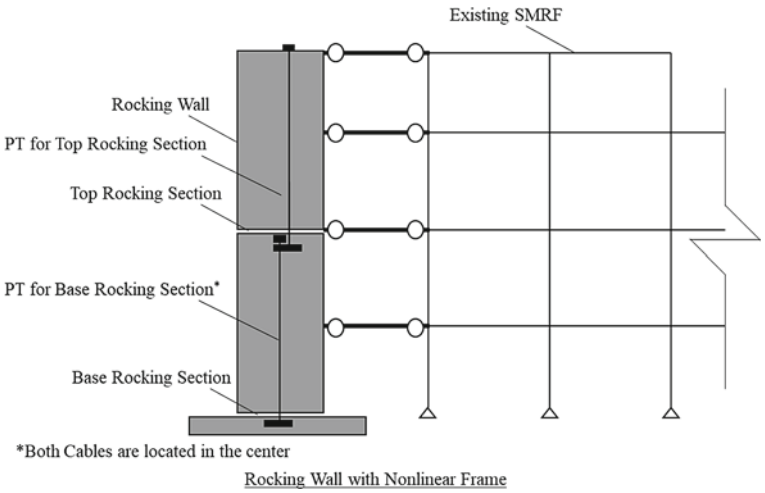

Fig. 2 Description of the numerical model of multiple rocking wall with SMRF

story weights (from dead load) and the weight of the frame elements. Gravity loads were applied as uniform distributed loads acting on the beam elements.

The mass of the rocking wall was neglected. In addition, the wall is used as a retrofitting system of an existing SMRF. Therefore, it is assumed that the gravity

loads in the building are carried only by the frame and the wall is subjected only to lateral loads due to the ground acceleration.

4 Case Study

A setback irregular frame as shown in Fig. 3 is examined. This frame represents a lateral load resisting system of a fourteen-story building. The frame has six bays with 7 [m] width each, and 3.5 [m] story height for the first three stories. The setback starts on the fourth floor of the building where the number of bays is reduces to two. Pinned connections between the frame columns and their foundations are assumed.

The frame has H.E.A 500 and H.E.A 900 type beams and columns, respectively for the entire structure. The structural steel for the beams and columns has an elastic modulus of 200,000 [MPa] and a yield strength of 400 [MPa]. Strain hardening behaviour was assumed for the structural steel. The seismic mass at the story levels including dead load and self-weight is 170 [ton] for each level before the setback. After the setback, the story mass reduces to 57.2 [ton]. The frame was subjected to the LA01, LA03, LA05 LA07 and LA09 ground accelerations.

The displacements profile and the ISDs for the bare frame are shown in Fig. 4 for each ground acceleration. In addition, the average of these ISDs is presented. Large average ISDs are observed at the higher levels of the frame. The largest average of the inter-story drift is in the 6th level and it is equal to approximately 2.6% (Fig. 4a) of the story level. The drifts at story levels that are before the setback are smaller.

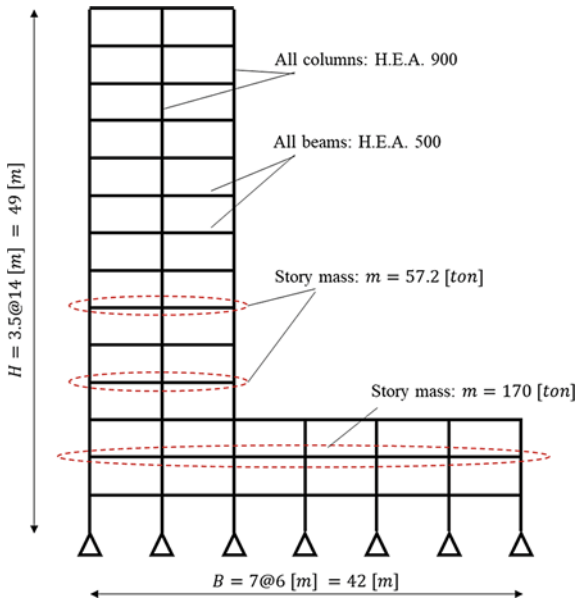

Fig. 3 Elevation plan of the studied setback irregular SMRF

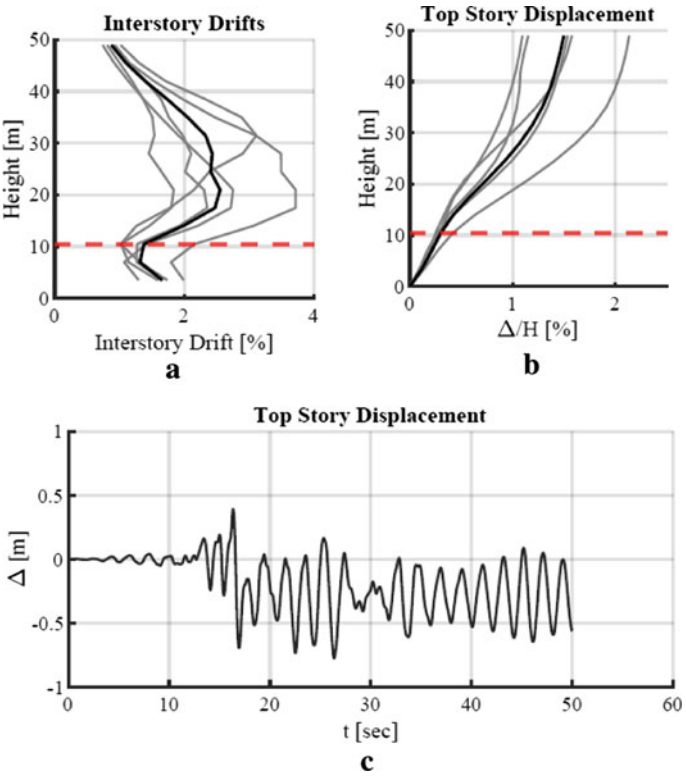

Fig. 4 Results for bare frame subjected to a set of ground excitations (average results are shown in bold line): **a** ISDs, **b** story displacements, **c** displacement of the top story of when the frame is subjected to the LA09 ground excitation

The observed large drifts cause a high amount of damage to the frame elements. In addition, large residual deformations are observed. Figure 3c shows the displacements of the top story of the building. It is observed that the residual displacement of the top story, when the structure was subjected to the LA09 excitation, is approximately 0.3 [m] which is 0.6% of the total building height. Therefore, in the next sections, different configurations for the retrofitting of this frame based on adding multiple rocking walls are examined.

5 Base Rocking

The traditional base rocking section is added to the bare frame from the previous section. This system includes a concrete PT wall with 4.5 [m] width and 0.25 [m] depth. The wall was post-tensioned vertically with an unbonded cable connecting its foundation to the top of the wall with a sectional area of 40 [cm^2]. The cable was post

tensioned with a force the is equal to half of its ultimate stress. The ultimate stress of the cable was 1860 [MPa]. Metallic yield dampers were provided at the rocking section. Two bars with a sectional area of 26.6 [cm^2] and 30 [cm] length were located at the edges of the rocking section. These bars have an elastic modulus of 200,000 [MPa] and a yield strength of 400 [MPa].

The behaviour of the structure is significantly improved after implementing the system described above. The ISDs are regulated and decreased as shown in Fig. 5a. The residual displacements of the top story were highly reduced as shown in Fig. 5c. These residual displacements are due to large plastic rotations in the frame elements. It should be noted that the design of such a system could be tuned to prevent these residual deformations.

The moment envelops are shown in Fig. 6a for each ground motion. It is observed that large flexural moments develop at the setback level. These moments may lead to the requirement of a high amount of reinforcement in the wall elements. This

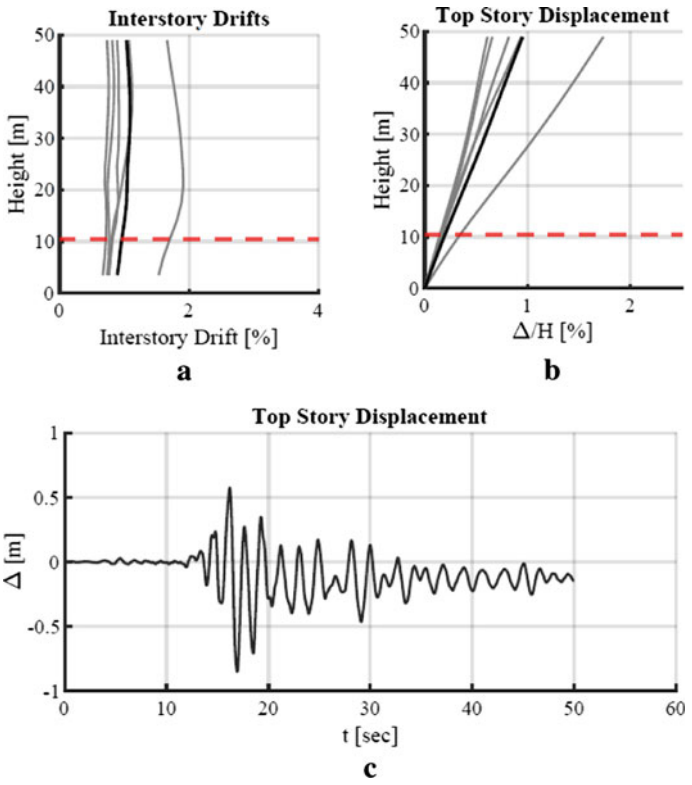

Fig. 5 Results for a frame retrofitted with a base rocking system subjected to several ground excitations (average results are shown in bold line): **a** ISDs, **b** story displacements, **c** displacement of the top story due to the LA09 ground excitation

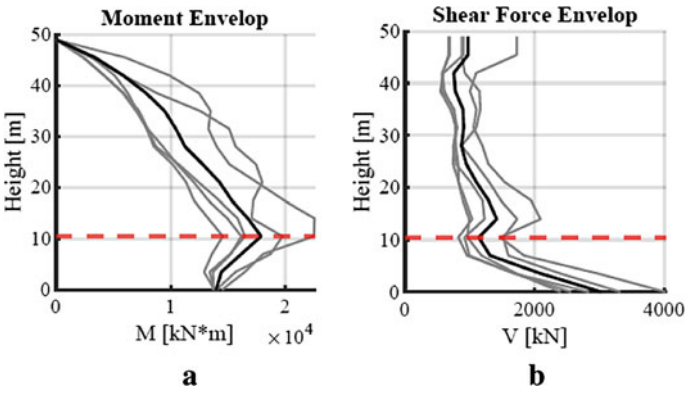

Fig. 6 Results for a frame retrofitted with a base rocking system subjected to several ground excitations (average results are shown in bold line): **a** moment envelops, **b** shear envelops

might lead to uneconomic designs of the retrofitting system. Therefore, an additional rocking section is provided at higher level of the rocking wall to reduce these demands.

6 Multiple Rocking

An additional rocking section is added to the system described in Sect. 4 which includes an SMRF with a rocking wall with a base rocking section. The additional rocking section was located at different story levels varied from the floor of the second story to the floor of the 14-th story. The decomposition flexural moment of the second rocking level was designed for different portions of the base rocking section decomposition moment. This ratio is referred to herein as Top to Bottom moment Ratio (TBR).

The behaviour of the structure was examined for the different potential combinations of location of top rocking section and TBRs. The contour maps in Fig. 8 show different responses of the structure. These represent the average (over all ground motions) of the maximum (over all stories or floors) of peak responses. The responses are normalized with the corresponding responses obtained for a system with base only rocking section except the ISDs that were normalized with the base rocking solution.

It is shown from Fig. 8a that adding an additional rocking section increases the maximum ISD compared to a system with base only rocking section (in this case the maximum ISD was 0.43 of the bare frame maximum ISD). This result is expected since the additional rocking section adds flexibility to the wall system. However, it is shown that for TBR that is larger than 40% the additional rocking section increases

the ISD only by 10% for each rocking level. This might be in the acceptable limits of the maximum ISDs based on the selected design performance level.

The main target of adding the top rocking section is reducing the average moment demand envelop volume in the wall. It is shown in Fig. 8b that the average moment demand envelop volume can be reduced by 29% by designing the top rocking section at the third level (at the setback level) and with TBR of approximately 20% with only about 9% additional ISD. This solution reduces the shear force by approximately 5%. The ISD obtained using the previous solution gives an ISD of approximately 1.2%.

Designing the top decomposition moment to be larger than the external moment does not affect the results compared to a solution with base rocking section. This is since in this case, the top rocking section will be inactive (does not open). This can be seen clearly in Fig. 8 with a virtual line connecting between the point (20%, 14) and (180%, 3). All the designs located at the right of this line will not affect the results.

It is shown in the selected example that locating the top rocking section at the setback level is the most beneficial. In addition, it is expected that adding another rocking section (3rd rocking section) is expected to significantly reduce the moment demand envelop volume. The response of this system is compared with the bare frame and base rocking system as shown in Fig. 7. In this case, the ratio between the top to bottom decomposition moments is 20%. It is shown that moment envelop volume is significantly reduced compared to the case of the base rocking section while the ISDs remain within the acceptable limits (see Fig. 8).

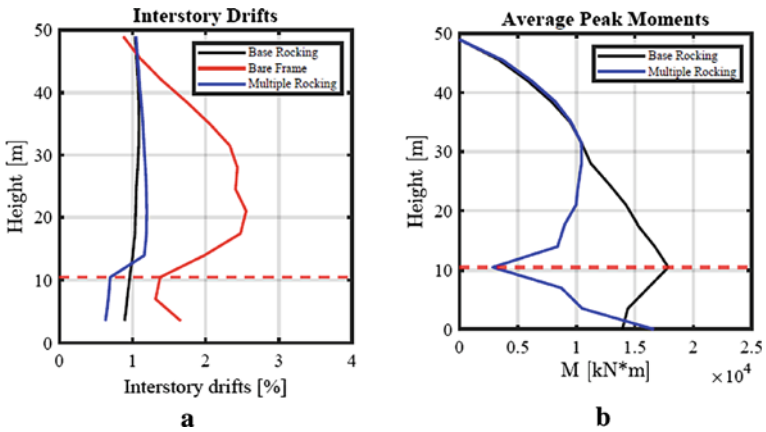

Fig. 7 **a** Average (over all ground motions) peak ISD, **b** average moment demands

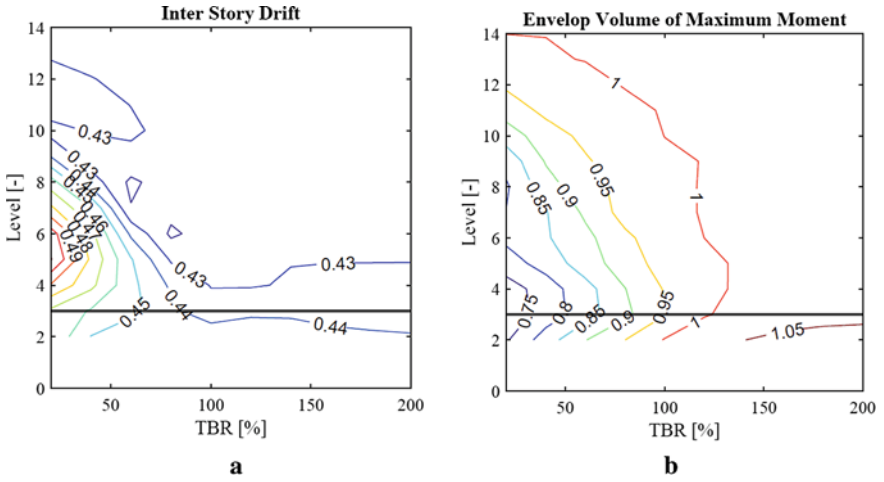

Fig. 8 **a** Normalized (by the base rocking corresponding responses), average (over all ground motions), maximum (over the height) peak responses inter-story drift, **b** average moment demand envelop volume

7 Conclusions

In this paper, the behaviour of an irregular SMRF retrofitted with multiple rocking wall system was investigated. The study was conducted using a nonlinear time history analysis of a fourteen story SMRF with a setback elevation that starts from the fourth floor. The effect of the location and the design moment of the top rocking section have been examined.

The results show that adding a rocking wall with a traditional base rocking section regulates the ISDs and reduces them significantly compared with the behaviour of the bare frame. Adding a rocking section at higher levels could potentially reduce the flexural moment and shear force demands while preserving acceptable ISDs and displacements.

For the presented case study, a reduction of 29 and 5% in the average flexural moment demand envelop volume and shear force design demand could be obtained while increasing the ISDs only by 9% compared to the base rocking solution. This result was obtained when the top rocking section was designed at the setback level. A reduction in these demands is expected to significantly reduce the initial cost of the retrofitting system.

References

1. Lignos DG, Asce AM, Hikino T, Matsuoka Y, Nakashima M, Asce M (2013) Collapse assessment of steel moment frames based on e-defense full-scale shake table collapse tests. 139:120–132. https://doi.org/10.1061/(ASCE)ST.1943-541X.0000608
2. Karavasilis TL, Bazeos N, Beskos DE (2008) Seismic response of plane steel MRF with setbacks: estimation of inelastic deformation demands. J Constr Steel Res 64:644–654. https://doi.org/10.1016/j.jcsr.2007.12.002
3. Kim J, Kim T (2009) Assessment of progressive collapse-resisting capacity of steel moment frames. J Constr Steel Res 65:169–179. https://doi.org/10.1016/j.jcsr.2007.12.002
4. Asgarian B, Sadrinezhad A, Alanjari P (2010) Seismic performance evaluation of steel moment resisting frames through incremental dynamic analysis. J Constr Steel Res 66:178–190. https://doi.org/10.1016/j.jcsr.2009.09.001
5. Pampanin S, Christopoulos C, Nigel Priestley MJ (2003) Performance-based seismic response of frame structures including residual deformations. Part II: multi-degree of freedom systems. J Earthq Eng 7:119–147. https://doi.org/10.1080/13632460309350444
6. Erochko J, Christopoulos C, Tremblay R, Choi H (2011) Residual drift response of smrfs and brb frames in steel buildings designed according to ASCE 7-05. J Struct Eng 137:589–599. https://doi.org/10.1061/(ASCE)ST.1943-541X.0000296
7. Gioiella L, Tubaldi E, Gara F, Dezi L, Dall'Asta A (2018) Modal properties and seismic behaviour of buildings equipped with external dissipative pinned rocking braced frames. Eng Struct 172:807–819. https://doi.org/10.1016/j.engstruct.2018.06.043
8. Nollet M-J, Smith BS (1993) ehavior of curtailed wall-frame structures. J Struct Eng 119:2835–2854
9. Rahman AM, Restrepo JI (2000) Earthquake resistant precast concrete buildings: seismic performance of cantilever walls prestressed using unbonded tendons. Christchurch, New Zealand
10. Tremblay R, Poirier L, Bouaanani N, Leclerc M, Rene V, Fronteddu L, Rivest S (2008) Innovative viscously damped rocking braced steel frames. In: 14th world conference on earthquake engineering (14 WCEE)
11. Marriott DJ, Pampanin S, Bull D, Palermo A (2008) Dynamic testing of precast, post-tensioned rocking wall systems with alternative dissipating solutions. In: 2008 NZSEE conference. University of Canterbury, Civil and Natural Resources Engineering
12. Eatherton M, Hajjar J, Ma X, Krawinkler H, Deierlein G (2010) Seismic design and behavior of steel frames with controlled rocking—Part I: concepts and quasi-static subassembly testing. ASCE Struct Congr 1523–1533. https://doi.org/10.1061/41130(369)138
13. Christopoulos C, Filiatrault A, Folz B (2002) Seismic response of self-centring hysteretic SDOF systems. Earthq Eng Struct Dynam 31:1131–1150. https://doi.org/10.1002/eqe.152
14. Wiebe L, Christopoulos C (2009) Mitigation of higher mode effects in base-rocking systems by using multiple rocking sections. J Earthq Eng 13:83–108. https://doi.org/10.1080/13632460902813315
15. Li T, Berman JW, Wiebe R (2017) Parametric study of seismic performance of structures with multiple rocking joints. Eng Struct 146:75–92. https://doi.org/10.1016/j.engstruct.2017.05.030
16. Qureshi MI, Warnitchai P (2017) Reduction of inelastic seismic demands in a mid-rise rocking wall structure designed using the displacement-based design procedure. Struct Des Tall Spec Build 26:1–22. https://doi.org/10.1002/tal.1307
17. Mazzoni S, McKenna F, Scott M, Fenves G, others (2006) Open system for earthquake engineering simulation (OpenSEES) user command-language manual. Pacific Earthquake Engineering Research Center, University of California, Berkeley
18. Perez FJ, Sause R, Pessiki S (2007) Analytical and experimental lateral load behavior of unbonded posttensioned precast concrete walls. J Struct Eng 133(11):1531–1540

Seismic Retrofitting of Irregular Mixed Masonry-RC Buildings: Case Study in Lisbon

João Rodrigues, Jelena Milosevic Ilic, and Rita Bento

1 Introduction

From the experience of the recent earthquakes, it is evident that unsatisfactory behaviour of many buildings is due to the insufficient lateral capacity, limited ductility and structural irregularity [1]. In fact, the existing real structures are often irregular, as perfect regularity is an idealization that rarely occurs.

Regarding buildings configuration, based on seismic codes, two irregularities can be distinguished: in plan and in elevation [2]. However, quite often buildings are characterized with a combination of both types of structural irregularities. Irregular configurations, either in plan or elevation, were often recognized as one of the leading causes of failure of buildings during past earthquakes.

Therefore, special attention should be paid on irregular structures, particularly the ones located in seismic zones. Besides, numerous existing old masonry and mixed masonry-reinforced concrete (RC) buildings were designed and built without using any seismic protection criteria and without considering the negative effect of the irregularities in plan and elevation during the building design. Consequently, to increase the safety of irregular existing structures and to reduce their seismic vulnerability, appropriate retrofitting techniques should be adopted.

In fact, this was confirmed in numerous studies, as for example in [3–8]. In these studies, nonlinear static or dynamic analysis on irregular masonry or mixed-masonry RC structures were performed, obtaining as the main conclusion that a proper retrofit solution has to be adopted to mitigate the seismic vulnerability.

J. Rodrigues · J. M. Ilic (✉) · R. Bento
CERIS, Instituto Superior Técnico, University of Lisbon, Av. Rovisco Pais, 1049-001 Lisbon, Portugal
e-mail: jelena.milosevic@tecnico.ulisboa.pt

R. Bento
e-mail: rita.bento@tecnico.ulisboa.pt

R. Bento et al. (eds.), *Seismic Behaviour and Design of Irregular and Complex Civil Structures IV*, Geotechnical, Geological and Earthquake Engineering 50,
https://doi.org/10.1007/978-3-030-83221-6_14

Due to this, the aim of this paper is twofold. Firstly, it evaluates the seismic behavior of selected irregular mixed masonry-RC (i.e. 'Placa') buildings located in Lisbon in their original stage. Then, secondly, based on the obtained results and the respective damage patterns, a set of seismic reinforcement solutions were proposed and analyzed.

The case study building was modelled based on the equivalent frame modelling approach using TREMURI software [9] and, subsequently, the seismic behaviour was assessed performing nonlinear static analyses by considering the effect of aggregate. The uniform load pattern has been selected as the reference one based on previous results of other authors performed on isolated buildings [10] and also in aggregate [11]. Indeed, it seems reasonable that uniform load distribution is sufficiently representative of the inertia actions acting on the aggregate since: (i) the aggregate is composed by buildings of medium–low height; and (ii) the confinement provided by adjacent buildings tends to inhibit the occurrence of uniform failure modes (i.e. mainly affected by the concentration of cracks in spandrels). In the future work, nonlinear dynamic analysis will be performed, since this type of analysis is considered as more accurate.

Additionally, a set of retrofitting solutions were implemented to the original models. Results between original and retrofitted models were compared in terms of the structural regularity, capacity curves and obtained damage patterns. On this way, it was possible to analyze and understand the impact and efficiency of the retrofit solutions, regarding the damage minimization and the guarantee of the regulatory safety requirement.

In the past decades, the popular seismic strengthening technique used for strengthening of masonry buildings was cement coatings, which efficiency was proved by performing laboratory or in situ experimental tests [12]. However, lately these materials are replaced by polymers which are being used for masonry as well as for reinforced concrete structures. The efficiency of these techniques is already confirmed in different studies by performing experimental tests [13–18] or numerical analysis [19–21].

Among the scenarios analyzed for the unreinforced buildings under study, the application of transversal steel connectors, reinforced plaster and a carbon fiber mesh, were applied as a solution for reinforcement of masonry walls. In contrast, for reinforcement of reinforced concrete elements, it was decided to analyze the effect of steel jacketing and CFRP sheets.

2 Case Study Building

The mixed masonry-RC building adopted as the case study, due to its structural characterization and the selected materials, represents a considerable portion of the buildings in the "Alvalade" neighborhood in Lisbon, as concluded in [22]. The chosen case study has an irregular shape in plan, the so called "Rabo de bacalhau" (Fig. 1).

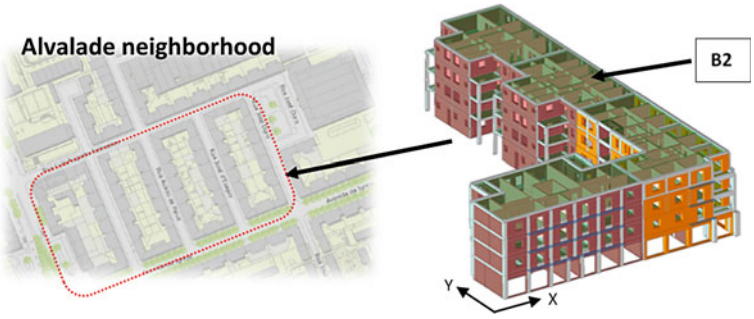

Fig. 1 Location of the case study building and 3D model

In the case study building, the three upper floors serve as housing, while the ground floor is dedicated exclusively to commercial use, with the reduction in the number of masonry walls in such floors causing structural irregularity and leading to soft-story types of collapse. Figure 2 shows the differences in floor plan between the ground floor (Fig. 2a) and the housing floors (Fig. 2b), as well as the arrangement of the reinforced concrete elements and the thickness of the walls.

The main and back façades, 0.40 m thick, consist of a reinforced concrete frame structure filled with hollow brick masonry. The side walls are also made up of a reinforced concrete frame system filled with 0.20 m thick hollow brick masonry. Regarding the type of material used in the interior walls, it was decided to consider the use of hollow brick in the last two floors and solid brick in the remaining lower floors, in accordance with the [23]. The thickness of the walls varies between 0.25 m and 0.15 m, whether it is the stairwell and partition walls, or other partitions, respectively.

The floors of the building consist of reinforced concrete slabs 0.12 m thick and reinforced in both directions. Reinforced concrete columns and beams are distributed

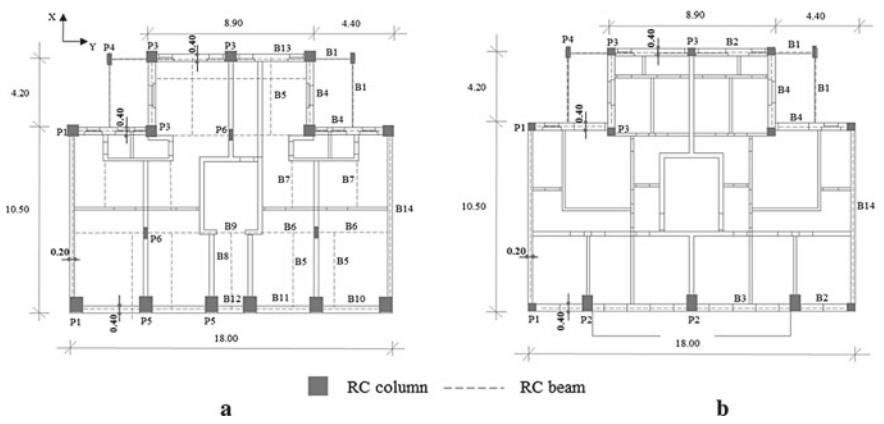

Fig. 2 **a** Ground floor, **b**Top floor (dimensions in [m])

essentially along the exterior walls of the building, except for a few exceptions on the ground floor: (i) interior columns that are discontinued on the upper floors, as well as (ii) some interior beams which are strategically positioned to assist in supporting the loads generated by other walls placed in this alignment on the upper floors. The distribution of RC elements is illustrated in Fig. 2. This represents one more irregularity in these structures.

As concluded in [24], the connections between exterior/exterior and exterior/interior walls in these buildings are weak. Consequently, the model was made considering bad connections. For more information, refer to [24]. The "block" effect is relevant to "Placa" buildings, which are usually located in the aggregate. Thus, this building was modelled in aggregate (see Fig. 1), then with the aim of defining the pushover curves, only the results for his building (B2) are considered.

The seismic response of the structure was assessed by performing nonlinear static analyses through the equivalent frame modelling approach, using Tremuri program [9], considering only in plane response of the masonry walls. It was assumed that out of plane response is prevented with the existing RC ring beams. Mechanical parameters used for the numerical model can be found in [24].

3 Reinforcement Techniques

Regarding the seismic retrofit techniques that were chosen, it was decided not to include more invasive solutions, such as the demolition of existing masonry walls to consequently add either reinforced concrete columns and/or shear walls or a steel bracing structure. In other words, it was decided to analyze only alternatives less invasive; i.e. solutions that did not result either in an excessive increase in the weight of the structure or in the eventual need to resort to the reinforcement of the foundation elements.

In this context, and with the objective of minimizing the damage observed in the building regarding the most demanding situations, it was chosen relatively common solutions in the current scenario of rehabilitation in Portugal, in accordance, whenever possible, with the efficiency regarding the cost and associated benefits.

Therefore, the study focused on the analysis of the following retrofit techniques:

- Strengthen of wall-to-wall connections using steel tie bars;
- Strengthen of masonry piers and spandrels using reinforced plaster, that is, by applying a steel mesh to the face of the masonry element to be reinforced;
- Strengthen of masonry elements with carbon fiber (CFRP). It corresponds to an approach similar to reinforced plaster, that is, through a reinforcement mesh, whose material (instead of steel) is based on carbon fibers, thus resembling the strengthen technique by the TRM system;
- Strengthen of reinforced concrete beams and columns by means of metal jacketing bonded to the structural element through epoxy resin;

- Strengthen of reinforced concrete beams and columns by means of jacketing with CFRP strips bonded to the structural element through epoxy resin.

4 Comparison Between Unreinforced and Reinforced Models

Nonlinear static analyzes were performed considering the X and Y directions (direction of the side walls and facades, respectively, see Fig. 1) in both the positive and negative senses, and considering uniform distribution (proportional to the mass of the building) and triangular distribution (proportional to the product between mass and height). Even two load distributions were considered and analyzed, it should be noted that uniform distribution is considered more relevant (as already mentioned above) since building was modelled in aggregate [24].

The pushover curves were defined, and the correspondent ultimate displacement was determined for the displacement associated with a reduction of 20% of the maximum base shear force in the nonlinear phase, as indicated in Part 3 of Eurocode 8 (EC8-3) [25]. To evaluate the seismic performance of the structure, the target displacement (dt) was determined. For this purpose, the bilinear pushover curves were defined and converted into the ADRS (Acceleration-Displacement-Response-Spectrum) format correlated with the seismic response spectrum. Accordingly, the building under study is located on type soil B, and in an earthquake zone 1.3 for earthquake type 1, determined from Part 1 of EC8 [26] and considered more demanding in comparison with earthquake zone 2.3 [24]. In the case of a social housing building, an importance coefficient $\Upsilon\mathrm{II} = 1.0$ was adopted, resulting in a soil acceleration (agr) of 1.13 m/s^2. Reduction for agr of 25% was made following the Portuguese Annex of EC8-3 [25], where is defined that for the existing buildings, there is no justification for considering the same return period adopted for the seismic design of new buildings.

Finally, the seismic performance of the structure was evaluated by taking into consideration the ratio between the ultimate displacement (du) and the target displacement (dt), such that the structural safety is verified when this value is higher than 1. Then, it was concluded that the structure does not verify safety only for uniform lateral loading distribution in the positive Y direction (parallel to the façade). Based on this result, the analysis of the structural damage pattern for the uniform lateral loading distribution in the Y direction and corresponding to the respective objective displacement was assumed as the most conditioning.

The nonlinear response of the masonry panels is modelled by nonlinear beams with a multilinear constitutive law. This law is provided the distribution of damage, which distinguishes the damage on five different levels, based on the shear strength reduction and drift of the elements (DL1—slight damage; DL2—moderate damage; DL3—extensive damage; DL4—near collapse damage; DL5—collapse) [27].

Figure 3 shows the damage pattern for the façades, considering the target displacement obtained for the most conditioning case, i.e. for Y direction and uniform load

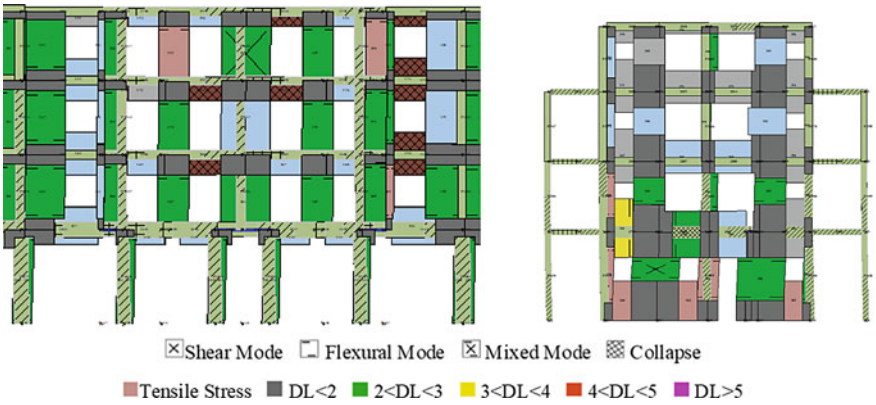

Fig. 3 Damage pattern in the façades for unreinforced building

distribution. As it can be observed, spandrels show the collapse by shear, while piers are characterized by the moderate flexural plastic damage (DL2).

Concerning the interior walls, except for a few cases, where collapse or near-collapse damage occurs (DL4), the remaining walls generally present only moderate damage (DL2). For sake of brevity, damage pattern for interior walls is not presented in this paper. About the reinforced concrete elements, bending damage in both the columns and the beam-column connecting knots stands out.

Comparing the capacity curves of the interior and exterior walls with the global capacity curve, it was observed that the behavior of the structure is quite conditioned by the walls of the back façade (W105 and W8), whose curves show a gradual decrease in their base shear force until reaching the target displacement ($dt = 0.84$ cm). This observation may be directly associated with the irregularity in plan provided by the configuration of the "*rabo de bacalhau*" in the back façade of the building. However, after the application of certain reinforcement solutions, it was possible to minimize the torsional effects and consequent damages of the façade, as it is shown below in this section (Fig. 4).

In total, 12 retrofit scenarios were selected and studied (Fig. 5) regarding the seismic retrofit techniques described in Sect. 3. Even all predicted strengthen scenarios met the seismic action safety criterion ($du/dt > 1$), a brief description will then be given only of the reinforcement scenarios which the results obtained were the most relevant and effective. It should be mentioned that technique C1, which corresponds to the improvement of the connections between walls is applied in all retrofitting scenarios.

Therefore, in one case (scenario 4), the application of a carbon fiber reinforcement mesh (CFRP) to the masonry walls was simulated. Consequently, the reinforcement was added to both façades in their integrity, as well as some interior walls where extensive or superior damage was observed ($DL > 3$).

The overall reinforcement of the masonry elements on the façades and main interior resistant walls with a CFRP reinforcement mesh has considerably improved

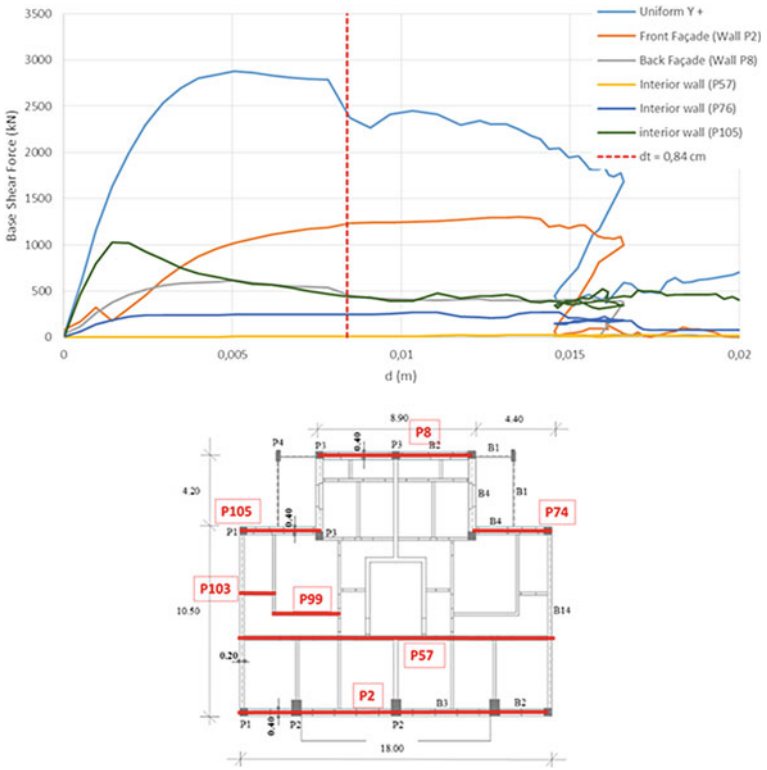

Fig. 4 Pushover curves for Y direction (up) and position of the walls in the building plan

performance to most reinforced walls. However, inducing partial rupture of the ground floor beams on the façades and some worse damage on masonry panels in the back façade (Fig. 6). As for the pushover curves (Fig. 7), it was concluded that the reinforcement using a carbon fiber mesh (CFRP), applied entirely to the façades, contributed to a significant increase in the resistance of the building in the Y direction (direction of the facade), as well as for the ultimate displacement value (du) of the structure.

Then, it was decided to analyze the possible reinforcement of the stairway walls, in order to determine its impact, both in reducing the displacement of the structure and in minimizing the torsional effects and consequent damages. In summary, this technique (scenario 5) describes the application of a CFRP reinforcement mesh on both sides of the stairway walls. Consequently, the reinforcement of the stairway walls indirectly promoted a better behavior of the masonry spandrels on the façades and also the interior beams on the ground floor (Fig. 8).

Scenario 8 consists on the reinforcement, to its full extent, of the corner columns of the building, as well as the remaining columns at ground floor level of the main façade and also the most damaged beams in the ground level. For the columns, the

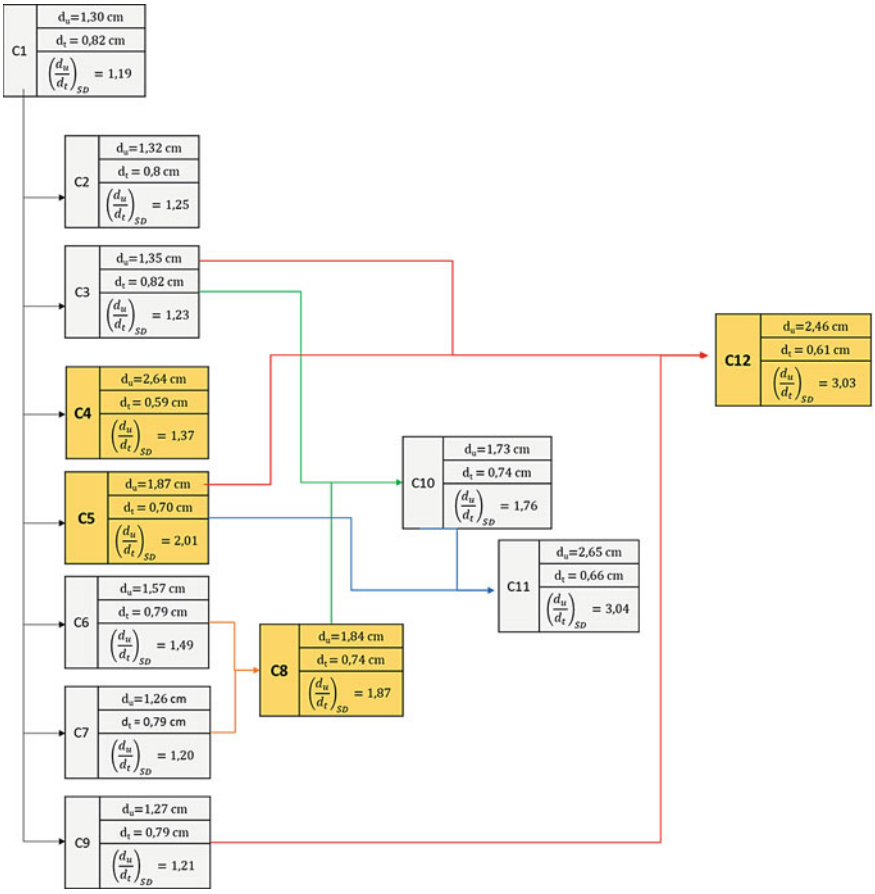

Fig. 5 Schematic correlation of the different reinforcement scenarios

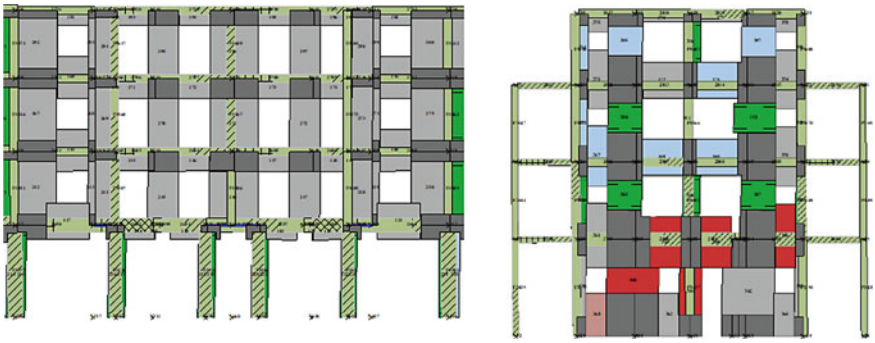

Fig. 6 Damage pattern for C4 (see Fig. 5)

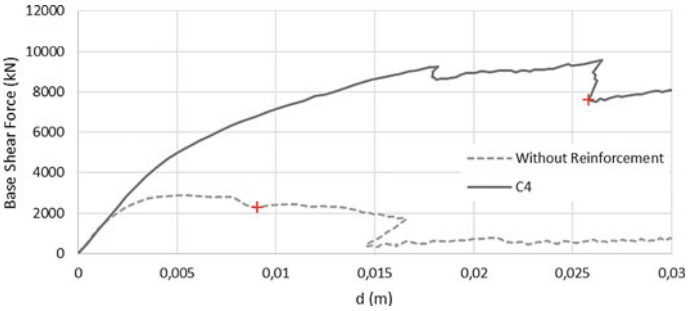

Fig. 7 Pushover curves for conditioning load distribution (+ represents d_u)

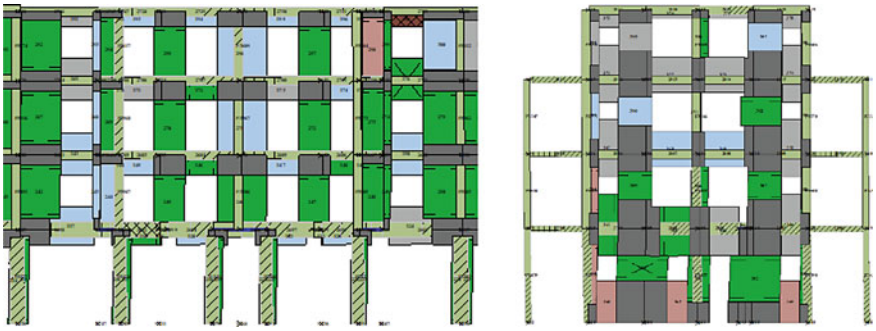

Fig. 8 Damage pattern for C5 (see Fig. 5)

simulated reinforcement solution consists on the application of metal angles (50 × 50 × 5 mm) attached to the surface in order to strengthen longitudinal reinforcement deficiencies and ensure better bending behavior. For the spandrels, it was considered the application of metal sheets. The modelling of the reinforcement solution was elaborated by calculating an equivalent reinforcement corresponding to the sum of the existing reinforcement with the addition of the new one.

The strengthening on the ground floor of the beams in the façade and some interior beams, allowed the complete suppression of shear collapse that were observed in some of these elements in the original case of the unstrengthen building. The strengthen, only on the ground floor, with metallic jacketing of the main façade columns, effectively mitigated the flexural damage on the respective columns both, on the floor where the reinforcement was applied, as well as on the upper floors. Combination of reinforcement with metal elements on both, the ground floor beams, and corner columns proved to be more efficient compared to separate reinforcement on beams and columns. Damage pattern for this technique is illustrated in Fig. 9. As can be seen in Fig. 10, the reinforcement contributed to a significant increase in the resistance of the building in the Y direction, as well as for the ultimate displacement value (du) of the structure.

Fig. 9 Damage pattern for C8 (see Fig. 5)

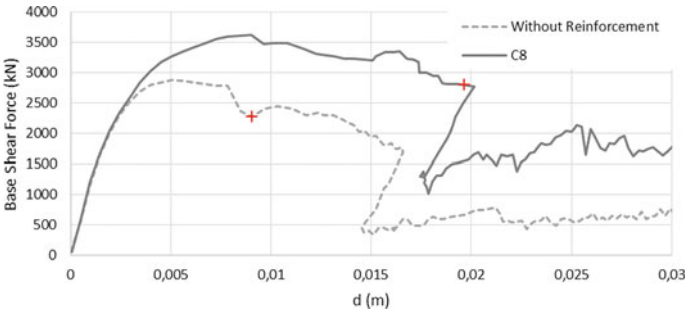

Fig. 10 Pushover curves for conditioning load distribution (+ represents d_u)

In scenario 12, all of the building's columns and also the interior beams present on the ground floor were reinforced by the CFRP confinement. In order to simulate the referred technique, it has been alternatively attempted to simplify the effect of CFRP confinement on the respective elements. Thus, based on the theoretical stress–strain model for confined concrete proposed in [28] and the expressions for predicting the action of FRP jacketing proposed in both [25, 29] different values of compressive strength and ultimate strain were determined for the respective sections of confined concrete. Therefore, these parameters were added to the mechanical properties that characterize the material of the reinforced elements and then analyzed. As for the masonry elements, all the spandrels present in the façades were reinforced with carbon fiber mesh (CFRP), as well as all masonry members perpendicular to the side walls.

The reinforcement solution contributed to the mitigation of damage to all columns above the ground floor, as well as to the precautionary of shear damage that had been evident in the interior beams. Also, the reinforcement proved to be particularly efficient in minimizing damage to the masonry lintels on the facades (Fig. 11). As for the remaining masonry walls, collapses are no longer observed, although damage is still occurring up to the level of extensive damage (DL3).

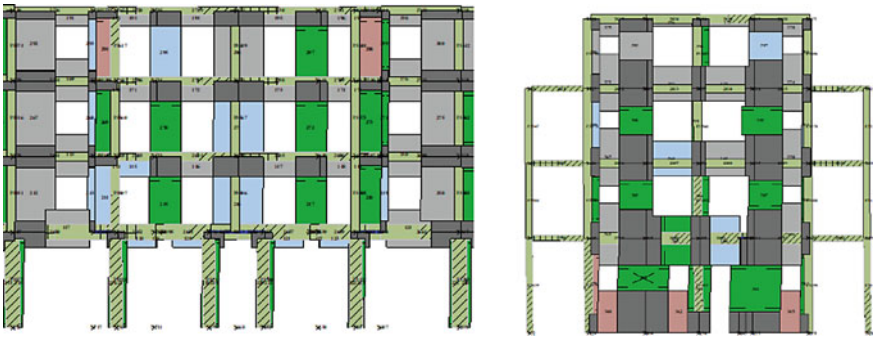

Fig. 11 Damage pattern for C12 (see Fig. 5)

As for the structural performance of the reinforcement solutions applied in scenario 12, its efficiency was proven, since the safety criterion for conditioning loading (Uniform Y +) is satisfactorily verified. For more information about strengthening techniques and results refer to [30].

5 Conclusions

The irregular mixed masonry-reinforced concrete buildings are reflected as a significant portion of the Lisbon building stock invariably exposed to a non-negligible seismic hazard. Therefore, to make safe irregular existing structures, it is necessary to mitigate the seismic vulnerability adopting a proper retrofit solution. In this paper, several retrofitting techniques are proposed for both masonry and RC elements. After applying the reinforced techniques, the overall structural safety of the building was satisfied, avoiding the global collapse of the structure. At the same time, the observed damage levels were appreciably mitigated.

The recommended solution should always be defined after an analysis of the costs associated with each intervention. However, based on the results obtained, it can be considered that one of the most appropriate recommendations should target the minimization of torsional effects due to the irregularities found in the back façade. Thus, it should consist mainly on reinforcing bad connections between walls, as well as a possible global reinforcement of the façades and walls of the stairwell, with the application of reinforced plaster or a reinforcement mesh in CFRP.

References

1. Ferraioli M, Avossa AM, Mandara A (2009) Performance-based seismic retrofitting of irregular RC building structures. Protection of Historical Buildings, PROHITECH 09
2. De Stefano M, Mariani V (2014) Perspective on European earthquake engineering and seismology, Chapter 13. https://doi.org/10.1007/978-3-319-07118-3
3. Simões A, Milosevic J, Meireles H, Bento R, Cattari S, Lagomarsino S (2015) Fragility curves for old masonry building types in Lisbon. Bull Earthq Eng 13(10):3083–3105
4. Simões A, Bento R, Lagomrasino S, Cattari S, Lourenço B (2019) Fragility functions for tall URM buildings around early 20th Century in Lisbon, Part 2: Application to different classes of buildings. Int J Archit Herit
5. Lamego P, Lourenço PB, Sousa ML, Marques R (2017) Seismic vulnerability and risk analysis of the old building stock at urban scale: application to a neighbourhood in Lisbon. Bull Earthq Eng 15(7):2901–2937
6. Parisi F, Augeni N (2011) Nonlinear seismic behaviour of irregular URM walls with openings. In: 14th Italian national conference on earthquake engineering
7. Cattari S, Maino S, Lagomarsino S (2015) Seismic assessment of plan irregular masonry buildings with flexible diaphragms. In: Proceedings of the tenth pacific conference on earthquake engineering building an earthquake-resilient pacific, Sydney, Australia
8. Mendes N, Lourenço PB (2014) Sensitivity analysis of the seismic performance of existing masonry buildings. Eng Struct 80:137–146
9. Lagomarsino S, Penna A, Galasco A, Cattari S (2013) TREMURI program: an equivalent frame model for the nonlinear seismic analysis of masonry buildings. Eng Struct 56:1787–1799
10. Marino S, Cattari S, Lagomarsino S (2018) Use of non-linear static procedures for irregular URM buildings in literature and codes. In: Proceeding of the 16th European conference on earthquake engineering, pp 18–21
11. Greco A, Lombardo G, Pantò B, Famà A (2018) Seismic vulnerability of historical masonry aggregate buildings in oriental sicily. Int J Architect Herit, 1–24
12. Tomaževič M, Sheppard P, Žarnić R (1985) Experimental studies of methods and techniques for the repair and strengthening of historic buildings in old urban and rural nuclei. In: US-Yugoslav workshop on Protection of Historic Buildings and Town Centres in Seismic Regions, 17–22 June 1985, Budva (in Slovene)
13. Dusi A, Mezzi M, Manzoni E, Dusi C (2007) The use of polymeric grids for the seismic enhancement of brick masonry buildings. 7º Congresso de sismologia e engenharia sísmica
14. Papanicolaou C, Triantafillou T, Karlos K, Papathanasiou M (2006) Textile-reinforced mortar (TRM) versus FRP as strengthening material of URM walls: In-plane cyclic loading. Mater Struct/Materiaux et Construct 40:1081–1097
15. Rahman A, Ueda T (2016) In-plane shear performance of masonry walls after strengthening by two different FRPs. Compos Constr 20(5):04016019
16. Gattesco N, Boem I, Dudine A (2015) Diagonal compression tests on masonry walls strengthened with a GFRP mesh reinforced mortar coating. Bull Earthq Eng 13:1703–1726
17. Triller P, Tomazevic M, Gams M (2019) Seismic strengthening of clay block masonry builings with composites: an experimental study of a full scale three-storey building model. Bull Earthq Eng 17:4049–4080
18. Guerreiro J, Proença J, Ferreira GJ, Gago A (2018) Experimental characterization of in-plane behaviour of old masonry walls strengthened through the addition of CFRP reinforced render. Compos Part B Rngineering 148:14–26
19. Marques R, Lamego P, Lourenço PB, Sousa ML (2017) Efficiency and cost-benefit analysis of seismic strengthening techniques for old residential buildings in Lisbon. Earthq Eng 1590–1625
20. Gattesco N, Amadio C, Bedon C (2015) Experimental and numerical study on the shear behaviour of stone masonry walls strengthened with GFRP reinforced mortar coating and steel-cord reinforced repointing. Eng Struct 90:143–157

21. Maio R, Estêvão J, Ferreira T, Vicente R (2017) The seismic performance of stone masonry buildings in Faial island and the relevance of implementing effective seismic strengtheing policies. Eng Struct 141:41–58
22. Milosevic J (2019) PhD Dissertation: Seismic vulnerability assessment of mixed masonry-reinforced concrete buildings in Lisbon, University of Lisbon
23. General Regulation of Urban Construction (1944) Direction of urbanization and construction services, 5th edn. City Hall, Portugal (in Portuguese)
24. Milosevic J, Cattari S, Bento R (2019) Definition of fragility curves through nonlinear static analyses: procedure and application to a mixed masonry-RC building stock. Bull Earthq Eng 513–545. https://doi.org/10.1007/s10518-019-00694-1
25. CEN (2017). NP EN 1998–3: Eurocódigo 8–Projecto de Estruturas para Resistência aos Sismos. Parte 3: Avaliação e Reabilitação de edifícios. Instituto Português da Qualidade. European Committee for Standardization. Bruxelas: Instituto Português da Qualidade. European Committee for Standardization
26. CEN (2003) European Standard EN 1998–1: Eurocode 8: Design of structures for earthquake resistance. Part 1: General rules, seismic actions and rules for buildings. Stage 51 Draft, Brusells: Comite Europeen de Normalisation, December 2003
27. Lagomarsino S, Cattari S (2015) Seismic performance of historical masonry structures through pushover and nonlinear dynamic analyses. Ansal A (ed), Perspectives on European earthquake engineering and seismology. Geotechnical, geological and earthquake engineering, vol 39, pp 265–292. Springer, Chamhttps://doi.org/10.1007/978-3-319-16964-4_11
28. Mander JB, Priestley MJN, Park R (1988) Theoretical stress-strain model for confined concrete. ASCE J Struct Eng 114(8):1804–1826
29. CNR-DT200 R1 (2013) Istruzioni per la Progettazione, l'Esecuzione ed il Controllo di Interventi di Consolidamento Statico mediante l'utilizzo di Compositi Fibrorinforzati. Consiglio Nazionale delle Ricerche. Roma, Itália
30. Rodrigues J (2019) MsC Dissertation: seismic retrofit of an old mixed masonry-reinforced concrete building, University of Lisbon, 2019, (in Portuguese)

Seismic Behaviour of Torsionally-Weak Buildings with and Without Base Isolators

Juan C. Reyes

1 Introduction

In recent years, new methods for seismic design and rehabilitation of irregular and complex structures have been developed. These techniques seek to reduce structural damage and maintain continuous operation of the structure after an earthquake. Among these techniques, base isolation is usually preferred because it is highly efficient in reducing seismic demands for buildings with fundamental periods in the equal velocity range of the design spectrum.

Seismic isolated buildings are initially designed assuming rigid super-structure, even if their plans are highly irregular. It is accepted that unfavourable torsional behaviour is eliminated by the seismic isolation system; however, this conclusion has been mostly supported by analyses of simplified buildings, in which plan asymmetry is not included explicitly [1–4]. Some researchers have worked with more realistic models of the system, but they do not consider nonlinear behavior of the super-structure [5–7]. To contribute to the understanding of actual effect of base isolation on the seismic behavior of unsymmetric-plan buildings, this paper presents results of a linear parametric study (considering super-structure flexibility) and nonlinear analyses of realistic irregular buildings. These analyses permit to quantify the importance of base isolation on reducing undesirable torsional effects.

J. C. Reyes (✉)
Universidad de Los Andes, Bogota, Colombia
e-mail: jureyes@uniandes.edu.co

R. Bento et al. (eds.), *Seismic Behaviour and Design of Irregular and Complex Civil Structures IV*, Geotechnical, Geological and Earthquake Engineering 50,
https://doi.org/10.1007/978-3-030-83221-6_15

2 Selected Structural Systems

To meet a large range of possibilities, unsymmetric-plan buildings can be classified as [8]: (i) "Torsionally-stiff" systems (A-type): lateral displacements dominate motion in the first two modes, while torsion controls motion in the third mode, indicating weak coupling between lateral and torsional components. Additionally, the period of the dominantly torsional mode is much shorter than the period of the dominantly-lateral mode. (ii) "Torsionally-similarly-stiff" systems (B-type): these systems have a high degree of coupling between translational and torsional motions. The first three modes of this kind of building have similar periods, and are strongly coupled. (iii) "Torsionally-flexible" system (C-type): in these systems, the first mode of vibration is essentially torsional. The period of the dominantly-torsional mode is longer than the period of the dominantly-lateral modes. For this study, buildings type B and C are the most relevant. The first task is to design realistic buildings that meet the requirements of systems B and C. Considering that new buildings' codes discourage the use of these systems, the buildings were designed according to an old code (UBC-85) [9]. Figure 1 presents the gallery of the shapes and frame layouts initially analyzed to get the definitive design. The thin lines represent the non-moment resisting frames (gravity-only framing) and the bold lines correspond to the earthquake resistant system (moment resisting frames). The selected systems are shown in Fig. 2. One important characteristic of these buildings is that all of them have similar area, weight and translational stiffness. They are three-story buildings with span length of 9.14 m

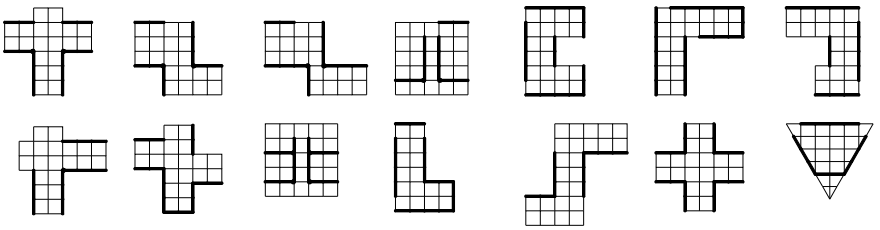

Fig. 1 Preliminary building layouts

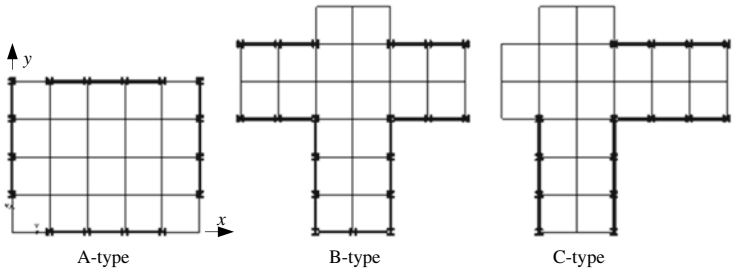

Fig. 2 Selected structural systems

(30 feet) and story height of 3.96 m (13 feet). The maximum plan dimension of B- and C-type buildings is 54.86 m (180 feet). "Good" engineering judgment and construction quality were assumed, especially in the issues related with beam-column connections. The sizes of the members were governed by drifts, and not by strength requirements. For this reason, B- and C-type buildings are stronger than the A-type building.

3 Ground Motions

The selected site is taken from [10]. The place corresponds to the LA Bulk Mail facility in Bell, CA (33.996 N, 118.162 W), located in south of downtown Los Angeles. The site is located on deep sediments, mostly Quaternary alluvial deposits, near the middle of the Los Angeles Basin. For this research, seven ground motions (Table 1) were selected from a set of 39 ground motions used in previous studies [10, 11]. These ground motions comply with the following criteria:

- Magnitude ranging from 6.5 to 7.6.
- Fault type: strike-slip and thrust faults, consistent with earthquake mechanisms present in California.
- Site class: selected records are all from site classes C or D. Average shear-wave velocity in upper 30 m of soil $V_{s30} > 180$ cm/s.
- Peak ground acceleration PGA > 0.2 g and peak ground velocity PGV > 15 cm/s.
- Lowest useable frequency < 0.25 Hz, to ensure that low frequency content was not removed by the ground-motion filtering process.
- Limit of two records from a single seismic event.
- No consideration of response spectral shape.
- Selected ground motions include close and far sources.
- Only horizontal components of the ground motions are considered in this study.

Table 1 Selected ground motions

ID	Earthquake name	M_w	Station name	V_{s30} m/s	Site	R_{JB} km
1	1994 Northridge	6.7	Beverly Hills—14,145 Mulhol	356	D	9.40
2	1999 Duzce, Turkey	7.1	Bolu	326	D	12.02
3	1979 Imperial Valley	6.5	Delta	275	D	22.03
4	1995 Kobe, Japan	6.9	Shin-Osaka	256	D	19.14
5	1999 Kocaeli, Turkey	7.5	Duzce	276	D	13.60
6	1989 Loma Prieta	6.9	Oakland—Outer Harbor Wharf	249	D	74.16
7	1999 Chi-Chi, Taiwan	7.6	TCU095	447	C	45.20

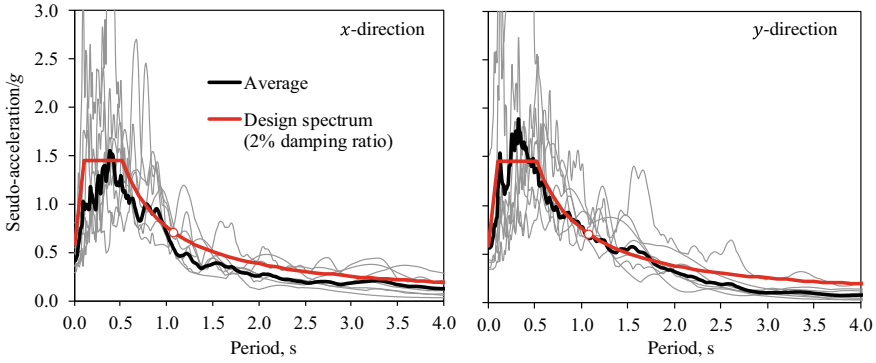

Fig. 3 Spectra for building type B

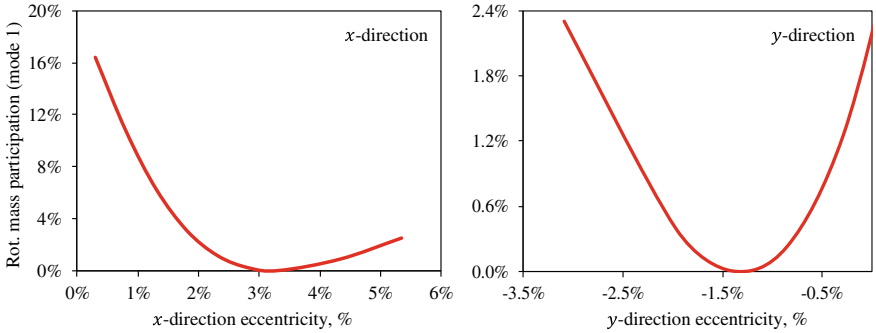

Fig. 4 Effect of the eccentricity of the isolation system in the rotational response

All ground motions were scaled to represent the same seismic hazard for the elastic fundamental period of the buildings. Figure 3 compares the spectra of the events with the code design spectrum (damping ratio $\zeta = 2\%$) for building type B.

4 Dynamic Characteristics of the Buildings

The modal analysis of the fixed base buildings was conducted in ETABS computer program. Table 2 shows vibration periods, and modal participation mass ratios (M_n^*/M_{total}) for the first three modes of vibration. For B-type building, the first modes of vibration have similar periods and they are highly coupled. For the C-type, it is evident that the first mode is essentially torsional, and its period is much larger than the second mode. In contrast, the A-type building has large participation mass in translation directions for the first two modes of the 3D model.

Table 2 Vibration periods and participation masses of the fixed-base and isolated buildings

System	Mode n	Period T_n, s		M_n^*/M_{total} in % (fixed)			M_n^*/M_{total} in % (isolated)		
		Fixed	Isolated	x-dir	y-dir	Rot	x-dir	y-dir	Rot
A	1	1.42	–	0	79	0	–	–	–
	2	1.35	–	79	0	0	–	–	–
	3	0.86	–	0	0	80	–	–	–
B	1	1.10	2.59	34	0	42	98	0	1
	2	0.96	2.54	43	0	35	0	99	1
	3	0.89	2.36	0	79	0	1	0	98
C	1	1.32	2.63	16	8	52	62	19	16
	2	0.93	2.54	48	30	3	27	72	17
	3	0.85	2.39	16	42	23	10	9	97

5 Parametric Linear Analyses

5.1 Preliminary Design of the Isolation System

One of the objectives of this work is to study the conditions that an isolated system should meet to reduce torsional behavior of buildings. This section presents a preliminary design of the isolation system conducted without any consideration of torsion. The selected base isolation system has the following characteristics:

- The bearings are Bridgestone high-damping rubber bearings.
- The average pressure on the bearings is 6.89 MPa (1.00 ksi).
- The maximum seismic shear strain is not to exceed 150%.
- The design response spectrum is the one specified for the site. This spectrum has constant velocity of 0.95 m/s (37.4 in/s).
- The maximum axial load is 1944 kN (437 kips), the minimum is 645 kN (145 kips), and the average is 1272 kN (286 kips). These axial loads are computed on one isolator, and correspond to dead load plus 0.50 times live load.

The design process was conducted using the above criteria, and laboratory test results. The final characteristics of the isolator system are the following:

- Diameter = 0.51 m (20 in).
- Thickness of rubber (12 layers of 5/8") = 0.19 m (7.50 in).
- Period of the isolated building = 2.6 s.
- Bearing displacement = 0.29 m (11.25 in).
- Base shear (fixed-base $\zeta = 2\%$)/Based shear (Isolated $\zeta = 14\%$) between 3 and 4.

5.2 Parametric Analysis

To study the effect of torsion in the dynamic behavior of the isolated building a parametric analysis was conducted. The equations of motions of a linear un-damped base isolated system considering rigid super-structure are:

$$\begin{bmatrix} m & 0 & 0 \\ 0 & I_o & 0 \\ 0 & 0 & m \end{bmatrix} \begin{Bmatrix} \ddot{u}_x \\ \ddot{\theta} \\ \ddot{u}_y \end{Bmatrix} + \begin{bmatrix} k_x & -k_x e_y & 0 \\ -k_x e_y & I_o & k_y e_x \\ 0 & k_y e_x & k_y \end{bmatrix} \begin{Bmatrix} u_x \\ \theta \\ u_y \end{Bmatrix} = -\begin{Bmatrix} m\ddot{u}_{gx} \\ 0 \\ m\ddot{u}_{gy} \end{Bmatrix} \tag{1}$$

where u_x, u_y and θ are the x, y and rotational displacements, respectively; m and I_o are the mass and the moment of inertia of the rigid super-structure; k_x and k_y are the stiffness of the isolation system in the x and y directions. In terms of torsion, one of the most important parameters are the eccentricities between the center of mass and the center of rigidity of the isolation system. If the superstructure is rigid and

the eccentricities (e_x and e_y) are close to zero, the system will be "torsionally-stiff" with negligible rotational mass participation in the fundamental mode.

The assumption of rigid super-structure for analyzing torsional properties of isolator systems is not valid when the eccentricities of the super-structure are large (i.e. bigger than 5% of the maximum plan dimension). For these cases, the isolation system should be designed to have some eccentricity in the opposite direction in order to reduce torsional behavior. A parametric study varying eccentricities (e_x and e_y), and considering a linear-flexible super-structure was conducted. In order to change the eccentricities of the system, the relative stiffness of the isolators was modified keeping constant the total stiffness of the system. Figure 4 shows the rotational mass participation ratio for the first mode of vibration versus the eccentricity of the isolation system. The eccentricity is expressed as percentage of the maximum plan dimension (54.86 m, 180 ft). For flexible super-structure, the figure confirms that the isolator system needs to have an opposite eccentricity in order to reduce the torsional response of the buildings. There is a theoretical optimal value of eccentricity that reduces the torsion of the first mode to zero. However, since the uncertainty associated with the stiffness of the isolators and the distribution of mass, this optimal eccentricity may be unrealistic. When the isolation system reaches the theoretical optimal eccentricity in one direction, Eq. 2 is satisfied.

$$\sum_{i=1}^{\#\text{floors}} m_i \phi_i e_i + m_b \phi_b e_b = 0 \tag{2}$$

In this equation, m_i and m_b are the masses of i th floor and the base (slab over the isolation system), respectively; similarly, e_i and e_b are the eccentricities of i th floor and the base; ϕ_i and ϕ_b are the fundamental mode shape displacements for the direction under consideration. This equation cannot be used directly to calculated the required eccentricity of the isolation system because the modal shapes ϕ are unknown. The equation is based on the modal expansion of floor masses.

Note that when the building is base isolated the torsional response of the building is reduced even if the eccentricity of the isolated system is not optimal. If buildings are base isolated using the same rubber bearing for all columns, the rotational mass participation ratio for the first mode drops from about 45% to 1% for B-type building and from 50 to 16% for C-type building (Table 2). The eccentricity of the isolation system with similar isolators in all columns is −0.29% and 0.30% for B- and C-type buildings, respectively.

6 Effects of Structural Nonlinearities

6.1 Modelling

The behavior of torsionally-weak buildings is strongly influenced by the higher modes and strength losses; therefore, nonlinear models should consider those effects. Three-dimensional models with fully axial load versus bi-directional moment interaction are strongly recommended for steel buildings because the behavior might be dominated by failures around the weak axis of the columns. In this study, the nonlinear model of the buildings was implemented in PERFORM-3D [12] considering the following features: (1) Girders of the moment resistant frames are modeled using a linear element with two plastic hinges at the ends characterized using trilinear models with strength loss. (2) Columns of the moment resistant frames use plasticity theory for axial-load interaction including strength loss. (3) Panel zones account for nonlinearity using the Krawinkler model. (4) Gravity frames are included in the model. (5) Beam-column connections for gravity frames are pinned. (6) The ductility capacities of girders, columns and panel zones are taken from ASCE-41 document. The isolators are represented using a trilinear model (including high-strain stiffening) with its parameters calculated by the equations presented in [13]. This model predicts very well the effective shear modulus, but it may under-estimate effective damping at low shear strains. For the B-type isolated building, all isolators have the same properties while, for the C-type building, some isolators are stiffer to reduce torsional behavior in the first modes of vibration. However, on purpose, the isolator systems did not have the optimal eccentricity because this situation was considered unrealistic. For comparison purposes, linear and nonlinear models were implemented for the isolated buildings.

6.2 Nonlinear Response History Analysis

The response of the buildings is examined using nonlinear response history analysis applying simultaneously both horizontal components of the ground motions described in Sect. 2. Figure 5 shows the absolute floor acceleration for fixed- and isolated-base buildings. It is evident that when the building is isolated floor accelerations drop noticeably for all floors. This means that the potential damage on acceleration sensitive non-structural components is reduced significantly, even if torsional effects are not completely eliminated. As shown in Table 3, the base shear is reduced by an average factor of 2. The actual reduction in base shear is less than expected because torsional effects were not accounted for in the initial design. Figure 6 show story drifts for the B- and C-type buildings. Note that drifts do not reduce in the same proportion than accelerations and base shears. This is partially due to the flexibility of the base beams. These beams should be as rigid as possible to neglect rotation

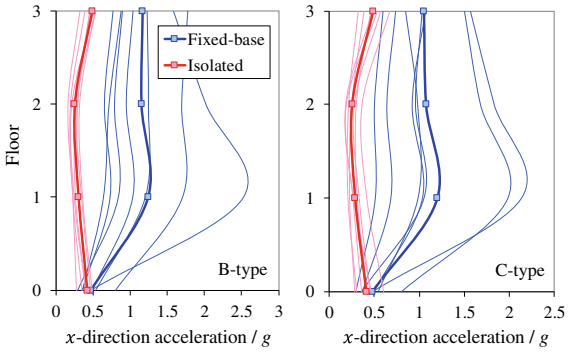

Fig. 5 Floor total acceleration of fixed-base and isolated buildings

Table 3 Base shear ratio (fixed/isolated)

Ground motion	1	2	3	4	5	6	7
Base shear ratio (fixed/isolated)	1.94	3.01	1.93	1.72	1.43	3.10	2.22

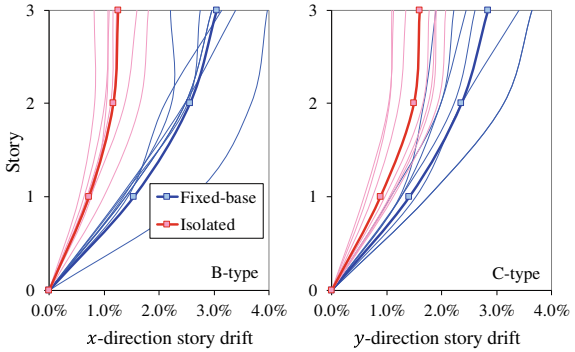

Fig. 6 Story drifts of fixed-base and isolated buildings

of the columns at the base. Seismic isolation reduces, but not eliminates torsional behavior of the structure leaving a residual torsion that is amplified by higher mode effects and nonlinearities of the super-structure.

6.3 Comparison Between Linear and Nonlinear Analyses

Figures 7 and 8 show roof displacements time series and story drifts for EQ1 and EQ3 records estimated using linear and nonlinear analyses. Although the maximum

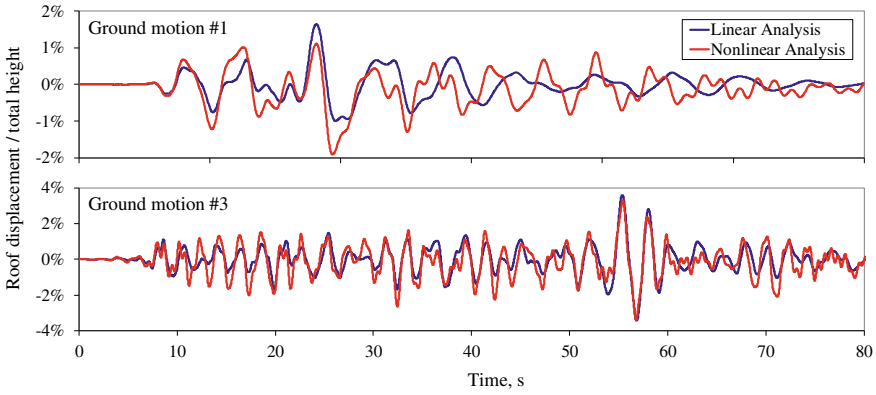

Fig. 7 Story drifts of fixed-base and isolated buildings

Fig. 8 Story drifts obtained from linear and nonlinear analysis

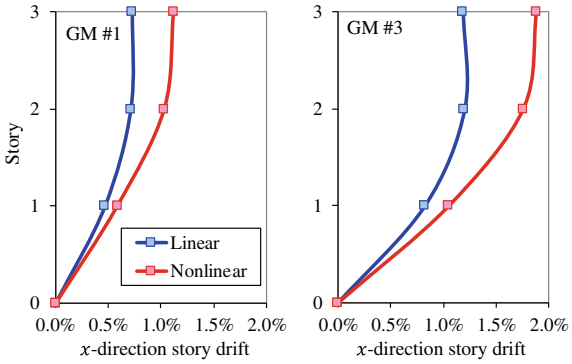

roof displacements are acceptably estimated using linear methods, the story drifts are underestimated. This may be due to the nonlinear behavior of some elements and the differences between the models used for the seismic isolators. The linear model has a specified damping and stiffness while the tri-linear model has variable hysteretical damping and stiffness. Higher modes effects may also significantly amplify nonlinear drifts.

7 Conclusions

This paper analyzes the efficiency of seismic isolation on reducing undesirable torsional effects. Based on the analysis conducted, the following conclusions were drawn:

- Using similar isolators for all columns of an unsymmetric plan building reduces, but not eliminates torsional behaviour of the structure leaving a residual torsion that is amplified by higher mode effects and nonlinearities of the super-structure. However, the isolated system can be designed to have an optimal eccentricity, which balances the eccentricity of the super-structure, and eliminates the torsional behavior of the first mode. Because of the uncertainty associated with the stiffness of the isolators and the distribution of mass, this optimal eccentricity may not be realistic. Therefore, accounting for these uncertainties in the design process is recommended.
- The flexural stiffness of the first-story beams has an important effect on the magnitude of story drifts of isolated buildings. The first-story beams should be as rigid as possible to neglect rotation of the columns at the base.
- Linear analyses provide important information about the global behavior of torsionally-weak buildings, and can be used for preliminary design of isolated buildings. However, these analyses can underestimate story drifts when the super-structure goes into the nonlinear range and the first modes have coupled torsional behavior.

References

1. Lee DM (1980) Base isolation for torsion reduction in asymmetric structures under earthquake loading. Earthq Eng Struct Dynam 8(4):349–359. https://doi.org/10.1002/eqe.4290080405
2. Murnal P, Sinha R (2004) Behavior of torsionally coupled structures with variable frequency pendulum isolator. J Struct Eng 130(7). https://doi.org/10.1061/(ASCE)0733-9445(2004)130:7(1041)
3. Becker TC, Keldrauk ES, Mieler MW, Mahin SA, Stojadinovic B (2012) Effect of mass offset on the torsional response in friction pendulum isolated structures. In: Proceedings of the 15th World conference on earthquake engineering Lisbon Portugal
4. Fallahian M, Khoshnoudian F, Loghman V (2015) Torsionally seismic behavior of triple concave friction pendulum bearing. Adv Struct Eng 18(12):2151–2166. https://doi.org/10.1260/1369-4332.18.12.2151
5. Di Sarno L, Chioccarelli E, Cosenza E (2011) Seismic response analysis of an irregular base isolated building. Bull Earthq Eng 9:1673–1702. https://doi.org/10.1007/s10518-011-9267-1
6. Cancellara D, Angelis F (2016) Assessment and dynamic nonlinear analysis of different base isolation systems for a multi-storey RC building irregular in plan. Comput Struct 180:74–88. https://doi.org/10.1016/j.compstruc.2016.02.012
7. Mazza F, Mazza M (2016) Nonlinear seismic analysis of irregular RC framed buildings base isolated with friction pendulum system under near-fault excitations. Soil Dyn Earthq Eng 90:299–312. https://doi.org/10.1016/j.soildyn.2016.08.028
8. Chopra AK, Goel RK (2004) A modal pushover analysis procedure to estimate seismic demands for unsymmetric-plan buildings. Earthq Eng Struct Dynam 33:903–927. https://doi.org/10.1002/eqe.380
9. International Conference of Building Officials (1985) 1985 Uniform Building Code, International Conference of Building Officials, USA

10. Goulet CA, Haselton CB, Mitrani-Reiser J, Beck JL, Deierlein GG, Porter KA, Stewart JP (2007) Evaluation of the seismic performance of a code-conforming reinforced-concrete frame building-from seismic hazard to collapse safety and economic losses. Earthq Eng Struct Dynam 36(13):1973–1997. https://doi.org/10.1002/eqe.694
11. Haselton CB (2006) PhD Dissertation: Assesing seismic collapse safety of modern reinforced concrete moment frame buildings. California, Stanford
12. Computers and Structures (CSI), Inc. (2006) PERFORM 3D, User Guide v4, Non-linear analysis and performance assessment for 3D structures. Computers and Structures Inc., USA
13. Naeim F, Kelly JM (1999) Design of seismic isolated structures. From theory to practice. John Wiley & Sons, Inc., USA

Use of Fluid Dampers in Order to Improve the Seismic Performance of Reinforced Concrete Buildings with Asymmetric Plan-View

Angelos Krystallis, Asimina Athanatopoulou, and Konstantinos Kostinakis

1 Introduction

Earthquake engineering aims at making new or existing structures resistant under seismic loads. In order to achieve this goal, various passive and active control devices have been proposed and developed during the past decades for the seismic retrofit of existing structures or the effective design of new ones under earthquake excitations. One of the most popular passive control devices for buildings subjected to seismic motions is viscous fluid dampers. These devices are supplementary damping devices, which increase the damping ratio of the structure and, consequently, the energy dissipation capacity. As a result, the need for other forms of energy dissipation, such as those associated with damages, is limited [1].

Reinforced concrete buildings with asymmetric plan-views are very common structural systems in countries with high seismicity. In case of these buildings the mass and stiffness centers do not coincide. The stiffness and strength are asymmetrically distributed, something that leads to the coupling between lateral and torsional components of vibration. Therefore, large rotation angles are observed for lateral seismic motion of the base and, consequently, the perimeter structural elements suffer from serious damages. In order to deal with such phenomena modern seismic codes (e.g., EC8 [2]) suggest to provide these structures with adequate and appropriately distributed stiffness, strength and ductility. However, in case of existing buildings with high values of eccentricity and of new buildings with certain architectural and

A. Krystallis · A. Athanatopoulou · K. Kostinakis (✉)
Aristotle University of Thessaloniki, Thessaloniki, Greece
e-mail: kkostina@civil.auth.gr

A. Krystallis
e-mail: aggelosfd@live.com

A. Athanatopoulou
e-mail: minak@civil.auth.gr

R. Bento et al. (eds.), *Seismic Behaviour and Design of Irregular and Complex Civil Structures IV*, Geotechnical, Geological and Earthquake Engineering 50,
https://doi.org/10.1007/978-3-030-83221-6_16

functional needs that do not allow the optimum choice of the structural system, an alternative solution would be the placement of appropriately selected passive control systems.

The present paper examines the appropriate distribution of viscous fluid dampers in order to improve the seismic performance of a structure with asymmetric plan-view. To achieve this goal, a multi-story building with fluid viscous dampers of certain viscosity is considered. Four different procedures of choosing the exact positions that the dampers should be placed in order to achieve the best seismic performance of the building are proposed. The evaluation of the building's seismic performance is carried out with the aid of linear, as well as nonlinear time history analyses, using nine real strong ground motions, and certain conclusions about the efficiency of the proposed procedures are drawn.

2 Fluid Viscous Dampers

The function of fluid viscous dampers is based on the principle of energy dissipation due to the flow of fluid through orifices. By this way these devices convert the kinetic energy of the seismic vibration into heat and then this energy is dissipated into the air [3–5]. A typical form of fluid damper is shown in Fig. 1 [5]. The activation of the dampers depends on the relative velocity between the two end points of the device, thus the force applied by a viscous damper is 90° out of phase with the forces applied by the seismic motion. The forces applied by the dampers to the structure are determined by the placement of the devices throughout the building. There have been developed several different approaches for the efficient distribution of the dampers. The basic idea that has been adopted by the most of them is the placement of the dampers diagonally between the stories, so that the edges of the devices move because of the stories' relative displacements (drifts) during the seismic motion. This approach has been proved to be effective in case of typical frame buildings.

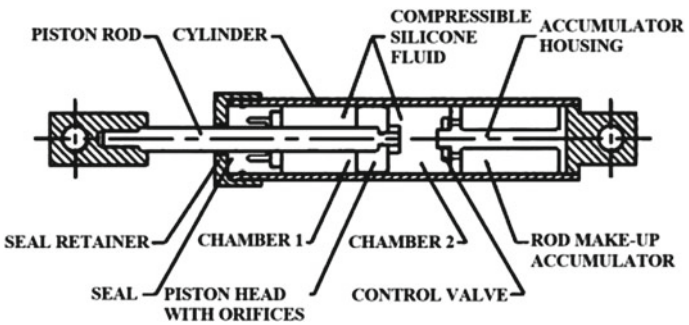

Fig. 1 Typical fluid viscous damper [5]

The function of the viscous dampers can be described by the following expression [6]:

$$\sum_{j=1}^{nd} c_j \left(f_j \cdot \Delta u_j\right)^2 \geq 2M_i^* \omega_i \xi_{d,i} \tag{1}$$

where c_j is the damper's viscosity, Δu_j is the relative modal horizontal displacement of the two stories adjacent to the damper, f_j is an effciency coeffcient (in case that the damper is positioned in the bracing between the two floors with inclination θ_j the effciency coeffcient equals $\cos\theta_j$), M^*_i and ω_i are the generalized mass and the circular frequency of eigenmode i respectively and $\xi_{d,i}$ is the critical damping ratio associated with the viscous dissipation.

3 Application to a Multi-story Building

3.1 Description, Design and Modelling

In the present section the appropriate distribution of viscous fluid dampers in order to improve the seismic response of an asymmetric in-plan structure is examined. For this aim, a five-story R/C building with asymmetric plan-view has been chosen. The plan-view of the typical building's story, as well as the dimensions of the structural elements, are shown in Fig. 2. The building is regular in-elevation, but irregular in-plan according to the criteria set by EC8 [2].

In Table 1 the design data of the investigated building are presented. The building was analyzed by means of the modal response spectrum analysis, as defined in EC8 [2]. The R/C structural elements were designed according to the provisions of EC2 [7] and EC8 [2]. The professional program for R/C building analysis and design ETABS [8] was adopted in both the analysis and design. Then, the nonlinear behavior of the structural elements was modeled using plastic hinges, located at the column and beam ends, as well as at the base of the walls. The properties of the plastic hinges were defined with the aid of ASCE 41–13 [9]. The capacity curves of the building model (without dampers) in X and Y directions are shown in Fig. 3.

3.2 Earthquake Records

For the analyses of the present study nine pairs of horizontal bidirectional earthquake strong motions obtained from the PEER [10] strong motion database were used (Table 2). The earthquake records were selected from worldwide well known sites characterized by strong seismic activity. The selected ground motions have been

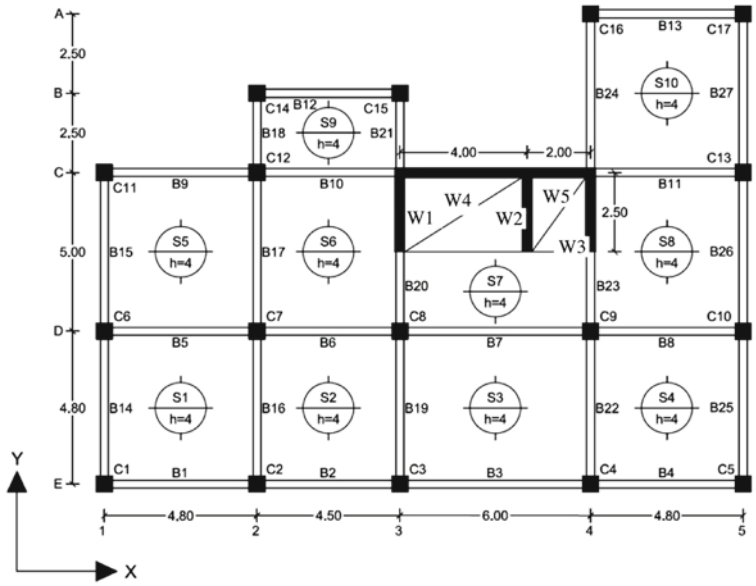

Storey	Beams	Columns	W1, W2, W3	W4	W5
1st-5th	25/50	50/50	250/30	400/30	200/30

Fig. 2 Plan view of the typical story and properties of the structural elements (in cm) (Bi denotes Beams, Ci denotes Columns, Wi denotes Walls, Si denotes Slabs and h denotes the story's height)

Table 1 Design data

Stories' heights H_i	Concrete	Steel	Slab loads	Masonry loads	Design spectrum (EC8)
1st: 4.0 m 2nd-5th: 3.0 m	*C30/37* $E_c = 3.3 \times 10^7$ kN/m^2 $\nu = 0.0$ w = 25 kN/m^3	*B500C* $E_s = 2 \times 10^8$ kN/m^2 $\nu = 0.3$ w = 78.5 kN/m^3	*Dead*: G = 1.4 kN/m^2 *Live*: Q = 2.0 kN/m^2	*Perimetric*: 3.6 kN/m^2 *Internal*: 2.1 kN/m^2	$a_{gR} = 0.24$ g *Ground type*: B *Behavior factor*: q = 2.0

recorded on Soil Type B according to EC8 [2] and are characterized by the following limits of the basic seismic record parameters: magnitude M5.6-M7.6, closest distance to the fault rapture $R_{rup} = 19.3 - 31.6$ km (far-fault ground motions according to the Uniform Building Code [11]) and significant duration $d_{5\text{-}95} = 3.7 - 0.2$ s. The elastic response spectra (5% damping) of the seismic records for the two horizontal directions are given in Fig. 4.

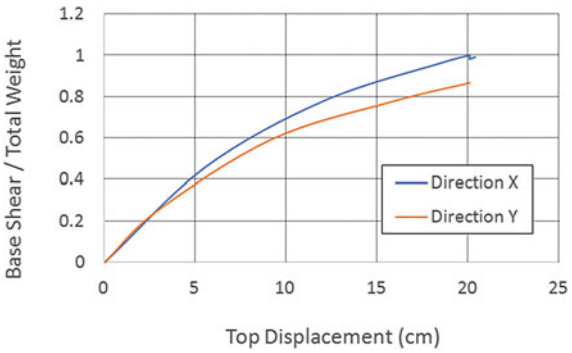

Fig. 3 Capacity curves of the building model (without dampers) in X and Y directions

Table 2 Earthquake records

No	Year	Earthquake name	Station	Component (deg)	PGA (g)
1	1994	Northridge	Castaic-Old Ridge Route	360/90	0.514/0.568
2	1999	Chi-Chi	CHY041	360/90	0.639/0.303
3	1991	Sierra Madre	Cogswell Dam -Right Abutment	155/65	0.304/0.263
4	1992	Cape Mendocino	Ferndale Fire Station	360/270	0.269/0.374
5	2000	Tottori	HRS002	360/90	0.482/0.417
6	2004	Niigata	NIGH06	360/90	0.363/0.417
7	2007	Chuetsu	YamakoshiTakezawa	360/90	0.356/0.325
8	2008	Iwate	MYG004	360/90	0.751/0.693
9	2010	Darfield	Heathcote Valley Primary School	206/116	0.577/0.632

3.3 Modelling and Position of the Dampers

In this section the appropriate distribution of viscous fluid dampers in order to improve the seismic response of the structure is investigated. To achieve this goal, four different procedures of choosing the exact positions that the dampers should be placed are proposed. The common choices that were made for all the procedures are the following:

- The dampers are placed only along the perimeter frames of the building, so there are 75 different possible locations along the building's height that they can be placed.
- A total number of 24 dampers has been chosen, since the analyses revealed that this number of dampers leads to a critical damping ratio associated with the viscous dissipation of approximately 20%, which was set as a target value [4].

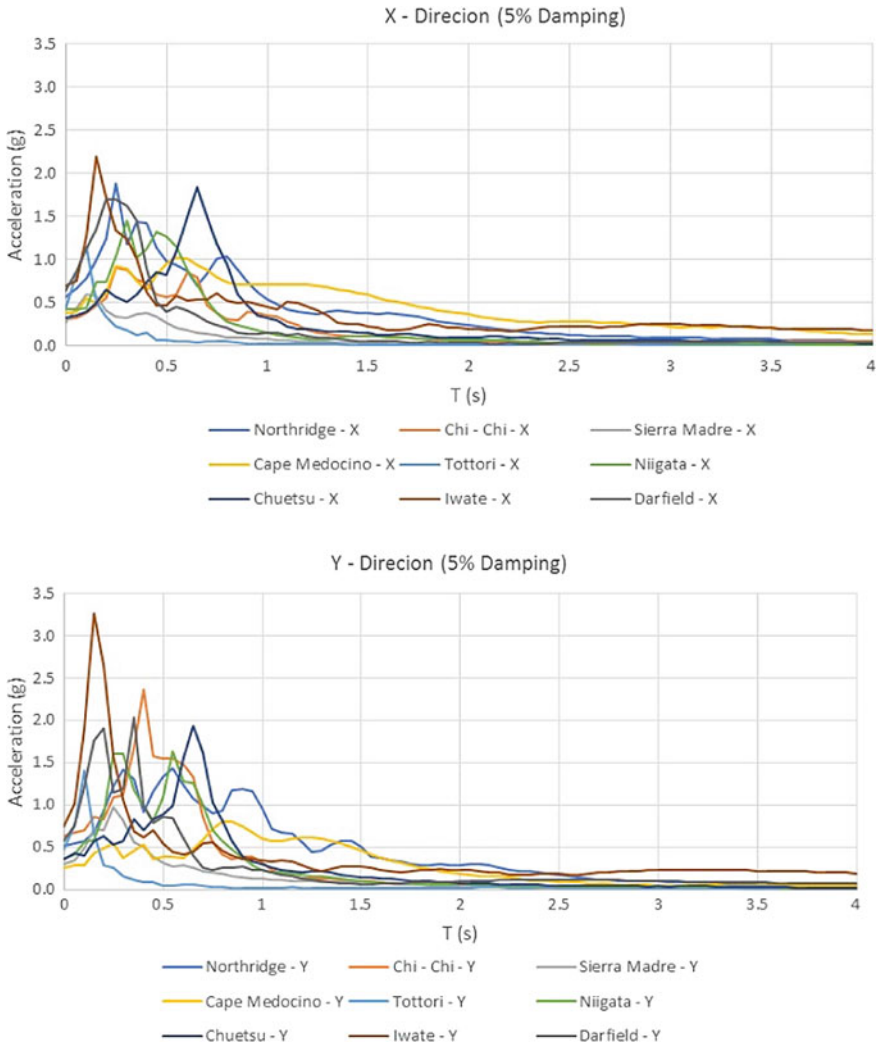

Fig. 4 Elastic response spectra of the seismic records for the two horizontal directions

- The viscosity of the dampers has been considered to be the same for all of them and equal to c = 2000 kNs/m, which is a typical value for this kind of devices.

The four procedures of choosing the positions of the dampers are the following:

(a) According to the first procedure (P1), the viscous damping of each damper was computed with the aid of Eq. 1 and using the results (f, Δu, M^*_i, ω_i) computed by the 1steigenmode. Then, the 24 dampers (out of the 75) with the larger damping ratio ξ_d were selected (Fig. 5a).

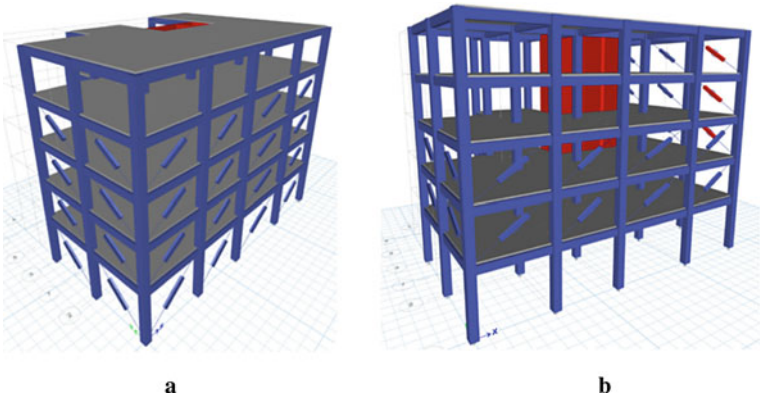

Fig. 5 Positions of the dampers according to procedures **a** P1 and **b** P3

(b) According to the second procedure (P2), the viscous damping of each damper was computed with the aid of Eq. 1 and using the results (f, Δu, M^*_i, ω_i) computed by the 2nd eigenmode. Then, the 24 dampers (out of the 75) with the larger damping ratio ξ_d were selected.

(c) According to the third procedure (P3), the 12 dampers with the largest damping ratio ξ_d according to P1 and the 12 dampers with the largest damping ratio ξ_d according to P2 were selected. So, in total 24 dampers were also used (Fig. 5b).

(d) According to the fourth procedure (P4), for each one of the nine chosen earthquake records (Sect. 3.2) linear time history analysis was conducted and the maximum force applied by each one of the 75 dampers was computed. Then, the 24 dampers with the largest applied force were selected.

Figure 6 illustrates the damping ratios ξ (%) of the structure with and without dampers (according to the four procedures described above). Moreover, the above procedures have been illustrated with the aid of a certain flow chart for the optimal placement of the viscous fluid dampers in case of any building (see also [12]) (Fig. 7).

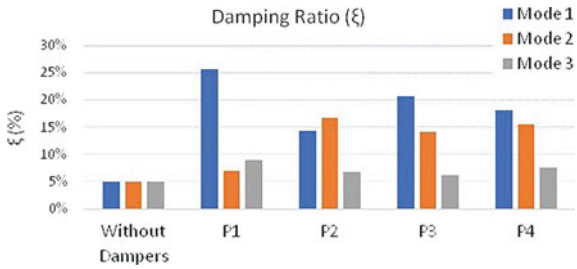

Fig. 6 Damping ratios of the structure with and without dampers

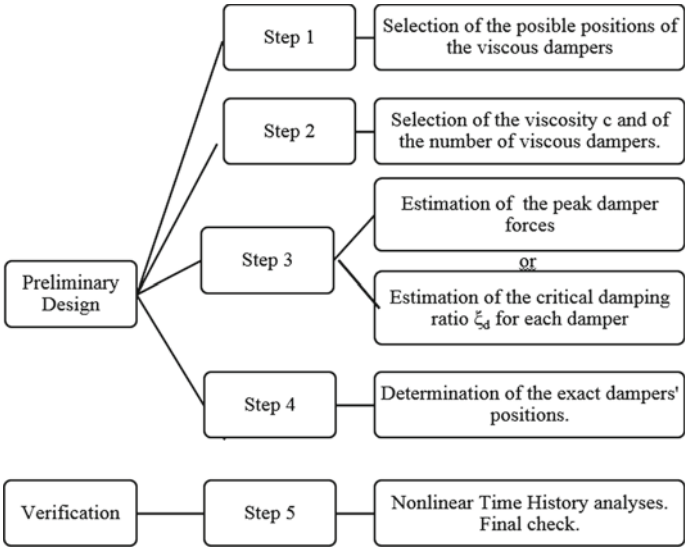

Fig. 7 Flow chart for the optimal sizing and distribution of the viscous fluid dampers

3.4 Analyses and Results

In this section the efficiency of the four aforementioned procedures of determining the dampers' positions in the improvement of the building's seismic response was evaluated. The assessment of the seismic performance was carried out with the aid of linear and nonlinear time history analyses using the nine real strong motion pairs presented in Sect.3.2. In order to account for the directionality of the seismic motions [13, 14], each pair of the earthquake records was applied along two horizontal orthogonal axes forming two different incident angles (0° and 90°) with the structural axes of the building. For each ground motion the relative displacements (drifts) along axes X (perimeter frames C, E and mass center) and Y (perimeter frames 1, 5 and mass center) (Fig. 2), as well as the rotations of the floors were computed as damage measures [e.g., 15]. More specifically, for each earthquake record and response measure the maximum of the values for the two incident angles was considered. Then, the average of these values for the nine records was determined according to the most seismic code provisions [e.g. 2, 16, 17]. In the following figures the results for the linear and the nonlinear analyses are presented.

From the figures below we can see that the maximum drifts along axis Y determine the seismic performance of the building, since they attain larger values than the drifts along axis X, so the assessment of the efficiency of the four procedures P1-P4 will be made based mainly on the drifts along Y axis. The analyses showed that procedure P1 was the least effective in reducing the maximum drift Y compared to the values of the building without the dampers in case of both the linear and the nonlinear analyses. Regarding the linear analyses the other three procedures (P2, P3 and P4)

led to very similar results (Figs. 8, 10a and 11a) reducing the drift along Y axis up to 30%, whereas in case of the nonlinear analyses procedure P4 seems to be the most effective for the majority of the stories (up to 67% reduction) followed by procedures P2 and P3 (Figs. 9, 10b and 11b).

With regard to the floor rotations, the results of the analyses revealed that procedure P1 was the most effective in both cases of linear and nonlinear analyses (up to 50% and 75% reduction compared to the values of the building without the dampers for linear and nonlinear analyses respectively), whereas procedure P2 was the one that led to the smallest reduction in rotations (Fig. 12).

Of significant importance is also the fact that the use of the dampers has been proved to be more efficient in improving the seismic performance of the building in case of the nonlinear analyses. This observation is valid for all the damage measures (drifts along the two horizontal axes, floor rotations) considered in the present study. Moreover, as it was shown above, note that the efficiency of a certain procedure of determining the dampers' distribution depends on the damage measure. As a general conclusion, we can state that procedures P4 and P1 led to the best results in case of drifts and floor rotations respectively.

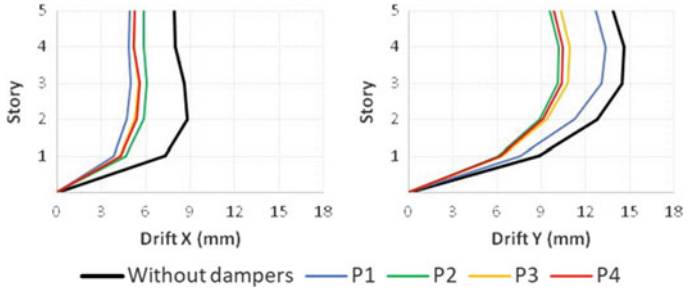

Fig. 8 Linear analyses: Average drifts along axes X and Y (mass center)

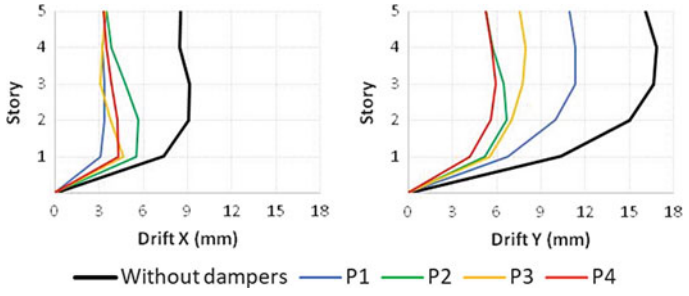

Fig. 9 Nonlinear analyses: Average drifts along axes X and Y (mass center)

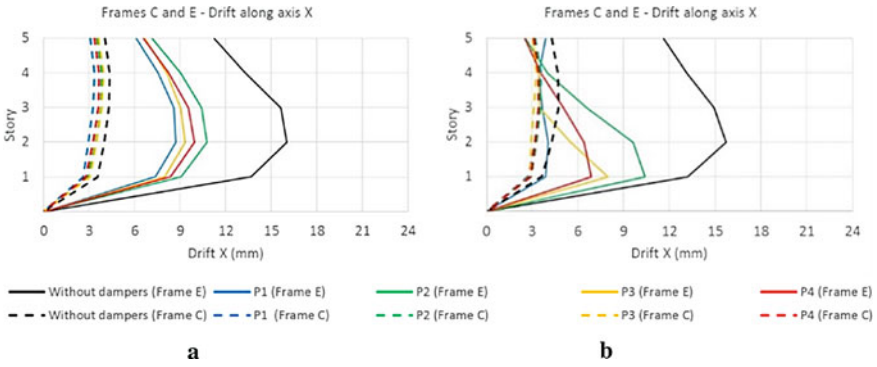

Fig. 10 Linear (**a**) and nonlinear (**b**) analyses: Average drifts along axes X (perimeter frames C and E)

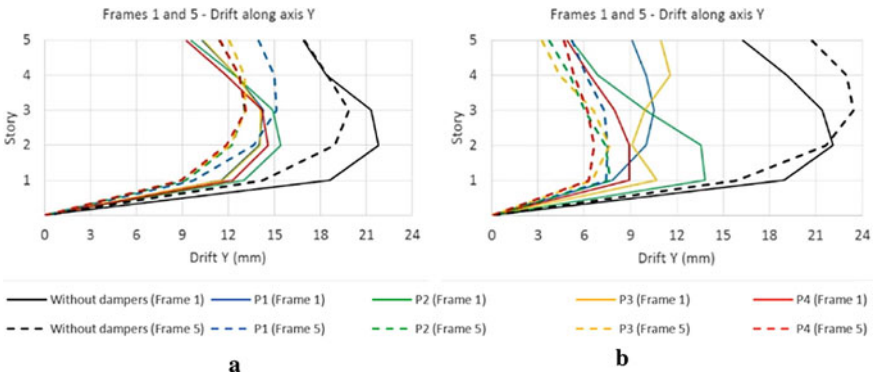

Fig. 11 Linear (**a**) and nonlinear (**b**) analyses: Average drifts along axes Y (perimeter frames 1 and 5)

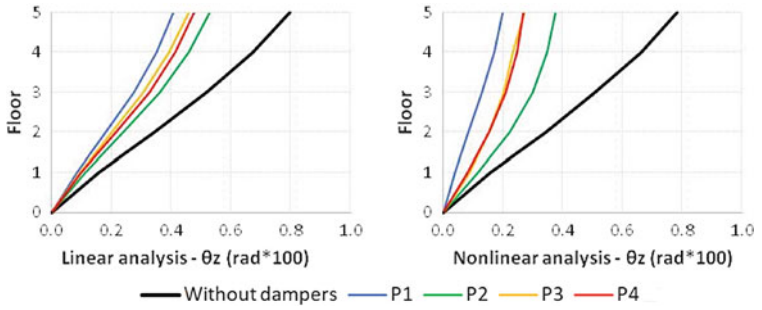

Fig. 12 Average floor rotations

4 Conclusions

The present paper investigated the appropriate distribution of viscous fluid dampers in order to improve the seismic performance of an asymmetric structure. To achieve this goal, a multi-story building with an asymmetrical plan-view and fluid viscous dampers with certain viscosity were considered. Consequently, the paper proposed four different procedures of choosing the exact positions that the dampers should be placed in order to achieve the best seismic performance of the building. The evaluation of the building's seismic performance was carried out with the aid of linear, as well as nonlinear time history analyses using nine real strong ground motions. Based on the results of the study, the following general conclusions can be drawn:

- The use of viscous fluid dampers reduces significantly both the drifts and the floor rotation of buildings with asymmetric plan view. In case of these buildings, the distribution of the dampers should also be asymmetric according to the proposed procedures.
- The use of the dampers is more efficient in improving the seismic performance of asymmetric buildings in case of the nonlinear analyses.
- The efficiency of the procedures depends on the damage measure. Procedures P4 and P1 led to the best results in case of drifts and floor rotations respectively.
- A flow chart for the optimal placement of the viscous fluid dampers in case of any asymmetric building is proposed.

References

1. Zare AR, Ahmadizadeh M (2017) Design of passive viscous fluid control systems for nonlinear structures based on active control. J Earthq Eng 23(6):1033–1054
2. EC8-Part 1: Eurocode 8 (2005) Design provisions for earthquake resistance of structures. Part 1–1: General rules – seismic actions and general requirements for structures. ENV 1998–1, CEN: Brussels
3. Klembczyk A (2009) Introduction to shock and vibration isolation and damping systems. Taylor Devices Inc., New York-USA
4. Christopoulos C, Filiatraut A (2006) Principles of passive supplemental damping and seismic isolations. IUSS Press, Pavia-Italy
5. Taylor Devices Inc (2017) Fluid viscous dampers and lock up devices, Technical Note.
6. Denoël V, Duflot P (2016) Technical note on the preliminary design of viscous dampers. Taylor Devices Inc., Brussels-Belgium
7. EC2-Part 1: Eurocode 8 (2004) Eurocode 2: Design of concrete structures - General rules and rules for buildings. ENV 1992–1, CEN, Brussels
8. ETABS v17.1. A computer program for static and dynamic nonlinear analysis of framed structures, 2018. Developed by Computers and Structures Inc., California, USA.
9. ASCE, SEI 41–13 (2014) Seismic evaluation and retrofit of existing buildings. American Society of Civil Engineers, Reston, VA
10. Pacific Earthquake Engineering Research Centre (PEER) (2003) Strong Motion Database. http://peer.berkeley.edu/smcat/

11. UBC. Structural Engineering Design Provisions. Uniform Building Code (1997) International Conference of Building Officials. vol 2. Whittier, CA
12. Palermo M, Silvestri S, Gasparini G, Dib A, Trombetti T (2017) A direct design procedure for frame structures with added viscous dampers for the mitigation of earthquake-induced vibrations. Proced Eng 199:1755–1760
13. Athanatopoulou A (2005) Critical orientation of three correlated seismic components. Eng Struct 27(2):301–312
14. Fontara I-K, Kostinakis K, Manoukas G, Athanatopoulou A (2015) Parameters affecting the seismic response of buildings under bi-directional excitation. Struct Eng Mech 53(5):957–979
15. Naeim F (2011) The seismic design handbook, 2nd edn. Kluwer Academic, Boston
16. FEMA 356 (2000) Prestandard and commentary for the seismic rehabilitation of buildings. Federal Emergency Management Agency, Washington, DC
17. ASCE, SEI 41–06 (2008) Seismic rehabilitation of existing buildings. American Society of Civil Engineers, Reston, VA

Evaluating the Effect of the Various Directions of Seismic Input on an Irregular Building: The Former Uto City Hall

Kenji Fujii

1 Introduction

The main building of the former Uto City Hall, a five-story reinforced-concrete building damaged severely in the 2016 Kumamoto earthquakes, was an irregular building [1]. The earthquake series included a foreshock that occurred on 14 April and a main shock that occurred on 16 April 2016. In a previous study, the present author evaluated the seismic capacity of the building adopting a pushover-based procedure [2]. It was found that the seismic capacity of the building may have been insufficient to withstand the foreshock. However, this conclusion relied on the assumption that the GMRotD50 [3] (the medium of the set of geometrical means obtained using all possible rotations) spectrum represents bidirectional ground motion in a real earthquake. The effect of rupture directivity may not be negligible as the epicenter of the foreshock was not far from the target building.

The effect of the various directions of seismic input on the response of irregular (asymmetric) buildings has attracted interest from researchers (e.g., [4–6]). However, the nonlinear response makes it difficult to gain a deep understanding of the behavior. The present author considers that the mode shape changes from the initial (elastic) stage appreciably, making analysis based on the modal response complicated and difficult. Another important point for the understanding of this behavior is the energy input of each modal response: when the energy input of the first modal response were larger, some of local responses would be larger. Therefore, it is expected that the effect of the various directions of seismic input to the local response can be explained in terms of the variation of energy input of the first modal response.

K. Fujii (✉)
Department of Architecture, Chiba Institute of Technology, 2-17-1Narashino-shi Tsudanuma, Chiba 275-0016, Japan
e-mail: kenji.fujii@it-chiba.ac.jp

R. Bento et al. (eds.), *Seismic Behaviour and Design of Irregular and Complex Civil Structures IV*, Geotechnical, Geological and Earthquake Engineering 50,
https://doi.org/10.1007/978-3-030-83221-6_17

This paper reports on the nonlinear time-history analysis of the main building of the former Uto City Hall using the acceleration recorded during the foreshock, considering various directions of seismic input. Then the nonlinear first modal response is calculated from the results of nonlinear time-history analysis and pushover analysis. The following discussion focuses on (a) the relation of the variation of the peak equivalent displacement of the first modal response and the peak local responses (story drift), (b) the variation of the maximum momentary input energy [7, 8] per unit mass of the first modal response, (c) the relation of the maximum momentary input energy per unit mass of the nonlinear first modal response and the maximum momentary input energy spectrum of linear system [7–9].

2 Building and Ground Motion Data

2.1 Building Data

Figure 1 shows the simplified structural plan and elevation of the main building of the former Uto City Hall. This building was a five-story reinforced-concrete building constructed in 1965.

Damage to the building was first reported on the morning of 16 April 2016, after the main shock, even though the building experienced the foreshock on 14 April 2016. Details of the building were reported in the previous study [2].

The present nonlinear analysis uses one of the three-dimensional nonlinear frame structural models constructed in the previous study [2] (Model-RuW4-100) because this model may explain the observed structural damage of the main building of the

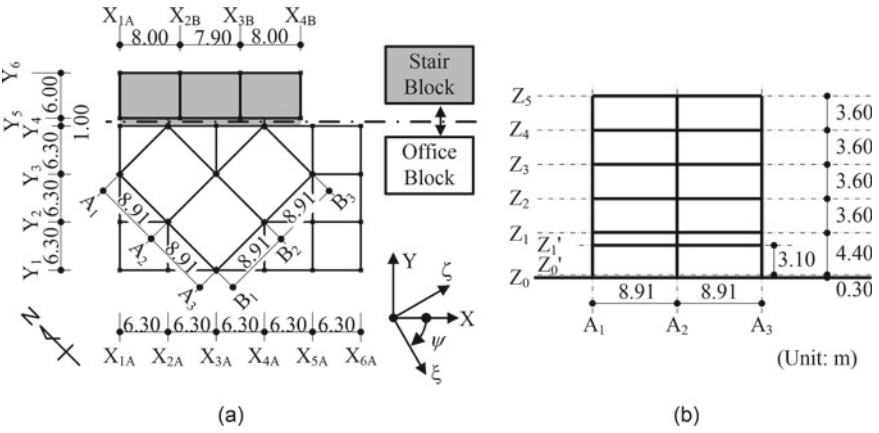

Fig. 1 Simplified structural plan and elevation of the main building of the former Uto City Hall. **a** Structural plan (level Z_0), **b** Simplified structural elevation (frame B_1)

former Uto City Hall. Figure 2 shows the structural model. As shown in Fig. 2a, this structural model is irregular in plan and elevation.

In the numerical model, a one-component model with nonlinear flexural spring at each end and the shear spring in the middle of the line element is used for all beams and columns. The concrete walls in stair block are modeled as two diagonal braces as shown in Fig. 2c, assuming that the shear behavior is predominant. Nonstructural concrete block walls are neglected in the numerical modeling, due to the lack of drawings. Other details can be found in the previous paper [2].

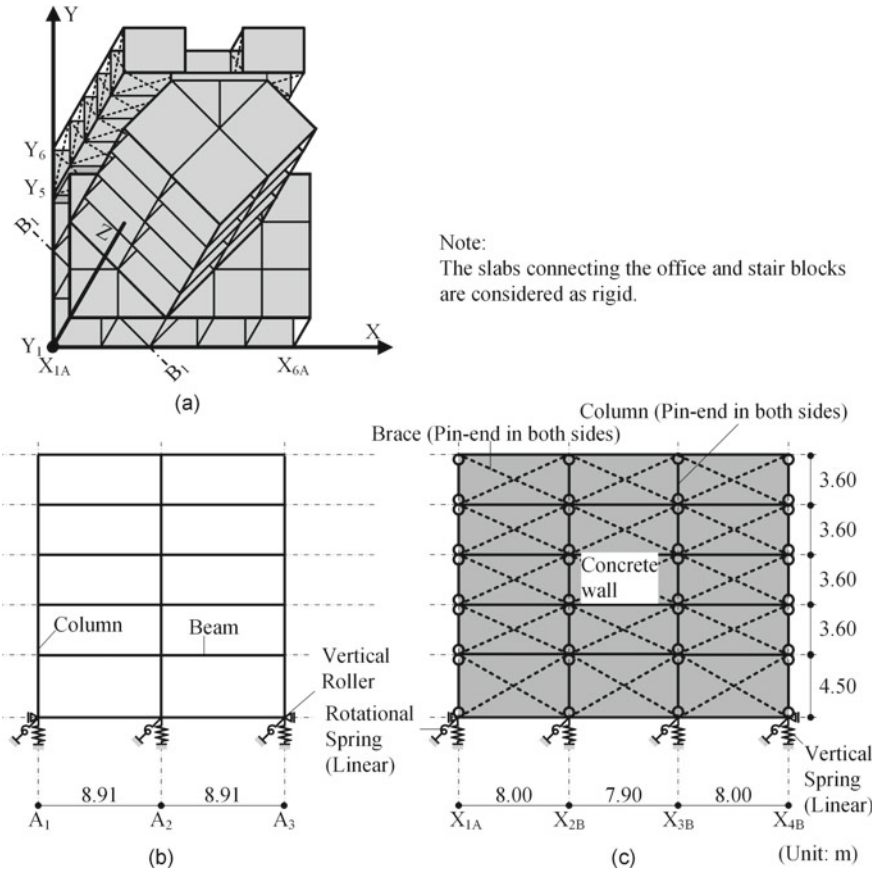

Fig. 2 Structural model [2]. **a** Overview, **b** Frame B_1, **c** Frame Y_5

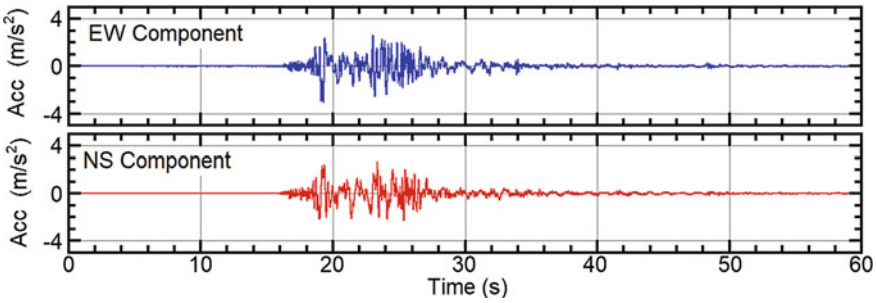

Fig. 3 EW and NS components of the foreshock acceleration recorded on 14 April at the K-NET Uto Station

2.2 Ground Motion Data

Figure 3 shows the acceleration of east–west (EW) and north–south (NS) components of the record of the foreshock (14 April 2016) obtained at the K-Net Uto Station, which is the station closest to the former Uto City Hall.

3 Nonlinear Time-History Analysis

3.1 Analysis Cases

The two components of the recorded acceleration of the foreshock are scaled by factoring constant λ ($\lambda = 0.8$, 0.9, and 1.0) in the present study. The EW and NS components are respectively input parallel to ξ- and ζ-axes, as shown in Fig. 1a. The angle of incidence of the ξ- axis with respect to the X-axis, ψ, varies at intervals 15° from 0° to 345°. Therefore, a total of $3 \times 24 = 72$ nonlinear time-history analyses are carried out. The actual EW axis is approximately 45° counterclockwise from the X-axis, and the case that $\psi = 315°$ is considered as the actual case in this study.

3.2 Analysis Results

Figure 4 shows the peak interstory drift at columns A_1B_1, A_3B_1 and A_3B_3 in the case that $\psi = 315°$. The figure also shows the drift limit assumed in the previous study [2] ($R = 1/75$). The peak responses of the "flexible" side columns (A_1B_1 and A_3B_1) are larger than the peak response of column A_3B_3, which is consistent with the fact that the observed damage to frame B_1 is more severe than that to frame A_3. In addition, the responses of columns A_1B_1 and A_3B_1 exceed $R = 1/75$ when $\lambda = 0.9$ and 1.0.

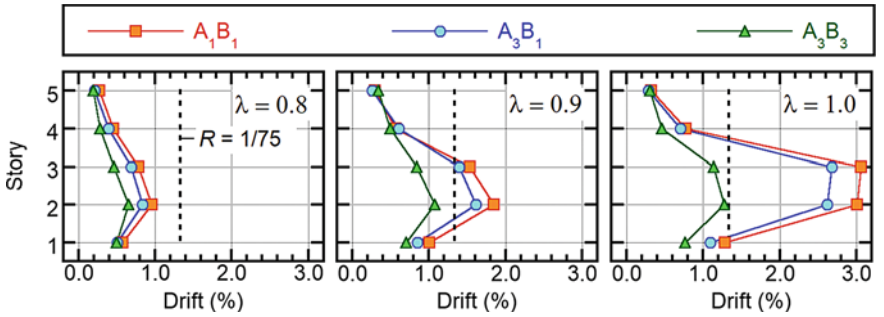

Fig. 4 Peak interstory drift at columns A_1B_1, A_3B_1 and A_3B_3 in the case that $\psi = 315°$

Figure 5 shows the distribution of the yield hinges at frame B_1. It is seen that for $\lambda = 0.9$ and 1.0, flexural yielding occurs at the top of column A_2B_1 on the third story and the right-side end of beam A_1-A_2 on level Z_3 and the left-side end of beam A_2-A_3 on level Z_3, as shown in the dotted rectangle in the figure. Note that a red triangle at a beam end indicates that the yielding of the beam–column joint occurs. Therefore, in the cases that $\lambda = 0.9$ and 1.0, the yielding of the beam–column joint and the column end occur simultaneously at the top of column A_2B_1 on the third story.

The analysis results presented here suggest that the main building of the former Uto City Hall suffered some level of structural damage during the foreshock. This finding is consistent with the results obtained in the previously conducted pushover-based evaluation [2].

Figure 6 shows the peak responses of columns A_1B_1, A_3B_1 and A_3B_3 on the second story for various directions of seismic input. As shown in plots (a) and (b),

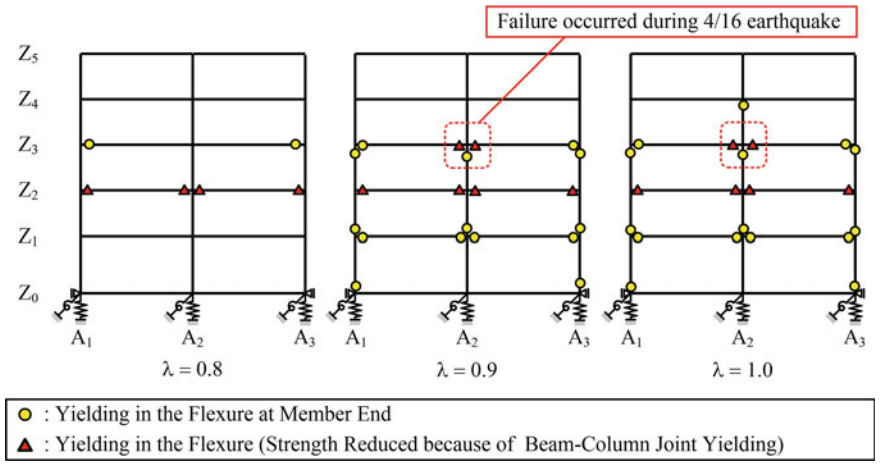

Fig. 5 Distribution of the yielding hinges at frame B_1 in the case that $\psi = 315°$

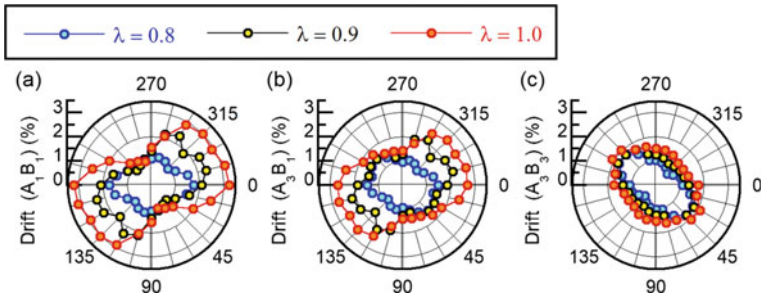

Fig. 6 Peak response at columns on the second story for various directions of seismic input. **a** Column A_1B_1, **b** Column A_3B_1, **c** Column A_3B_3

the peak responses of columns A_1B_1 and A_3B_1 are larger in the ranges of $120° \leq \psi \leq 180°$ and $300° \leq \psi \leq 360°$. In contrast, the peak response of column A_3B_3 is larger in the ranges of $0° \leq \psi \leq 75°$ and $180° \leq \psi \leq 255°$ as shown in plot (c). This implies that the damage to frame A_3 is more severe than that to frame B_1 if the direction of the seismic input is different from that of the actual earthquake.

4 Evaluation of the Effect of Various Directions of Seismic Input on the Peak Drift

4.1 Calculation of the Nonlinear First Modal Response

The nonlinear first modal response is calculated from the pushover analysis results following a procedure proposed by Kuramoto [10] for planar frame analysis.

Figure 7 compares parameters between an N-story irregular building and the equivalent single-degree-of-freedom (SDOF) model representing the first modal response [2]. Here, vectors ${}_{\mathbf{n}}\mathbf{d}$ and ${}_{\mathbf{n}}\mathbf{f}_{\mathbf{R}}$ are the displacement and restoring force vectors obtained from the pushover analysis results while $\mathbf{M}$ is the mass matrix determined from the mass and mass moment of inertia, m_j and I_j respectively, for the jth floor. Meanwhile, ${}_nD_{1U}{}^*$ and ${}_nA_{1U}{}^*$ are respectively the equivalent displacement and acceleration of the first modal response, and $M_{1U}{}^*$ is the effective first modal mass with respect to the principal axis of the first modal response (U-axis).

Figure 8 shows the flow of the calculation of the nonlinear first modal response. In this calculation, displacement-based mode-adaptive pushover (DB-MAP) analysis [2, 11] is applied to consider the change in the first mode shape at each nonlinear stage. Here, vectors $\mathbf{d}(t)$ and $\mathbf{f}_{\mathbf{R}}(t)$ are the displacement and restoring force vectors obtained from the results of nonlinear time-history analysis.

Knowing the first mode vector corresponding to ${D_{1U}}^*{}_{peak}$, $\Gamma_{1Uie}\varphi_{\mathbf{1ie}}$, the tangent of the angle of incidence of the U-axis from the X-axis, $\tan\psi_{1ie}$, is determined as.

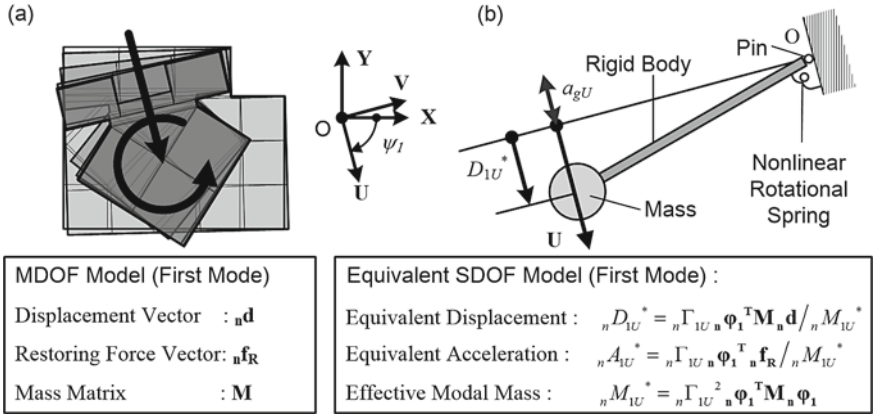

Fig. 7 Comparison of parameters between an N-story irregular building and the equivalent SDOF model. **a** An N-story irregular building with deformation similar to the first mode shape, **b** Equivalent SDOF model representing the first modal response

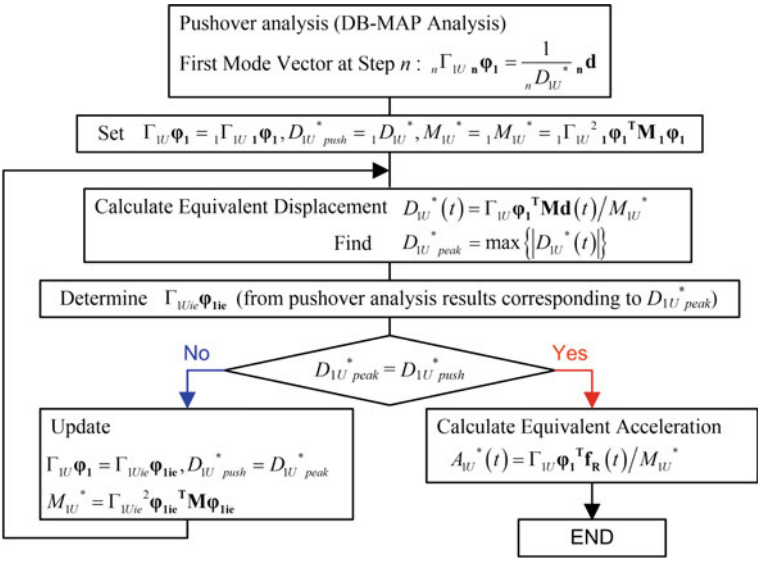

Fig. 8 Flow of the calculation of the nonlinear first modal response

$$\tan\psi_{1ie} = -\sum_j m_j\phi_{Yj1ie} \Big/ \sum_j m_j\phi_{Xj1ie} \tag{1}$$

$$\varphi_{\mathbf{1ie}} = \left\{ \phi_{X11ie}\cdots\phi_{XN1ie}\ \ \phi_{Y11ie}\cdots\phi_{YN1ie}\ \ \phi_{\Theta 11ie}\cdots\phi_{\Theta N1ie} \right\}^{\mathbf{T}}. \tag{2}$$

4.2 *Effect of Various Directions of Seismic Input on the Nonlinear First Modal Response*

Figure 9 shows the results of calculating the peak of the first modal response ($D_{1U}{}^{*}{}_{peak}$ and $A_{1U}{}^{*}{}_{peak}$) from all results of time-history analysis. Plot (a) compares the peak of the first modal response and $A_{1U}{}^{*} - D_{1U}{}^{*}$ relationship obtained from the pushover (DB-MAP) analysis. Those peaks of the nonlinear first modal response fairly agree to $A_{1U}{}^{*} - D_{1U}{}^{*}$ relationship obtained from the pushover analysis. This confirms that the nonlinear first modal response is properly calculated by the procedure presented herein. Plot (b) shows the peak equivalent displacement $D_{1U}{}^{*}{}_{peak}$ for various directions of seismic input. As shown in plot (b), $D_{1U}{}^{*}{}_{peak}$ is larger in the ranges of $120° \leq \psi \leq 180°$ and $300° \leq \psi \leq 360°$.

A comparison of Figs. 9b and 6 shows that the range in which $D_{1U}{}^{*}{}_{peak}$ is largest corresponds to the range in which the peak responses of columns A_1B_1 and A_3B_1 are largest, while this is not so for column A_3B_3.

Figure 10 shows the relation of the peak equivalent displacement of the first modal response and the peak drift of the columns on the second story. The figure

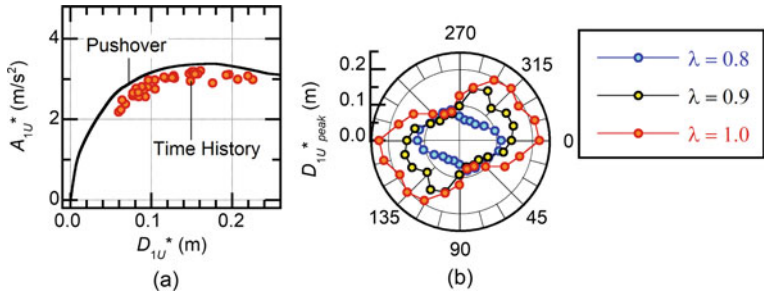

Fig. 9 Calculation results of the peak of the first modal response. **a** Equivalent acceleration-equivalent displacement ($A_{1U}{}^{*} - D_{1U}{}^{*}$) relationship, **b** $D_{1U}{}^{*}{}_{peak}$ for various directions of seismic input

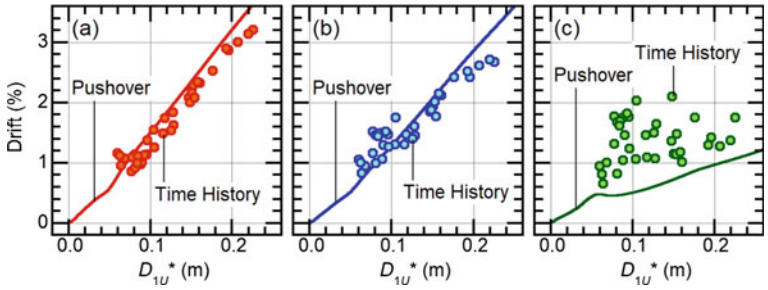

Fig. 10 Relation of $D_{1U}{}^{*}{}_{peak}$ and the peak drift of columns on the second story. **a** Column A_1B_1, **b** Column A_3B_1, **c** Column A_3B_3

compares the results of nonlinear time-history analysis and pushover analysis. For columns A_1B_1 and A_3B_1, the results of nonlinear time-history analysis agree well with the results of pushover analysis, as shown in Fig. 10a, b. In contrast, there is an appreciable difference between the results of nonlinear time-history analysis and pushover analysis for column A_3B_3 as shown in Fig. 10c.

From this observation, the drift responses of columns A_1B_1 and A_3B_1 on the second story can be approximated using the first modal response, while the contributions of the second and higher modal responses are appreciable for column A_3B_3. The variation in the peak drift on the second story at the "flexible" side columns (A_1B_1 and A_3B_1) due to the direction of the seismic input can therefore be explained in terms of the variation of the first modal response.

4.3 *Momentary Energy Input of the Nonlinear First Modal Response*

The momentary input energy of the first modal response per unit mass is next calculated. The present study follows studies by Inoue and coauthors [7, 8]. The energy input during a half cycle of the structural response is considered. The momentary input energy of the first modal response per unit mass, $\Delta E_{1U}{}^*/M_{1U}{}^*$, is defined as.

$$\frac{\Delta E^*_{1U}}{M^*_{1U}} = -\int_t^{t+\Delta t} a_{gU}(t)\dot{D}^*_{1U}(t)dt \tag{3}$$

where $a_{gU}(t)$ is the ground acceleration component along the U-axis while t and $t + \Delta t$ are the beginning and end times of a half cycle of the structural response. The maximum momentary input energy of the first modal response per unit mass, $\Delta E_{1U}{}^*{}_{\max}/M_{1U}{}^*$, is defined as the maximum value of $\Delta E_{1U}{}^*/M_{1U}{}^*$ over the course of the seismic event.

Figure 11 illustrates the definition of $\Delta E_{1U}{}^*{}_{\max}/M_{1U}{}^*$. In the figure, the case in which the largest $D_{1U}{}^*{}_{peak}$ occurs ($\lambda = 1.0$, $\psi = 0°$) is shown as an example. As shown in the figure, $\Delta E_{1U}{}^*{}_{\max}/M_{1U}{}^*$ is the input energy from $t = 24.34$ s (beginning of a half cycle as shown in (a)) to $t + \Delta t = 25.06$ s (end of the half cycle).

For the following discussions, the equivalent velocity of the maximum momentary input energy of the first modal response, $V_{\Delta E1U}{}^*$, is defined as.

$$V_{\Delta E1U^*} = \sqrt{2\Delta E_{1U^*}\max/M_{1U^*}} \tag{4}$$

Figure 12 shows the results of calculating $D_{1U}{}^*{}_{peak}$ and $V_{\Delta E1U}{}^*$ from all results of time-history analysis. Plot (a) shows a clear relation between $D_{1U}{}^*{}_{peak}$ and $V_{\Delta E1U}{}^*$, as was pointed out by Inoue and coauthors for the nonlinear SDOF model [7, 8]. Plot (b) shows the peak equivalent velocity $V_{\Delta E1U}{}^*$ for various directions of seismic input.

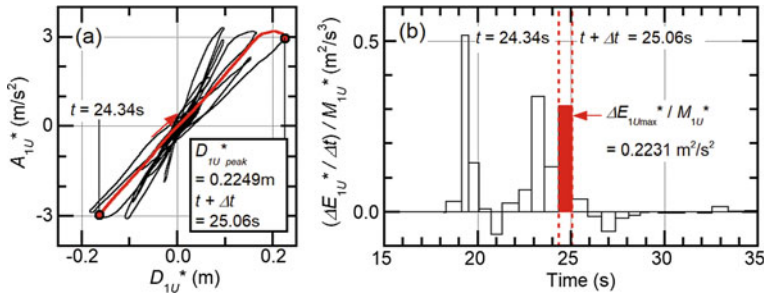

Fig. 11 Definition of the maximum momentary input energy of the first modal response per unit mass. **a** Hysteresis loop of the first modal response, **b** Time-history of the momentary energy input

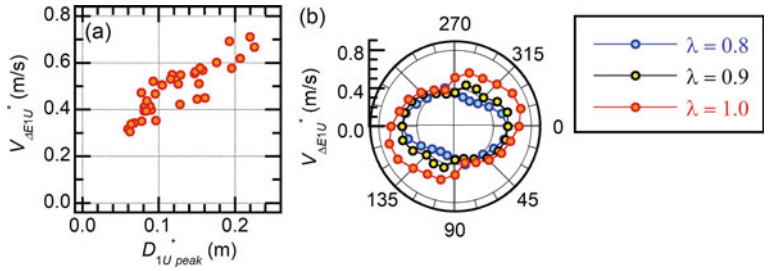

Fig. 12 Calculation results of $D_{1U}{}^{*}{}_{peak}$ and $V_{\Delta E1U}{}^{*}$. **a** Relation of $D_{1U}{}^{*}{}_{peak}$ and $V_{\Delta E1U}{}^{*}$, **b** $V_{\Delta E1U}{}^{*}$ for various directions of seismic input

As shown in plot (b), $V_{\Delta E1U}{}^{*}$ is larger in the ranges of $135° \leq \psi \leq 180°$ and $315° \leq \psi \leq 360°$. The trend of $V_{\Delta E1U}{}^{*}$ is consistent to that of $D_{1U}{}^{*}{}_{peak}$ shown in Fig. 9b. Therefore, the variation in the peak drift on the second story at the "flexible" side columns (A_1B_1 and A_3B_1) due to the direction of the seismic input can be explained in terms of the variation of $V_{\Delta E1U}{}^{*}$.

4.4 Comparison of the Maximum Momentary Input Energy with the Linear Spectrum

Next, the maximum momentary input energy of the first modal response shown above is compared with the linear spectrum. In this study, the following linear spectra are calculated: (i) the maximum and minimum linear unidirectional $V_{\Delta E}$ spectra with viscous damping ratio $h = 0.10$ [7, 8] considering various angle of incidence of seismic input, and (ii) linear bidirectional $V_{\Delta E}$ spectrum [9] with viscous damping ratio $h = 0.10$. Since the angle of incidence of the U-axis from the X-axis varies gradually as the equivalent displacement $D_{1U}{}^{*}{}_{peak}$ increases due to the nonlinearity, the intervals for calculating the maximum and minimum $V_{\Delta E}$ spectrum should be

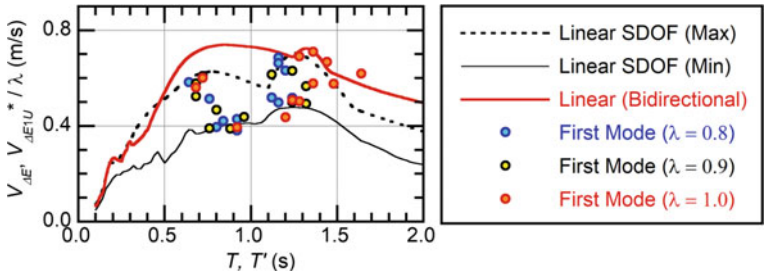

Fig. 13 Comparisons of the normalized $V_{\Delta E1U}{}^{*}$ and linear $V_{\Delta E}$ spectrum

smaller. Therefore, the maximum and minimum $V_{\Delta E}$ spectrum is calculated for a for a natural period of the linear SDOF model T when the angle of incidence of the seismic input ψ varies in 1° intervals from 0° to 359°. Figure 13 compares the $V_{\Delta E1U}{}^{*}$ normalized by the scaling factor λ and linear $V_{\Delta E}$ spectrum with viscous damping ratio $h = 0.10$. In the figure, the notations Max and Min respectively indicate the maximum and minimum $V_{\Delta E}$, while the notation Bidirectional is the bidirectional momentary input energy spectrum calculated using time-varying function [9]. The response period T' is defined from the time for a half cycle of the structural response at $\Delta E_{1U}{}^{*}{}_{\max}/M_{1U}{}^{*}$ as.

$$T' = 2\Delta t \tag{5}$$

In the figure, most plots of the normalized $V_{\Delta E1U}{}^{*}$ are within the band between Max and Min $V_{\Delta E}$ spectra. In addition, the bidirectional $V_{\Delta E}$ spectrum approximates the upper bound of the plots of the normalized $V_{\Delta E1U}{}^{*}$. Therefore, for the conservative prediction of the peak response, the bidirectional $V_{\Delta E}$ spectrum formulated in [9] may be used as the seismic intensity parameter.

5 Conclusions

A nonlinear time-history analysis of the main building of the former Uto City Hall was carried out, considering various directions of seismic input. The effect of various directions of seismic input on the peak response was then discussed based on the nonlinear first modal response. The main conclusions of the study are as follows.

(a) The angle of incidence where the peak drift at the "flexible" side column (A_1B_1 and A_3B_1) is the largest is close to that where the peak equivalent displacement of the first mode, $D_{1U}{}^{*}{}_{peak}$, is largest.

(b) The equivalent velocity of the maximum momentary input energy of the first modal response, $V_{\Delta E1U}{}^{*}$, is clearly related to $D_{1U}{}^{*}{}_{peak}$. This is consistent to

the results by Inoue and coauthors for the nonlinear SDOF model. In addition, the trend of the variation of $V_{\Delta E1U}{}^{*}$ is consistent to that of $D_{1U}{}^{*}{}_{peak}$.

(c) Most plots of the evaluated $V_{\Delta E1U}{}^{*}$ are within the band between the maximum and minimum spectra obtained from the linear elastic analysis considering all possible angles of incidence. In addition, the bidirectional $V_{\Delta E}$ spectrum formulated in [9] approximates the upper bound of $V_{\Delta E1U}{}^{*}$.

Based on these findings, the presenting author considers the effect of the various directions of seismic input to the local response at "flexible" side can be explained in terms of the variation of energy input of the first modal response. In addition, the equivalent velocity of the bidirectional maximum momentary input energy may be one of the possible seismic intensity parameters available for discussion of the nonlinear peak response under bidirectional excitation. Further investigation is needed for confirmation.

Acknowledgements Ground motions used in this study were taken from the websites of the National Research Institute for Earth Science and Disaster Resilience (NIED) (http://www.kyoshin.bosai.go.jp/kyoshin/, last accessed on 14 December 2019).

References

1. Fujii K, Yoshida S, Nishimura T, Furuta T (2017) Observations of damage to Uto City Hall suffered in the 2016 Kumamoto Earthquake. In: Proceedings of the 8th European workshop on the seismic behaviour of irregular and complex structures, Bucharest, Romania
2. Fujii K (2019) Pushover-based seismic capacity evaluation of Uto City Hall damaged by the 2016 Kumamoto Earthquake. Buildings 9(6):140. https://doi.org/10.3390/buildings9060140
3. Boore DM, Watson-Lamprey J, Abrahamson NA (2007) Orientation-independent measures of ground motion. Bull Seismol Soc Am 96:1502–1511
4. López OA, Torres R (1997) The critical angle of seismic incidence and the maximum structural response. Earthq Eng Struct Dynam 26:881–894
5. Athanatopoulou AM (2005) Critical orientation of three correlated seismic components. Eng Struct 27:301–312
6. Faggella M, Gigliotti R, Mezzacapo G, Spacone E (2018) Graphic dynamic prediction of polarized earthquake incidence response for plan-irregular single story buildings. Bull Earthq Eng 16(10):4971–5001
7. Inoue N, Wenliuhan H, Kanno H, Hori N, Ogawa J (2000) Shaking table tests of reinforced concrete columns subjected to simulated input motions with different time durations. In: 12th World conference on earthquake engineering. Auckland, New Zealand
8. Hori N, Inoue N (2002) Damaging properties of ground motion and prediction of maximum response of structures based on momentary energy input. Earthq Eng Struct Dynam 31(9):1657–1679
9. Fujii K, Yoshiki Murakami Y (2020) Bidirectional momentary energy input to a one-mass two-DOF system. In: Proceedings of the 17th world conference on earthquake engineering. Sendai, Japan

10. Kuramoto H (2004) Earthquake response characteristics of equivalent SDOF system reduced from multi-story buildings and prediction of higher mode responses. J Struct Construct Eng. Trans AIJ 580:61–68 (in Japanese)
11. Fujii K (2014) Prediction of the largest peak nonlinear seismic response of asymmetric buildings under bi-directional excitation using pushover analyses. Bull Earthq Eng 12:909–938

Performance of RC Beam Column Joint with Varying Hoop Reinforcement

Ashish B. Ugale and Suraj N. Khante

1 Introduction

The performance of framed structures depends not only upon the individual structural elements but also upon the integrity of the joints. In most of the cases, joints of irregular framed structures are more critical and subjected to the most critical loading under seismic conditions. In an earthquake region, the expected deficiency in seismic performance of gravity load designed RC frames has been widely attributed to reinforcing details that are typical in that type of construction. Beam-column joints in seismically susceptible zones are critical regions in the reinforced concrete framed structure [1]. The joint is usually neglected in Indian practice for specific design and attention being restricted to provision of sufficient anchorage for beam longitudinal reinforcement and can be acceptable when the frame is not subjected to earthquake loads. A beam column joint becomes structurally less efficient when subjected to large lateral loads. The earthquakes in India in past decades reported catastrophic failures and casualties. The innovative joint designs that are able to reduce congestion of reinforcement in the joint are desirable. ACI-352 (2002) recommends additional research on use of T-headed bar (mechanical anchorage) in design of beam-column joints in concrete structures [2]. The horizontal hoop reinforcement in joint for seismic resistance design plays an important role. It is observed that hoops carry a substantial portion of the joint shear directly with the remainder being carried by the concrete core in the form of a diagonal compression strut [3]. Transverse hoops in a joint contribute to the shear resistance of joints indirectly by confining the concrete core, thus enhancing its diagonal compressive strength. But confining transverse reinforcement improves the performance of the joint and at the same time it increases the congestion at joint. Therefore, it is necessary to evaluate

A. B. Ugale (✉) · S. N. Khante
Applied Mechanics Department, GCOE, Amravati, Maharashtra, India

R. Bento et al. (eds.), *Seismic Behaviour and Design of Irregular and Complex Civil Structures IV*, Geotechnical, Geological and Earthquake Engineering 50,
https://doi.org/10.1007/978-3-030-83221-6_18

the exact behavior of beam-column joint by studying the joint shear strength, stiffness, displacement ductility, crack patterns etc. The objective of this experimental study is to satisfy such structural demands by introducing headed bar and different types of transverse hoops in joint so as to achieve expected confinement with ease of placement of reinforcement and concrete.

2 System Developments

ACI codes details prerequisites for the minimum area of joint transverse reinforcement and the greatest possible spacing of transverse reinforcement to obtain satisfactory concrete confinement. The anchorage capacity of a headed bar is to a great extent owe to its bearing, which may require less confinement as compared to a joint with hook bars. Some tests were conducted to investigate the part of joint hoops in the shear strength, displacement ductility and stiffness of exterior beam-column joints with headed bars subjected to reverse cyclic loading [4, 5].

As per Sect. 21·7·4 [6], nominal shear strength (V_n) is based on

$$V_n = 15A_j\sqrt{f'_c} \tag{1}$$

where A_j is the effective cross-sectional area within a joint in a plane parallel to the plane of reinforcement and f'_c is characteristic strength of concrete cylinder; the code surveys the nominal shear strength capacity based on strut mechanism. The design shear force, $V_{jh,u}$ based on capacity design concept, can be estimated using

$$V_{jh,u} = T - V_{col} = 1.25(A_{st}\, f_y - Ast\, f_y\, j_d / L_c) \tag{2}$$

where T is the tensile force in the beam reinforcement; V_{col} is the horizontal column shear; 1.25 is the overstrength factor; A_{st} is the area of tension reinforcement of the beam; f_y is the specified yield strength of the beam longitudinal reinforcement; L_c is the distance between column inflection points; and j_d is the internal lever arm of the beam section (approximately 7/8 of the effective depth of the beam) [4, 5].

3 Test Program

Six exterior beam-column joint designed as per IS 456 [7] with variations such as joint shear reinforcement and headed bars. The specimens are tested under cyclic and reverse cyclic loading.

3.1 Material Properties

The concrete mix with medium workability is designed for the M25 grade. Portland Pozzolana Cement of 53 grade and natural sand with specific gravity 2.72 of grading zone I are used as fine aggregate. Course aggregates of a maximum size of 20 mm and specific gravity 2.78 are used. HYSD bars of Fe 450 grade 8 mm dia. are used as longitudinal reinforcement of beam and column, whereas Fe 250 grade 6 mm dia. bars are used as transverse reinforcement [7, 8].

3.2 Test Specimens

The specification details of individual specimen are mentioned in Table 1.

In the current research work, headed bars are used in place of conventional reinforcing bars with necessary development length. A bar with a short head in the form of welded steel plate at the end of a straight reinforcing bar is provided in the zone of the diagonal compression strut. In all the specimens, minimum clear cover for all headed bars is $2d_b$ and provided clear cover is 20 mm, where d_b is diameter of bar. By using headed bar, development length available is equal to 160 mm i.e. 20db which is measured from the inner face of the head plate to the outer face of the joint hoop. Details of headed bar is shown below in Fig. 1 as against of development length as per IS 456 [7]. The beam and column are provided with stirrups and lateral ties of 6 mm in diameter. All details of the specimens are shown in Fig. 2.

Table 1 Specification details of test specimen

Sr. no	Specimen designation	Specification
1	J_1	Control specimen using headed bars
2	J_{11}	Specimen using headed bars with extra single tie in joint
3	J_{12}	Specimen using headed bars with extra two ties in joint
4	J_{13}	Specimen using headed bars with extra three ties in joint
5	J_{14}	Specimen using headed bars with extra single stirrup in joint
6	J_{15}	Specimen using headed bars with extra two stirrup in joint

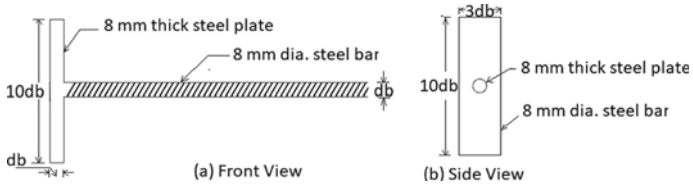

Fig. 1 Details of headed bar

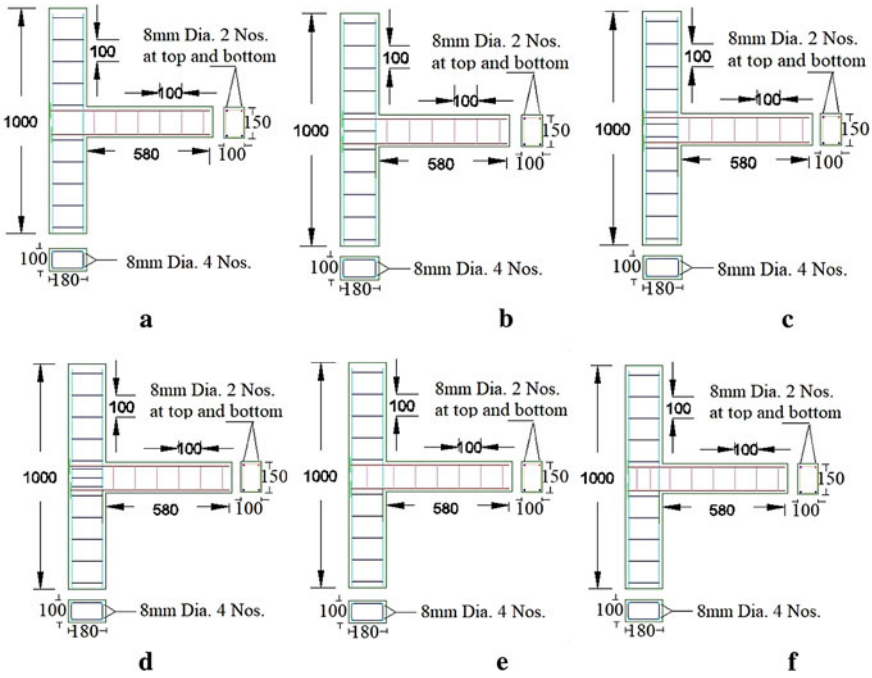

Fig. 2 Reinforcement details of specimens **a** J_1, **b** J_{11}, **c** J_{12}, **d** J_{13}, **e** J_{14}, **f** J_{15}

3.3 Test Setup and Loading Procedure

All the six specimens are tested using reaction frame in the laboratory. The details of experimental test set-up are shown in Fig.3a, b. Each of the test specimens is subjected to cyclic and reverse cyclic loading to simulate earthquake loading. An

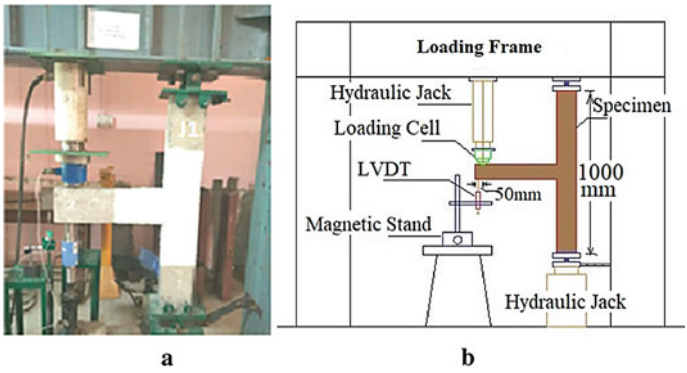

Fig. 3 **a** Photograph of experimental setup, **b** Schematic diagram of set up

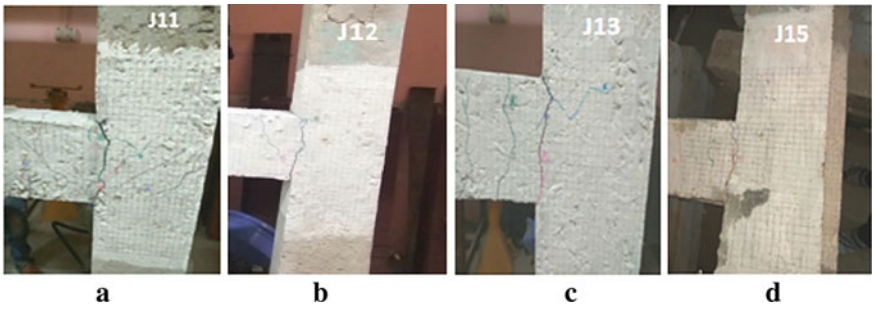

Fig. 4 Beam flexure failure (BF) in specimens **a** J_{11}, **b** J_{12}, **c** J_{13}, **d** J_{15}

axial load on the column is applied by using hydraulic jack mounted on the frame. The loaded column ends are supported with hinge supports at top and bottom. Two jacks are used to apply cyclic and reverse cyclic load to the beam, which is applied at a distance of 50 mm from free end. The applied load is measured with the help of loading cell inserted in between jack and beam. The experimental test carried out is displacement controlled; hence drift ratio is constant for the cycle for the specimens considered. The deflection at the beam free end tip is measured by linear variable differential transducers (LVDTs) as shown in Fig. 3b.

4 Strength Predictions and Cracking Behavior

Generally three types of failures are observed in joint i.e. Joint shear failure, Beam flexure failure and Beam Joint Failure or a combination thereof.

Minor cracks are observed in all specimens during initial cycles. At higher displacement cycle, specimen J_{11}, $J_{12,}$ J_{13} and J_{15} shows the vertical flexure cracks in beam at joint interface and finally fails due to beam flexure failure. Failure is recognized by steady loss of load-conveying limit after the formation of the plastic hinge in the adjacent beam and same is evident from Fig. 4a–d. The formation of combined horizontal and vertical cracks in joint area results in failure of joint as observed in specimen J_1 and J_{14} as shown in Fig. 5a, b. It is also called as beam joint failure, whereas horizontal crack is due to shear and vertical crack is due to flexure.

5 Force-Drift Study

The displacement ductility (μ) is the ratio of the final displacement and the yield displacement i.e. d_u/d_y, wherein d_u is the vertical displacement of the beam corresponding to maximum loading P_u and d_y is the yield displacement [9, 10]. The different strength parameters of individual specimens are accounted for and analyzed

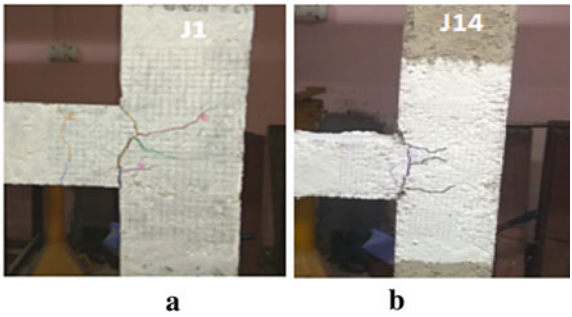

Fig. 5 Beam joint failure (BJF) in specimens **a** J_1, **b** J_{14}

Table 2 Joint Shear Strength, Nominal flexural strengths, displacement ductility, stiffness, and energy dissipation of specimens

Specimen	P_{max} (kN)	Nominal flexural strength, M_n (kNm)	Yielding displacement in mm (d_y)	$V_{jh,test}$ (kN)	Displacement ductility factor, $\mu = (d_u/d_y)$	Stiffness (Initial) kN/mm	Stiffness (final) kN/mm
J_1	12.01	4.74	2.24	50.29	5.36	5.36	1.00
J_{11}	13.03	4.74	1.73	54.56	6.94	7.54	1.05
J_{12}	16.04	4.74	1.63	67.16	7.36	9.84	1.09
J_{13}	13.75	4.74	1.43	57.57	8.39	9.62	1.15
J_{14}	12.58	4.74	1.98	52.68	6.07	6.37	1.05
J_{15}	12.99	4.74	2.21	54.39	5.44	5.89	1.12

in Table 2. The specimen J_1 displayed lower displacement ductility and poor execution as no confining reinforcement is provided in the beam– column section. The addition of hoop reinforcement improves displacement ductility values as compared to J_1. The specimen J_{13} exhibited large displacement ductility values 56.53% more due to good confinement in the beam-column joint region as a result of proper anchorage and an effective joint shear-resisting mechanism. Specimen J_{15} shows least improvement amongst the other confined specimens and 8.15% more than control specimen J_1. Horizontal hoops (ties) contribute to compression strut in the direction of longitudinal beam reinforcement. Hence, confinement due to horizontal ties is more effective as compared to vertical stirrups.

6 Comparisons of Predictions of Experimental Responses

The drift ratio (DR) is defined as the ratio of deflection Δ of the loading point to the distance between the centreline of the column and loading point. In hysteresis curves the load is plotted against displacement. All the specimens exhibited a satisfactory response up to drift (DR) 2% and same is shown in Fig. 6.

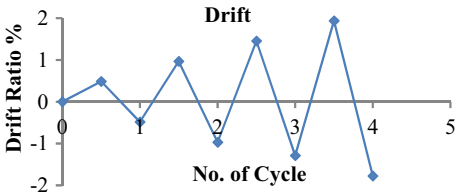

Fig. 6 Loading regime

The shape of hysteresis curves indicates energy dissipation accomplished. The hysteresis curves of specimens J_{11}, J_{12}, J_{13} and J_{15} are looking wide and stable, with higher energy dissipation in each primary loading cycle. Specimens J_1 and J_{14} although they failed in the joint, exhibited a satisfactory hysteretic response up to drift 2%. Figure 7a–f shows corresponding hysteresis curves of force drift performance for individual specimen. It is observed that an improved level of performance can be executed with headed bars even without joint hoop reinforcement. The hysteresis loops indicates proper energy dissipation accomplished for all the tested specimens [10].

7 Stiffness

It can be found in Fig. 8 that all specimens demonstrated a comparable pattern of stiffness degradation with higher displacement cycle. It is noticed that the deviations are remarkable for all the specimens huge at lower displacement. Gradual degradation of stiffness is observed until failure. The specimen J_1 had the lowest initial as well as final stiffness owing to non-confinement. The hoop confinement in other specimen resulted in a higher stiffness compared to control specimen.

8 Shear Strength

The joint shear strength $V_{jh,test}$ [5] is calculated using Eqs. (3) and (4),

$$Vjh, test = T_{max} - V_{col} \tag{3}$$

$$= P_{max}\left\{(L_b/j_d) - (L_b + 0.5hc)/L_c\right\} \tag{4}$$

where T_{max} is the maximum tensile force in the longitudinal reinforcement of the beam; V_{col} is the horizontal column shear in equilibrium with applied loading, L_b is length of the beam from the column face and h_c is depth of column. The specimen J_1 possesses the least value of joint shear strength as compared to other specimens

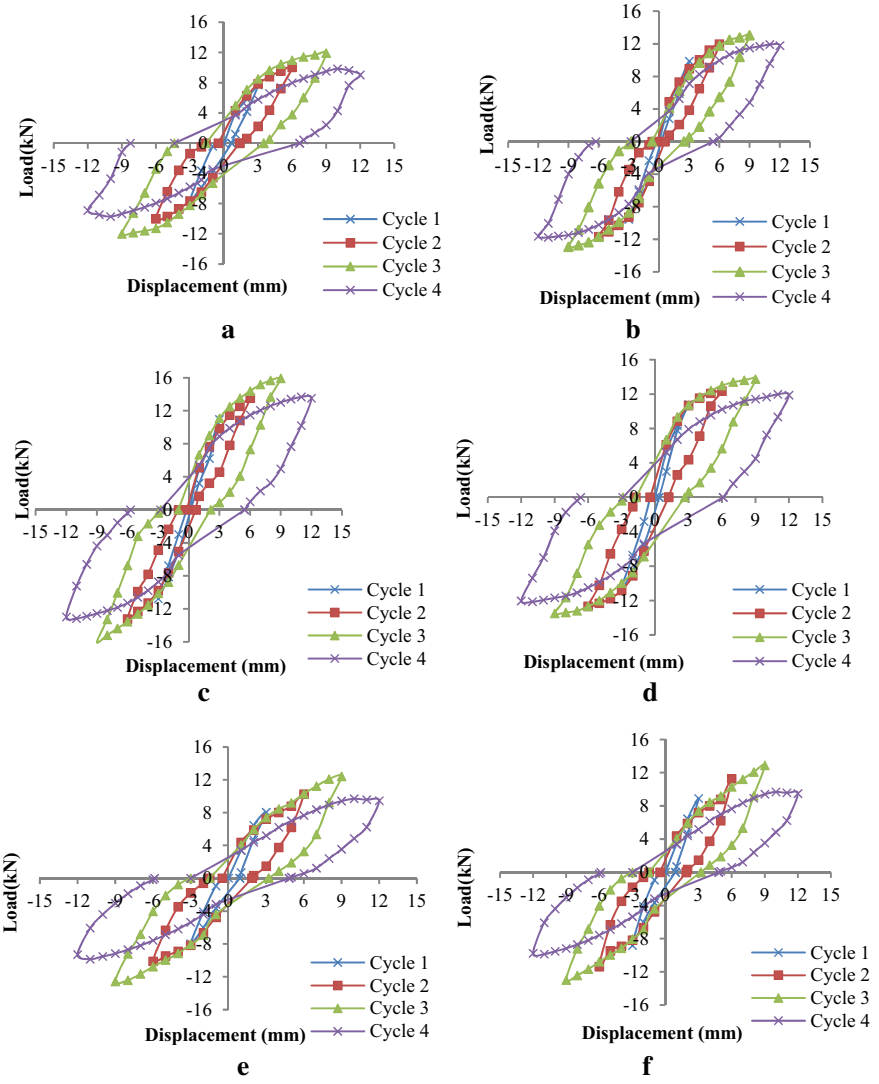

Fig. 7 Comparison of force-drift responses of specimens **a** J_1, **b** J_{11}, **c** J_{12}, **d** J_{13}, **e** J_{14}, **f** J_{15}

and the maximum shear strength is revealed by the specimen J_{12}. Joint shear strength increases with increase in confinement of joint due to presence of hoops. Based on the capacity design concept, the estimated design shear force, $V_{jh,u}$ (Eq. 2) is 46.43 kN for all the specimens with ultimate displacement (d_u) 12 mm. All joint specimens perform better by an amount of 8.30, 17.51, 44.65, 23.99, 13.46 and 17.44% more than the estimated value of shear strength i.e. 46.43 kN. Specimen J_{11}, J_{12}, J_{13}, J_{14} and J_{15} exhibited more value of actual shear force than control specimen J_1 by an

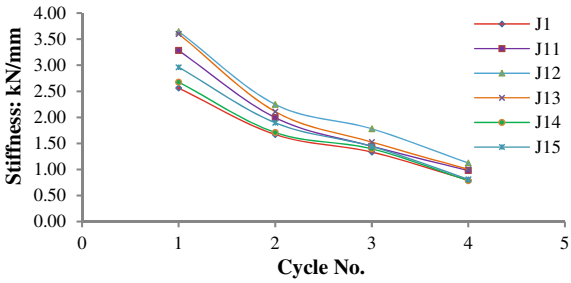

Fig. 8 Stiffness degradation of test specimens

amount of 8.49, 33.54, 14.48, 4.75 and 8.15 respectively. Table 2 shows the joint shear strength of individual specimen.

9 Conclusions

This paper deals with research on six exterior beam-column joint specimens with differing joint hoops in quality (orientation) and quantity to examine the role of joint hoops on the shear strength of exterior beam-column joints by utilizing headed bars under cyclic loading. The following conclusions are drawn from the tests.

- The measure of joint hoops impacts the global response of the beam-column joint, especially at high inelastic cyclic load reversals when shear requirement at the intersection approaches the shear limit of the joint.
- The beam-column joint specimens without joint hoop reinforcement experience remarkable dislodging with extensive cracks.
- Confinement in either direction i.e. horizontal or vertical enhances extreme load-carrying capacity, displacement ductility, joint shear quality and stiffness of the specimen. However ties are predominantly effective.
- Increase in the confinement of joint by using ties generally increases the ductility of the joint, shear strength and initial stiffness of joint. However, the shear strength increases with increase in the confinement using extra ties up to two, but it decreases with further increase in confinement.
- Increase in the confinement of joint by using stirrups invariably increases the shear strength; but reduction observed in ductility and initial stiffness of joint.
- Confinement of joint using extra single tie or stirrup gives equal stiffness at final stage but it is more at initial stage in case of horizontal hoop.
- Increasing ties for joint confinement resulted in enhancing the shear strength, displacement ductility and initial stiffness of joint. However, increase in stirrups for confinement also increases shear strength but there is a reduction in ductility and initial stiffness

- Specimen J_{12} shows overall better performance amongst all the other specimens. I.e. confinement of joint using two additional ties enhanced the general seismic performance of joint when compared with others.

References

1. Celik OC, Ellingwood BR (2008) Modeling beam-column joint in fragility assessment of gravity load designed reinforced concrete beams. J Earthquake Eng 12:357–381
2. Rajagopal S, Prabavathy S (2014) Exterior beam-column joint study with non-conventional reinforcement detailing using mechanical anchorage under reversal loading. Sadhana 39–5:1185–1200
3. Shyh-Jiann Hwang, Hung-Jen Lee, Kuo-Chou Wang (2004) Seismic design and detailing of exterior reinforced concrete beam-column joints. In: 13th World conference on earthquake engineering. Vancouver BC, Canada, August 1–6, 2004, p 397
4. Dhake PD, Patil HS, Patil YD (2015) Anchorage behavior and development length of headed bars in exterior beam-column joints. Mag Concr Res 67–2:53–62. https://doi.org/10.1680/macr.14.00144
5. Dhake PD, Patil HS, Patil YD (2015) Role of hoops on seismic performance of reinforced concrete joints. Struct Build 168-SB10:708–717. Doi: 10.1680 /stbu.14.00107
6. ACI American Concrete Institute (2008) Committee 318: building code requirements for structural concrete and commentary. ACI, Farmington Hills, MI, USA, ACI 318–08
7. IS 456:2000 Indian standard plain and reinforced concrete code of practice. Bureau of Indian Standards, New Delhi, India
8. BIS Bureau of Indian Standards (1970) IS 383–1970 (reaffirmed1997): specification for coarse and fine aggregates from natural sources for concrete. Bureau of Indian Standards, New Delhi, India.
9. Hwang SJ, Lee HJ, Liao TF, Wang KC, Tsai HH (2005) Role of hoops on shear strength of reinforced concrete beam–column joints. ACI Struct J 102(3):445–453
10. Ugale AB, Khante SN (2019) Energy dissipation of RC beam-column joint confined by different types of lateral reinforcements. In: Proceeding of international conference on innovative trends in civil engineering for sustainable development (ITCSD–2019). 89–91

Dynamic Identification and Structural Behavior of an Irregular School Building

Riccardo Mario Azzara, Vieri Cardinali, Mario De Stefano, Marco Tanganelli, and Stefania Viti

1 Introduction

In existing buildings, the modifications occurred during the years generally increase their complexity and irregularity, introducing further uncertainties. Intuitive and no-engineering interventions are commonly made over the structures in order to improve their performances pursuing new uses or destinations.

Concerning the seismic assessment of the structures, the evaluation of their structural performances requires the preliminary definition of the structural model and of the mechanical properties of materials used. While the *knowledge path* described in the Italian National Code permits a general comprehension of the structural organism, the determination of the mechanical properties is affected by a higher number of uncertainties. To this aim, several experimental procedures may be used; destructive campaigns are the most reliable, since they directly define the numerical values of the investigated parameters. Nevertheless, their applicability is strongly reduced because of the costs, difficulty in the executions, and their invasive effects.

R. M. Azzara
Istituto Nazionale di Geofisica e Vulcanologia, Osservatorio Sismologico di Arezzo, c/o Villa Severi Via Francesco Redi 13, 52100 Arezzo, Italy
e-mail: riccardo.azzara@ingv.it

V. Cardinali (✉) · M. De Stefano · M. Tanganelli · S. Viti
Department of Architecture, University of Florence, Piazza Brunelleschi n 6, 50121 Florence, Italy
e-mail: vieri.cardinali@unifi.it

M. De Stefano
e-mail: mario.destefano@unifi.it

M. Tanganelli
e-mail: marco.tanganelli@unifi.it

S. Viti
e-mail: stefania.viti@unifi.it

R. Bento et al. (eds.), *Seismic Behaviour and Design of Irregular and Complex Civil Structures IV*, Geotechnical, Geological and Earthquake Engineering 50,
https://doi.org/10.1007/978-3-030-83221-6_19

During the years, different no-destructive or partial destructive methodologies have been studied [1, 2]. Based on empirical correlation with destructive data, they are able to give reliable result, despite the randomness of the materials' behavior. In fact, in the existing buildings, the variability of conditions can be extremely high [3–6], so that the definition of the mechanical characteristics through a limited number of tests may bring to wrong results. Therefore, in order to achieve reliable information regarding the mechanical properties of existing buildings, a lot of time and effort is needed. Moreover, concerning existing buildings (in particular with historical masonry structures) engineer practice has to face with building aggregates. As known, the interaction between adjacent buildings and co-participant structures still represent an open field and enlarges the number of variables. Because of these reasons, the use of ambient vibration techniques in order to match the dynamic behavior of the buildings and to characterize the mechanical properties of the structures has widely grown. The dynamic identification is an effective tool in order to obtain experimental results for the dynamic behavior of the buildings [7–12]. Moreover, its use has been preferred in cultural heritage contexts, where, considering the relevance of the structures studied, the execution of destructive campaigns is not recommendable [13–15]. In this paper, the assessment of the structural performances of a building hosting the School of Architecture of the University of Florence is presented. It consists of a rectangular and regular building altered during past intervention through the insertion of reinforced concrete structures.

2 The School of Architecture in Florence

The case study consists in the School of Architecture of Florence. It is located in the historical center of the city, in an old building erected since the fourteenth century. The School nowadays is characterized by an irregular and complex structure; in fact, the University is located over the fabrics of a Medieval monastery. During the ages, many changes occurred; in the second half of XIX century, the structure hosted also the Municipal prison. From the 80's of the XX century, the complex is hosting the School of Architecture of Florence. In this phase, new buildings were built, and the organization of the entire planimetry has been redesigned. New structures in RC have been put as adjacent structures to the existing ones. The final result is a complex building characterized by several interactions with the adjacent structures and an irregular shape (both for his plan configuration, both for his heights).

The analyzed building, named "*Block B*", is shown in Fig. 1. It has three stories; with respect of the main entrance, it is symmetric to another building (*Block A*), characterized by the same shape but built with a different technology. They both present a rectangular shape, whose sides measure 14.10×20.20 m. *Block B* presents walls with a relevant thickness (around 35 cm) made of clay bricks. At the center of the volume four couples of pillars hold bohemian vaults covering the central navy at the upper level of the building. As written before, the building has been widely strengthened during past interventions.

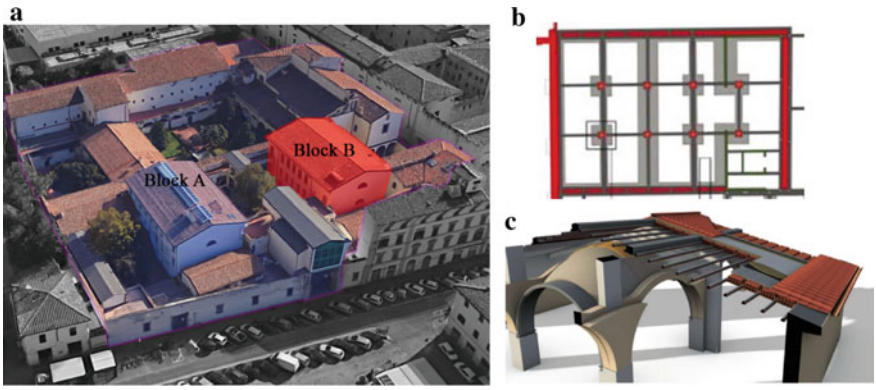

Fig. 1 From left: **a** view of the university complex with the highlight of the case study **b** structural planimetry of the building considered **c** 3D-section of the particular of the vaults and the roof of the structure analyzed

The pillars have been reinforced; injections of epoxy resins were made on the core of the masonry pillars, while the perimeter has been confined through a layer of RC plaster (15 cm thickness). The bohemian vaults have been treated by a second order of epoxy resins shell put over the old one, to the purpose of confining and reinforcing it. In the perimetral walls, new RC beams has been introduced in order to confine and reinforce the masonries. The slabs have been re-built during this phase of interventions, through the realization of RC floors characterized by RC joists alternated by hollow clay elements and topped by a reinforced concrete slab. Finally, the openings in the masonry structures have been confined by steel hoops. Figure 1b, c show the general layout of the building structure, together with the details of the bohemian vaults and the roof of the building.

The structural survey has been defined on the basis of the archive research conducted; the evidences from the found documentation have been compared with a laser-scanner survey (in order to check the reliability of the drawings) and with a thermography campaign (to confirm the presence of the RC elements). The veracity of the documents has been verified; in order to limit the impact of the survey to the building, no destructive tests have been planned, and the "minor" Knowledge Level, *KL1*, has been used (Confidence Factor, *CF*, equal to 1.35). However, a dynamic identification of the case study has been performed.

2.1 Dynamic Identification

The dynamic identification of *Block B* has been made through the use of 6 seismometers (2 for each level) disposed across the main walls of the structure. The seismic stations, by SARA Electronic Instruments S.R.L., consist of an AD converter (SL06/24 bit) coupled to a three-axial seismometer with eigenfrequency 2 Hz (SS20).

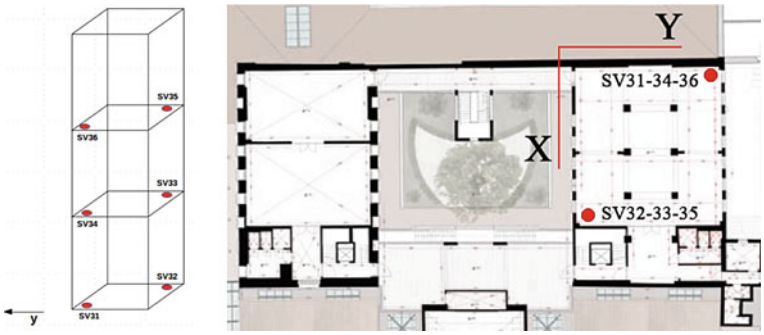

Fig. 2 The setup of the experimental campaign with the vertical alignment of the seismic stations over the two considered nodes

The total amount of data consists of about three hours of signals recorded at 100 sps, the times of the stations have been synchronized by GPS. In Fig. 2 the setup of the experimental test is shown.

2.1.1 Time-Domain Analysis

The analysis of the data recorded during the experimental campaign has revealed some interesting aspects about the response of the structure. For sake of brevity, the paper focuses on some aspects only, related to the performed identification analysis. Figure 3 shows an example of the horizontal waveforms recorded during the test. The vibrations recorded along the horizontal components show an increase in amplitude along the vertical alignment, still maintaining an excellent correlation of the waveforms. Along the *X* component the oscillation exhibits systematically higher

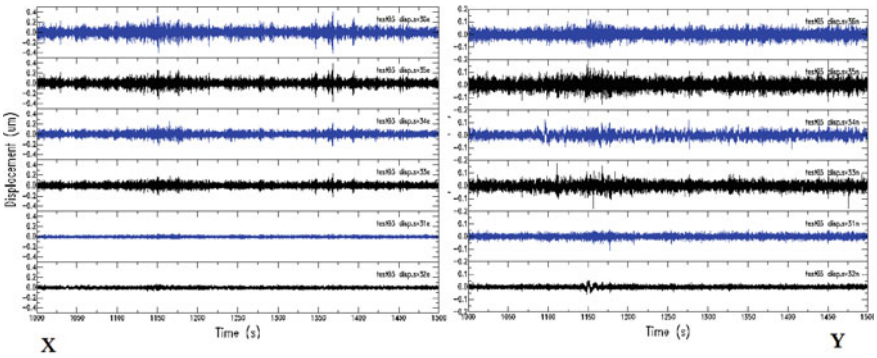

Fig. 3 Horizontal waveforms recorded along the two main directions; from the bottom, each couple of signals (black and blue) is referred to a specific level (ground floor, first and second level). The black is for seismic stations SV 32–33-35, while the blue is for SV 31–34-36

amplitudes than those recorded along *Y* direction (the scale of each panel of Fig. 3 is set at the maximum value of the top stations, the amplitude of the *X* component is about twice than that of the *Y*). This behavior could suggest a different response of the two parts of the structure. Overall, along the *X* direction the building keeps a regular global behavior, while in the *Y* direction it shows a displacements trend that may express a torsional effect.

2.1.2 Frequency Analysis

The recorded signals have been analyzed in the frequency domain in order to point out the frequencies of the vibrational modes of the building. The average *Fast Fourier Transform* (FFT) has been computed for each components and devices. The *FTTs* in Fig. 4 have been computed by averaging the Fourier spectra evaluated over consecutive intervals lasting 120 s. Spectral analysis provides a particularly complex image of the behavior of the structure, that seems to confirm what hypothesized in the time-domain analysis, probably due to the different external constraints produced by the connections of each corner with the other parts of the complex.

From Fig. 4, along the *X* direction it is possible to highlight at each station a single spectral peak around 5.2–5.3 Hz with amplitude increasing from the ground to the highest floor (please see the black arrows in Fig. 4). At each level the spectra show the same amplitudes and shapes for each couple of seismic stations located in the opposite corners. Moreover, at the base stations it is possible to recognize a secondary spectral peak at about 9.5 Hz that doesn't propagate inside the building.

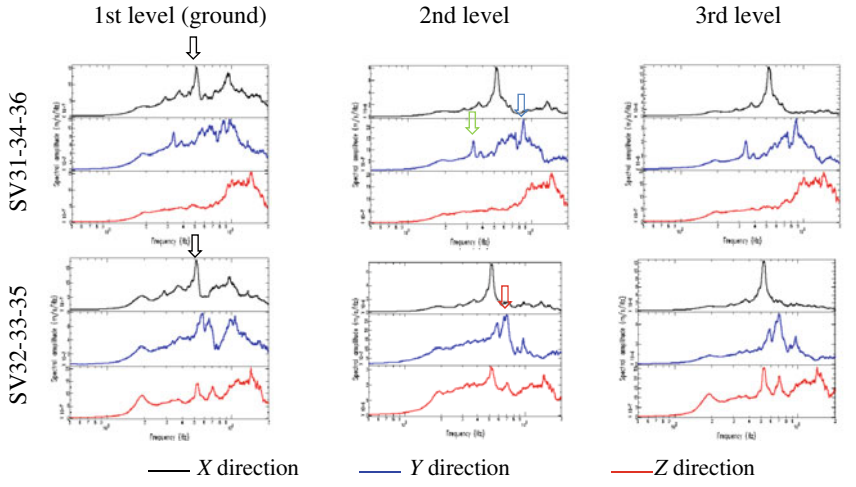

Fig. 4 Mean fourier spectra calculated over the full registration time for each seismic station *X* direction *Y* direction *Z* direction

In the *Y* direction (Fig. 4), a very different behavior is found at the two monitored corners. The vertical alignment SV31-SV34-SV36 presents a peak centered on 3.4 Hz (green arrow), that disappears in the opposite corner (SV32-SV33_SV35). At this side of the building two different peaks arise centered at frequencies 5.2–5.3 and 7.3 Hz, respectively (blue and red arrows).

3 Structural Modelling

An equivalent frame modelling (EFM) has been made. The 3Muri program, which is the commercial version of the Tremuri [16, 17] code, has been used. The software discretizes the walls into piers, spandrels and rigid nodes. A bi-linear constitutive law coherent with the Italian National Code prescription is adopted. For the RC elements, it considers beams with lumped plasticity. The obtained structural model is shown in Fig. 5.

3.1 Modelling Calibration and Linear Dynamic Analysis

The dynamic identification is an effective tool for the modeling calibration. The calibration of the model requires several assumptions, regarding the elastic modulus of the adopted materials, the stiffness of the diaphragms and the considered boundary conditions. In the definition of mechanical characteristics of materials and the boundary conditions several uncertainties are involved; in particular, a qualitative assessment of the strengthening interventions occurred in the past years is quite difficult to make, and several values could be assumed for the mechanical properties of the single components introduced in the model.

Two different models have been considered, i.e. *M#1* and *M#2* (Table 2). In *M#1* the building has been considered without any boundary condition along the external walls. In *M#2*, instead, proper boundary conditions have been considered to account

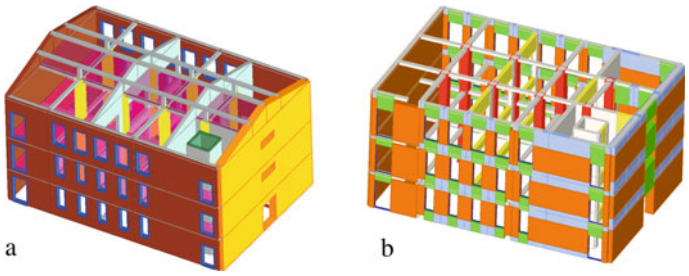

Fig. 5 The structural model of the studied building; **a** the 3Muri Model; **b** the discretized form in piers, spandrels, rigid nodes and RC elements

for the adjacent buildings; namely, the perimetral walls of the structure have be assumed to be blocked by the adjacent constructions, through the introduction of carriages with an infinite stiffness, which avoid the displacement orthogonal to the wall planes. Therefore, the two models represent the limit conditions (free and fixed) for the external walls' behavior. The other difference presented between M#1 and M#2 is that in the second model the Elastic Modulus of the materials has been reduced for the 50% according with the codes and which correspond to estimate a "cracked configuration" of the masonry.

In this work, the mechanical properties of the materials, listed in Table 1, have been assumed on the basis of the standard values provided by the current Italian Technical Code NTC 2018 [18] (Table 1). The considered values follow the codes recommendation for the assumed *KL*, adopting the *mean* value of the range provided by the Code for the density (ρ) and the Elastic Moduli E and G, and the *minimum* values for Compressive strength (f_m) and Shear resistance (τ_0). Two different masonry typologies have been identified, clay brick masonry and stone masonry; then, based on the strengthening intervention occurred, the typologies have been split assuming four different mechanical characteristics. The mechanical properties of both the masonries have been differently increased to account for the strengthening intervention made in the past years. The values assumed for these mechanical quantities can be found in Table 1.

For the clay bricks masonry, two different types of modeling have been considered (type A and B). In both the clay bricks typologies a reinforced plaster has been added together with the assumption of a good quality mortar; moreover, in the typology B, the presence of thin joints has been taken in account. The reinforced plaster and the good quality mortar have been considered also for the stone masonry and the pillars, which are still made of stones. Moreover, in the pillars, coherently with the

Table 1 Mechanical properties of the masonry presented in the models

Quantity	Unit	Clay bricks reinf. *A*	Clay bricks reinf. *B*	Stone masonry reinforced	Stone masonry Pillars
f_m	MPa	5.40	8.10	5.07	5.85
τ_0	MPa	0.135	0.168	0.109	0.126
E	MPa	3375	5062	3393	3915
G	MPa	1125	1687	1131	1305
ρ	KN/m^3	18	18	21	21

Table 2 Main assumptions made for the two models

Model	Mechanical properties		Boundary conditions
	Elastic modulus	Masonry description	
Model #1	$E_{cracked} = E_{uncracked}$	"Uniform"	Free
Model #2	$E_{cracked} = 50\%\ E_{uncracked}$	"Differentiated"	Fixed

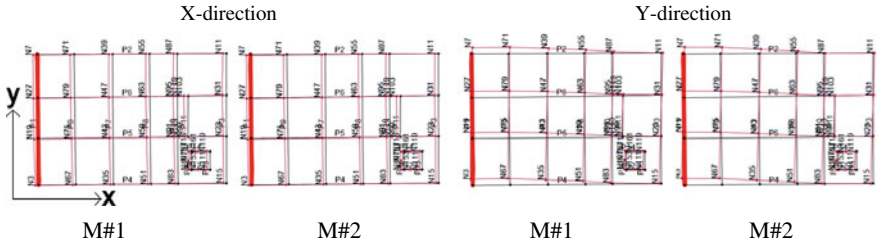

Fig. 6 Deformation shapes of the two first modes for the two considered structural models

strengthening documentations, a binder injection has been added. For the considered materials, the final increment coefficients have been assumed equal to 2.25, 3.375, 1.95 and 2.25, respectively. For the RC elements, a Concrete C20/25 with B450 steel bars has been considered.

For the mesh discretization, concerning the coupling between spandrels and RC elements such as the perimetral ring beam, a deformable portion of 50% of the total length of the elements has been adopted. A linear dynamic analysis has been performed. Concerning the first modes in the two directions, both the numerical results present a good match with the values obtained from the experimental campaign. The difference is presented in percentage through:

$$1 - \frac{Frequency_{\text{exp}}}{Frequency_{an}} \tag{1}$$

where at the numerator there is the frequency provided by the experimental campaign and at the denominator there is the analytical frequency of the 3Muri models. For M#1 a difference of 3.8% in X direction and -0.47% in Y direction is found, while M#2 shows a difference of 8.77% in the X and 1.77% in the Y direction.

Finally, in terms of deformation, the results provided by the modal analysis show a good correspondence between the results of the two numerical models and of the analysis on the experimental data. Specifically, in the Y direction there is some torsional effect that allows an irregular deformed shape. As known, The execution of an the experimental campaign allows only few control points of the structures, while the selected modal shapes highlight how some internal parts (such as the vaults structures) appear more sensitive to irregular displacements (Fig. 6).

3.2 Seismic Analysis

Finally, in order to assess the seismic performances of the building, a pushover analysis has been performed. Two different load patterns have been considered: one proportional to the mass (uniform pattern) and one with the inverse triangular trend.

The results have been expressed in terms of capacity curves and seismic performances. The N2 Method [19] has been adopted, by assuming a soil type B and a return period of 712 years for the *Life Safety* Limit State (*SLV*). Two different Limit States have been considered, i.e. the *Damage* (SLD) and the *Life Safety* (SLV) limit states. In Fig. 7 the bilinear capacity curves of the two models are shown. As it can be seen, M#2 exhibits a higher capacity especially in the *Y* direction. This result is certainly related to the boundary conditions applied to the structure, since the presence of the hinges prevents displacements (and deformations) along the considered direction. It is worth noting that the M#2 is characterized by a cracked configuration of the masonries, while in M#1 the masonries have been taken with their full stiffness.

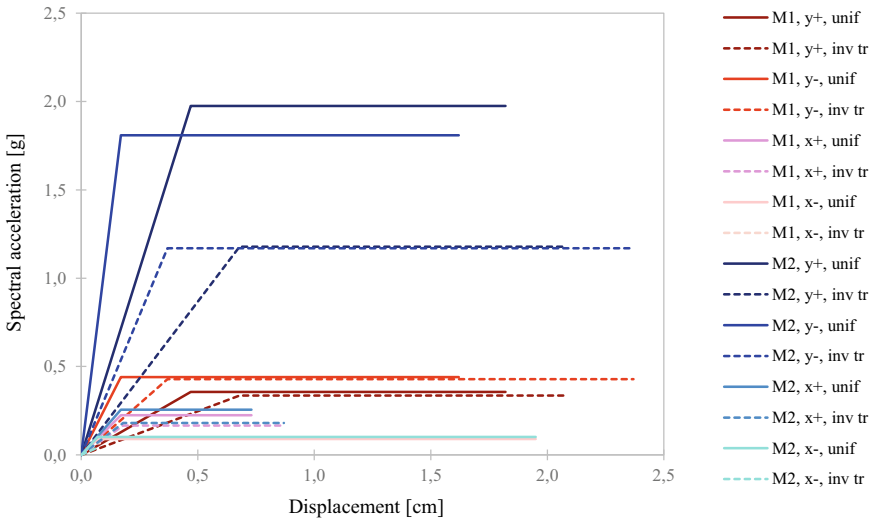

Fig. 7 Bilinear capacity curves for the two structural models along the two directions

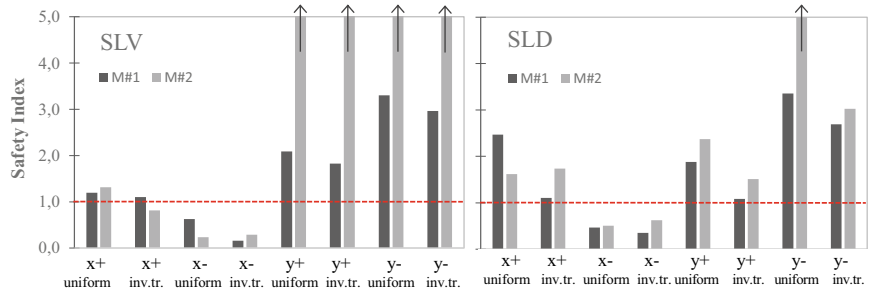

Fig. 8 Safety Index comparison between the two models for the two considered limit states

Finally, a comparison in terms of Safety Index is presented in Fig. 8. The Safety Index is computed as the ratio between the acceleration for the attainment of a specific limit state (Capacity) and the site acceleration with a 712 years return period and soil typology B (Demand). For the seismic verification, the Index is verified for values greater than 1. As for the capacity curves, the graphics evidence higher performances of M#2, especially in *Y* direction. Both the structural models highlight a good response in *Y* direction, which is offered from the RC elements along this direction. On the other side, in *X* direction, the resistance mass is not so relevant. In this case it is worth noting the influence of the analysis'direction, since the boundary conditions are able to "sustain" the structure against their action.

4 Conclusions

In this paper the dynamic identification and the structural behavior of an irregular school building have been presented. The building consists of a regular structure which has been altered during the years through interventions which introduced a structural irregularity. Moreover, the presence of adjacent buildings, and their consequent interaction, increases the number of uncertainties of the assessment and their contribution. The knowledge path recommended by the Italian standards has been applied and the structural model has been set. A dynamic identification of the structure through the use of triaxial seismometers has been performed. The results show a predominant irregular deformation along the *Y* direction, corresponding to the main frequency of the building. In absence of destructive campaign, the dynamic response of the structure has been used to check the suitability of the assumptions made for representing the mechanical properties of the materials. Namely, since the effective behavior of the masonry walls of the building could not be exactly known, two different level of confinement have been assumed for the masonry. As a consequence, two equivalent frame models have been produced, which differ for their boundary conditions and mechanical characteristics. The modal behavior provided by the two models has been compared to the one found through the identification analysis; the comparison evidenced that both the models provided a modal response close to the one found the experimental data.

Finally the two models have been adopted to predict the inelastic behavior of the building; to this purpose, a non-linear static analysis has been performed. The results show how the modeling approach can produce different results in terms of seismic assessment. Indeed, the analysis is very sensitive to the boundary conditions of the structure. In particular, along the *Y* direction there are differences (in terms of safety index) ranging between 1 to 5. In conclusion, taking into account the discussed uncertainties, the obtained results lead to assess the general capacity of the building and its vulnerabilities. This study points out the role of the irregularity in masonry-mixed structures through the detection by dynamic identification. Further analysis will be needed, in order to characterize the mechanical properties of materials through destructive tests and reduce the amount of uncertainties. In-depth studies concerning

the role of the adjacent buildings are recommended. Their investigation may pass through the assess of additional modeling approaches such as yielding boundaries to simulate the interaction of the buildings, or modeling the portions of adjacent structures.

References

1. Cristofaro MT, Tanganelli M, Viti S (2020) New predictive models to evaluate concrete compressive strength using the SonReb method. J Build Eng 27(2020):100962
2. Maio R, Santos C, Ferreira TM, Vicente R (2018) Investigation techniques for the seismic response assessment of buildings located in historical centers. Int J Arch Herit 1–14. https://doi.org/10.1080/15583058.2018.1503363
3. Morandi P, Magenes G, Albanesi L (2012) Mechanical characterization of diferent typologies of masonry made with thin shell/web clay units. In: Proceeding of the 12th Canadian masonry symposium
4. De Stefano M, Tanganelli M, Viti S (2015). Seismic performance sensitivity to concrete strength variability: a case-study. EarthqS Struct 9:321–337, ISSN:2092–7614
5. Vignoli A, Boschi S, Modena C, Cescatti E (2016) In-situ mechanical characterization of existing masonry typologies: a research project in Italy fnalized to update the structural codes. In: Proceedings of XVI international brick and block masonry conference 27–29 Giugno 2016, Padova, Italia, pp. 1983–1991.ISBN: 978–1–138–02999–6
6. Milosevic J, Cattari S, Bento R (2018) Sensitivity analysis of the seismic performance of ancient mixed masonry-RC buildings in Lisbon. Int J Mason Res Innov 3(2):108–154
7. Bindi D, Petrovic B, Karapetrou S et al (2015) Seismic response of an 8-story RC-building from ambient vibration analysis. Bull Earthquake Eng 13:2095–2120. https://doi.org/10.1007/s10518-014-9713-yG
8. Fabbrocino C Rainieri, Verderame GM (2007) L'analisi dinamica sperimentale e il monitoraggio delle strutture esistenti. In: Controllo e monitoraggio di edifici in calcestruzzo armato: il caso-studio di Punta Perotti Giornata di Studio ENEA.
9. Gentile C, Saisi A (2007) Ambient vibration testing of historic masonry towers for structural identification and damage assessment. Constr Build Mater 21(6):1311–1321
10. Brownjohn JMW (2003) Ambient vibration studies for system identification of tall buildings. Earthq Eng Struct Dyn 32:71–95
11. Ventura C, Liam Finn W-D, Lord JF, Fujita N (2003) Dynamic characteristics of a base isolated building from ambient vibration measurement and low level earthquake shaking. Soil Dyn Earthq Eng 23:313–322
12. D'Ambrisi A, Mariani V, Mezzi M (2012) Seismic assessment of a historical masonry tower with nonlinear static and dynamic analyses tuned on ambient vibration tests. Eng Struct 36:210–219
13. Azzara RM, Girardi M, Padovani C, Pellegrini D (2019) Experimental and numerical investigations on the seismic behaviour of the San Frediano bell tower in Lucca. Ann Geophys 61 2018. doi.org/https://doi.org/10.4401/ag-8025
14. Azzara RM, De Falco A, Girardi M, Pellegrini D (2017) (2017) Ambient vibration recording on the Maddalena bridge in Borgo a Mozzano (Italy): data analysis. Ann Geophys 60(4):S0441. https://doi.org/10.4401/ag-7159
15. Baraccani S, Palermo M, Azzara RM, Gasparini G, Silvestri S, Trombetti T (2017) Structural interpretation of data from static and dynamic structural health monitoring of monumental buildings. Key Eng Mater 747:431–439
16. Lagomarsino S, Penna A, Galasco A, Cattari S (2013) TREMURI program: an equivalent frame model for the nonlinear seismic analysis of masonry buildings. Eng Struct 56:1787–2179

17. Penna A, Lagomarsino S, Galasco A (2014) A nonlinear macroelement model for the seismic analysis of masonry buildings. Earthq Eng Struct Dynam 43(2):159–179
18. NTC (2018) Aggiornamento delle «Norme tecniche per le costruzioni». GU. No. 42 del 20 Febbraio DM Ministero Infrastrutture e Trasporti 17 gennaio 2018, Roma (in Italian). NTC (2008) Norme tecniche per le costruzioni. DM. ministero infrastrutture e Trasporti 14 gennaio 2008, GURI. 4 febbraio 2008, Roma, 2018. (in Italian)
19. Fajfar P (1999) Capacity spectrum method based on inelastic demand spectra. Earthq Eng Struct Dyn 28:979–993

Influence of Plan Irregularity in the Seismic Vulnerability Assessment of Existing Unreinforced Masonry Buildings with RC Slabs

Vieri Cardinali, Marco Tanganelli, Mario De Stefano, and Rita Bento

1 Introduction

In civil engineering, irregularity can highly affect the seismic performance of structures. The irregularity may regard both the structural organization and the non-structural one, involving alterations that may portend to torsional effects and non-uniform behaviors. The role of irregularity has been particularly investigated during the last years by the scientific community, introducing rules in national and international codes [1, 2]; the topics regard both the comprehension of the structural behavior of irregular structures, both the reliability of existing procedures for their seismic assessment [3–6]. While nowadays the regimentations have been improved specifically regarding the design of new structures, most of the problems are referred to the existing buildings. Concerning the masonry and the mixed masonry-RC buildings, the lack of versatility of such type of structures reduces the problems that may be found in RC or steel structures. By the way, their intrinsic relationship between structural organism and architectonical design makes masonry and mixed buildings particularly vulnerable because of the contribution of irregularity. This paper aims to

V. Cardinali (✉) · M. Tanganelli · M. De Stefano
Department of Architecture, University of Florence, Piazza Brunelleschi n. 6, 50121 Florence, Italy
e-mail: vieri.cardinali@unifi.it

M. Tanganelli
e-mail: marco.tanganelli@unifi.it

M. De Stefano
e-mail: mario.destefano@unifi.it

R. Bento
CERIS Instituto Superior Técnico, University of Lisbon, Av. Rovisco Pais, 1049-001 Lisbon, Portugal
e-mail: rita.bento@tecnico.ulisboa.pt

R. Bento et al. (eds.), *Seismic Behaviour and Design of Irregular and Complex Civil Structures IV*, Geotechnical, Geological and Earthquake Engineering 50,
https://doi.org/10.1007/978-3-030-83221-6_20

investigate the role of irregularity in masonry buildings with RC slabs. Such category refers to modern not-historical structures built during the XXth century. A relevant part of the Italian (and European) urban stock has been built in this period through the use of masonry walls as an alternative to the more modern reinforce concrete. Moreover, even if the design of the urban stock during this period was pretty standardized and uniformed through the use of few schemes and typological plans, most part of this urban stock was built in the absence of seismic codes. Because of their technological characteristics, the behavior of those buildings under seismic loads is not ascribable to the one of the historical constructions. In fact, they generally present a global box-behavior where the in-plane capacity is mostly driven by the shear capacity of the walls. In order to assess the role of irregularity for what concerns the masonry buildings with RC slabs, two existing case-studies settled in Florence have been selected as benchmarks. The case studies have been built after the 2nd World War (WWII) in two different external districts. Complexly, 27 buildings have been made just using two different plan configurations. They consist in a scattered linear aggregation of regular block-type based on central stairs and two apartments for each floor. Even if the original block-design is completely regular, the aggregation proposed makes the final buildings affected by a plan irregularity.

2 The Case-Studies

2.1 Architectonical and Structural Design

The two selected districts are residential settlements realized during the 50's in external areas around Florence: the Galluzzo area, on the southern hills surrounding the city and in Via della Casella, located at the extreme western territory of the municipality. The two interventions are part of the national program INA-Casa promoted by the National Government after the WWII in order to provide houses for the population [7]. The stocks have been built following the same building typologies, attributable to two standard models (Type A and Type B). Both the benchmarks are based on the duplication of regular building characterized by a central stair and serving two apartments for floor. The two typologies differ for the dimensions of the residential units (60 sqm Type A, 45 sqm Type B) and for the aggregation in which they are composed. Indeed, Type A presents a scattered linear combination of only two units, while the Type B is obtained by three scattered units. The planimetries of the interventions are shown in Fig. 1. While the Galluzzo buildings have conserved their geometry, in the Casella area some interventions occurred over the years. Specifically, around the 80's the apartments at the ground levels have been replaced by garages for the upper units (Fig. 1).

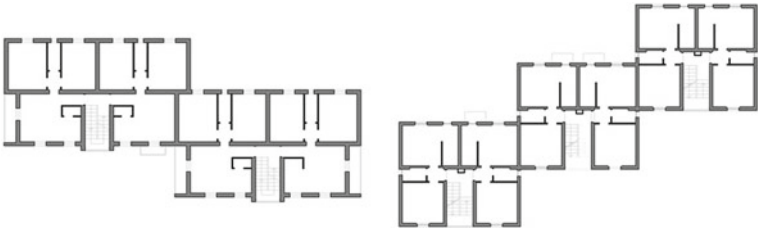

Fig. 1 Plan configuration for the two typologies presented; type A (on the left) and type B (on the right)

2.2 Investigation Campaign and Mechanical Characteristics

The knowledge path recommended by the Italian Standards [8] has been applied. Starting from an archive and historical research, a detailed investigation campaign has been carried out. Specifically, it started with non-destructive tests like thermography campaigns performed over all the building. The removal of the plaster layers verified the accuracy of the evidence of thermography. Over the visible masonries, penetrometric tests in order to check the resistance of the mortars have been made; for the masonries, in-situ flat-jack tests have been performed, while some resistant element has been removed in order to perform compressive crushing tests in the laboratory. Ambient vibration tests over the two buildings typologies have been performed in order to match the global behavior of the structural models with the real modes of the residential complexes. A more accurate description of the tests performed can be found in [9].

The buildings consist of three floors. The bearing walls have a thickness of 26 cm; the structure of the first two levels is made by semi-hollow concrete blocks (55 × 40 × 25 cm) while the third level is composed by hollow-clay blocks (26 × 26 × 13 cm) disposed with the internal cavities in a horizontal way. A perimetral concrete ring beam (16 × 16 cm) guarantee at each level the box-behavior; it is connected to the slabs made by RC beams alternated by hollow clay elements and topped by a RC screed. The only difference is presented at the top level where the ceiling is realized through RC prefabricated beam (*Varese* joist) connected with hollow flat tiles. The roofs are built in the same way by Varese joists. In Type A, the terrace walls are realized using a clay brick masonry wall. In Table 1 are shown the main mechanical characteristics associated with the masonries of the buildings after the campaign performed. The values are coherent with the mechanical characteristics shown in Table C8A.2.1 of [10] for the same typology classifications.

Table 1 Property table of the materials adopted and obtained

		Clay bricks	Concrete blocks	Hollow blocks
Compressive strength	f_m [MPa]	2.4	4.4	3.0
Shear resistance	τ_0 [MPa]	0.06	0.24	0.10
Young's modulus	E [MPa]	1500	2960	3150
Shear modulus	G [MPa]	500	987	1050
Specific weight	ρ [KN/m^3]	18	14	12

3 Structural Modelling and Seismic Analyses

In order to assess the influence of the plan irregularity in the seismic performance of the buildings, three different configurations for each typology have been considered. Starting from the original Single-Unit configuration, that represents a regular symmetric building, it has been combined in a linear way and finally in a scattered way. It is worth noting as the first benchmark just represent the original cell which the buildings are composed and analyzed as independent. The second cases (Double Unit and Triple Unit) represent linear aggregations of the elementary cell along the main façades (X direction). Finally, the third case is the real existing case studies (Type A and B). In Fig. 2, the concept of the presented study is showed.

3.1 Equivalent Frame Modelling

The modelling discretization has been made through an equivalent frame (EF) approach. The scientific community has widely used EF models for their reliability and less computational demand. To this aim, the Tremuri program [11, 12], which is the scientific version of the commercial 3Muri developed by Stadata, has been adopted for the analyses. The structural models have been realized by different levels, defining the geometrical and the structural characteristics of the real buildings. As known, EF modelling is based on the evidences of damage patterns in masonry structures; discretizing the masonry panels into piers, spandrels and rigid nodes. The RC elements such as the ring beams are modelled through beam with

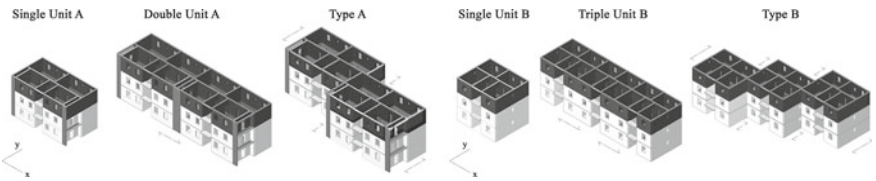

Fig. 2 The main phases of analyses performed; from the single-unit buildings to their linear aggregations, to the final type A and B through the scattered connections

lumped plasticity. For the masonry elements, a multilinear constitutive law with strength decay implemented in the software has been adopted [13]. Both for piers and spandrels different Damage Levels (DL1–*Slight Damage*; DL2–*Moderate Damage*; DL3–*Extensive Damage*; DL4–*Near Collapse*) have been associated with different values of drift in the panels.

3.2 Pushover Analysis

The influence of the seismic irregularity has been evaluated performing pushover (PO) analyses over the typologies showed before. Two different load patterns have been considered: one proportional to the mass and one following the inverse triangular pattern. In PO, the selection of a control node in the upper part of the building is needed. Usually, considering stiffness slabs in their plane, the selection of such control point is made between the central points of the building. In this study, for each building, different control nodes have been selected in order to assess how the duplication of the original cell (and the consequent movement of the control point) affects the results. By the way, the previous analyses showed how the presence of the ring beams with rigid slabs revealed that this selection was not relevant. The PO curves presented are referred to the mean displacement of the upset level in the models. Graphics in Fig. 3 have been plotted considering the displacement (d) over the height (h) of the models (abscissa) and the base shear (V) normalized by the weight (W) of the buildings (ordinate).

In both the case studies, the PO curves referred to the X and Y directions are significantly different. In X direction, the increase of resistant due by the doubling of the original cell makes the capacity of the structures increase so that the second configurations always present the highest values of V/W. This is clearer in Type B, where the Triple configuration increase the number of masonry walls in this direction. Finally, the realized ones (Type A and Type B) have the maximum V/W in an intermediate position between the original cell and the duplicate one. In Y direction, the results are more variable, depending on both on the verse of the analyses and on the load pattern. Especially in the case study A, the bearing walls in this direction present openings that generate small piers sensible to the pushing verse. However, some difference is involved. Because of the scattering presented in Y direction, the realized Type A and Type B have longer resistant walls in the considered direction. This is evident with the mass proportional load pattern in the Type A, while the inverse triangular load pattern highlights it in Type B.

The study aims to investigate not only the PO curves in themselves but also the performance points for the attainment of each limit state. The Performance Levels PL, so defined, are based on the damage levels (DL) of the structure. In this work, a multi-scale approach proposed by [14] has been adopted. It considers three different levels of interest, such as the global scale (defining thresholds over the PO curve), macroelement scale (involving the drift limits for macroelement walls) and element scale (considering the cumulative rate of damage in piers and spandrels).

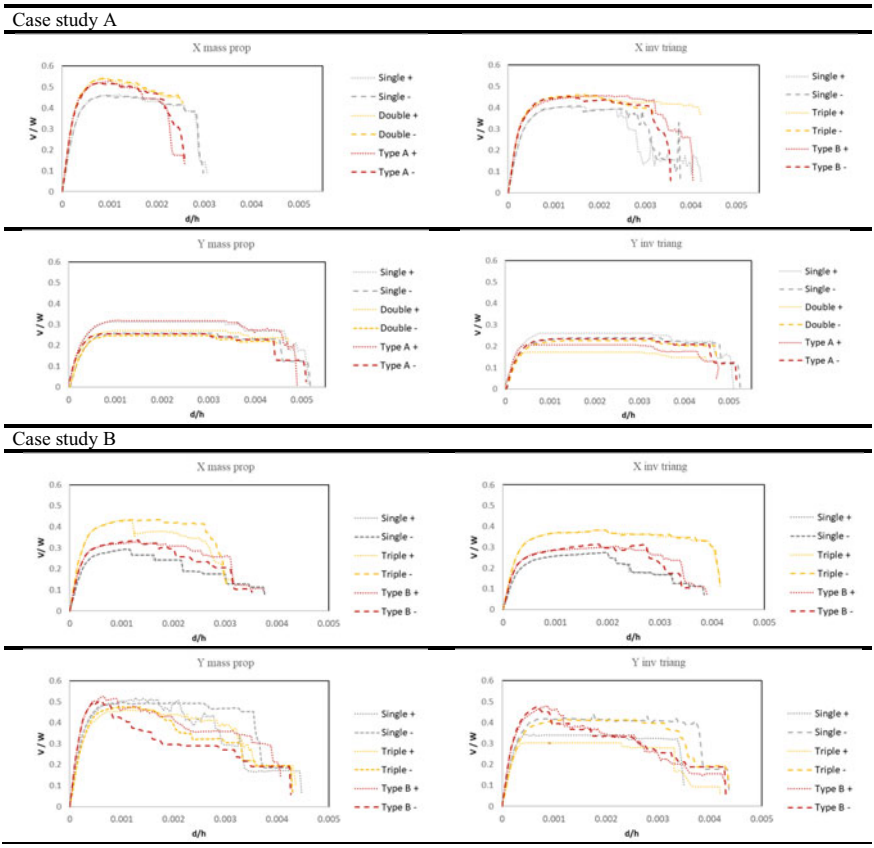

Fig. 3 Comparative PO curves for the real type A and B and their simplified configurations

The minimum attainment between the three criteria defines the performance point for the four damage levels previously described.

The PLs have been defined adopting the PGA as Intensity Measure IM by the Capacity Spectrum Method [15]. For the seismic demand, the seismic hazard of the city of Florence for a return period of 475 years has been considered, while for the soil classification, a soil of type B has been selected. The comparison, expressed in percentage, takes as reference the Single-Unit Case Study for both the typologies, which are considered representative of regular buildings. The difference is represented by:

$$\frac{IM_{x,DLi} - IM_{s,DLi}}{IM_{s,DLi}} \tag{1}$$

Table 2 Expressed percentage of the increment or decrement of PGA values for the case studies compared to the regular single unit case studies

X Direction				
[%]	DL1	DL2	DL3	DL4
Double	23.35	8.87	26.17	38.30
Type A	50.86	10.75	14.10	17.19
[%]	DL1	DL2	DL3	DL4
Triple	57.62	42.09	47.00	82.80
Type B	−6.81	7.64	14.75	47.71
Y Direction				
[%]	DL1	DL2	DL3	DL4
Double	−16.47	−21.05	−28.33	−18.47
Type A	−3.47	−14.52	−20.92	−13.78
[%]	DL1	DL2	DL3	DL4
Triple	53.60	−10.21	−13.40	−21.74
Type B	93.17	68.76	31.74	3.58

where $IM_{x,DLi}$ is referred to the Intensity Measure (PGA) of the generic model x, for the Damage Level *i*, while $IM_{s,DLi}$ is referred to the Single Unit Case Study *S*. In Table 2 the results for both the case studies are presented.

In X direction, for the attainment of the same PLs the results show relevant it is the addition of resistant wall with few openings, which brings to higher values of the PGA. By the way, because of the scattered in the Y direction and the related asymmetry, some negative contributions are presented; so, in terms of PGA the values for the final Type A and Type B are lower than the Double and Triple configurations. In Y direction, the results are slightly different. In fact, since the bearing walls are shared between different units, the linear addition of the cells is not directly correlated by an increase of the resistant in the same direction and the seismic performance of the Unit configurations are better than the Double and Triple ones.

Finally, the Type A and B, due to the scattered disposition, present an increment in the length of the resistant walls in Y directions, so, the final configurations highlight an increase in terms of PGA. In Fig. 4, a comparison in terms of capacity/demand ratio is shown.

3.3 Consideration of the Torsional Effects in Top Displacements

In order to analyze the torsional effects on the seismic performance of the three presented configurations, a comparison in terms of top displacement has been made. It considers the displacement of selected control nodes at the top of the buildings

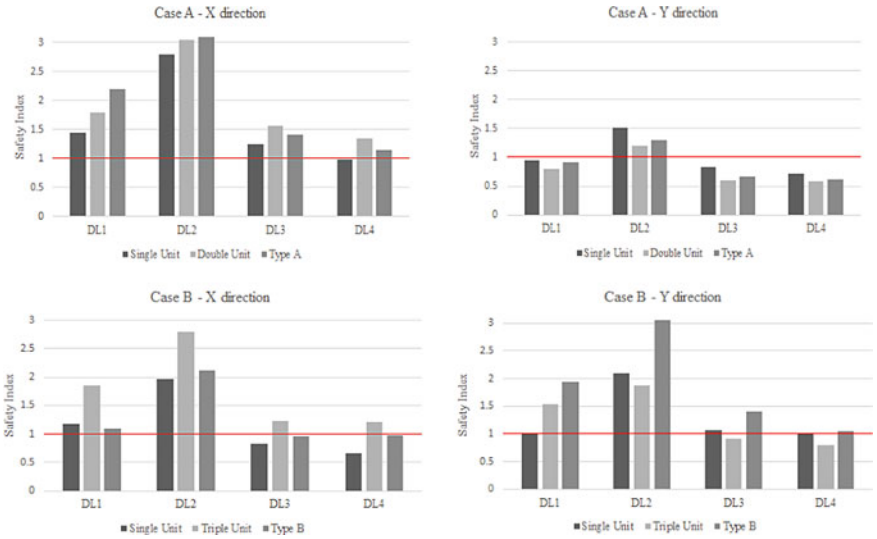

Fig. 4 Safety index for each damage level for the different benchmarks. the safety indexes over 1 are verified

referring to the lateral external walls and the central control point. The evaluation of the scattered in terms of displacement is expressed by:

$$1 - \frac{\mu_i}{\mu_X} \tag{2}$$

where μ_i is the displacement of a generic node i and μ_x is the displacement of the control node. For sake of brevity, the results, presented in Fig. 5 are shown only in the Y direction, referred to the mass proportional load pattern for the Type A and to the inverse triangular for Type B, which are the patterns highlighting the behavior of the structures. The benchmarks present a torsional-deformable behavior, where the central masses are more involved by the seismic actions. However, the differences between the perimetral nodes and the selected control points (which are in central positions) are below the 4% of the referred displacement. Concerning the final Types A and B, in the case of DL4 torsional-rigid effects are activated, with the rotation of the buildings around the central part. This is most apparent for the Type B because of the longitudinal length of the structure, where a maximum difference of 5.6% occurs.

Finally, a comparison in terms of damage pattern in the external walls of the buildings has been made. The Performance Points of the PO curves have been fitted by the performance of the Single Unit case studies. In Fig. 6, the Base-Shear/Displacement for the building Type B and for the correspondent external walls (Wall #1) in Y direction is presented, while the damage patterns are shown in Fig. 7. It is worth noting as the capacity of the walls in the real building present a previous decay so

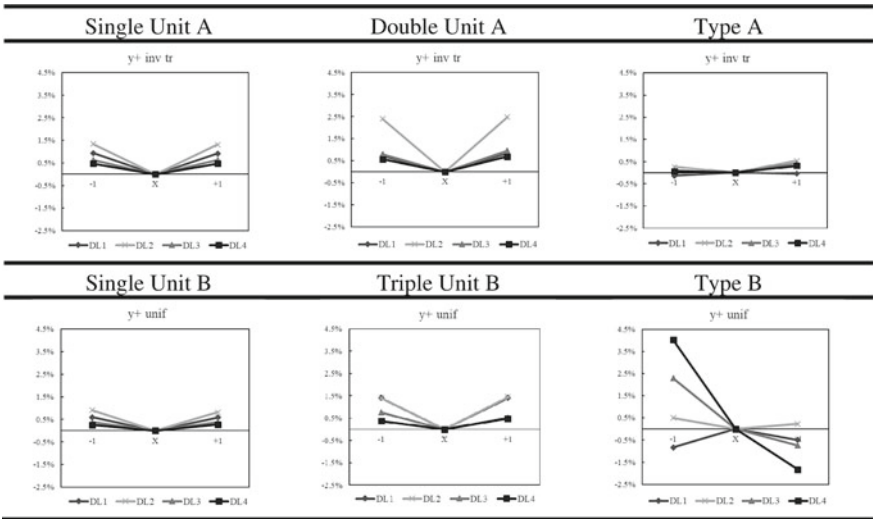

Fig. 5 Normalized top displacement of the nodes at the upset level of the structures; − 1: node on the external wall on the left; x: node on the central position; + 1: node on the external wall on the right

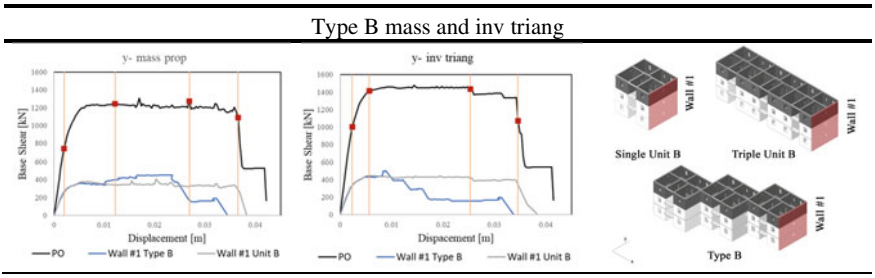

Fig. 6 PO curve of the single-unit B and base-shear displacement curves for the building and for the Wall #1 in the single unit case study B and in Type B. the vertical lines state the DLs of the single-unit benchmark

that, fitting the displacement of each PL, higher levels of damage occur. In particular, for DL1 and DL2 the damage patterns are the same, while, in Type B the damage levels increase for DL3 since the collapse of the walls before the attainment of the DL4 point for the Single Unit.

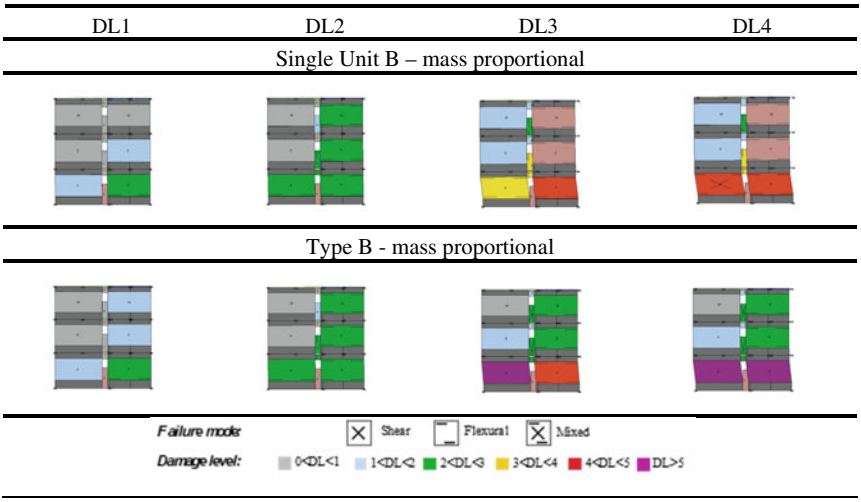

Fig. 7 Damage pattern comparison between the single unit B and the type B for the perimetral Wall 1 in Y direction for the two considered load patterns

4 Conclusions

In this paper, an assessment of the influence of plan irregularity in masonry buildings with RC slabs has been presented. Due to the presence of rigid slabs these buildings allow specific appraisals concerning the planar irregularity. In fact, differently from other buildings with no-rigid diaphragms, the occurring torsional phenomena can only be assured by the mass and stiffness distribution. To this aim, two projects settled in Florence have been selected as case studies. They consist of two different typologies used to build 27 different buildings. An accurate diagnostic campaign through both no-destructive and destructive tests has been performed, and the structural and mechanical characteristics have been defined. From the real typologies, six different benchmarks have been investigated. An EF discretization has been adopted, and non-linear static procedures have been selected to evaluate the performance of the buildings. Comparisons between the PO curves and the Performance Points for each LS have shown how the design influences the capacity of the buildings. Finally, the torsional effects have been assessed through the analyze of the distribution of top displacement in the plane and the damage pattern of the external walls. Complexly, the performance of the structures in the two directions is different; the increase of resistant generally leads to higher values of PGA to attain the same PLs. Some torsional phenomena occur, especially for DL3 and DL4, and the differences are shown in terms of Damage pattern. However, it is possible to assume that the structures express a uniform behavior; the plans studied have complex and irregular layouts but, for what concern the torsional effects and their amplitudes, torsional shapes are limited. Further analyses are expected; in-depth studies concerning the

role of eccentricity in the application of the load patterns are recommended, together with the use of other non-linear static procedures which consider high mode effects or/and non-linear dynamic analyses in order to check the reliability of the non-linear static procedure adopted in this research.

References

1. EN 1998–1 (2004) English: Eurocode 8: design of structures for earthquake resistance–part 1: general rules, seismic actions and rules for buildings. authority: the European Union per regulation 305/2011, directive 98/34/EC, directive 2004/18/EC
2. Agency FEM (2000) FEMA-356. Prestandard and Commentary for Seismic Rehabilitation of Buildings, Washington DC
3. De Stefano M, Pintucchi BL (2008) A review of research on seismic behaviour of irregular building structures since 2002. Bull Earthq Eng 6(2):285–308, ISSN:1570–761X
4. Lavan O, De Stefano M (2013) Seismic behaviour and design of irregular and complex civil structures. di AAVV, Springer, Berlin, pp. 1–374, 978–94–007–5376–1
5. Bhatt C, Bento R (2014) The extended adaptive capacity spectrum method for the seismic assessment of plan-asymmetric buildings. Earthq Spectra 30(2):683–703. https://doi.org/10.1193/022112eqs048m
6. Marino S, Cattari S, Lagomarsino S (2019) Are the nonlinear static procedures feasible for the seismic assessment of irregular existing masonry buildings? Eng Struct 2001 Dec 2019
7. Cardinali V, Viti S, Tanganelli M (2019) Seismic vulnerability of the residential buildings of Florence. In: COMPDYN 2019 7th ECCOMAS thematic conference on computational methods in structural dynamics and earthquake engineering Papadrakakis M, Fragiadakis M (eds). Crete, Greece, 24–26 June 2019
8. NTC (2018) Italian code for structural design (Norme Tecniche per le Costruzioni–NTC) DM. 14/1/2008, Official Bulletin N° 29 of Feb 4, 2008 (in Italian)
9. Palermo O, Cardinali V, Azzara MR, Tanganelli M (2019) Seismic assessment of public housing interventions: two INA-CASA settlements in Florence, VII Convegno Internazionale ReUSO Matera, 23–26 Ottobre 2019 (in Italian)
10. MIT I (2009) Instructions for the application of the Italian code for structural design (Norme Tecniche per le Costruzioni–NTC) DM. 14/1/2008, Ministero delle Infrastrutture e dei Trasporti (MIT), Roma (In Italian)
11. Lagomarsino S, Penna A, Galasco A, Cattari S (2013) TREMURI program: an equivalent frame model for the nonlinear seismic analysis of masonry buildings. Eng Struct 56:1787–2179
12. Penna A, Lagomarsino S, Galasco A (2014) A nonlinear macroelement model for the seismic analysis of masonry buildings. Earthq Eng Struct Dynam 43(2):159–179
13. Cattari S, Lagomarsino S (2013) Masonry structures. pp.151–200. in Sullivan T, Calvi GM (eds): developments in the field of displacement based seismic assessment, IUSS Press, (PAVIA) and EUCENTRE, p. 524, ISBN: 978–88–6198–090–7
14. Lagomarsino S, Cattari S (2015) Seismic performance of historical masonry structures through pushover and nonlinear dynamic analyses. In: Perspectives on European earthquake engineering and seismology, Springer, p 265–292
15. Freeman SA (1998) The capacity spectrum method ASA tool for seismic design. In: Proceedings of 11th European conference of earthquake engineering, Paris, France

Multidirectional Lateral Loads and Combination Rules in Pushover Analysis

Cristina Cantagallo, Francesco A. Pellegrini, Enrico Spacone, and Guido Camata

1 Introduction

When seismic loads are applied on a structure, the randomness of the seismic phenomenon in space must be taken into account, as it is not possible to know a priori the position of the earthquake epicenter and therefore the direction from which the earthquake propagates towards the structure. The generic response, R, in a point of a structure varies with the angle of incidence of the earthquake, which is defined by the position of the epicenter and the orientation of the structure. Since the position of the epicenter of far source seismic events is not generally known, the angle of incidence θ is not known and the direction generating the maximum structural response (i.e. the critical response) could vary between 0° and 360° [1].

In order to compute a structural response that take into account for the multi-directionality of the seismic load, various researchers proposed to combine the structural demands obtained by applying the response spectrum analysis simultaneously in the two principal structural directions. More specifically, [2] stated that the total quadratic response r^2 of n seismic components acting simultaneously can be estimated by adding the quadratic responses ${r_k}^2$ to each seismic component k ($k = 1; n$). This formulation is called the Square-Root-of-the-Sum-of-the-Squares (SRSS) rule and it arises simply from the supposition that each component is a Gaussian stochastic process. The first application of this rule in seismic engineering is due to Goodman

C. Cantagallo (✉) · F. A. Pellegrini · E. Spacone · G. Camata
Department of Engineering and Geology (INGEO), University "G. D'Annunzio" of Chieti-Pescara, viale Pindaro, 42, 65127 Pescara, Italy
e-mail: cristina.cantagallo@unich.it

E. Spacone
e-mail: espacone@unich.it

G. Camata
e-mail: guido.camata@unich.it

R. Bento et al. (eds.), *Seismic Behaviour and Design of Irregular and Complex Civil Structures IV*, Geotechnical, Geological and Earthquake Engineering 50,
https://doi.org/10.1007/978-3-030-83221-6_21

et al. [3] for combining the contributions of vibration modes in the Response Spectrum Method when the modes are well separated. Subsequently, [4, 5] formulated the Complete Quadratic Combination (CQC) rule, applied for closely-spaced modes. Further considerations about the application of the multicomponent earthquake excitation in linear analysis were performed by Wilson et al. [6] and Newmark [7]. They proposed the Percentage Rule, which approximates the multicomponent response as the sum of the 100% of the response resulting from one component and a percentage λ of the responses resulting from the other components. More specifically, [6, 7] suggested λ to be 40% and 30%, respectively. More recently, [8] concluded that the Percentage Rule could underestimate the design forces in certain members. Smeby and Der Kiureghian [9] proposed an extension of the CQC rule, known as the CQC3 rule, to combine modal responses due to the three seismic components. Subsequently, as [2], also [10] proposed a response spectrum rule for combining the contributions from three orthogonal components of ground motion. This rule, denoted as CQC3, determines the generical response quantity in function of the seismic orientation angle θ, taking into account for the correlation between individual seismic components. Moreover, CQC3 is able to identify the most critical orientation of the ground motion components for each response quantity of interest obtained in linear range. It can be considered the most general case of the 30, 40% and SRSS rules [11, 12]. Camata et al. [13] reveled that that the structural responses obtained by the application of the SRSS rule provides values always greater than the CQC3 critical response. Moreover, they showed that the 30% rule can underestimate the response obtained applying the SRSS rule up to 9%.

In order to consider multidirectional (orthogonal) excitation effects in the linear field, most current seismic codes require the use of the SRSS rule and alternatively the application of the 30% rule [14]. Other codes indicate as primary choice the use of the 30% rule, indicating as an alternative the SRSS rule [15]. Furthermore, some standards indicate only the possibility of using the 30% rule [16–18]. Despite these two rules were originally formulated for linear structural responses, the current regulatory codes prescribe their application also for Non-Linear Static (pushover) Analyses (NLSAs). In order to investigate the validity of these directional combination rules in NLSA, the pushover analyses of three irregular reinforced concrete structures are performed and the corresponding capacity curves are obtained in their structural direction $\pm x$ and $\pm y$. Subsequently, for each considered orthogonal direction the structural demand is calculated using the N2 method [19]. The obtained results are then combined using the 30% and the SRSS combination rules. Moreover, other pushover analyses are performed rotating the pushover seismic force with incident angles θ_i and the corresponding structural demands with the N_2 method are calculated. Finally, the structural demands obtained from the different NLSAs are compared with those computed by Non-Linear Time History Analyses (NLTHA) performed by using suites of real and generated ground motion records.

2 Application of the Combination Rules in Non-linear Static Analyses

EC8-Part 1 states that when a NLSA is used applying a spatial model, the SRSS or 30% combination rules should be applied. Equations 1 and 2 indicates the formulation of these two rules taking into account for the signs of the structural responses.

$$R_{SRSS} = \sqrt{\left|E_{Edx}^2\right| + \left|E_{Edy}^2\right|} \tag{1}$$

$$R_{30\%} = max\left\{\left(\pm E_{Edx} \pm 0.3E_{Edy}\right); \left(\pm 0.3E_{Edx} \pm E_{Edy}\right)\right\} \tag{2}$$

E_{Edx} and E_{Edy} represent the forces and deformations due to the application of the target displacement in the x and y directions, respectively.

Although there are many studies in the literature on the application of pushover analysis on irregular 3D structures subjected to bidirectional ground motions (for example, [20–23]), few authors apply the combination rules to NLSA. Magliulo et al. [24] apply the pushover analysis with the N2 method to plan irregular buildings considering accidental eccentricity. They propose different procedures where the SRSS rule is applies to the results of NLSA. Reyes and Chopra [25] use 3D modal pushover analysis calculating the total dynamic response for each ground motion component, r_x and r_y, with the CQC modal combination. The SRSS combination rule is then applied to the responses r_x and r_y so calculated. Cimellaro et al. [26] recommended a 100–60% rule for NLSA after having applied the pushover forces simultaneously in the two main structural directions.

In the current work, for each considered structure, four NLSA are performed in the main structural directions $\pm x$ and $\pm y$, obtaining for each direction the corresponding base shear—top displacement pushover curves. Subsequently, the structural demands are calculated according to the N2 method and the EC8—Part 1. The EDPs evaluated in this work, i.e. the inter-story drift and the shear in the columns, are obtained in the structural direction $\pm x$ and $\pm y$ at the steps corresponding to the structural demands. They are combined according to the SRSS and 30% combination rules shown in Eq. 1 and Eq. 2, respectively.

3 Case Studies

Three irregular reinforced concrete structures (referred to as Structure 1, Structure 2, Structure 3) are selected according to their structural configuration (Fig. 1). They have increasing plan irregularity and complexity. The non-linear analyses are carried out with the computer software Opensees [27] using the pre- and post- processor STKO [28]. Force-based fiber-section frame model [29] with five Gauss–Lobatto integration points are used both for beams and columns. The shear stiffness is added

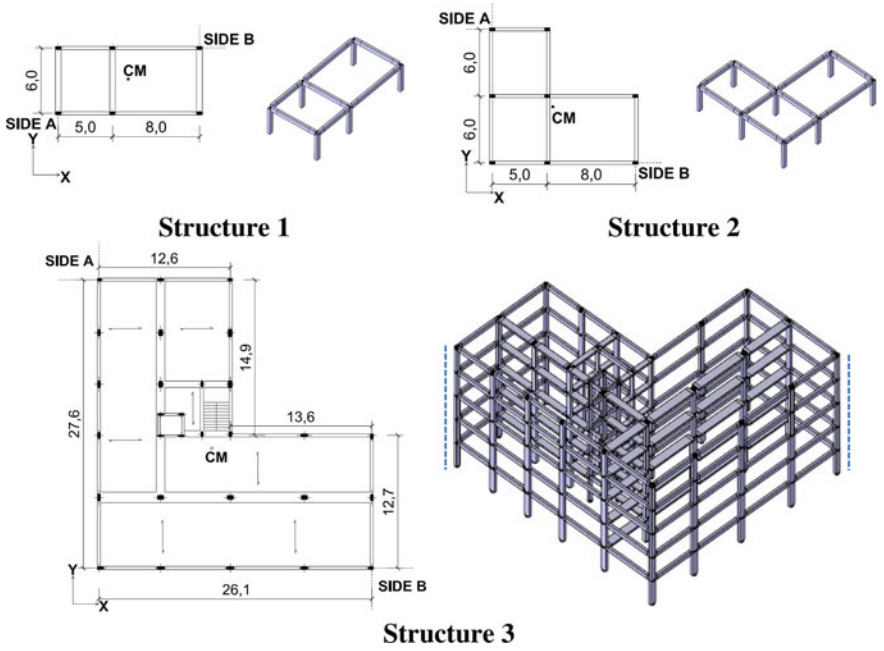

Fig. 1 Structural models of the three analysed structures

to the section behavior using the OpenSees section aggregator command. Rigid diaphragms are used at all floor levels. The concrete is modeled with the Kent-Scott-Park constitutive law [30] with $f_c = 20$ MPa and strain at maximum compressive strength $\varepsilon_{c0} = 0.002$. The Giuffré-Menegotto-Pinto constitutive law [31] is used for the reinforcing steel, with $f_y = 400$ MPa, E = 210 GPa and strain hardening ratio $b = 0.02$. Gravity loads are applied statically before the non-linear analyses. Floor masses include all dead loads and 30% of live loads according to EC8-Part1.

Structure 1 and Structure 2 are torsionally deformable 1-storey plan irregular frames having height equal to 3.32 m. Beam and column cross sections of both buildings are 30 × 50 cm. Structure 3 is an irregular realistic structure designed in the 1970s having different cross sections, including flat beams and columns with very reduced size in one direction (ex. 20 × 60, 20 × 50). The main modeling features and the dynamic properties of the three analyzed RC frame structures are briefly summarized in Fig. 1 and Table 1, respectively.

Table 1 Elastic periods and mass participation ratios obtained from the modal analyses of the three considered structures

	Structure 1				Structure 2				Structure 3			
Mode no.	T_i (s)	m_x (%)	m_y (%)	m_z (%)	T_i (s)	m_x (%)	m_y (%)	m_z (%)	T_i (s)	m_x (%)	m_y (%)	m_z (%)
1	0.32	0	98.3	1.7	0.35	0	99.9	0	1.12	30.6	30.7	16.7
2	0.25	0	1.7	98.3	0.26	5.50	0.1	94.4	1.06	44.1	32.2	1.8
3	0.21	100	0	0	0.24	94.5	0	5.5	0.88	3.2	15.6	60.2

4 Analysis and Discussion of Results

4.1 Non-linear Static Analyses

NLSAs are performed considering two invariant lateral load patterns: a mass proportional distribution and a load pattern proportional to the story forces calculated in a linear dynamic analysis, including a number of modes with a total mass participation of not less than 85%. As indicated in the Italian Building Code (NTC2018), this distribution must be applied if mass participation of the fundamental vibration mode in the considered direction is less than 75%. Clearly, for 1-storey structures, the two load patterns coincide. Each force distribution is applied on each considered structure according to the main structural axes x and y, with both positive and negative signs. Subsequently, the mass proportional force distribution is then applied along the directions θ_i from 0° to 360°, with steps of 22.5°. In this work, this procedure is called "multi-directional NLSA". For each direction and structure, the corresponding shear-displacement curve of the Multi Degree of Freedom (MDOF) system is obtained and then transformed into a bilinear elasto-perfectly plastic curve corresponding to an equivalent Single Degree of Freedom (SDOF) system. The structural demands are then calculated comparing the response spectrum of the considered site with the bilinear equivalent curve obtained considering a building lateral capacity until a 20% reduction of the maximum base shear.

4.2 Non-linear Time History Analyses

NLTHA of Structure 1 and Structure 2 are performed using 20 pairs of natural records. The reference site for the analyses is located on rock soil in L'Aquila (AQ-Italy)—42.350° latitude and 13.399° longitude. 55 unscaled ground motion records (each consisting of two orthogonal horizontal components) are pre-selected from two databases: Engineering Strong-motion Database ESM [32] and European Strong-motion Database ESD [33]. For each selected record and for each period T_i, a single spectral acceleration $S_a(T_i)$ is obtained as geometric mean of the two corresponding horizontal spectral components. As stated in Beyer and Bommer [34], the geometric mean is the most widely used definition of the horizontal component of motion. A single spectrum is therefore computed from the spectral values of the x and y components. The spectra corresponding to the un-scaled records are then scaled to the spectral acceleration $S_a(T^*)$ corresponding to the "non-linear period" T^*. As shown by a previous study [35], $S_a(T^*)$ produces the lowest variability in structural demand among the most common input intensity measures. It considers the elongation of the effective structural period during the non-linear analysis and is well correlated with the deformation demand. The "non-linear period" T^* is obtained from NLSAs carried out according to EC8-Part 1 in the direction of the first linear period T_1. A group of 20 pairs of scaled records is obtained from the pre-selected 55 ground

motion records so that in the 0.2 T^*–2 T^* spectrum-compatibility range, the mean elastic spectrum calculated from all time histories is within the 90–110% window of the uniform hazard spectrum. In order to reduce the influence due to the record selection, the NLTHAs of Structure 2 are performed with both natural and generated records. Seven pairs of ground motion records are generated using Simqke based on the approach proposed by Gasparini and Vanmarcke [36]. Because of its structural complexity, in order to reduce the variability of structural demand due to seismic input, NLTHAs on Structure 3 are performed by using seven pairs of generated records.

4.3 Results

Figure 2 shows the displacement demands obtained in the two main structural direction x and y for each considered structure. In Structure 1 the maximum non-linear

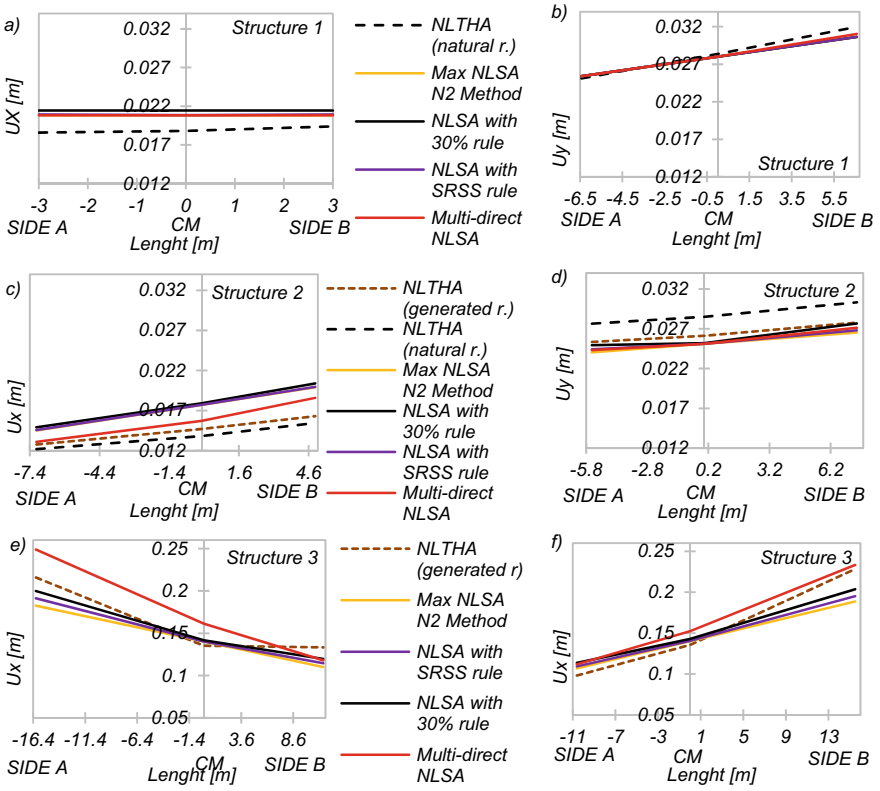

Fig. 2 Displacement demands obtained in the three analysed structures on the main structural axes x and y

static displacement obtained applying the $\pm x$ pushover forces are conservative with respect to the results of NLTHAs (Fig. 2a). The combination rules further increase this result up to a maximum of 11% with the 30% rule. In weak direction (Fig. 2b), all non-linear analyses generate similar displacements.

Figure 2c shows that the displacement demands obtained from all NLSAs in the strong structural direction of Structure 2 are greater—and therefore conservative -than the corresponding results of NLTHAs. Conversely, the pushover displacements on the weak direction (Fig. 2d) are lower than those calculated with NLTHAs performed with natural records probably due to the ground motion variability. The results provided by generated records are closer to those obtained from NLSAs.

Figure 2e and f show the absolute displacements on the top floor of Structure 3. More specifically, Fig. 2e shows that the displacement demands obtained from NLSAs provide in general unconservative displacements (except for multi-directional NLSAs, which produce conservative results on side A). In y direction, N2 structural demands with and without combination rules are conservative with respect to the results of NLTHAs only on side A, probably due to the strong torsion of the deck. By contrast, multi-directional NLSAs are in this case always conservative and very close to NLTHAs. All NLSAs of Fig. 2e and f refer to the mass proportional load pattern.

Figure 3 shows the ratios between the shear demands obtained from NLSAs and NLTHAs in the x and y structural directions. NLSAs are obtained considering a mass proportional load pattern and the corresponding shear demands are calculated according the following three different methods:

(a) maximum shear values obtained from the application of the N2 method in the $\pm x$ and $\pm y$ structural directions,
(b) application of the SRSS and 30% combination rules to the shear demands in the $\pm x$ and $\pm y$ structural directions and
(c) application of pushover forces at different incident angles θ_i and calculation of the maximum shear values obtained at each θ_i.

In Fig. 3, NLTHAs of Structure 1 and Structure 2 are both performed with 20 pairs of natural ground motion records. Conversely, the results of NLTHAs of Structure 3 are obtained considering 7 pairs of generated records. For Structure 1 and 2 the shear demands on all columns are evaluated, while for Structure 3, only the angle columns highlighted with dotted blue lines in Fig. 1 are considered.

5 Conclusions

Existing structures have structural irregularities that affect the reliability of NLSAs. Hence there is the need to extend pushover procedures to irregular buildings subjected to bidirectional inputs. In this work, the NLSAs are applied first separately along the two main structural directions. Then, the EDPs obtained in these directions are

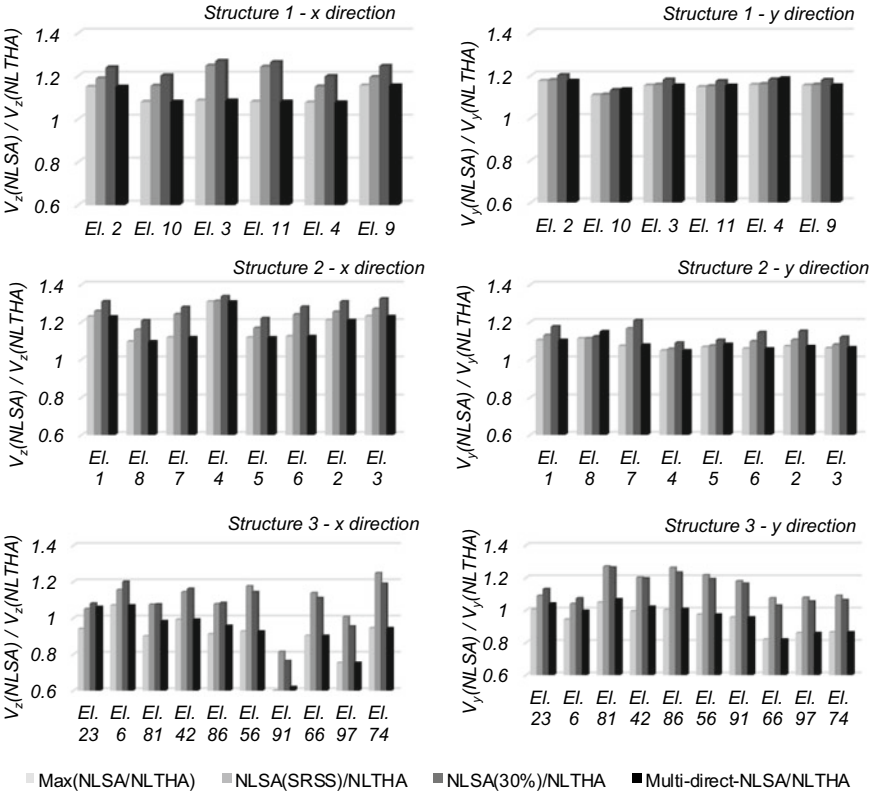

Fig. 3 Comparison between the shear demands obtained from NLSAs and NLTHAs in the *x* and *y* structural directions

combined according to the SRSS and 30% rules. Subsequently, the pushover forces are applied at different angles θ_i, from 0° a 360° with steps of 22.5°. For each θ_i, the maximum EDPs corresponding to the steps of the structural demands are obtained. Finally, NLTHAs are performed in order to compare the results obtained with the different methods. This comparison reveals as follows:

– The combination rules applied on displacement demands of single-story buildings do not provide results very different from the conventional N2 method.
– The prediction of displacement demands obtained from multi-directional NLSAs is very effective for the multi-story building, where the method also provides accurate predictions of floor rotations.
– All pushover procedures provide an overestimation of shear demand in single-story structures, in both directions and for all columns. Conversely, for the multi-story structure, the shear demands obtained from NLSAs are greater than the results of NLTHAs (and therefore conservative) only if combinations rules are

applied. For many columns, the N2 method and the multi-directional NLSAs provides un-conservative shear demands and this result is more evident on the upper levels.

The adequacy and precision of the pushover procedures depend on the structural configuration and the degree of plan irregularity. Therefore, future research should further investigate the effects of different pushover procedures on further load patterns, EDPs and structural configurations.

References

1. Anastassiadis K, Avramidis IE, Panetsos P (2002) Concurrent design forces in structures under three-component orthotropic seismic excitation. Earthq Spectra 18(1):1–17
2. Newmark NM, Rosenblueth (1971) Fundamentals of earthquake engineering. Prentice-Hall, New Jersey
3. Goodman LE, Rosenblueth E, Newmark NM (1952) A seismic design of elastic structures founded on firm ground. Technical Report. University of Illinois Engineering Experiment Station. College of Engineering, University of Illinois at Urbana-Champaign
4. Der Kiureghian A (1981) A response spectrum method for random vibration analysis of MDF systems. Earthquake Eng Struct Dynam 9(5):419–435
5. Wilson EL, Der Kiureghian A, Bayo EP (1981) A replacement for the SRSS method in seismic analysis. Earthquake Eng Struct Dynam 9(2):187–192
6. Newmark NM (1975) Seismic design criteria for structures and facilities, Trans-Alaska pipeline system. In: Proceedings of the U.S. national conference on earthquake engineering. Earthq Eng Inst Michigan, 94–103
7. Rosenblueth E, Contreras H (1977) Approximate design for multicomponent earthquakes. J Eng Mech Div 103(5):881–893
8. Wilson EL, Suharwardy I, Habibullah A (1995) A clarification of the orthogonal effects in a three-dimensional seismic analysis. Earthq Spectra 11(4):659–666
9. Smeby W, Der Kiureghian A (1985) Modal combination rules for multi-component earthquake excitation. Earthquake Eng Struct Dynam 13:1–12
10. Menun C, Der Kiureghian A (1998) A replacement for the 30, 40% and SRSS rules for multi-component seismic analysis. Earthq Spectra 14(1):153–156
11. López OA, Chopra AK, Hernández JJ (2001) Evaluation of combination rules for maximum response calculation in multicomponent seismic analysis. Earthquake Eng Struct Dynam 30(9):1379–1398
12. López OA, Chopra AK, Hernández JJ (2004) Adapting the CQC3 rule for three seismic components with different spectra. J Struct Eng 130(3):403–410
13. Camata G, Canducci G, Spacone E (2007) Input sismico multidirezionale: regole di combinazione direzionale e di progetto (in Italian). XII Proceeding ANIDIS L'ingegneria sismica in Italia. Pisa
14. EC8-Part 1: Eurocode 8 (2005) Design provisions for earthquake resistance of structures. Part 1–1: general rules—seismic actions and general requirements for structures. ENV 1998–1, CEN: Brussels
15. FEMA-273 Building Seismic Safety Council (1997) NEHRP guidelines for the seismic rehabilitation of buildings. Federal emergency management agency, Washington, D.C
16. NTC2018 (2018) DM 17 January 2018: updating of technical codes for constructions (in Italian). Official gazette n.42 of 20/02/18 ordinary supplement n. 8, Roma
17. ASCE 41 (2017) Seismic evaluation and retrofit of existing buildings. American society of civil engineers. ASCE41–17

18. ASCE/SEI 7–10 Minimum design loads for buildings and other structures. ASCE standard, American society of civil engineers, structural engineering institute
19. Fajfar P (2000) A nonlinear analysis method for performance-based seismic design. Earthq Spectra 16(3):573–592
20. D'Ambrisi A, De Stefano M, Tanganelli M (2009) Use of pushover analysis for predicting seismic response of irregular buildings: a case study. J Earthq Eng 13(8):1089–1100
21. Kreslin M, Fajfar P (2012) The extended N2 method considering higher mode effects in both plan and elevation. Bull Earthq Eng 10(2):695–715
22. Bosco M, Ghersi A, Marino EM (2012) Corrective eccentricities for assessment by the nonlinear static method of 3D structures subjected to bidirectional ground motions. Earthquake Eng Struct Dynam 41(13):1751–1773
23. Fujii K (2016) Assessment of pushover-based method to a building with bidirectional setback. Earthq Struct 11(3):421–443
24. Magliulo G, Maddaloni G, Cosenza E (2012) Extension of N2 method to plan irregular buildings considering accidental eccentricity. Soil Dyn Earthq Eng 43:69–84
25. Reyes JC, Chopra AK (2011) Evaluation of three-dimensional modal pushover analysis for unsymmetric-plan buildings subjected to two components of ground motion. Earthquake Eng Struct Dynam 40(13):1475–1494
26. Cimellaro GP, Giovine T, Lopez-Garcia D (2014) Bidirectional pushover analysis of irregular structures. J Struct Eng 140(9):04014059
27. McKenna F, Fenves GL, Scott MH (2000) Object oriented program opensees; open system for earthquake engineering simulation. http://www.opensees.berkeley.edu
28. Petracca M, Candeloro F, Camata G (2017) STKO user manual. ASDEA software technology, Pescara Italy
29. Spacone E, Filippou FC, Taucer F (1996) Fiber beam-column model for nonlinear analysis of R/C frames: I formulation Earthq Eng Struct Dyn 25(7):711–725
30. Scott BD, Park P, Priestley MJN (1982) Stress-strain behavior of concrete confined by overlapping hoops at low and high strain rates. J Am Concr Inst 79(1):13–27
31. Filippou FC, Popov EP, Bertero VV (1983) Effects of bond deterioration on hysteretic behavior of reinforced concrete joints. Report EERC 83–19, earthquake engineering research center. University of California, Berkeley
32. Luzi L, Hailemikael S, Bindi D, Pacor F, Mele F, Sabetta F (2008) ITACA (ITalian ACcelerometric Archive): a web portal for the dissemination of Italian strong-motion data. Seismol Res Lett 79(5):716–722
33. Ambraseys N, Smit P, Sigbjornsson R, Suhadolc P, Margaris B (2002) Internet-site for European strong-motion data. In: European commission, research-directorate general, environment and climate programme
34. Beyer K, Bommer JJ (2006) Relationships between median values and between aleatory variabilities for different definitions of the horizontal component of motion. Bull Seismol Soc Am 96(4A):1512–1522
35. Cantagallo C, Camata G, Spacone E, Corotis R (2012) The variability of deformation demand with ground motion intensity. Probab Eng Mech 28:59–65
36. Gasparini D, Vanmarcke EH (1976) Simulated earthquake motions compatible with prescribed response spectra. In: department of civil engineering, research report R76–4. Massachusetts institute of technology

Effects of Column Base Flexibility on Seismic Response of Steel Moment-Frame Buildings

Tomasz Falborski, Ahmand Hassan, and Amit Kanvinde

1 Introduction

SMRFs are popular lateral load resisting systems in earthquake-prone areas, due to their ductility and the architectural versatility offered by unbraced bays. Despite availability of many design procedures [1, 2], one area where the guidance is relatively less developed is the simulation of column base connections. This is because research on column base connections has lagged other SMRF connections (e.g., beam-column connections), such that the focus in the context of base connections has been on developing strength models [3] rather than stiffness or load-deformation response. The lack of research has been further fueled by the presumption that base connections respond either as fixed (with capacity designed to be stronger than the attached column) or as pinned (if designed otherwise). Following this presumption, base connections are simulated as either fixed or pinned in current design and performance assessment practice [4, 5]. Recent research has shown this practice to be highly problematic for two reasons. First, experiments on various types of column base connections ranging from exposed base plate connections [6], slab-overtopped base plate connections [7] and embedded base connections [8] indicate that base connections exhibit partial fixity, which contravenes both the fixed and pinned assumptions. Second, the erroneous characterization of fixity (as either fixed or pinned) has significant implications

T. Falborski (✉)
Faculty of Civil and Environmental Engineering, Gdańsk University of Technology, Gdańsk, Poland
e-mail: tomfalbo@pg.edu.pl

A. Hassan · A. Kanvinde
Department of Civil and Environmental Engineering, University of California, Davis, CA, USA
e-mail: askhassan@ucdavis.edu

A. Kanvinde
e-mail: kanvinde@ucdavis.edu

R. Bento et al. (eds.), *Seismic Behaviour and Design of Irregular and Complex Civil Structures IV*, Geotechnical, Geological and Earthquake Engineering 50,
https://doi.org/10.1007/978-3-030-83221-6_22

for structural response. For both these reasons, structural response is highly sensitive to estimates of base fixity, underscoring the need for its accurate characterization. Motivated by this, base fixity models have been proposed for various base connection details, including exposed [9], slab-overtopped [10], and embedded [11]. However, each of these models has been developed using (and validated against) a limited set of laboratory test data. Therefore, applying these models with confidence to simulate the rotational fixity of as-built field details is challenging for the following reasons: (1) the laboratory specimens investigate only a limited set of configuration details (i.e., anchor rod configurations, base plate shape and aspect ratio, surrounding reinforcement), such that extrapolation of the models to field details that are different has not been verified, (2) all laboratory specimens are loaded laterally under a constant axial load, whereas in the field, the axial load varies due to seismic motions – this is an important effect because axial load has a strong effect on the fixity of exposed base plate connections [9], (3) in practice, base connections are loaded under biaxial bending, whereas none of the models or tests have interrogated the effect of biaxial bending on rotational fixity, and (4) the laboratory specimens are anchored to a strong floor, such that the effect of soil deformations is not reflected in the test data.

Against this backdrop, this paper seeks to introduce best practices for simulation of column base fixity in SMRFs using recorded time history data from two buildings instrumented as part of the California Strong Motion Instrumentation Program (CSMP). Sophisticated three-dimensional frame models of these buildings are constructed, and various options (including the previously published models introduced above) for simulating column bases are evaluated by comparing the simulated response of these buildings to the recorded response under the seismic excitations.

2 Types of Column Base Connections and Flexibility Models

SMRF column base connections in seismically active regions take numerous forms, depending on the loading, soil type, system design and architectural considerations, and local economies. Broadly, these may be categorized into exposed base plate connections, or embedded connections (see Fig. 1), with detailing variations (e.g., placement of anchor rods) within each form. The following subsections describe these connections, outlining the physical mechanisms by which they deform and resist loads, along with the models proposed to estimate their flexibility.

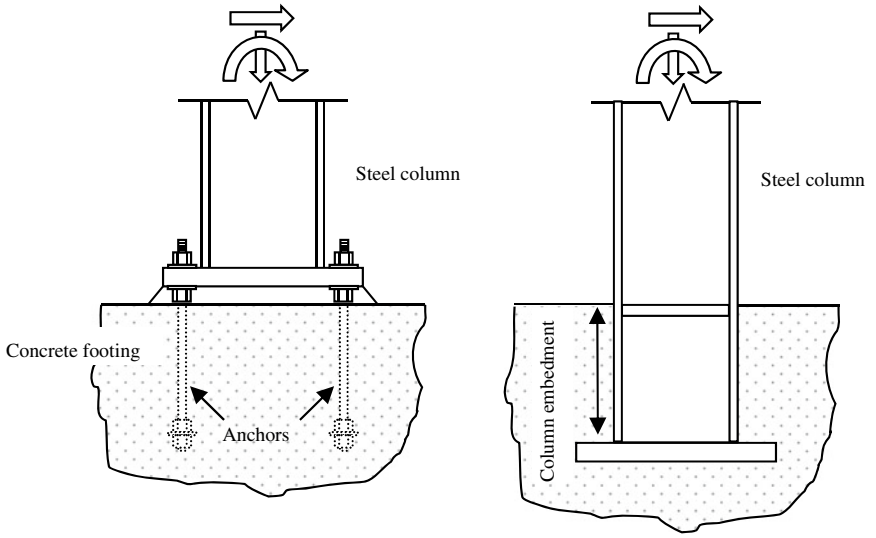

Fig. 1 Common types of column base connections: exposed base plate, (left) and embedded column base (right)

2.1 Exposed Base Plate Connections

In an exposed base plate connection the column is welded to a base plate, which is anchored to a footing using anchor rods, or post installed anchors [3]. The connection itself is designed for the limit states of flexural yielding of the base plate, bearing failure in the footing, or anchor rode failure—by yielding, pullout or breakout [3]. Kanvinde et al. [9] presented a model to estimate the rotational flexibility of laboratory specimens with good accuracy. Subsequent research conducted by Trautner et al. [12] corroborates the validity of this model for other laboratory test data. It should be noted that exposed base plate type connections are preferred for low- to mid-rise (less than 3–4 stories) SMRFs because it is economically unfeasible to transfer larger base moments through anchor rods (in such cases embedded base connections are typically specified).

Sometimes, exposed base connections are overtopped with a slab on grade. This is often the case in residential or commercial (as opposed to industrial) construction. The slab-on-grade is usually not considered in design, assuming that the connections respond in a manner similar to exposed base plate connections. However, studies by Barnwell [7] indicate that although the primary mechanism of load resistance is similar to the exposed base plate connections, the slab on grade increases the rotational fixity and provides additional strength as well. Tryon [10] proposed a model to estimate the rotational fixity of slab-overtopped connections.

2.2 *Embedded Base Plate Connections*

In contrast to slab-overtopped exposed base plate connections (where the embedment is sometimes incidental), columns may be embedded in the footing by design in order to improve their bearing capacity when exposed base plate connections become economically unfeasible. These connections are typically specified in mid- to high-rise buildings in which the moment demands are high. In this type of connection the load is resisted through a combination of horizontal bearing of the footing against the column flange, and vertical bearing against the embedded base plate. These mechanisms (identified by Grilli et al. [8] based on full-scale experiments) are the basis for a fixity model proposed by Torres-Rodas et al. [11].

3 Characteristics of Instrumented Buildings

Two SMRF buildings instrumented as part of the CSMIP were selected for analysis in this study. Table 1 shown below summarizes key characteristics of these buildings as well as the base connections used in these frames. Figure 1 illustrates these frames—each row within the figure represents one building (as indicated in the figure), whereas the columns show the photographs and structural models (first column), the moment frames (second column), and the gravity frames with the nonstructural components represented as braces (third column).

Table 1 Building and CSMIP data characteristics

Bldg	Location (all in CA)	CSMIP station	Stories	Period (NS, EW)	Base and foundation type	Number of records
1	Richmond	58,506	3	0.60 s, 0.76 s	Exposed base plates with overtopping slabs concrete pile caps and grade beams	8
2	Burbank	24,370	6	1.29 s, 1.33 s	Embedded column bases connected to concrete pile caps and grade beams	7

4 Building Simulation Models and Estimation of Nonstructural Stiffness

Three-dimensional simulation models were constructed for the buildings using the software program ETABS [13]. In addition to the moment frames, the models included the gravity frames, nonstructural components (i.e., partition and exterior walls) as well as diaphragms. Nonstructural components contribute significantly (up to 40%) to the elastic stiffness of the building [14], significantly affecting dynamic response. Thus, accurate characterization of nonstructural component stiffness is essential for effective simulation of building response. The nonstructural stiffness within each story of the building may be estimated based on configuration of partition/external walls and cladding, based on test data [15] and stiffness models [16] for similar types of nonstructural components. The stiffness of nonstructural wall and cladding details is sensitive to their geometry, the presence of doorways, captive ends, as well as construction details, e.g., type of studs (cold formed or wood, nail/screw patterns, sill plates [17, 18]). As a result, literature-based estimates of nonstructural stiffness are approximate at best. Consequently, a direct approach for estimation of nonstructural stiffness was developed in this study:

a. During any ground motion, the instantaneous horizontal components of the total story shear may be represented as ${V_I^{story}}_{x,y}(t)$ in which the subscript (Roman) I represents the Ith story, located directly below the ith floor. The subscripts x and y represent the two horizontal directions.
b. This instantaneous story shear may be decomposed into three components, which must equilibrate the inertial forces of all the floors above story I:

$$\begin{aligned} {V_1^{story}}_{x,y}(t) &= {V_1^{NS}}_{x,y}(t) + {V_l^{strucut}}_{x,y}(t) + {C_l^{damping}}_{x,y}\dot{u}_{lx,y}(t) \\ &= \sum_{i=1}^{N} m_i \ddot{u}_{i,x,y}(t) \end{aligned} \tag{1}$$

In the above equation, the terms ${V_I^{NS}}_{x,y}(t)$ and ${V_I^{struct}}_{x,y}(t)$ represent the instantaneous story shears (in the x and y directions) carried by the nonstructural and structural (i.e., SMRF and gravity frames) elements, respectively, whereas ${C_I^{damping}}_{x,y} \cdot \dot{u}_{I,x,y}(t)$ is the instantaneous damping force in which the term $\dot{u}_{I,x,y}(t)$ represents the instantaneous interstory velocities in the x and y directions. The term on the right hand side represents the inertial forces of all the floors above story I, in which $\ddot{u}_{i,x,y}(t)$ represents the instantaneous absolute accelerations of these floors.

Following the observations above, the instantaneous force carried by the nonstructural elements ${V_I^{NS}}_{x,y}(t)$ may be determined if the remaining quantities in Eq. (1) are estimated. More specifically, ${V_I^{struct}}_{x,y}(t)$, may be obtained by conducting, for example, simple static analysis. Following procedure may be adopted: for a given story and direction within the building recorded time histories time instants at which the interstory velocity equals zero (or are negligible) are selected. At these instants, the damping force within the story is zero. Consequently, at each of these instants, the

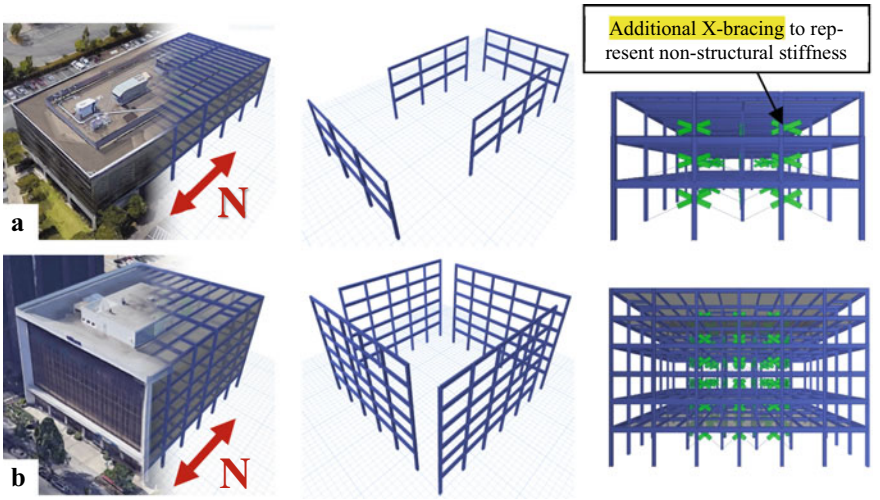

Fig. 2 **a** Building #1, **b** Building #2 (left column—ETABS models, middle column—SMRFs, right column—non-structural bracing locations)

sum of the story shears carried by the structural frames and the nonstructural components must equal the inertial forces induced by stories above. For these time instants, instantaneous values of the floor lateral displacements represent the deformations of the structural frames (i.e., SMRF and gravity frames) as well. Consequently, the story shear carried by these frames may be suitably estimated by applying these displacements in a static manner to the simulation model of the building. Given this observation the shears in the upper stories may be directly determined as $V_I^{struct}{}_{x,y}(t)$.

Once determined in this way, the nonstructural stiffness is applied in the form of equivalent bracing members (see Fig. 2, third column). These bracing members (whose cumulative stiffness equals the estimated story nonstructural stiffness) are inserted into bays where nonstructural elements (e.g., partition walls) are present.

5 Results and Discussion

Once the building models have been developed as described in the previous section, they are used to examine the effect of base fixity on seismic response. For each of the buildings, column base connections are represented in five alternate ways. These include pinned (denoted k_0 to indicate zero fixity), fixed (denoted k_∞ to indicate infinite fixity) and three intermediate values. These values denoted k_{model}, $0.5 \times k_{model}$, and $1.5 \times k_{model}$ represent the model-based estimates of base fixity. Of these, the first k_{model} is the best-estimate of base fixity estimated using the appropriate model for each base detail within each building (referring to Table 1). The estimates $0.5 \times k_{model}$, and $1.5 \times k_{model}$ (in which the base fixity is set to $\pm 50\%$ of the best estimate) are also

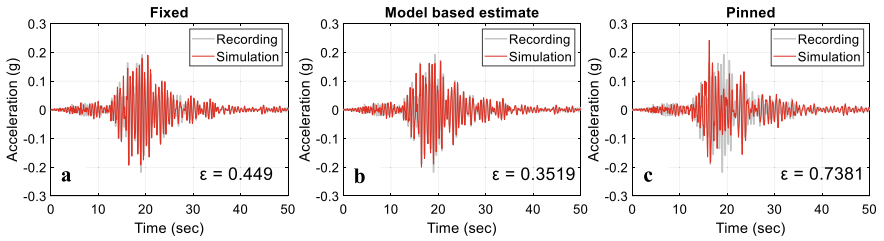

Fig. 3 Sample recorded and simulated acceleration time histories for Building #1

queried to examine the sensitivity of frame response to uncertainty in base fixity estimates. Zero-length rotational springs with properties corresponding to each of these stiffness estimates are provided at the column bases. The parametrization outlined above results in 10 building simulation models; five of these models (with k_0, k_∞, k_{model}, $0. \times k_{model}$, and $1.5 \times k_{model}$) correspond to each of the two buildings. All 10 models are subjected to all ground motions available for the corresponding building. Each of the 75 nonlinear time history analysis runs (obtained from two buildings) produces acceleration time histories that may be directly compared to recordings from the instrumented buildings. As an illustrative example, Fig. 2 shows graphical comparisons of recorded and simulated acceleration histories for Building #1.

Referring to Fig. 3, it is observed that simulations with the fixed base k_∞ and the model based best-estimate k_{model} cases appear to track the recorded most closely, whereas simulations with the pinned base, i.e., k_0 show greater error. Although such visual assessments are informative, an objective error measure is needed to quantify agreement between simulated and recorded time histories, and to examine trends across various buildings or base details and inform modeling practices in general. Naeim et al. [19] provide best practices for such quantification, in the specific context of utilizing CSMIP data. Consequently, these practices to calculate the error between any pair of recorded and simulated time histories are selected for this study—see Eq. (2).

$$_{i,x,y} = \left[\frac{\int \left| \ddot{u}_{i,x,y,recorded} - \ddot{u}_{i,x,y,simulated} \right| \cdot dt}{\int \left| \ddot{u}_{i,x,y,recorded} \right| \cdot dt} \right] \tag{2}$$

The error denoted as ε_{total} represents the error from the acceleration time histories averaged over all instruments within the building, whereas the error denoted as $\varepsilon_{10\%}$ represents the error calculated by considering only the strong motion portion of each time history (for only those values of acceleration that exceed 10% of the maximum acceleration within a time history).

Referring to Fig. 4 the following observations may be made:

- The pinned base assumption results in the greatest value of error. This suggests that simulating bases as pinned is grossly inaccurate. In fact, this error is quite large, i.e., both ε_{total} and $\varepsilon_{10\%}$ are greater than 0.5 even for Building #1 which

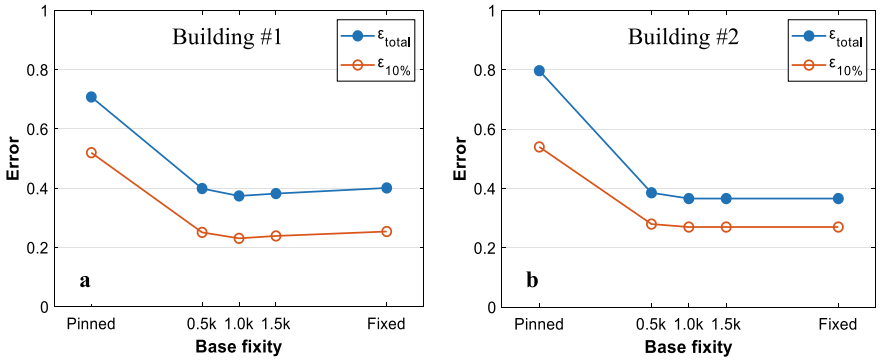

Fig. 4 Error between simulated and recorded acceleration time histories

includes only exposed type base connections. This suggests that the practice of simulating exposed base connection as pinned is not well-founded, and that the connection has significant rotational fixity, which is possibly enhanced by various factors including the presence of axial force as well as the overtopping slab.

- For Building #1 (i.e., Fig. 2b) which features exposed base plate connections, the lowest error corresponds to k_{model}, such that the error increases as the fixity is increased beyond this value. Specifically, the simulations with k_∞ result in roughly 2.5% more error (for both ε_{total} and $\varepsilon_{10\%}$) as compared to the simulations with k_{model}. This is unsurprising, given the higher flexibility of exposed base plate connections and suggests that for these connections, simulating the bases with model-based estimates of stiffness is appropriate.
- For Building #2 (i.e., Fig. 2b), the errors (both ε_{total} and $\varepsilon_{10\%}$) decrease substantially as the base fixity is increased, and saturate around the fixity corresponding to k_{model} – such that increasing the stiffness to infinity (i.e., a fixed base) results in essentially the same response. Referring to Table 1, Building #2 has embedded base connections. This suggests that embedded base connections may be suitably represented either based on the appropriate model [11] or even as fixed, especially since the former requires more effort and familiarity with the model.
- The lowest errors for Building #1 with the exposed bases are in the range of $\varepsilon_{total} = 0.374$, and $\varepsilon_{10\%} = 0.231$; these are obtained using k_{model}. The lowest errors obtained for Building #2 with the embedded bases are $\varepsilon_{total} = 0.366$, and $\varepsilon_{total} = 0.27$; as noted above, these are obtained for base stiffness between k_{model} and k_∞. In absolute terms these errors may be considered low/acceptable, considering the following: (1) Previous work, e.g., Naeim et al. [18] used genetic algorithms to tune building properties to minimize errors between CSMIP recordings and simulations—these algorithms resulted in errors (defined similarly) not significantly lower than the ones reported in Fig. 4. The simulations in this study were not optimized in this manner, and used best estimates of structural properties, to provide a realistic assessment of expected errors in building simulation. From this standpoint, the error values noted above are encouraging, and (2) Referring

to Fig. 4, the error corresponding to values in this range represents good visual agreement between the recordings and simulations.
- In all cases, the sensitivity of error to the base flexibility in the neighborhood of k_{model} is modest (as illustrated by the errors for the $0.5 \times k_{model}$, and $1.5 \times k_{model}$ simulations).

6 Conclusions

The main findings of this study, based on the observations from Figs. 3 and 4 and associated discussion may be interpreted to provide guidance for the modeling of column base connections in steel moment frames. The key takeaways are:

- Simulating column bases as pinned, even when they are constructed as exposed base plates results in gross mischaracterization of frame response
- For exposed base plate connections, simulating the bases using model-based estimates is advisable, since it results in the best agreement (minimum errors) between the recorded and simulated time histories for both acceleration and displacement.
- For embedded base connections, simulating the bases as fixed or with the model based estimates result in the lowest error. This suggests that from a standpoint of elastic building response estimation, it is reasonable to simulate the bases as fixed, given the higher effort and expertise required for model-based estimation.
- Since the response appears to be relatively insensitive to the flexibility in a $\pm$ 50% neighborhood of the model based estimates, explicit consideration of soil or footing flexibility may not be critical, since previous studies [4] indicate that these effects do not alter the stiffness by more than 50%. Nevertheless, the flexibility of the whole foundation system (where vertical displacements of the footings are also allowed which may result, for example, in rigid rotation of the building) needs to be additionally analyzed in a separate study.

Although this study provides the first field-recording based examination of column base fixity, it has limitations, which must be considered while interpreting or applying its recommendations. First, it is important to note that even the best overall agreement between simulated and recorded time histories is not ideal (errors on the order of 30% for the integrated measure), indicating that the representation of the base connections is only one source of error. Nonetheless, the lowest errors noted in this study are comparable to or better than those noted in other comparisons between recorded and high-fidelity simulations. The implications are the following: (1) although the remaining error may be reduced further by making some adjustments to the structural models, e.g., providing irregular strength, stiffness or damping values over various parts of the building, such adjustments are arbitrary with respect to the nominal or best-estimates of these properties, (2) as a result, the remaining error is challenging to minimize further, since it may be attributed to inherent uncertainty in these properties, and (3) the recommendations for simulating base fixity presented herein are justifiable within this overall context. Second, for the buildings studied in this paper, the ground

motions were of relatively low intensity, selected to not induce inelastic actions in the structure. This has an additional implication. The rotational response of base connections is nonlinear even in the pre-yield stage. This may be attributed to the following factors: (1) the nonlinearity of concrete, (2) gapping and contact between the steel and concrete components of the connection, and (3) for exposed base plate connections, the change in axial load during seismic loading, which results in a change in stiffness. This must be considered in extrapolating results of this study to buildings subjected to stronger shaking. Notwithstanding these limitations, the analyses presented in this paper are encouraging because they provide the first field-recording based guidance for simulating column base connections in SMRFs.

Acknowledgements The authors are grateful to the California Department of Conservation and the California Strong Motion Instrumentation Program (CSMIP) for providing major funding for this project. The advice of Professor Farzin Zareian at the University of California, Irvine, and of Professor Pablo Torres at Universidad San Francisco de Quito, Ecuador is also greatly appreciated. The findings and opinions in this paper are solely of the authors.

References

1. American Institute of Steel Construction, Inc. (AISC) (2016) Seismic provisions for structural steel buildings (ANSI/AISC 341–16). American Institute of Steel Construction, Chicago, (IL, USA)
2. American Institute of Steel Construction, Inc. (AISC) (2016) Prequalified connections for special and intermediate steel moment frames for seismic applications (ANSI/AISC 358–16). American Institute of Steel Construction, Chicago, (IL, USA)
3. Fisher JM, Kloiber LA (2006) Base plate and anchor rod design. In: AISC steel design guide one, 2nd edn. American Institute of Steel Construction, Chicago, IL
4. Zareian F, Kanvinde AM (2013) Effect of column-base flexibility on the seismic safety of steel moment-resisting frames. Earthq Spectra 29(4):1537–1559
5. Falborski T, Torres-Rodas P, Zareian F, Kanvinde AM (2020) The effect of base connection strength and ductility on the seismic performance of steel moment resisting frames. J Struct Eng, ASCE 146 (5)
6. Gomez IR, Kanvinde AM, Deierlein GG (2010) Exposed column base connections subjected to axial compression and flexure. In: Final report presented to the American institute of steel construction. Chicago, IL
7. Barnwell N (2015) Experimental testing of shallow embedded connections between steel columns and concrete footings. Master thesis, Brigham Young University, Provo, UT
8. Grilli DA, Jones R, Kanvinde AM (2017) Seismic performance of embedded column base connections subjected to axial and lateral loads. J Struct Eng ASCE 143(5):04017010
9. Kanvinde AM, Grilli DA, Zareian F (2012) Rotational stiffness of exposed column base connections: experiments and analytical models. J Struct Eng ASCE 138(5):549–560
10. Tryon JE (2016) Simple models for estimating the rotational stiffness of steel column to footing connections. Master thesis, Brigham Young University, Provo, UT
11. Torres-Rodas P, Zareian F, Kanvinde AM (2017) Rotational stiffness of deeply embedded column-base connections. J Struct Eng, ASCE 143(8)
12. Trautner CA, Hutchinson T, Grosser PR, Silva JF (2016) Effects of detailing on the cyclic behavior of steel baseplate connections designed to promote anchor yielding. J Struct Eng, ASCE 142(2)

13. Computers and Structures, Inc. (CSI) (2016) ETABS integrated building design software. Computers and Structures Inc., Berkeley, CA. http://docs.csiamerica.com/manuals/etabs/Analysis%20Reference.pdf
14. ATC (2017) Seismic analysis, design, and installation of nonstructural components and systems—background and recommendations for future work. Report no. NIST GCR-917–44, Applied Technology Council, Redwood City, CA
15. McMullin K, Merrick D (2001) Seismic performance of gypsum walls—experimental test program. In: Report W-15, CUREE woodframe project
16. Kanvinde AM, Deierlein GG (2006) Analytical models for the seismic performance of gypsum drywall partitions. Earthq Spectra 22(2):391–411
17. Jampole E, Deierlein GG, Miranda E, Fell B, Swensen S, Acevedo C (2016) Full-scale dynamic testing of a sliding seismically isolated unibody house. Earthq Spectra 32(4):2245–2270
18. Davies R, Retamales R, Mosqueda G, Filiatrault A, Allen D (2012) cold-formed steel framed gypsum partition walls on the seismic response of a medical facility. In: Twenty-first international specialty conference on cold-formed steel structures. St. Louis, Missouri
19. Naeim F, Hagie S, Alimoradi A, Miranda E (2005) Automated post-earthquake damage assessment and safety evaluation of instrumented buildings. In: John A (ed) Martin and associates research report—JAMA report number 2005–10639. Los Angeles, CA

Seismic Risk Assessment of Existing RC Frame-Buildings with Shear Walls

Beatrice Belletti, Enzo Martinelli, Elena Michelini, Michela Tavano, and Francesca Vecchi

1 Introduction

Vulnerability assessment of existing buildings plays a major role in seismic risk mitigation policies. According to the data collected in the last ISTAT survey [1], a large proportion of the Italian residential building stock was designed considering only gravitational loads or according to obsolete seismic codes. So far, the most of the studies related to the risk assessment of Reinforced Concrete (RC) structures have been focused on moment-resisting frames and infilled frames (among others, e.g. [2–6]), whereas only few works are available on RC dual frame-wall systems, and on wall-equivalent dual systems (e.g. [7–9]). However, core structural systems represent a quite common construction solution for old residential RC buildings in Italy, especially in large urban areas with higher population density. In this typology, the bearing structure is formed by RC frames, mainly subjected to vertical loads, and by RC walls, which are usually placed around the staircases or elevator shafts. If wisely designed,

B. Belletti (✉) · E. Michelini · M. Tavano · F. Vecchi
Department of Engineering and Architecture, University of Parma, Parco Area delle Scienze 181/A, 43124 Parma, Italy
e-mail: beatrice.belletti@unipr.it

E. Michelini
e-mail: elena.michelini@unipr.it

M. Tavano
e-mail: michela.tavano@studenti.unipr.it

F. Vecchi
e-mail: francesca.vecchi@unipr.it

E. Martinelli
Department of Civil Engineering, University of Salerno, via Giovanni Paolo II 132, 84084 Fisciano, SA, Italy
e-mail: e.martinelli@unisa.it

R. Bento et al. (eds.), *Seismic Behaviour and Design of Irregular and Complex Civil Structures IV*, Geotechnical, Geological and Earthquake Engineering 50,
https://doi.org/10.1007/978-3-030-83221-6_23

RC walls may have a positive effect on the seismic performance of the framed structure [10] and may help preventing soft-story collapse mechanisms. Nevertheless, in existing buildings the position of RC walls is often asymmetric in plan, representing a source of structural irregularity and creating torsional effects under seismic action. Another quite common problem is related to the poor quality of structural detailing, especially in the critical zones (i.e. reinforcement amount and thickening), which might not ensure a ductile collapse mechanism of the walls. Therefore, a realistic description of the vulnerability of this structural typology appears to be worthy of interest, not only from a scientific point of view, but also for socio-economic reasons.

In this work, the problem is tackled by referring to a specific case study, representative of a typical Italian residential multi-story building with an asymmetric stairwell core. To this end, a Finite Element (FE) model of the structure is first defined, by simulating frames though beam and truss elements, and shear walls through shell elements. The nonlinear behaviour of RC is taken into account through PARC_CL 2.1 constitutive model [11], implemented into the FE Code ABAQUS [12]. The structural behaviour is analysed by performing pushover (PO) analyses with two different lateral load distributions, and damage threshold levels are identified along PO curves following different criteria. Different Engineering Demand Parameters (EDPs) are considered and compared to verify their suitability for the case of frames with shear walls, such as the attainment of predefined levels of inter-story drift and the attainment of predefined values of damage state in the materials (i.e. crack widths, or strain levels in concrete and longitudinal and transverse reinforcement). The obtained results are finally used for drawing fragility curves.

2 Case Study

The case study selected in this work represents a typical example of Italian existing RC multi-story building designed for gravity loads only, without specific provisions for earthquake resistance. The geometry of the building and its structural features (including reinforcement amount and arrangement) are described in detail in two well-known Italian university textbooks [13, 14], to which reference is made. The typical floorplan of the building and its longitudinal sections along the two main directions X, Y are reported in Fig. 1a, b respectively. The building, which serves as private housing, is formed by a lower ground floor and five floors above the ground level, and has a rectangular plan, whose dimensions are 11.7 m $\times$ 24.4 m. The bearing structure is conceived so that that vertical loads are mainly resisted by RC frames, while the lateral loads are mainly absorbed by the stairwell core, so realizing a wall-equivalent dual system.

The eccentric position of the core is the major reason for in-plan irregularity, shifting the centre of mass (CM) away from the centre of stiffness (CR), with a larger eccentricity along Y-direction (approximately equal to 2.5 m, with slight differences from one level to the other) as shown in Fig. 1a. Since the considered case study refers to an existing building designed without seismic provisions, the reinforcement

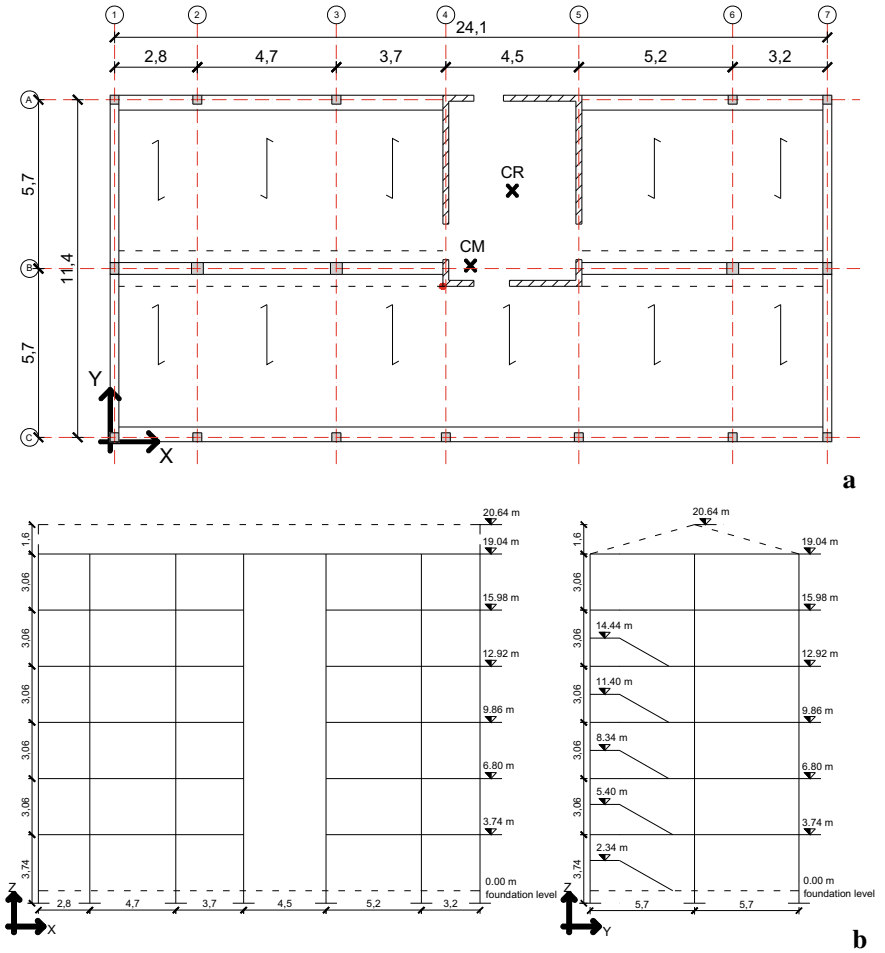

Fig. 1 Geometry of the examined building: **a** typical floorplan, with indication of the centre of mass CM and of the centre of stiffness CR (dimensions in m), **b** longitudinal sections along the two main directions X, Y

of the 200 mm thick walls forming the stairwell core is dimensioned with reference to wind action and to a conventional horizontal load equal to 0.5% of the weights [13]. This conventional load aims to take into account the unfavourable effects caused by geometric imperfections, which may be due to possible deviations in the geometry of the structure and in the position of loads, according to [15].

The reinforcement layout of the core walls, taken from [13], is summarized in Table 1 for reading convenience. The reinforcement amount for lintels in Table 1 is referred to the ground floor only, and it slightly decreases passing to the upper floors.

Table 1 Reinforcement layout of the core walls [13]

	Longitudinal reinforcement	Transverse reinforcement
Walls (current section)	ϕ 12/300 mm	ϕ 8/300 mm
Lintels above openings	2 ϕ 12 + 3 ϕ 16	ϕ 8/250 mm
Ring beams	2 + 2 ϕ 16	ϕ 8/250 mm

Both inter-story floors and the roof floor are composed with parallel RC joists and interposed hollow clay blocks, with a 400 mm thick RC topping, and are assumed to act as rigid diaphragms. The walls and the frames are constituted of C25/30 concrete, and the reinforcement is made of B450C steel.

3 Finite Element Model

The behaviour of the above described building is studied numerically by using the commercial software ABAQUS [12]. All the simulations include the effects of both geometric and mechanical non-linearity. The latter is taken into account through PARC_CL 2.1 crack model, implemented in ABAQUS as a User MATerial (UMAT) subroutine, as better described in Sect. 3.2.

Since the structure of the building is conceived as a wall-equivalent dual system, numerical analyses are repeated twice, by adopting two different modelling assumptions on frame behaviour and on its interaction with the core. In the first simplified FE model, beams and columns are considered as elements of pendulum frames, and their interaction with the core under seismic action is neglected. For the same reason, all the sources of nonlinearity are attributed only to RC walls, while the behaviour of the elements belonging to the pendulum frames is assumed linear-elastic. In the second FE model, the interaction between the frame and the core is instead taken into account, and the nonlinear behaviour of frame elements is schematized through a concentrated plasticity approach, by assigning a nonlinear moment–curvature law to the ends of beams and columns. The moment–curvature relation is evaluated by adopting the Saenz law with ultimate strain equal to 3.5×10^{-3} for concrete, and an elastic-perfectly plastic law for steel. In both cases, the effect of masonry infills on the structural response under seismic action is not included in the model, to avoid the introduction of further variables in the problem. This assumption seems reasonable at this first stage of the research, since the focus of the work is the identification of the best-suited EDPs and the corresponding damage thresholds in case of core systems, in comparison to the case of naked framed buildings.

Pushover analyses are carried out to investigate the behaviour of the building under seismic action, by considering two distributions of lateral forces: a uniform pattern, based on lateral forces that are proportional to masses regardless of elevation, and a

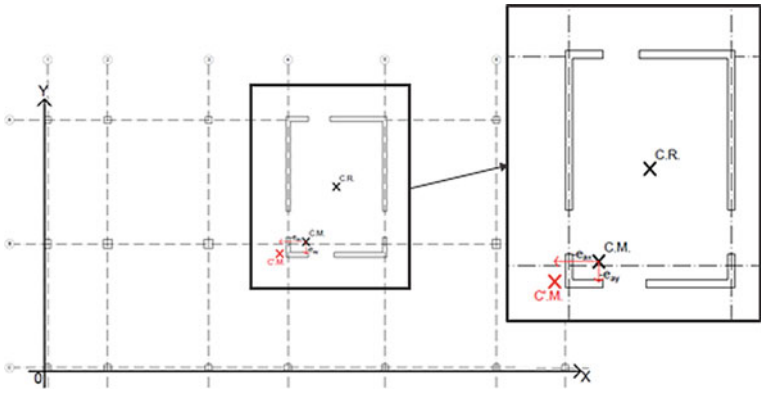

Fig. 2 Effect of accidental eccentricity: shift of CM so to maximise its distance from CR

triangular pattern, proportional to the product of the seismic masses at a given story for the height of the same story [16, 17]. Lateral loads are applied independently in the two X, Y positive/negative directions. For each of the 8 resulting loading cases, the chosen target displacement is the average roof displacement, calculated as the average of the displacements recorded at the nodes placed at the two opposite corners of the floorplan, i.e. corresponding to the upper-right corner and to lower-left one of Fig. 1a. The effect of accidental eccentricity prescribed by Standard codes (i.e., [17]) is taken into account in a simplified way, by combining the two eccentricities in X and Y-directions so to maximize the distance between the centre of mass and the centre of stiffness (as depicted in Fig. 2).

3.1 Modelling Choices

A general view of the adopted 3D FE model is shown in Fig. 3a. RC core walls are modelled through 8-node one-layered shell elements, with 4 Gauss integration points in the shell plane and 5 Simpson integration points in the thickness.

Three-node beam elements with 2 integration points are used for RC columns, while RC beams are modelled through two-node truss elements with one integration point in case of pendulum frames, and through two-node beam elements with one integration point in case of collaborating frames.

Rigid diaphragm condition is imposed to the structure by constraining the motion of the nodes belonging to each floor to the rigid motion of a predefined node belonging to the core, through kinematic coupling conditions. The chosen "master" node corresponds to the bottom left corner of the core (red dot in Fig. 1a), whose position is very close to the centre of mass.

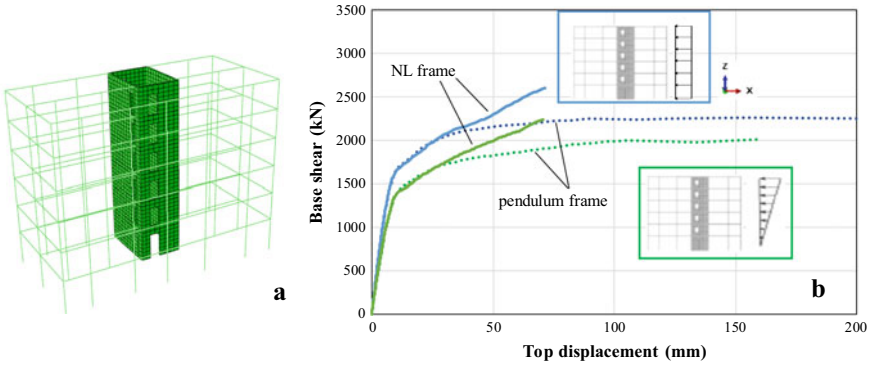

Fig. 3 **a** FE model of the building; **b** Different modelling choices for frame: effects on PO curves

A comparison among PO curves obtained from the two considered FE models (with pendulum or collaborating frames) is shown in Fig. 3b, in the case of lateral forces acting along the negative X direction.

3.2 PARC_CL 2.1 Model

The nonlinear behaviour of RC walls is taken into account through PARC_CL 2.1 crack model. This model is based on a fixed crack approach, in which the reinforcement is assumed to be smeared in the hosting concrete element.

PARC_CL 2.1 represents the extension to cyclic loads of a well validated constitutive model originally conceived for the analysis of RC structures under static actions based on total strain approach (PARC model, [18]). An alternative model for the analysis of RC structures under static actions based on a strain decomposition approach (2D-PARC model, [19, 20]) has been also developed at the University of Parma. PARC_CL 2.1 crack model allows taking into account plastic and irreversible deformations in the unloading–reloading phase and it can be suitable for the prediction of the cyclic and dynamic response of RC structures. It represents the last release of the previous PARC_CL 2.0 crack model [21], including new features, like buckling of longitudinal reinforcement [11], time-dependent effects and corrosion of reinforcement [22].

4 Choice of EDPs and Damage Thresholds for the Construction of Fragility Curves for RC Core Systems

The procedure followed in this work for the damage assessment of the considered case study is based on the application of a capacity spectrum method. The approach is similar to the one described in HAZUS [23] and followed in the Risk-UE project [24, 25]. In short, the response of the building under seismic action is assumed to be represented by the so-called "performance point", which is defined as the intersection between a properly reduced earthquake demand curve, and the capacity curve of an equivalent SDoF system. The response of the non-linear SDoF system, deriving from the above described PO analyses, is schematized by means of an equivalent bilinear capacity curve. Both the demand and the capacity curves are represented in the ADRS domain, in terms of spectral acceleration versus displacement. Fragility curves are then derived by comparing the so obtained performance point, in terms of displacement, with that corresponding to the reaching of a predefined damage threshold, following a procedure based on incremental static analysis. Therefore, the construction of fragility curves is clearly strictly related to the individuation of the damage threshold associated to each damage state, and to the corresponding EDP.

As reported in [2, 3, 9], story-level EDPs are commonly adopted for the damage assessment of individual buildings or generic building types, since they can be easily obtained from both numerical analyses and structural monitoring. As an example, the well-known Hazus methodology [23] estimates seismic damage based on the average inter-story drift ratio, also in case of building with complex configurations, or which are susceptible to torsion. For pre-code mid-rise buildings (4–7 floors) with RC shear walls, the Hazus method suggests to adopt the threshold values summarized in Table 2. However, the Hazus manual specifies that these values are derived for generic building types, and that building with particular irregularities or vulnerable configurations may have significantly lower damage-state thresholds.

The mechanical method developed within Risk-UE project (known as Risk-UE LM2) directly identifies 4 limit states on the capacity curve as a function of the yielding and ultimate displacements (d_y and d_u, respectively), as discussed in [25] and summarized in Table 3. The first 3 damage states (from slight to extensive) are assumed to have a direct correspondence with the first 3 damage grades of the European macroseismic scale EMS-98 [26], while the last 2 damage grades of EMS-98 (very heavy damage and destruction) are assumed to be hardly distinguishable from each other in a mechanical model and are consequently represented by the same damage state in Risk-UE LM2 ("complete damage"). For each considered

Table 2 Average inter-story drift ratios at threshold damage states according to Hazus method for pre-code mid-rise building with concrete shear walls [23]

Damage level	Slight	Moderate	Extensive	Complete
ISDR	0.0021	0.0041	0.0105	0.0267

Table 3 Spectral displacements at threshold damage states according to [25]

Spectral displacement	Slight	Moderate	Extensive	Complete
S_d (m)	0.7 d_y	d_y	$d_y + 0.25\ (d_u - d_y)$	d_u

building typology, the parameters defining the capacity curve have been derived from simplified force-based procedures within the Risk-UE project (see [24, 25] for further details). In case of pre-code mid-rise RC buildings, the following values of yielding and ultimate displacements are suggested in [24]: for concrete shear walls $d_y = 0.03$ m and $d_u = 0.0904$ m; for dual systems $d_y = 0.0259$ m and $d_u = 0.0781$ m.

A more straightforward approach that can be followed in case of RC shear wall buildings is the introduction of material-level EDPs, which are usually represented by material strains. Although a correct determination of material strains requires the adoption of sophisticated numerical analyses, their use as EDPs for the construction of fragility curves seems to be more appropriate, since it allows to clearly monitor the evolution of the damage state of the building. By following an approach conceptually similar to that suggested in FEMA 356 [27], the damage thresholds (LS) reported in Table 4 are assumed in this work for the model with RC walls and pendulum frames.

In case of collaborating frames, further checks should be also carried out on frame elements. Having excluded the possibility of anticipated brittle failures, chord rotation is assumed as additional EDP for damage state definition, according to Standard Codes prescriptions (i.e., [17]), as follows: $\theta = \theta_y$ for LS2, $\theta = 3/4\ \theta_u$ for LS3, $\theta = \theta_u$ for LS4.

Figure 4 shows a comparison among the three above described criteria for defining the damage thresholds (according to Hazus, Risk UE and material-based EDPs), with reference to the model with pendulum frames and to the PO analysis with uniform distribution of lateral forces acting along the positive X direction. It can be seen that the damage thresholds based on ISDR are significantly different from the others reported in the graph. For the specific lateral force distribution shown in Fig. 4, the LS obtained from the evolution of the strain field in constituent material are instead almost coincident with those obtained from spectral displacements S_d. However, when considering other PO curves, some differences between the two approaches appear more evident, especially for higher damage levels (LS3 and LS4). Figure 5

Table 4 Material-based EDPs and definition of damage levels for RC core (or shear wall) buildings

Damage level	EDPs
LS1—Slight	C1: $\varepsilon_c = \varepsilon_{cracking}$ (cracking)
LS2—Moderate	C2: $\lvert\varepsilon_c\rvert = 3.5‰$ (in concrete cover) S1: $\varepsilon_s = \varepsilon_y$
LS3—Extensive	C3: $\lvert\varepsilon_c\rvert = 3.5‰$ (in confined concrete) S2: $\varepsilon_s = 1\%$
LS4—Complete	C4 = C3 for pre-code RC walls without confinement S3: Bucking/Failure of longitudinal rebars

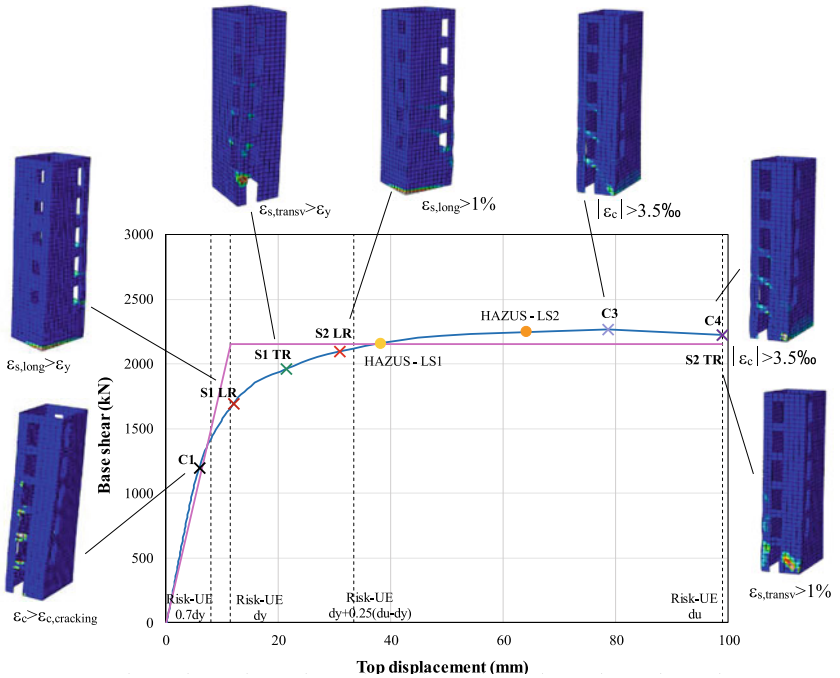

Fig. 4 Identification of the damage thresholds by considering different EDPs, with reference to the PO curve obtained with uniform lateral forces, acting along the positive X direction, and contours highlighting the evolution of strains in the materials with increasing loads. The results are relative to the model with pendulum frames

shows the application of the damage thresholds defined in Table 4 to the FE model with collaborating frames; in this case, further checks on frame elements are also carried out in terms of limit values of chord rotation. As can be observed, the inclusion of frame elements in the model has a negligible influence on the definition of LS1 and LS2, while it strongly affects the definition of the thresholds related to higher damage levels (especially complete damage). The limit values of chord rotation are reached in some columns of the first level belonging alignment C (see Fig. 1a), as a result of torsional effects related to the in-plan irregularity of the building (Fig. 5).

Generally speaking, this last approach seems the most suitable for RC core building, since it allows to monitor the different damage mechanisms that take place both in the frames and in the walls as loading increases.

The displacement values corresponding to the reaching of the damage thresholds depicted in Figs. 4 and 5, are also summarized in Table 5 to allow an easier comparison.

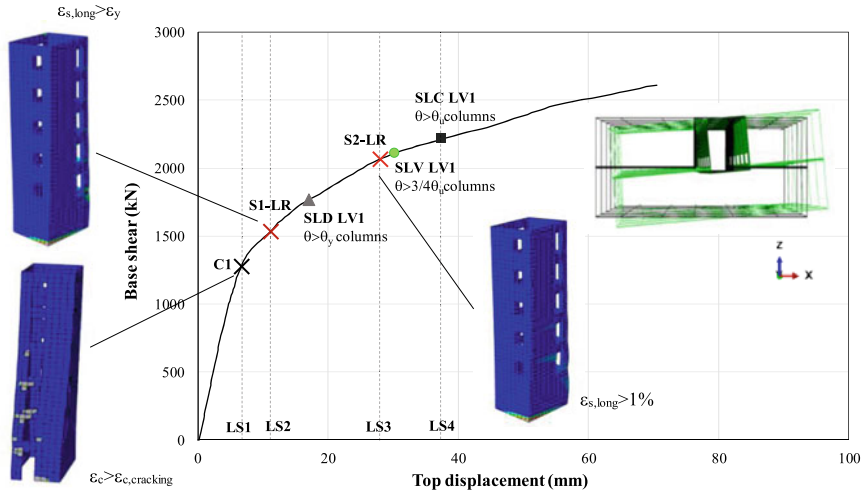

Fig. 5 Damage thresholds with reference to the PO curve obtained with uniform lateral forces, acting along the positive X direction, and contours highlighting the evolution of strains in the materials with increasing loads. The results are relative to the model with collaborating frames

Table 5 Top displacement values (in mm) corresponding to the reaching of the damage thresholds for the models with pendulum and collaborating frames (see Figs. 4 and 5)

	Pendulum frame			Collaborating frame		
	Risk-UE	Hazus	Material-based EDPs	Risk-UE	Hazus	Material-based EDPs + chord rotation control
LS1	8.04	38.11	5.62	12.12	39.95	6.75
LS2	11.48	64.01	12.10	17.31	70.52	11.21
LS3	33.35		30.83	30.61		28.03
LS4	98.95		98.95	70.52		37.46

5 Construction of Fragility Curves

Fragility Curves (FC) are obtained through a numerical code (implemented in VBA for Excel) and based on incremental static analysis [28]. The required input data are the number of storeys with the associated seismic masses, an appropriate selection of spectrum-compatible accelerograms, the 8 PO curves obtained from FE analyses with indication of the 4 considered damage states, the maximum PGA and the corresponding incremental value.

In this work, 125 accelerograms elaborated by the task group 4.2 within the WP4 "MARS" research activities (DPC-ReLUIS 2019–2021 Project) and referred to rigid soil are applied [29]. For each explored value of PGA, the program iteratively searches

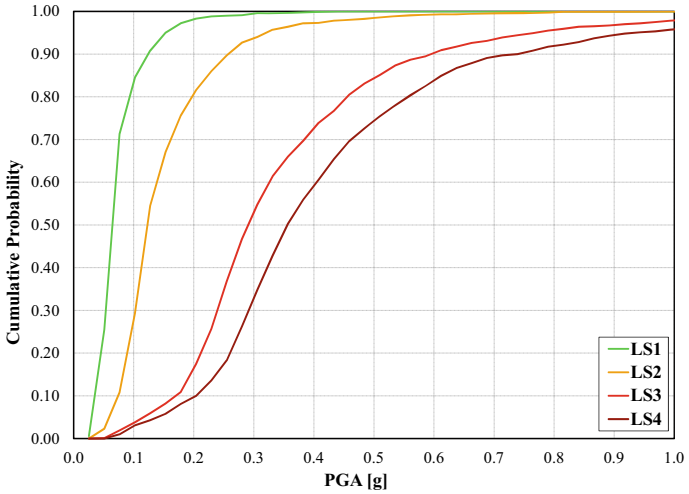

Fig. 6 Fragility curves for the considered core building with collaborating frames

for the performance point, by considering all the input spectra and bilinear capacity curves. With respect to the assessed target displacement, the probability of exceeding each of the damage state thresholds is evaluated and the cumulative probability is then calculated. Figure 6 shows the fragility curves obtained by considering the PO curves derived from the FE model with collaborating frames, and the LS definition reported in Fig. 5.

These numerical fragility curves are compared in Fig. 7 with empirical ones presented in [30] for Italian residential RC buildings with more than 4 storeys and designed for gravity loads only. Empirical curves, which are referred to moment resisting frame (MRF) buildings, were directly derived from post-earthquake damage data, on the basis of the maximum damage level attained by vertical structures and infills/partitions [30].

6 Conclusions

In this study, material based EDPs are proposed for the damage assessment of existing RC shear wall systems, and fragility curves are generated for a reference mid-rise RC core building. The specific features of core buildings, which are characterized by a very stiff response and usually present in-plan irregularities, are indeed different from those of framed structures, and displacement based EDPs might not be appropriate for a realistic definition of damage thresholds. The results obtained from the proposed procedure seem promising, even if further validation is required. Future works will be also focused on the influence of infill modelling on the results.

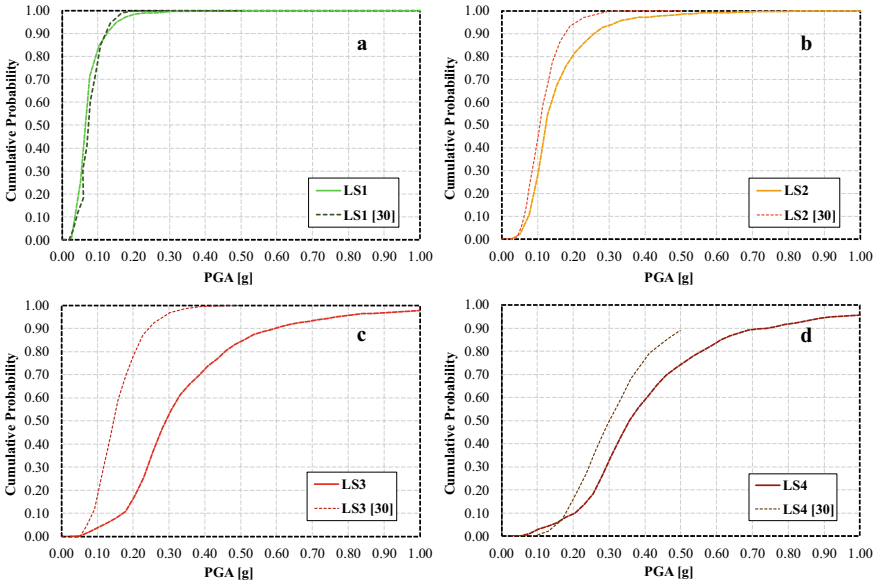

Fig. 7 Comparison between numerical FC for the considered core building with collaborating frames and empirical FC for MRF RC buildings with more than 4 storeys [30]

Acknowledgements This work was performed within DPC-ReLUIS2019-2021, WP4 "MARS".

References

1. ISTAT (2011) http://dati-censimentopopolazione.istat.it/Index.aspx?DataSetCode=DICA_EDIFICIRES. Last Accessed Feb 2020
2. Maio R, Tsionis G, Sousa ML, Dimova S (2017) Review of fragility curves for seismic risk assessment of buildings in Europe. In: Proceedings of the 16th world conference on earthquake. Santiago Chile, p 3823
3. Maio R, Tsionis G (2015) Seismic fragility curves for the European building stock. Technical report, European Commission, Brussels JRC
4. Masi A, Digrisolo A, Manfredi V (2015) Fragility curves of gravity-load designed RC buildings with regularity in plan. Earthq Struct 9:1–27
5. Akkar S, Sucuoğlu H, Yakut A (2005) Displacement-based fragility functions for low-and mid-rise ordinary concrete buildings. Earthq Spectra 21:901–927
6. Martinelli E, Lima C, De Stefano G (2015) A simplified procedure for nonlinear static analysis of masonry infilled RC frames. Eng Struct 101:591–608
7. Dumova-Jovanoska E (2000) Fragility curves for reinforced concrete structures in Skopje (Macedonia) region. Soil Dyn Earthq Eng 19:455–466
8. Bilgin H (2013) Fragility-based assessment of public buildings in Turkey. Eng Struct 56:1283–1294
9. Xiong C, Lu X, Lin X (2019) Damage assessment of shear wall components for RC frame–shear wall buildings using story curvature as engineering demand parameter. Eng Struct 189:77–88

10. Belletti B, Damoni C, Gasperi A (2013) Modeling approaches suitable for pushover analyses of RC structural wall buildings. Eng Struct 57:327–338
11. Belletti B, Vecchi F (2018) Implementation of steel constitutive model including buckling in PARC_CL 2.1 crack model. In: Proceedings of the 5th fib congress. Melbourne, Australia
12. ABAQUS user's manual. Dassault Systèmes Simulia Corp, Providence, RI, USA
13. AICAP Eds (2008) Seismic design of RC buildings—guide to the application of Eurocode 2, with reference to the Italian Code DM 14.1.2008. Pubblicemento
14. Toniolo G, Di Prisco M (2009) Design of structures volume. 2B—reinforced concrete. design for limit states (in Italian), 3rd edn. Zanichelli
15. EC2-Part1: Eurocode 2 (2015) Design of concrete structures—part 1–1 : general rules and rules for buildings. UNI EN 1992–1–1:2015, CEN, Brussels
16. Fajfar P (2000) A nonlinear analysis method for performance-based seismic design. Earthq Spectra 16:573–592
17. EC8-Part 1: Eurocode 8 (2013) Design of structures for earthquake resistance. UNI EN 1998–1:2013, CEN, Brussels
18. Belletti B, Cerioni R, Iori I (2001) Physical approach for reinforced-concrete (PARC) membrane elements. ASCE J Struct Eng 127:1412–1426
19. Cerioni R, Iori I, Michelini E, Bernardi P (2008) Multi-directional modeling of crack pattern in 2D R/C members. Eng Fract Mech 75:615–628
20. Bernardi P, Cerioni R, Michelini E, Sirico A (2016) Numerical modeling of the cracking behavior of RC and SFRC shear-critical beams. Eng Fracture Mechanics 167:151–166
21. Belletti B, Scolari M, Vecchi F (2017) PARC_CL 2.0 crack model for NLFEA of RC structures under cyclic loadings. Comput Struct 191:165–179
22. Belletti B, Vecchi F, Bandini C, Andrade C, Montero JS (2020) Numerical evaluation of the corrosion effects in PC beams without shear reinforcement. Struct Concr
23. FEMA. Multi-hazard loss estimation methodology—Hazus–MH 2.1 technical manual. earthquake model. www.fema.gov/plan/prevent/hazus
24. Lagomarsino S, Giovinazzi S (2006) Macroseismic and mechanical models for the vulnerability and damage assessment of current buildings. Bull Earthquake Eng 4:415–443
25. Milutinovic ZV, Trendafiloski GS (2003) RISK-UE—WP4 vulnerability of current buildings. Technical report, European Commission
26. Grunthal G (1998) European Macroseismic scale. Chaiers du Centre Européen de Gèodynamique et de Séismologie, vol. 15. Luxemburg
27. FEMA 356 (2000) Prestandard and commentary for the seismic rehabilitation of buildings. Washington DC, USA
28. Korkmaz KA (2008) Evaluation of seismic fragility analyses. In: Proceedings of the 14th world conference on earthquake engineering. Beijing, China
29. Smerzini C, Galasso C, Iervolino I, Paolucci R (2014) Ground motion record selection based on broadband spectral compatibility. Earthq Spectra 30(4):1427–1448
30. Rosti A, Del Gaudio C, Rota M, Ricci P, Di Ludovico M, Penna A, Verderame GM (2020) Empirical fragility curves for Italian residential RC buildings. Bullettin Earthq Eng

Seismic Assessment of RC Buildings Considering the Influence of Vertical Irregularities: Framed and Wall-Frame Structures

Maria-Victoria Requena-Garcia-Cruz, Rita Couto, Rita Bento, and Antonio Morales-Esteban

1 Introduction

The reinforced concrete (RC) buildings represent a significant percentage of the cities' building stock in many countries all over the world. In the case of Portugal, in 2011, these buildings were 50% of the total stock of the country [1]. Furthermore, they host 60% of the national population since they mainly contain dwellings.

This study is focused on the RC structures located in the neighbourhood of "*Alvalade*" (Lisbon). Characteristics such as their date of construction, number of floors and RC structural configuration have been obtained from the blueprints available at the "*Arquivo Municipal do Lisboa*". Later, they were all gathered in ArcGIS [2]. A total of 2,249 buildings have been identified, of which, 28% are RC structures. They were mainly constructed before 1980 (97% of them), when the first demanding Portuguese seismic code was published [3]. Furthermore, 70% of them were built between 1950 and 1970. Two structural configurations have been identified: framed and wall-frame, which represent 46% and 42% of the RC structures of the area, respectively [4].

M.-V. Requena-Garcia-Cruz (✉) · A. Morales-Esteban
Department of Building Structures and Geotechnical Engineering, University of Seville, Av. Reina Mercedes, 2, 41012 Seville, Spain
e-mail: mrequena1@us.es

A. Morales-Esteban
e-mail: ame@us.es

R. Couto · R. Bento
CERIS, Instituto Superior Técnico, Universidade de Lisboa, Av. Rovisco Pais, 1049-001 Lisboa, Portugal
e-mail: rita.g.couto@tecnico.ulisboa.pt

R. Bento
e-mail: rita.bento@tecnico.ulisboa.pt

R. Bento et al. (eds.), *Seismic Behaviour and Design of Irregular and Complex Civil Structures IV*, Geotechnical, Geological and Earthquake Engineering 50,
https://doi.org/10.1007/978-3-030-83221-6_24

According to this assessment, two RC buildings of both structural configurations have been selected as case studies. They are representative of the current building stock of Lisbon and present a considerable seismic vulnerability. First, they were built between 1950 and 1980, before the application of the seismic codes. Second, they share similar constructive and structural characteristics with respect to the rest of the European RC buildings constructed during that period. Third, they have short columns, soft-floors, smooth rebars and irregularities in height and plan.

In fact, irregularities can be commonly found in RC buildings. They are mainly divided into two groups that can be both present in this kind of buildings: in plan or in elevation. Different approaches have been proposed to properly account for their effects [5]. Works like [6, 7] highlighted the importance of adopting adequate nonlinear modelling strategies and assumptions to predict the suitable seismic response of asymmetric buildings or buildings with vertical irregularities. The typical vertical irregularities identified in the present study have been: (i) the heterogenic distribution of infills; and (ii) the irregular height of columns. These types of irregularities are often related to the generation of additional torsional effects and soft-floor mechanisms that can worsen the seismic performance of RC buildings [8].

Hence, this paper aims to analyse the influence of these irregularities on the seismic behaviour of RC buildings. Different versions of the buildings have been defined varying the position of the infills and the height of the columns and the shear walls. Nonlinear static analyses have been carried out and the N2 method and its extended version have been considered to assess their seismic behaviour.

2 Seismic Assessment

This section describes the case-study RC buildings and the procedures adopted in their seismic behaviour assessment.

2.1 Description of the Buildings

The case-study buildings are representative buildings of each structural configuration (Fig. 1). Building A is a five-storey RC wall-frame, with a total height of 15.5 m. The stairs and the lift are in the central bays of the X direction. There is also a shear wall in this direction in the centre of the plan. In the ground floor, it has a soft-story configuration. Building B is a six-storey framed RC building, with a total height of 17.0 m. The height of all floors is irregular. Furthermore, it has short columns between the ground and the first floor. In this case, the first floor has a soft-storey configuration.

In both cases, the slabs are of 15 cm of thickness, which are supported in both orthogonal directions by the vertical elements. The characteristic corresponding to both buildings are listed in Table 1. The mass of the structure has been calculated

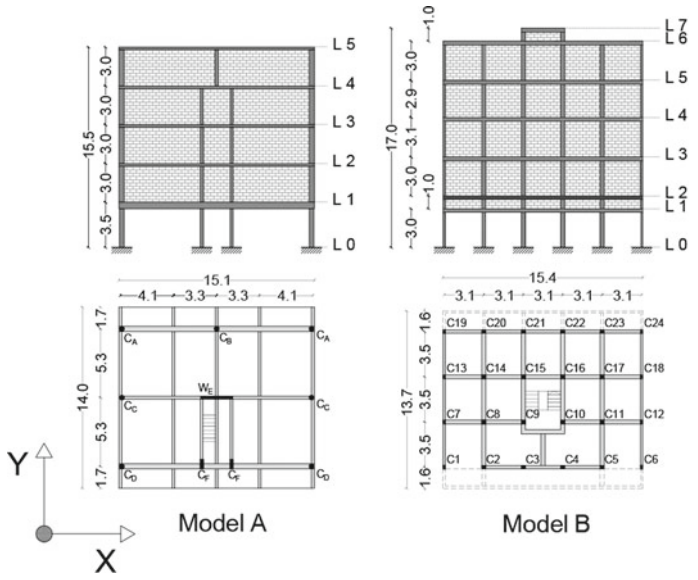

Fig. 1 Structural schemes and plans of the buildings

Table 1 Geometrical characteristics of the buildings

Type	Total mass (Tn)	Columns		Beams		Walls	
		bxh (cm)	Rebars (cm^2)	bxh (cm)	Rebars (cm^2)	bxh (cm)	Rebars (cm^2)
Building A	720	23 × 25–25 × 87	L: 0.63–7.29 T: 0.18–0.71	13 × 31–25 × 68	L: 2.26–33.58 T: 1.48	250 × 25	15.78
Building B	1507	20 × 31–30 × 40	L: 0.31–38.79 T: 1.58	10 × 40–20 × 60	L: 0.63–16.46 T: 2.11–2.47	–	–

Note L and T refer to Longitudinal and Transversal rebar. Rebar ratios are maximum and minimum values

considering the dead and the live loads. The dead loads have included the self-weight of the structural elements, the internal partitions, the exterior infills, the ceiling and the pavement. The live loads have been defined according to Part-1 of Eurocode 8 (EC8-1) [9] for residential buildings.

Table 2 Material properties

Concrete	f_c (MPa)	ε_c (‰)	ε_{cu} (‰)	E_c (GPa)
Cover	28	2	200	30
Core	28	2	2	30
Steel	f_y (MPa)	f_u (MPa)	ε_{su} (‰)	E_s (GPa)
Ribbed rebar	370	360	240	210
Smooth rebar	222	216	168	126

Note Compressive maximum strength (fc), strain at maximum strength (εc), ultimate strain (εcu) and modulus of elasticity (Ec) for concrete; yielding strength (fy), ultimate strength (fu), ultimate strength (εsu) and modulus of elasticity (Es) for steel

2.2 Numerical Modelling

The different 3D numerical models of the case-study buildings have been developed in OpenSEEs [10]. Columns, beams and shear wall have been modelled using 'nonlinearBeamColumn' elements to consider their nonlinear behaviour. The 'Section Fibre' approach has been used to discretize sections into fibres. The uniaxial materials 'Concrete04' [11] and 'Steel02' [12] have been used to model the concrete cover and core and the steel, respectively. The safety factor defined in EC8-1 [9] has been used to reduce the strength of the materials. The effects of the smooth rebar have been taken into account by modifying the steel constitutive law as in [13]. The materials properties are shown in Table 2. The RC beams have been connected by rigid diaphragms at each floor level due to the effect of the slabs. The masses have been applied at each floor's centre. Due to the negligible results, the accidental eccentricity has not been considered.

2.3 Infills Modelling

The infills panels have been modelled through the two-diagonal truss approach [14]. In order to model the diagonal trusses, a four branches force–displacement relationship has been determined as defined in [15] and a uniaxial hysteretic material has been implemented in Opensees. The influence of openings has been taken into account by reducing the initial stiffness of the infills by λ_0 as considered in [8]. This approach does not distinguish between the type of opening (door or window). Following these authors' suggestions, the infills' strength has been reduced by 50% only in the case of doors. The models' infills thickness ranges from 10 to 30 cm in both cases. Table 3 shows the infills properties.

Table 3 Infills material properties

t (m)	G_w (MPa)	E_w (MPa)	τ_{cr} (MPa)	α
0.25	1240	4092	0.28	0.05

Note Thickness of the infill (t), elastic shear modulus (Gw), modulus of elasticity of the masonry (Ew), shear cracking stress (τcr), elastic modulus of the frame (Ew), post-capping degrading branch coefficient (α)

2.4 Sensitivity Analysis

According to the *Alvalade*'s survey, two types of vertical irregularities have been identified: (i) the distribution of infills; and (ii) the height of columns. Horizontal irregularities have been observed in the blueprints and although their influence should also be studied, it is not the goal of this paper.

Different configurations have been defined varying the position of the infills and the height of the columns. Regarding the infills, three different distributions have been considered: bare frame, partially and totally infilled. For the bare frame models, no infills have been added. In the case of the partially infilled models, they have been added in all the floors except for the ground floor. For the totally infilled models, infills have been considered for all floors. Concerning the height of the columns, three situations have been studied: regular and irregular (soft-story mechanism) height and the presence of short columns in an intermediate floor. Figure 2 shows the schematic configurations of the nine analysed versions of the buildings. Short columns have been added in different locations. For Building A, they have been included in all the floor's area. For Building B, the short columns have been added in the first frame (similarly to the real configuration of the building).

3 Analysis of the Results

The results obtained are shown and analysed in this section. In Table 4, the fundamental periods for each model in the directions analysed are listed. All models' periods are lower in the X direction due to the higher stiffness of the structures in this direction. It can be observed that the periods have been reduced when increasing the number of infills. This is due to the increase of the model's stiffness and the alterations of the models' seismic performance.

The pushover curves for the bare frame, partially and totally infilled models have been obtained considering two horizontal load patterns in each direction: uniform mass-proportional pattern; and modal pattern (proportional to the fundamental mode of vibration). Nevertheless, only the curves for the modal load pattern have been plotted in Figs. 3, 4 and 5 for bare frame, partially and totally infilled models, respectively. This pattern is sufficiently representative of the inertia actions affecting the models and produces the most demanding results. The curves have been normalised

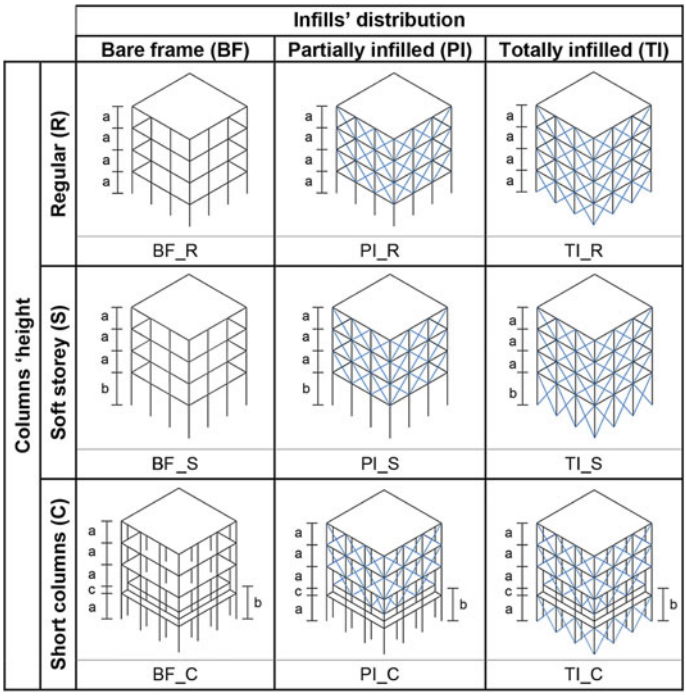

Fig. 2 Schematic configurations analysed for Building A and B with respective nomenclature. Where: *a*, *b* and *c* are 3 m, 4 m and 1 m, respectively. The blue trusses represent the infills panels' distribution

Table 4 Fundamental periods (s) for each model and each analysis in both directions

Building	Dir	Bare frame			Partially infilled			Totally infilled		
		BF_R	BF_S	BF_C	PI_R	PI_S	PI_C	TI_R	TI_S	T_C
A	X	0.55	0.56	0.53	0.35	0.37	0.35	0.32	0.34	0.12
	Y	0.63	0.65	0.65	0.36	0.42	0.36	0.18	0.19	0.14
B	X	0.69	0.84	0.83	0.41	0.52	0.61	0.33	0.36	0.44
	Y	0.84	0.93	1.00	0.51	0.65	0.71	0.38	0.40	0.48

to compare the results. To do so, the base shear force (V_b) and top displacement (d) have been divided by each model's entire weight (W) and height (H_t), respectively.

The pushover curves for the bare frame models differ considerably (Fig. 3). For Building A, the influence of both types of irregularities has been negligible. However, for Building B, the columns' irregularities have affected the response of the models, reducing the capacity up to a 25%.

Adding the infills partially has strongly affected all the models' response (Fig. 4). The maximum strength has been increased up to 300% and 25% for Building A and B,

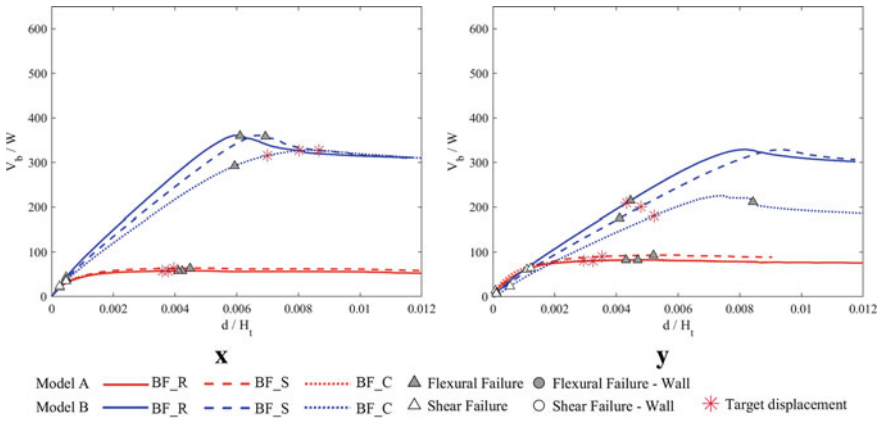

Fig. 3 Pushover curves and failures for the bare frame models in the **x** and **y** directions

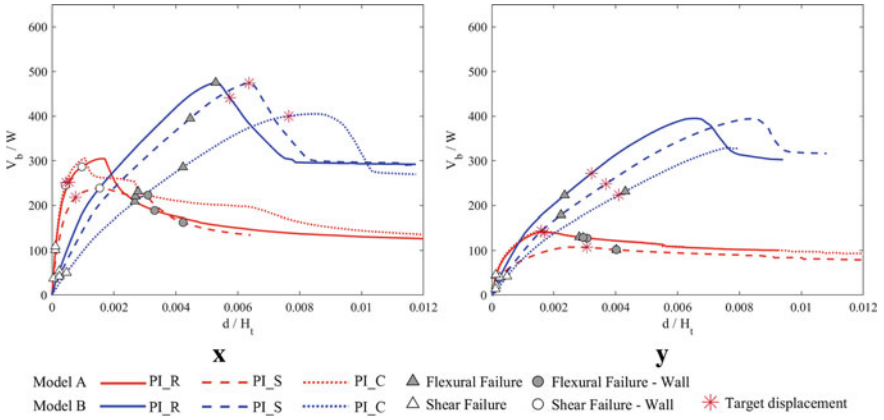

Fig. 4 Pushover curves and failures for the partially infilled models in the **x** and **y** directions

respectively. However, this increase has not been that outstanding in the Y direction due to the lower infills' strength. Despite the resistance improvement, the shear and bending failures have been obtained for smaller displacement. Thus, the increase of the capacity does not lead to the improvement of the seismic performance. The columns' irregularities have affected Building B more than Building A. For Building A, the R and S configurations have resulted in similar initial stiffness and resistance. The S configuration has presented the lowest capacity. For Building B, the initial stiffness and capacity have been reduced considerably for each irregularity.

Regarding the totally infilled models (Fig. 5), Building A's capacity has significantly increased compared to the partially infilled ones. However, for Building B, the difference has been negligible. For Building A, the most seismic vulnerable structural elements are located at the ground floor for the partially infills models; for

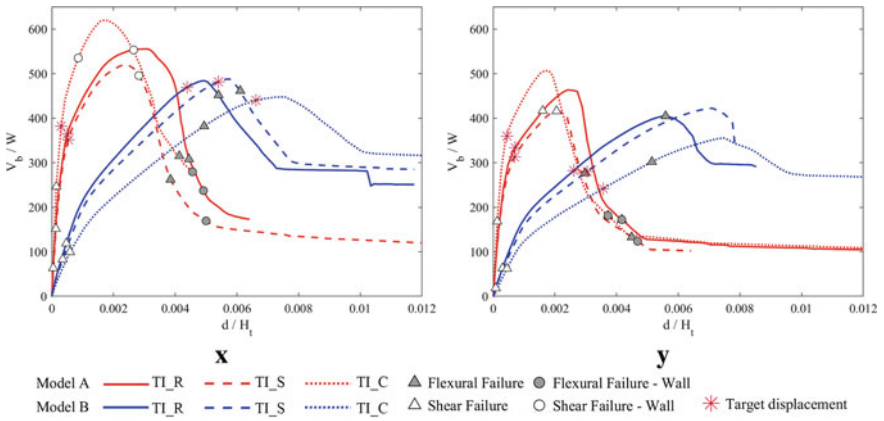

Fig. 5 Pushover curves and failures for the totally infilled models in the **x** and **y** directions

totally infilled models, the seismic demand of these elements have been reduced. In the case of Building B, the effect of horizontal load pattern has been homogeneously distributed in height, resulting in minor differences between the partially and the totally infilled configurations.

The safety verification of the RC buildings has been checked in accordance to the recommendations of the Part 3 of Eurocode 8 EC8-3 [16]. The seismic demand in terms of chord rotation and internal shear forces should be smaller than the correspondent capacity values. Hence, it has been demonstrated that the models do not comply the safety checks for the shear behaviour. By contrast, they comply the flexural bending requirements. Therefore, retrofitting solutions should be applied in order to prevent shear collapse.

The damage distribution in the vertical elements (columns and shear wall) for the partially and totally infilled models (PI_R, PI_S, PI_C, TI_R, TI_S and TI_C) for buildings type A and B is presented in Fig. 6. Only the worst direction has been shown. The bare frame models have not been included since it is not a real configuration. Different levels have been determined according to the Demand Capacity Ratio (DCR) for flexural and shear failures. It has been assumed that the Significant Damage limit state (SD) is attained when the ratio between the story shear (V_{demand}) or the storey chord rotation (θ_{demand}) and the capacity is equal or greater than 1 ($V_{demand}/V_R \geq 1$ and $\theta_{demand}/\theta_{um,SD} \geq 1$, respectively), where V_R is the cyclic shear resistance and $\theta_{um,SD}$ is the ultimate total chord rotation capacity for the SD limit. [16]. For the flexural damage, two more levels have been determined to visualise the elements that almost reached the DCR for the SD limit state ($\theta_{demand}/\theta_y > 0.9$) and the elements that already exceeded the chord for yielding ($\theta_{demand}/\theta_y > 1$). Thus, for each model, the distribution of damage when the first vertical structural element reaches the criteria for the SD limit state for chord rotation or shear force, has been displayed.

In the case of Building A, for the partially infilled configuration (PI), the vertical elements have been damaged in the ground floor despite of the columns' irregularity.

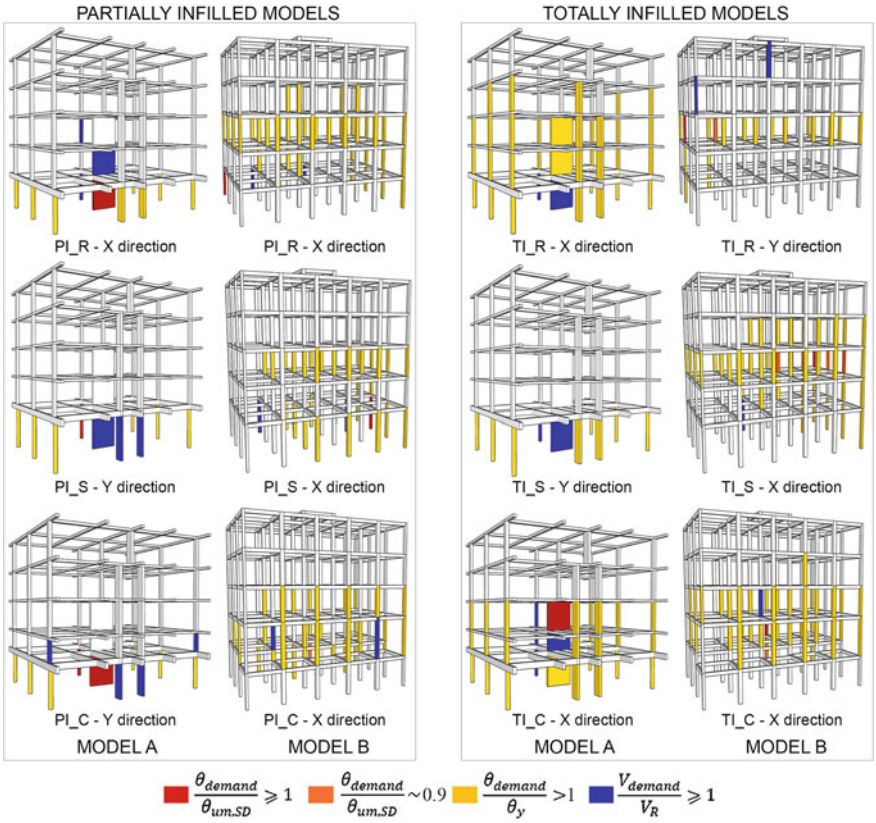

Fig. 6 Damage in vertical elements for the configurations that presented the highest number of elements damaged

Regarding the totally infilled situation, for the regular configuration (TI_R), the damage has been located on the first four floors and the ground floor's wall has collapsed by shear. For the soft-storey configuration (TI_S), the damage has been concentrated on the soft-storey floor and one wall and column have been collapsed by shear. For the short columns configuration (S), the damage has been concentrated on the floor with short columns and on the surrounding floors.

In the case of Building B, the damage on the vertical elements has been concentrated on the middle floors for all irregularities. However, for the soft-storey (S) and short columns (C) configurations, the damage has been also located on the soft-storey floor and on the floor with short columns, respectively.

4 Conclusions

Results have shown that the increase on the number of infills have reduced the fundamental period of the buildings. It has been demonstrated that when the infills are regularly distributed, the seismic performance of the building, can be improved. In contrast, when irregularly distributed, the results have worsened. The infills' influence has been similar in both building's directions. However, modifying the infills distribution in plan (i.e. creating an in plan irregularity) could affect the seismic performance of RC buildings due to the infill's influence. After the infills failure, all curves tend to present an alike residual capacity i.e. the capacity of the bare frame models.

For Building A, the partially infilled soft-story configuration (PI_S) has led to the worst seismic performance with lower values of initial stiffness and resistance and poor performance. This configuration has concentrated the damage on the ground floor and produced the shear failure of the columns and the wall mainly at this level. For Building B, the partially infilled short column configuration (PI_C) has been the worst configuration. This has been due to the shear failure of the short columns and to the bending failure of the columns of the floor above. In fact, this is the real configuration of the building. Based on the results obtained, retrofitting measures should be taken into account to prevent the shear failure of the RC building structures analysed to comply with the safety requirements of the EC8-3.

Acknowledgements The authors would like to acknowledge the financial support of *Fundação para a Ciência e a Tecnologia* (FCT, *Ministério da Educação e Ciência*, Portugal) through the scholarship BL105/2019 through the FCT Research Program: MitRisk—Framework for seismic risk reduction resorting to cost-effective retrofitting solutions, POCI-01-01456-Feder-031865. In addition, the scholarship provided by the VI-PPI of the University of Seville is acknowledged.

References

1. Silva V, Crowley H, Varum H, Pinho R, Sousa L (2015) Investigation of the characteristics of Portuguese regular moment-frame RC buildings and development of a vulnerability model. Bull Earthq Eng 13(5):1455–1490. https://doi.org/10.1007/s10518-014-9669-y
2. Environmental Systems Research Institute (ESRI) (2011) ArcGIS desktop: release 10
3. Diário do Governo (1983) Regulamento de Segurança e Acções para Estruturas de Edifícios e Pontes (RSA), Decreto-Lein. 235/83, Lisbon, Portugal. (in Portuguese)
4. Couto R, Requena-García-Cruz, M, Bento R, Morales-Esteban A (2020) Seismic capacity and vulnerability assessment considering ageing effects. Case study: three local Portuguese RC buildings. Bull Earthq Eng. https://doi.org/10.1007/s10518-020-00955-4
5. De Stefano M, Pintucchi B (2008) A review of research on seismic behaviour of irregular building structures since 2002. Bull Earthq Eng 6(2):285–308. https://doi.org/10.1007/s10518-007-9052-3
6. Stathopoulos KG, Anagnostopoulos SA (2005) Inelastic torsion of multistorey buildings under earthquake excitations. Earthquake Eng Struct Dynam 34(12):1449–1465. https://doi.org/10.1002/eqe.486

7. Chintanapakdee C, Chopra AK (2004) Seismic response of vertically Irregular frames: response history and modal pushover analyses. J Struct Eng 130(8):1177–1185. https://doi.org/10.1061/(ASCE)0733-9445(2004)130:8(1177)
8. Dolšek M, Fajfar P (2008) The effect of masonry infills on the seismic response of a four storey reinforced concrete frame-a probabilistic assessment. Eng Struct 30(11):3186–3192. https://doi.org/10.1016/j.engstruct.2008.04.031
9. CEN (2004) Eurocode 8: design of structures for earthquake resistance—part 1: general rules, seismic actions and rules for buildings. European Committee for Standardization. 1 (English): 231. (Authority: The European Union per Regulation 305/2011, Directive 98/34/EC, Directive 2004/18/EC)
10. McKenna F, Fenves G, Scott M (2007) OpenSees: open system for earthquake engineering simulation. Pacific Earthquake Engineering Research Center, University of California, Berkeley. http://opensees.berkeley.edu
11. Popovics S (1973) A numerical approach to the complete stress-strain curve of concrete. Cem Concr Res 3(5):583–599. https://doi.org/10.1016/0008-8846(73)90096-3
12. Filippou FC, Popov EP, Bertero VV (1983) Effects of bond deterioration on hysteretic behaviour of reinforced concrete joints. Report to the National Science Foundation, Berkeley, California. http://www.ce.berkeley.edu/~filippou/Research/Publications/Reports/EERC-83-19.pdf
13. Caruso C, Bento R, Sousa R, Correia AA (2019) Modelling strain penetration effects in RC walls with smooth steel bars. Mag Concr Res 71(17):894–906. https://doi.org/10.1680/jmacr.18.00052
14. Celarec D, Ricci P, Dolšek M (2012) The sensitivity of seismic response parameters to the uncertain modelling variables of masonry-infilled reinforced concrete frames. Eng Struct 35:165–177. https://doi.org/10.1016/j.engstruct.2011.11.007
15. Panagiotakos TB, Fardis MN (1996) Seismic response of infilled RC frame structures. In: Proceedings of the 11th world conference on earthquake engineering, pp 1–8
16. European Union (2005) Eurocode-8: design of structures for earthquake resistance. Part 3: assessment and retrofitting of buildings. Belgium

Analysis of the Influence of Atriums in Seismic Performance of RC Primary School Buildings

Beatriz Zapico-Blanco, Maria-Victoria Requena-Garcia-Cruz, Emilio Romero-Sánchez, Jaime de-Miguel-Rodríguez, and Antonio Morales-Esteban

1 Introduction

Most of the Spanish primary school buildings were built prior to the enforcement of the PGS-1 [1], the seismic code that first introduced a seismic action value for Huelva. The code provided basic considerations, only applicable to the design of new buildings. It was not until 1994 that a more demanding and enforcing code was released: the NCSE-94 [2]. This code was more rigorous, including a probabilistic seismic hazard analysis and more advanced guidance for new buildings seismic design. Consequently, buildings constructed prior to that date were designed with very little or no seismic considerations.

Moreover, primary schools present a high child-to-adult ratio, which compromises the effectiveness of the evacuation plans [3]. In addition to this, it has been observed that children can be severely traumatized by catastrophic events [4] and have a comparatively difficult recovery process.

B. Zapico-Blanco (✉) · M.-V. Requena-Garcia-Cruz · E. Romero-Sánchez · J. de-Miguel-Rodríguez · A. Morales-Esteban
Department of Building Structures and Geotechnical Engineering, University of Seville, Av. Reina Mercedes, 2, 41012 Seville, Spain
e-mail: bzapico@us.es

M.-V. Requena-Garcia-Cruz
e-mail: mrequena1@us.es

E. Romero-Sánchez
e-mail: eromero13@us.es

J. de-Miguel-Rodríguez
e-mail: jdemiguel@us.es

A. Morales-Esteban
e-mail: ame@us.es

R. Bento et al. (eds.), *Seismic Behaviour and Design of Irregular and Complex Civil Structures IV*, Geotechnical, Geological and Earthquake Engineering 50,
https://doi.org/10.1007/978-3-030-83221-6_25

In brief, the school community is characterized by a low seismic resilience [5]. In this context, the European project named PERSISTAH (*Projetos de Escolas Resilientes aos SISmos no Território do Algarve e de Huelva*, in Portuguese) aims to increase the seismic resilience of the schools located in the Algarve (Portugal) and Huelva (Spain) regions [6]. The south-western Iberian Peninsula is affected by far away earthquakes of long return period and of large magnitude [7], due to its proximity to the Eurasia-Africa plate boundary. Buildings in this area have been severely damaged in the past by relevant seisms such as the 1344, 1531, 1722, 1755, 1859 and 1909 earthquakes [8]. In order to achieve the goal of the project, two parallel paths are undertaken: to increase the awareness of the school community and to analyse the seismic performance of the buildings. This paper concentrates on the latter.

When assessing the seismic vulnerability of the existing building stock, several paths can be followed. In this case, the assessment was performed at a regional level, which requires data of a large number of buildings. Resorting to detailed inspections in this scenario is not realistic, and the use of simplified methods, such as the Index Building Approach, for gathering enough data and information is required [9]. The first step to assess the vulnerability of the school buildings is to properly classify the population under study. Several groups which could potentially share a similar seismic behaviour have been identified. Within each group, a representative building has been selected as index of the typology, which has been assessed in detail. The conclusions of the analysis, as well as the retrofitting schemes prescribed, can thus be conceived at typology level, and then be slightly adapted to each individual building.

With the aim of determining the characteristics that define each typology, several sensitivity analyses have been done, quantifying the relative relevance of each feature studied. This paper is focused on the existence of an atrium and its position. This is the most recurrent irregularity of the population studied and a potential weak point of these building, together with the existence of short columns in the basement, which is the object of separated study [10]. To assess the influence of this parameter, different versions of the index building model, varying the position of the atrium, have been analysed. Nonlinear static analyses have been used to study the respective seismic performance of these models, with special attention to the effect of the addition of the atrium on the torsional behaviour and hence the modal participation mass, which could invalid the method (see Sect. 3.3).

2 Characterization of the Schools

First, the schools of the Spanish province of Huelva (139 in total) have been characterized. The school complexes are composed of one to six individual buildings, adding up to 267 buildings. Data about the buildings have been gathered employing the available information sources in each case: original and rehabilitation projects, aerial images, visits, *ad-hoc* surveys sent to the schools, etc. Then, the information has been processed. First, a general classification, based on the structural type (Fig. 1a), has been carried out. The buildings present three main structural types:

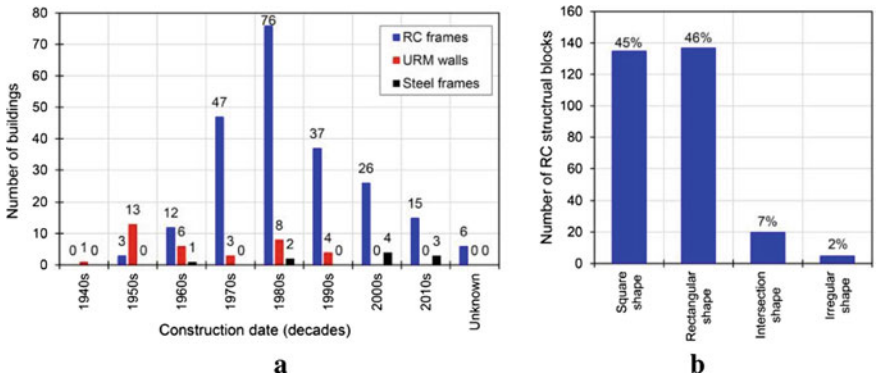

Fig. 1 **a** Number of buildings per construction date and structural system, **b** Number and percentage of RC structural blocks based on their general geometry

reinforced concrete frames (RC), unreinforced masonry, and steel structures. The most represented type is the RC structure which is a 83% of the total (Fig. 1a).

The work described in this paper is focused on the study of the aforementioned group and the paper will refer exclusively to it from now onwards. The RC structures studied present structural joints, which divide the buildings in different structural blocks that need to be analysed separately. 297 blocks have been identified.

The RC blocks have been divided into groups depending on their geometrical shapes: *square*, *rectangular*, *intersection* and *irregular* (Fig. 1b). *Square* blocks are the most regular, with similar dimensions in both directions. *Rectangular* blocks are characterised by a predominant dimension, which is at least twice as big as the orthogonal one. *Square* and *rectangular* are the predominant types, with a 45% and a 46% of the total population, respectively. The other two groups are not representative (<10% of the population). The present paper focuses on the *rectangular* RC blocks, since they are potentially more vulnerable than the *square* ones, given their comparatively larger asymmetry.

Rectangular RC blocks can be divided in four subgroups: *small*, *medium*, *large* and *L shape*. Again, the first two groups are the most representative ones, being 42% and 40% of the population, respectively. *Small rectangular* blocks are very regular in both plan and elevation, and present one single storey. *Medium rectangular* blocks are similar to them, but bigger in plan and with two storeys, which makes them potentially more vulnerable to the seismic action. The index building selected for the present work belongs to this sub-group.

In these buildings, the RC structure is completed with perimeter infill walls. Infill walls can influence the seismic behaviour of the buildings, especially when irregularly distributed [11]. A recurrent characteristic of the population studied is the presence of atriums. Where an atrium is present, some infill walls are removed and others are added, creating an irregularity and potentially changing the seismic performance of the building. In the present work, the sensitivity of this typology to the existence and the position of the atriums is studied.

In the case of *rectangular blocks*, one or more atriums are present in 39% of the buildings, while it has not been possible to verify their presence in 33% of them. Atriums can be found in the corner or in the middle bays of the block and on one or two floors. They can be distributed either symmetrically or asymmetrically.

3 Method

3.1 Building Configurations

The analysis has been carried out considering a case study/index building (Fig. 2). The index building has been selected on the basis of its representativeness of the typology under study (*Medium regular RC blocks*) and because of the completeness of the available information about it (blueprints and specifications). The building is a two-storey RC structure constructed during the 70s, like most of the buildings of this typology. It presents nine RC frames in the Y direction and four irregular bays in the X direction. The building has a slab on the ground floor, which generates short columns. This is another important irregularity of the building with a strong effect on its seismic behaviour, as can be seen in [10]. All floors are composed of ribbed slabs spanning in the Y direction. The building's initial situation (IS) can be observed in Fig. 2.

The geometrical characteristics of the RC frames are listed in Table 1. The RC compressive strength (f_{ck}) is 17.5 MPa and the steel minimum yield stress (F) is

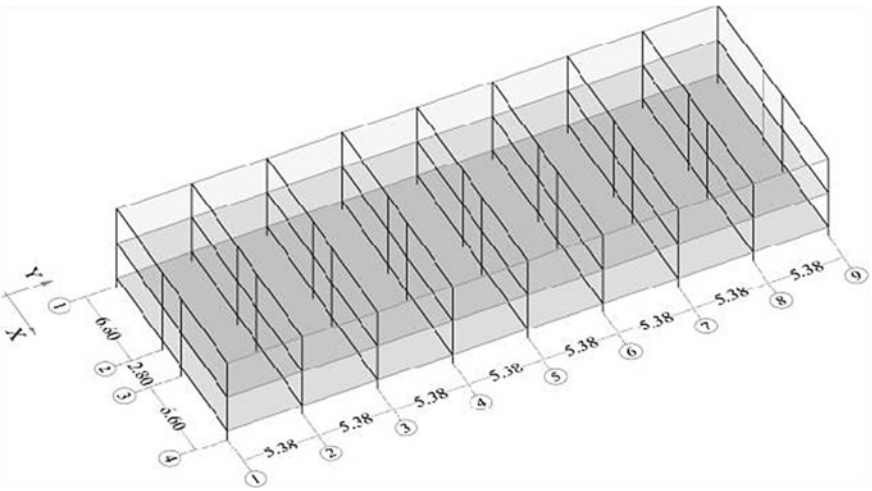

Fig. 2 3D model of the case study building, Initial Situation (IS)

Table 1 Geometrical characteristics of the RC frames

Structural element	Columns	Load beams	Tied beams
Dimensions	40 × 30 cm	40 × 30 cm	30 × 30 cm
Longitudinal Rebar	4Ø12 mm	Top: 2Ø12 mm	Top: 2Ø12 mm
		Lower: 4Ø16 mm	Lower: 2Ø12 mm
Transversal rebar	Ø6 mm/20 cm	Ø6 mm/20 cm	Ø6 mm/20 cm

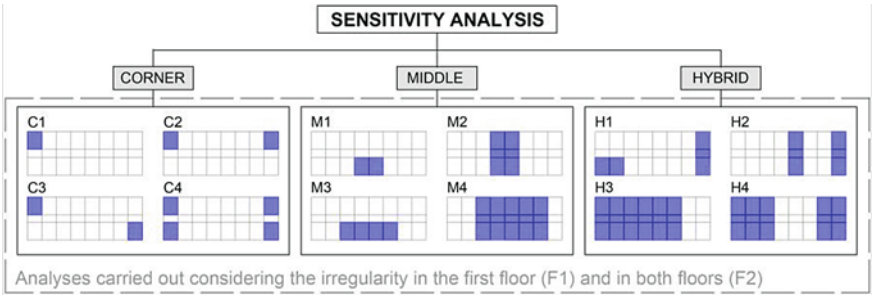

Fig. 3 Different positions of the atrium considered in the sensitivity analysis

420 MPa. The modulus of elasticity (E_c) are 25 000 MPa and 200 000 MPa for the concrete and the steel, respectively.

3.2 Sensitivity Analysis Set-Up

In the typology studied, atriums are located in either the corners (C), the middle bay (M) or both (i.e. hybrid, H). Based on this, the configurations presented in Fig. 3 have been used to study the influence of the position of the atrium on the seismic performance of the blocks. Combinations of the possible locations which were not observed in the population or which were not logical have not been considered.

3.3 Nonlinear Static Analysis

The capacity of the models has been determined by means of nonlinear static analyses performed with OpenSEEs [12] in both orthogonal directions of the models (X and Y). It is important to notice that the existence of an atrium might lead to torsional effects, which can in turn invalid the results from nonlinear static analyses. Hence, for

this specific case, a validation of the procedure is carried out considering the results of modal analyses, as will be described. Two load patterns have been taken into account as established in the EC8-1 [13]: uniform and modal. However, reference will be made only to the modal load pattern since it is the most restrictive one [10]. From these modal analyses, the eigen vectors in each direction (X and Y) for all of the master nodes (located in the middle of each slab) have been obtained according to the corresponding mode of vibration. The solver *fullGenLapack* (available in OpenSEEs) has been used, since the models analysed present few interactions. This solver performs a displacement normalization of the eigenvectors. It has been checked that the principal mode of vibration of each model according to each direction is lower than mode 1 and 2. If the principal modes of vibration are higher than those, then, it would mean that not enough mass is moving and the torsional effects are heavily affecting the analyses. Therefore, it proves that the procedure is valid in this specific case. Then, these vectors have been mass-normalised, resulting in the effective modal pattern.

The frames have been modelled using fibres and OpenSEEs nonlinear elements. The concrete and the steel have been simulated using 'Concrete04' and 'Steel02' materials. The concrete slabs present significant stiffness. Therefore, their effects have been simulated by connecting the RC beams by a rigid diaphragm at each floor level. Infills have been modelled following the two diagonal truss approach as in [14]. Only perimeter infills, which present a minimum thickness of 200 mm, have been included in the model. Internal partitions have not been considered due to their slenderness (thickness < 100 mm), which makes their contribution to the global behaviour negligible. Special attention has been paid to the modelling of the short columns, taking into account the geometrical characteristics of the building.

4 Analysis of the Results

The results obtained from the analyses are shown and discussed in this section. In Fig. 4, the pushover curves obtained for each of the models are plotted. Although both uniform and modal load patterns have been taken into account, only the curves corresponding to the modal pattern are shown, since they are the most restrictive.

It can be observed that the changes produced in the behaviour of the building by the addition of an atrium are different when considering the X and the Y direction. The curves have been normalized by considering the total weight (W) and the total height (H_t) of the structure.

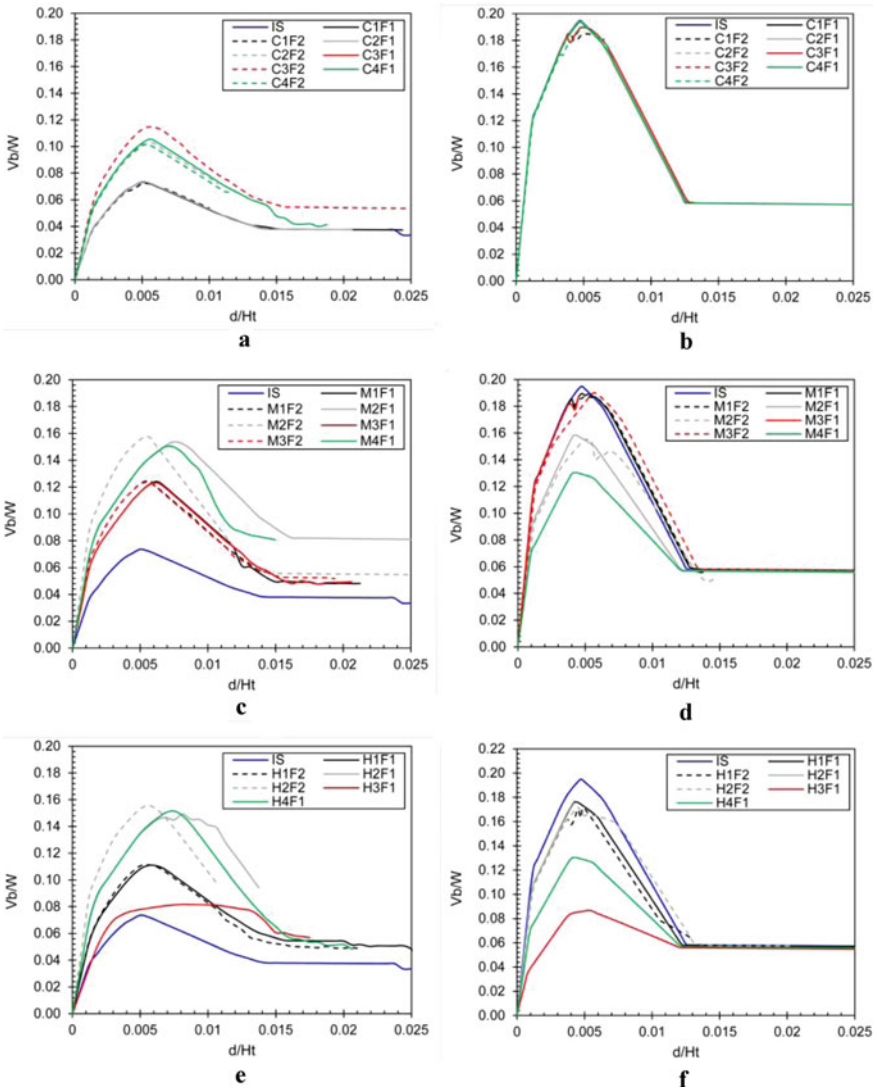

Fig. 4 Pushover curves for models with (**a, b**) corner, (**c, d**) middle and (**e, f**) hybrid atriums. X and Y direction curves are on the left and right, respectively. Irregularity is present only in the first floor for the F1 models and in both floors for the F2 models

4.1 Pushover in the X Direction

The maximum capacity of the building (IS) in the X direction is of about 7500 kN, for a displacement of the control node of 0.04 m. The residual capacity is of about 4000 kN, after a displacement of 0.1 m, when the infills fail.

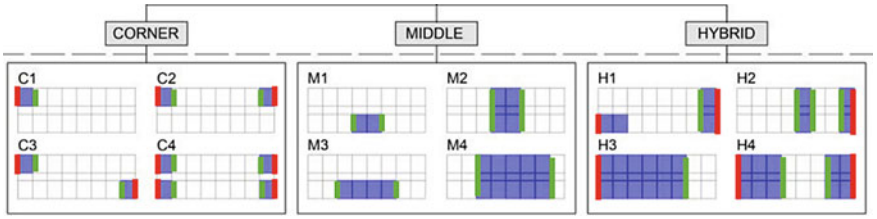

Fig. 5 Added (green) and removed (red) infill walls related to each atrium configuration, affecting the X direction

The addition of one or more atriums has, in most of the cases selected, a positive effect on the global strength, the initial stiffness, the residual capacity, the displacement for maximum shear and the point of the infills failure of the models. The figure below shows the added (green) and removed (red) infill walls related to each atrium configuration, contributing to the capacity in X.

In particular, when the atrium added is located at the building corners (see Figs. 4a and 5), the total capacity is increased up to a 46% and the peak takes place for a displacement of the control node slightly larger than in the IS. The initial stiffness in these models is also slightly bigger.

When the atrium is located in a middle bay (see Figs. 4c and 5), the total capacity of the model can even double the IS, as does the initial stiffness and residual capacity. The maximum shear peak takes place at a larger displacement, up to 0.06 m. This effect is more important when the atrium is pass-through (M2 and M4). The same applies to the models when the atriums are located in hybrid positions (see Figs. 4e and 5), especially in H1 and H2. In model H3, the increase in capacity is not so significant and a torsional effect is observed (see Fig. 7).

4.2 Pushover in the Y Direction

The maximum capacity of the building (IS) in the Y direction is of about 20000 kN, for a displacement of the control node of 0.04 m. The residual capacity is of about 6000 kN, after a displacement of 0.1 m, when the infills fail.

The addition of one or more atriums in the Y direction diminishes the global strength of the building, while the initial stiffness, residual capacity and displacement for maximum shear and point of infills failure remain similar. This is due to the fact that the addition of an atrium entails the removal of contributing perimeter infill walls and the addition of new ones, in different locations depending on the atrium configuration. In the case of the Y direction, as can be seen in Fig. 6, the number of walls added (in green) are equal or less than the number of walls removed (in red).

In particular, when the atrium is located at the building corners (models C1 to C4, see Figs. 4b and 6), the reduction in capacity is negligible.

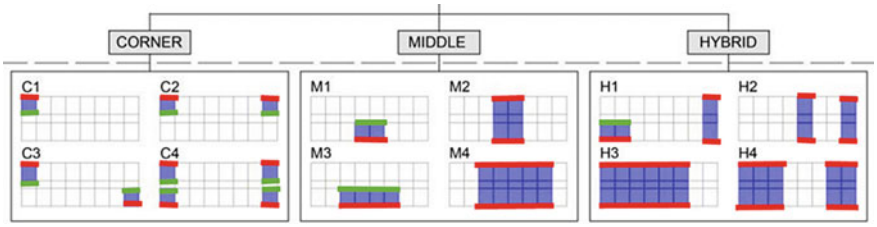

Fig. 6 Added (green) and removed (red) infill walls related to each atrium configuration, affecting the Y direction

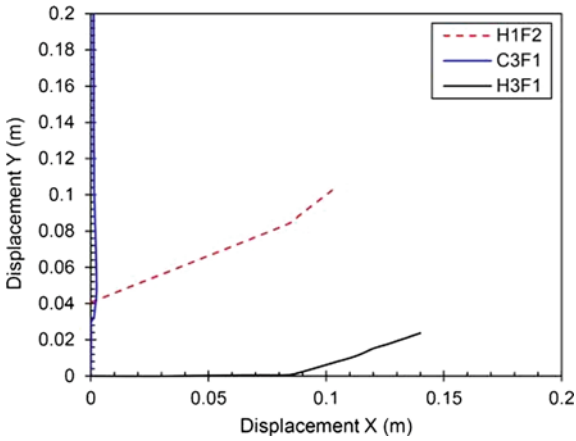

Fig. 7 Displacement of the control node. Solid lines: pushover in the X direction. Dashed lines: pushover in the Y direction

When the atrium is located in a middle bay (see Figs. 4d and 6), two situations are possible: (a) if the atrium is only in one side of the building (models M1 and M3), its influence is not noticeable; (b) if the atrium is pass-through (M2 and M4), the total capacity of the building is reduced up to a 35%, depending on the total area of the atrium.

When the atriums are located in hybrid positions (see Figs. 4f and 6), a reduction of the total resistance has been observed in all the models, in this case, up to a 58% compared with the IS model.

In both directions, whether the atrium is present both in the ground floor and in the first floor or only on the ground floor, no effect in the results have been observed.

4.3 Torsional Effects

Torsional effects, which are not present in the behaviour of the original building, arise when the atrium is in a non-central location and/or the atrium to building surface

ratio is high (see Fig. 7). This effect is especially noticeable in models H1F2 (see Fig. 4e), and H3F1 (see Fig. 4f).

5 Conclusions

In this work, the schools of the Spanish region of Huelva, mainly RC framed buildings from the 70s, have been studied. It has been observed that the existence of atriums is a recurrent irregularity and a seismic vulnerability. This paper has focused on quantifying the relative relevance of this irregularity by means of a sensitivity analysis. To do so, different versions of an index building model (rectangular in plan), varying the position of the atrium, have been analysed. Nonlinear static analyses have been used to study the seismic performance of these models.

The results show that the existence of an atrium produces quite different effects in the X and Y directions.

When a pushover is performed in the X direction (see Fig. 2), six infill panels, located at each side of the long dimension of the building, per floor contribute to the resistance of the building if no atrium is present. The addition of an atrium entails the introduction of additional contributing infill walls, separating the interior of the building from the new open space (which was not present in the original configuration). Those extra walls will contribute to the global capacity of the building. However, given the configuration of the building under study, a new atrium will introduce additional walls only in the X (short) direction. Figure 5 shows the added (green) and removed (red) infill walls related to each atrium configuration, contributing to the capacity in X. The infills added are located closer to the centre of the building than the perimeter ones, which could also increase the total stiffness of the system. These positive effects have been observed in all the models studied; although they could be impaired by the torsional effects caused by a big non-central atrium (see case H3F1 in Fig. 4e).

By contrast, when a pushover is performed in the Y direction (see Fig. 2), 16 infill panels per floor contribute to the resistance of the building in the initial situation. Adding an atrium can cause the reduction in number of contributing infill panels in this direction, especially, when the atrium is pass-through and panels are eliminated in both facades (see Fig. 6). This negative effect can be observed only at a total capacity level (shear strength at the peak), but not in the shape of the capacity curve, which indicates that the stiffness of the system remains basically unchanged. The existence of torsion enhances this effect, as can be seen in H3F1 (see Fig. 4f). In this model, then total number of infills is not reduced, and yet, the peak shear reaches a lower value when compared with the IS.

In the light of the results observed it can be concluded that not taking into account the effects of an atrium, when analysing a block similar to the index building, could lead to unrealistic results. However, the presence of the atrium has an effect on the response of the building only when located at the ground floor.

Further studies are required to determine to what extent the effects described depend on the number of bays, on the total length of the façades and/or on the length to width ratio of the building.

Acknowledgements This work has been supported by the INTERREG-POCTEP Spain-Portugal programme and the European Regional Development Fund through the 0313_PERSISTAH_5_P project and the VI-PPI of the University of Seville by the granting of a scholarship.

References

1. Presidency of Goverment [Presidencia del Gobierno] (1968) Seismic code PGS-1. Part A. [Norma sismorresistente PGS-1. Parte A]
2. Spanish Ministry of Public Works [Ministerio de Fomento de España] (2002) Spanish Seismic Construction Code of Buildings [Norma de Construcción Sismorresistente: Parte general y edificación (NSCE-02)], Spain
3. Arup International (2013) Arup International Development for the Global Program for Safer Schools. Characteristics of safer schools
4. Galante R, Foa D (1986) An epidemiological study of psychic trauma and treatment effectiveness for children after a natural disaster. J Am Acad Child Psychiatry. 25(3):357–363. https://doi.org/10.1016/S0002-7138(09)60257-0
5. Masten AS (2014) Global perspectives on resilience in children and youth. Child Dev 85(1):6–20. https://doi.org/10.1111/cdev.12205
6. Estêvão J, Ferreira M, Morales-Esteban A, Martínez-Álvarez F, Fazendeiro Sá L, Requena-García-Cruz MV, Segovia-Verjel ML, Oliveira C (2018) Earthquake resilient schools in Algarve (Portugal) and Huelva (Spain). In: 16th European conference on earthquake engineering, pp 1–11
7. Amaro-Mellado JL, Morales-Esteban A, Martínez-Álvarez F (2017) Mapping of seismic parameters of the Iberian Peninsula by means of a geographic information system. CEJOR. https://doi.org/10.1007/s10100-017-0506-7
8. Sá L, Morales-Esteban A, Durand Neyra P (2018) The 1531 earthquake revisited : loss estimation in a historical perspective. Bull Earthq Eng 16(10):4533–4559. https://doi.org/10.1007/s10518-018-0367-z
9. Lagomarsino S, Giovinazzi S (2006) Macroseismic and mechanical models for the vulnerability and damage assessment of current buildings. Bull Earthq Eng 4(4):415–443. https://doi.org/10.1007/s10518-006-9024-z
10. Requena-Garcia-Cruz MV, Morales-Esteban A, Durand-Neyra P, Estêvão JMC (2019) An index-based method for evaluating seismic retrofitting techniques. Application to a reinforced concrete primary school in Hulva. PlosOne 14(4):e0215120. https://doi.org/10.1371/journal.pone.0215120
11. Dolšek M, Fajfar P (2008) The effect of masonry infills on the seismic response of a four storey reinforced concrete frame-a probabilistic assessment. Eng Struct 30(11):3186–3192. https://doi.org/10.1016/j.engstruct.2008.04.031
12. McKenna F, Fenves GL, Scott MH (2000) OpenSees: open system for earthquake engineering simulation
13. European Union (2004) Eurocode 8: design of structures for earthquake resistance. Part 1: general rules, seismic actions and rules for buildings, Belgium
14. Razzaghi MS, Javidnia M (2015) Evaluation of the effect of infill walls on seismic performance of RC dual frames. Int J Adv Struct Eng 7:49–54. https://doi.org/10.1007/s40091-015-0081-x

Modified Modal Response Spectrum Analysis of Plan Irregular Highly Torsionally-Stiff Structures Under Seismic Demands

Saúl López, Daniel Pancardo, Mario De Stefano, Gustavo Ayala, and Valerio Alecci

1 Introduction

Modal response spectrum analysis is the most widespread analysis method for seismic assessment and design of building structures. It is used in the standard force-based procedures given in most of the building codes and in displacement-based procedures for assessment/design considering serviceability and ultimate limit states such as the N2 Method [1]. However, the use of modal spectral analysis is strictly valid for elastic systems, hence, it can only provide a rough estimation of the maximum response of structures in the inelastic range under design demands associated with the ultimate limit state.

Moreover, an issue of concern is the application of modal response spectrum for the analysis of plan irregular buildings which may exhibit torsional response in the

S. López (✉) · D. Pancardo
Programa de Ingeniería Civil, FES Acatlán UNAM, Avenida Alcanfores y San Juan, Totoltepec s/n, Santa Cruz Acatlán, Naucalpan de Juárez, Mexico
e-mail: selopezrios@comunidad.unam.mx

D. Pancardo
e-mail: dan.pancardo@comunidad.unam.mx

M. De Stefano · V. Alecci
Dipartimento Di Architettura, Università Degli Studi Di Firenze, Piazza Brunelleschi 6, 50121 Florence, Italy
e-mail: mario.destefano@unifi.it

V. Alecci
e-mail: valerio.alecci@unifi.it

G. Ayala
Coordinación de Ingeniería Estructural, Instituto de Ingeniería UNAM, Ciudad Universitaria, Mexico City, Mexico
e-mail: gayalam@iingen.unam.mx

R. Bento et al. (eds.), *Seismic Behaviour and Design of Irregular and Complex Civil Structures IV*, Geotechnical, Geological and Earthquake Engineering 50,
https://doi.org/10.1007/978-3-030-83221-6_26

inelastic range of behaviour. De Stefano and Pintucchi, [2], showed, through an extensive parametric analysis of one-storey shear building models, that the key parameter to assess the suitability of modal response spectrum analysis is the ratio of uncoupled torsional to lateral frequencies, Ω. For moderately torsional stiff systems ($\Omega < 1.5$) maximum inelastic floor rotations are smaller than the corresponding elastic ones, thus, the use of modal response spectrum analysis of elastic models provides a conservative estimate of the maximum inelastic floor rotations and maximum displacement of the flexible side of the plan. However, for highly torsional stiff systems ($\Omega \geq 1.5$), such as buildings with shear-walls, maximum floor rotations and displacements of the flexible side of inelastic buildings are larger than those of elastic ones, therefore, the results of modal response spectrum analysis of elastic models are unconservative.

For this reason, this paper presents an artifice that allows an improved estimation of the in-plan displacement profile of highly torsional stiff systems with monosymmetric rectangular plan and given stiffness/strength eccentricity values. The artifice consists of performing modal response spectrum analysis of a modified elastic model where the actual centre of mass of the building is displaced a distance termed additional mass eccentricity, e_{ad}, which is a function of the plan aspect ratio, B/L; the uncoupled translational period, T_y; the stiffness/strength eccentricity, e_{sx}, and the seismic behaviour factor q. Modal spectral analysis of such model provides a sufficient approximation of the ratio of maximum displacement of the flexible side of the building to that of the centre of mass, δ_F/δ_{CM}, and the floor displacement profile under inelastic response of the actual structure. The results obtained from the linear analysis of the modified elastic model with e_{ad}, are corrected by an appropriate scaling factor which accounts for the inelastic displacement demand at the centre of mass.

Design values for e_{ad} were defined from an extensive parametric analysis of highly torsionally stiff one-storey shear buildings. The seismic input considered was a suite of 7 accelerograms from the European Ground Motion Database compatible with the EC8 elastic design spectrum for Zone I and Soil Type B, [3]. Dynamic analyses of the case studies were performed from which δ_F/δ_{CM} was obtained. From the results of such analysis, e_{ad} was calculated via an iterative scheme consisting of a series of dynamic analyses of elastic models where eccentricity was varied until δ_F/δ_{CM} approximated that of the corresponding inelastic model. Equations to calculate e_{ad} were derived from linear and nonlinear regression analyses for its use in seismic assessment and design applications.

2 Case Studies

The case studies considered, herein denoted as X-Systems, were one-storey shear buildings with rigid diaphragm of rectangular plan B x L, representative of buildings with perimetral shear walls, previously studied by De Stefano and Pintucchi, [2]. Even though the limitations of shear buildings models are well recognized [4], they can provide useful insight on the global behaviour of MDOF systems. Moreover,

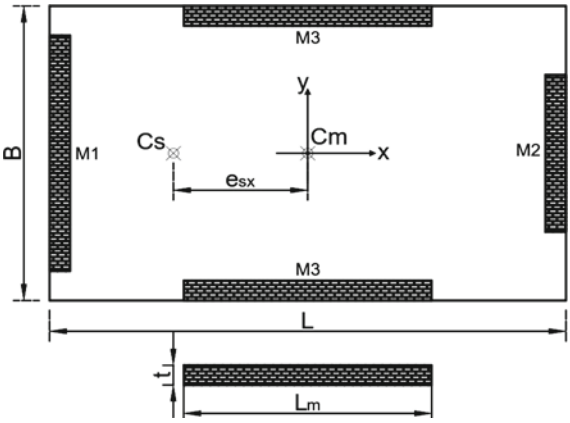

Fig. 1 Structural plan configuration of the X-System case studies

considering that the present study required several linear and nonlinear dynamic analysis, shear beam models were deemed appropriate for such purpose.

The X-systems are composed of four vertical wall-type elements of thickness t and length L_m, distributed along the perimeter of the building (Fig. 1). The thickness to length ratio, t/L_m, of all elements is equal to 0.1 and their out-of-plane stiffness is equal to 0.001 of its in-plane stiffness. The plan configuration considered was monosymmetric, i.e., stiffness eccentricity is relative to a single horizontal axis. This type of configuration was chosen as seismic demands of monosymmetric systems usually provide an upper bound of demands for two-way asymmetric plan buildings, [5]. The centre of mass was located at the geometric centre of the plan and the centre of stiffness at a known distance from the centre of mass. The strength eccentricity was considered the same as the stiffness eccentricity, i.e., the centre of strength coincides with the centre of stiffness, which is representative of new buildings designed with current codes, [2].

The case studies were built for a wide range of values of the main parameters involved in torsional response, which covers those of actual buildings:

- Plan aspect ratio, B/L, of 0.50, 0.75 and 1.0
- Uncoupled translational period, T_y, of 0.05 to 2.0 s in increments of 0.05.
- Uncoupled translational stiffness ratio, R_T, with values of 1.0, 1.5 and 2.0.
- Stiffness/strength eccentricity along the x direction, e_{sx}, between 0.05 and 0.30 in increments of 0.05. It should be noted that for the type of plan configuration of the case studies, Ω depends on e_{sx} [2].
- Lateral strength associated with seismic reduction factors, q, between 1.0 and 6.0, which encompass the ductility classes given by EC8, [3].

3 Seismic Ground Motions

The seismic ground motions considered in this study were the horizontal orthogonal components of a suite of 7 earthquake records from the European Strong Motion Database, compiled by De Stefano and Pintucchi [2], which are compatible with the EC8 elastic design spectrum corresponding to Zone 1 and Soil Type B. For the purpose of reducing the dispersion of dynamic response of the case studies, the records were scaled using as intensity measure the maximum spectral acceleration of the elastic response spectrum with 5% damping ratio of both horizontal components at the fundamental period of the structures, $Sa_m(T_1)$ [6]. Hence, for every one-storey model, each pair of accelerograms of the set was scaled in such a way that $Sa_m(T_1)$ matched the ordinate of the elastic design spectra at the same period. Moreover, it was checked that the ordinates of the mean elastic response spectrum of all the earthquake records was at least 90% of those of the design spectrum in the period range $0.2T_1$ to $2T_1$ as required by EC8. In most cases the scaling scheme employed complied with such criterion; for the few cases where it did not, the scale factors were modified accordingly.

4 Modelling and Analysis of the Case Studies

The parametric analysis was performed using the OpenSees software [7]. To define the strength of the structural elements for different levels of inelastic action, modal-spectral analysis of the elastic models was performed using the reference design spectrum reduced by seismic reduction factors q between 1.0 and 6.0. Since it was considered that the centre of strength of the case studies was located at the same point as their centre of stiffness, *i.e.*, $e_{sx} = e_{rx}$, the strength of the structural elements was distributed in proportion to its stiffness.

Linear and nonlinear dynamic analyses were carried out using both horizontal components of the earthquake records selected to assess the seismic response of the case studies. The wall-type elements were modeled as in-plane uniaxial flexural elements. The solution of the dynamic equilibrium equation was attained via Newmark's average constant acceleration method, along with the Newton–Raphson method. The damping of the system was modeled using Rayleigh's model, considering a damping ratio of 5% for the first two modes of vibration.

5 Nonlinear Response

The trends of the dynamic response of the case studies can be identified in Fig. 2 where plots of the median δ_F/δ_{CM} *vs.* T_y are shown for systems with $e_{sx} = 0.10$ and 0.20, $B/L = 1.0$, $R_T = 1.0$ and for q values from 2 to 6. The Ω values corresponding to

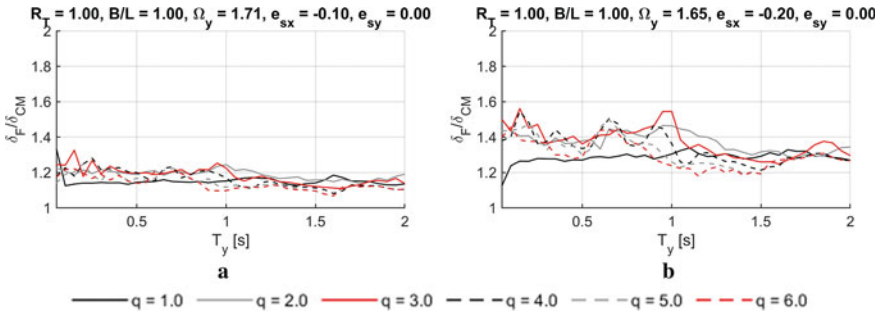

Fig. 2 Displacement amplification of the flexible side, δ_F/δ_{CM}, as a function of uncoupled period, T_y, for inelastic one-storey models q = 2 to 6 with B/L = 0.5; R_T = 1.0, and– **a** e_{xs} = 0.10, **b** e_{xs} = 0.20

the combination of such eccentricity values and the rest of the parameters are 1.71 and 1.65, respectively. As can be observed in such figure, as e_{sx} is larger, δ_F/δ_{CM} increases, which is due to e_{sx} being larger as Ω is smaller for the plan configuration of the case studies. Furthermore, δ_F/δ_{CM} is significantly larger for all q values, particularly for T_y smaller than 1.0 which is consistent with the findings of De Stefano and Pintucchi, [2]. Therefore, modal spectral analysis of elastic models underestimates the displacement response of the flexible side in most cases.

6 Additional Mass Eccentricity

In this study, an artifice is proposed to achieve a better estimation of maximum inelastic response for extremely torsionally stiff systems via modal spectral analysis. It consists on providing an additional mass eccentricity, e_{ad}, that when added to the actual eccentricity in the elastic model, e_{sx}, leads to approximately the same δ_F/δ_{CM}, with respect to the actual centre of mass, under inelastic response (Fig. 3). Therefore, the design eccentricity of the elastic model is defined as,

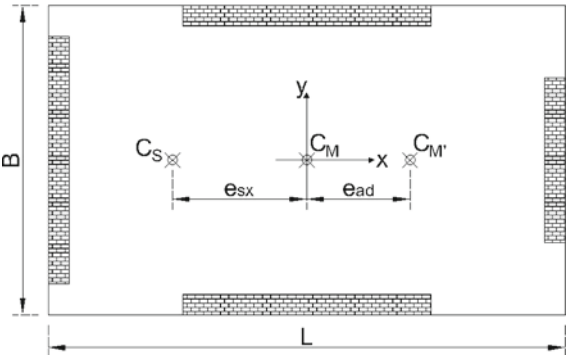

Fig. 3 Additional mass eccentricity in structural model

$$e_{dx} = e_{sx} + e_{ad} \tag{1}$$

The linear analysis of the elastic model with this modified eccentricity will provide an estimation of the δ_F/δ_{CM} only. To calculate the seismic demands of the structure associated to the actual in-plan displacements of the inelastic system, the results obtained from modal spectral analysis of the elastic model with e_{ad} should be corrected with the following factor

$$C_F = \frac{\delta_{CM}}{\delta_{CM'} - \theta_{CM'}\, e_{ad}} \tag{2}$$

where δ_{CM} is an approximation of the actual inelastic displacement of the centre of mass obtained from modal spectral analysis of an elastic model without e_{ad} or via pushover analysis of an inelastic model; $\delta_{CM'}$ and $\Theta_{CM'}$ are, respectively, the displacement and rotation of the displaced centre of mass, C_M', obtained from modal spectral analysis of the elastic model with e_{ad}.

e_{ad} was determined via an iterative scheme consisting of a series of linear dynamic analyses of elastic models with the same properties, i.e., B/L, R_T, Ω, of a given inelastic model with lateral strength in terms of the q-factor. Specifically, e_{sx} was varied in constant steps of 0.01 until the median δ_F/δ_{CM} of all records of the modified elastic model exceeded the value sought and bisection was carried out afterwards to define the final e_{ad} value considering a tolerance of 5%. This tolerance was considered appropriate as the target is the median value for the whole set of records.

By means of such iterative scheme, e_{ad} was calculated for each of the case studies considered. A positive value of e_{ad} denotes that C_M should be displaced a distance e_{ad} along the x-axis in the opposite direction to C_S. Conversely, a negative value implies displacing CM towards CS.

Figure 4 depicts the plots of T_y *vs.* e_{ad} for B/L = 1.0, R_T = 1.0 and e_{sx} = 0.10 and 0.20, and q-values 2, 4 and 6. In general, e_{ad} exhibits a decreasing relation with respect to T_y which is more pronounced and less smooth as e_{sx} is larger. For e_{sx}

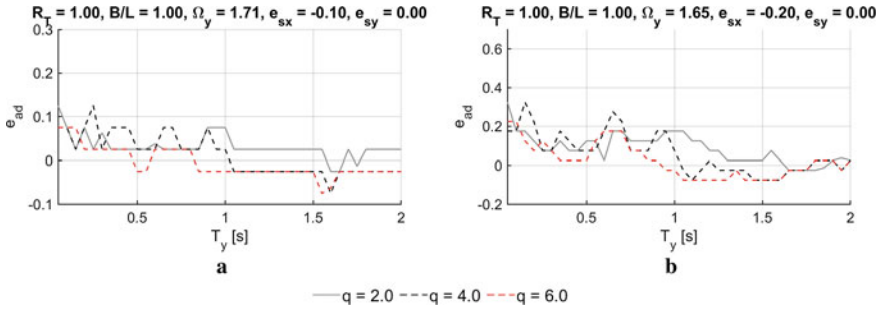

Fig. 4 Additional eccentricity, e_{ad}, as a function of uncoupled period, T_y, for inelastic one-storey models with B/L = 1.0; R_T = 1.0, q = 2, 4, 6 and two eccentricity values– **a** e_{xs} = 0.10, **b** e_{xs} = 0.20

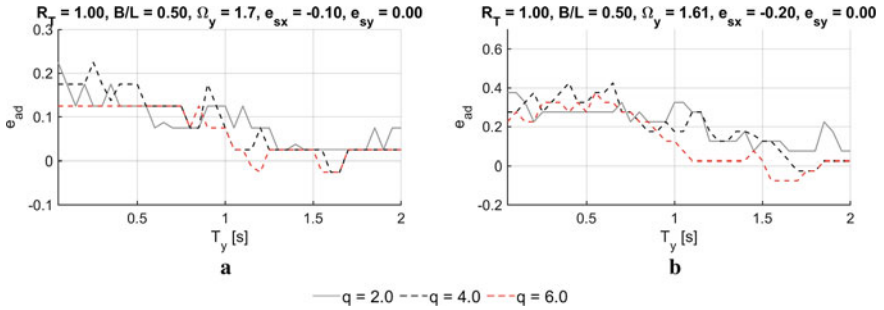

Fig. 5 Additional eccentricity, e_{ad}, as a function of uncoupled period, T_y, for inelastic one-storey models with B/L = 0.5; R_T = 1.0, q = 2, 4, 6 and two eccentricity values—**a** e_{xs} = 0.10, **b** e_{xs} = 0.20

= 0.10 and for all q values, e_{ad} fluctuates around 0.05 for $T_y \leq 1.0$ s, decreases to values close to 0 at $T_y = 1.3$ s, point from which it remains approximately constant; the maximum value of e_{ad} is 0.12 at $T_y = 0.25$ s. For $e_{sx} = 0.20$ e_{ad} shows larger variations with respect to T_y. For q = 2, e_{ad} fluctuates around 0.10 for $T_y \leq 1.0$ s and decreases to values close to 0 at $T_y = 1.5$ s, point from which it remains approximately constant except for a peak at $T_y = 1.8$ s. The maximum e_{ad} value is 0.15 at $T_y = 0.4$ s. For q = 4, e_{ad} fluctuates around 0.12 for $T_y \leq 1$ s and decreases to values around–0.05 at $T_y = 1.1$ s, period after which it increases up to a value close to 0 at $T_y = 1.6$ s. The maximum e_{ad} value is 0.25 at $T_y = 0.65$ s. For q = 6, e_{ad} fluctuates around 0.08 for $T_y \leq 0.7$ s and decreases to values around -0.05 at $T_y = 1.1$ s, after which it increases to a value close to 0 at $T_y = 1.6$ s and remains approximately constant for the rest of the periods. The maximum e_{ad} value is 0.20 at $T_y = 0.7$ s.

Figure 5 depicts the plots of T_y *vs.* e_{ad} for B/L = 0.5, R_T = 1.0, e_{sx} = 0.10 and 0.20, and q = 2, 4, 6; where it can be observed that the trends followed for such systems are similar to those of systems with B/L = 1.0, however, e_{ad} values are larger since Ω values are smaller.

7 Equations for the Calculation of e_{ad}

Equations for the calculation of e_{ad} were derived via regression analysis. Firstly, e_{ad} dependency on period T_y was defined using linear regression considering three regions: (1) a constant value for $T_y \leq 1.0$ s; (2) a decreasing linear function for 0.5 $< T_y \leq 1.5$ s; (3) a constant function for $T_y > 1.5$ s. Subsequently, the coefficients obtained from the linear regression were fitted considering as independent variables the parameters B/L, R_T, e_{sx} and q. This fitting was carried out via an artificial neural network using MATLAB [8]. Such neural network consists of a two-layer feedforward network with a logarithmic sigmoid transfer function in the hidden layer and

a linear function in the output layer. From the data obtained in the parametric function, 70% was used to train the neural network by means of a Levenberg–Marquardt backpropagation function. 15% was used for the validation of the neural network, where the mean squared error was considered for the assessment of performance. The remaining 15% was used for testing the neural network. The equations derived from the linear and nonlinear regression scheme are the following:

$$e_{ad} = \begin{cases} \beta_1; & T_y \leq T_1 \text{ s} \\ \frac{\beta_2 - \beta_1}{T_2 - T_1}\left(T_y - T_1\right) + \beta_1; & T_1 < T_y \leq T_2 \text{ s} \\ \beta_2; & T_2 < T_y \end{cases} \tag{3}$$

$$T_1 = \left\{ \begin{matrix} 1.0s;\ e_{sx} \leq 0.20 \\ 1.2s;\ e_{sx} > 0.20 \end{matrix} \right\} \quad T_2 = \left\{ \begin{matrix} 1.5s;\ e_{sx} \leq 0.20 \\ 1.7s;\ e_{sx} > 0.20 \end{matrix} \right\} \tag{4}$$

$$\beta_1 = -0.0113 + \frac{0.5050}{1.4054e^{\alpha_1} + 1} \tag{5}$$

$$\beta_2 = 2.4434 - \frac{2.4335}{0.1837e^{\alpha_2} + 1} - \frac{0.0265}{3.15 * 10^{14}e^{\alpha_3} + 1} \tag{6}$$

$$\alpha_1 = 2.9495B/L - 13.7448e_{sx} + 0.1312q \tag{7}$$

$$\alpha_2 = -1.7354B/L + 15.6739e_{sx} - 1.9476q \tag{8}$$

$$\alpha_3 = -38.6907B/L + 9.1984e_{sx} - 1.0516q \tag{9}$$

It should be noted that the equations are not a function of the uncoupled translational stiffness ratio, R_T, as results of the regression analysis indicated that this parameter is not correlated with e_{ad}. The equations proposed provide an acceptable approximation of the actual e_{ad} as the coefficient of determination R^2 attained is 0.89. Figure 6 depicts the comparison of actual e_{ad} values *vs.* those calculated with Eq. 3 for systems with B/L = 1.0; R_T = 1.0; q = 2.0, 6.0; e_{sx} = 0.20. As can be observed in such figure, the equations provide a good approximation of e_{ad} for most cases. However, for T_y > 1.0 s, the equations tend to be conservative and for very short periods, T_y < 0.25 s, they may provide unconservative results.

However, in general, the median floor displacements are sufficiently approximated with the displacements obtained from linear analysis of the elastic models with e_{ad} calculated with Eq. 3 and scaled with Eq. 2. However, for this validation, the scaling of Eq. 2 was carried out taking δ_{CM} equal to the actual inelastic displacement in order to show how well introduction of the additional mass eccentricity e_{ad} allows to predict amplifications of lateral displacement at the flexible side. Figure 7 presents the floor displacement profiles for X-Systems with T_y = 1.0 s, B/L = 1.0, R_T = 1.0, q = 2, 6 and e_{sx} = 0.20. The profiles shown are those obtained from non-linear dynamic analyses (continuous black line) and those obtained from the analyses of the elastic

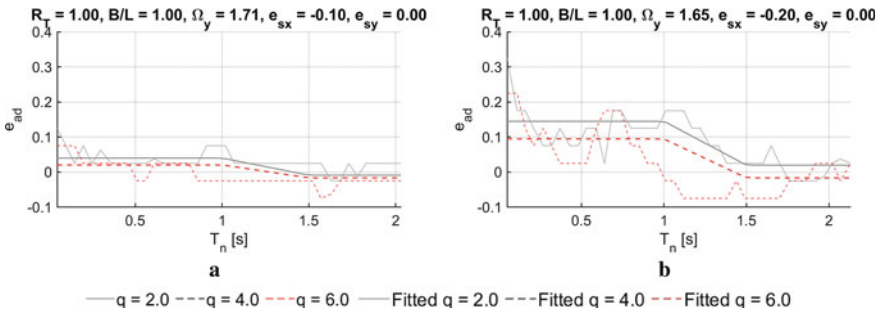

Fig. 6 Comparison of actual and fitted e_{ad} for inelastic one-storey models with q = 2, 4 and 6 with B/L = 0.5; R_T = 1.0, and two eccentricity values—**a** e_{xs} = 0.10, **b** e_{xs} = 0.20

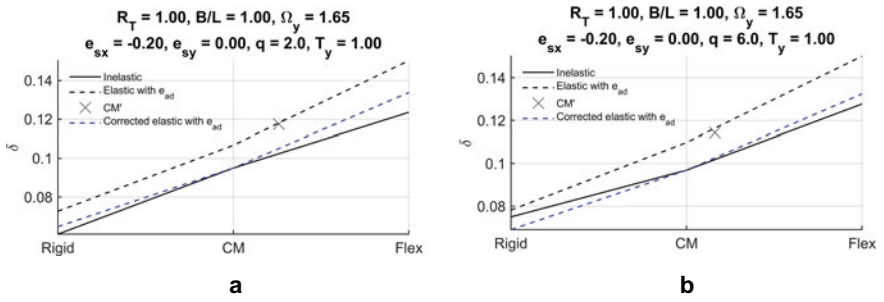

Fig. 7 Comparison of floor displacement profiles for systems with T_y = 1.0 s, R_T = 1.0, B/L = 1.0; e_{sx} = 0.20—**a** q = 2, **b** q = 6

model with modified eccentricity, both uncorrected (dashed black line) and corrected with Eq. 2 (dashed blue line), where it can be seen that a good correspondence was achieved.

For most cases, the displacements of the flexible side are slightly overestimated; the mean error among all case studies is 1.42% and the standard deviation is 7.18. Conversely, the displacements of the rigid side are in most cases underestimated; the mean error among all case studies is -10.5% and the standard deviation is 14%. Nonetheless, the underestimation of the displacements on the rigid side may be dealt by using the 'no reduction rule' [1], where the reductions in lateral displacements of the stiff side are conservatively neglected in the design process.

8 Conclusions

Current standard seismic design procedures based on modal spectral analysis of elastic models may lead to significant underestimations of maximum response of highly torsionally stiff buildings such as those composed of shear walls. This paper

shows that an improved estimation of the seismic demands of such type of structures can be achieved via modal spectral analysis of a modified elastic model where an additional mass eccentricity, e_{ad}, is provided. e_{ad} is the increment in eccentricity required in an elastic model to match the displacement amplification of the flexible side, δ_F/δ_{CM}, under inelastic response. The seismic demands obtained from the linear analysis of the modified model are scaled by a correction factor, C_F, to approximate the maximum inelastic floor displacement profile. The artifice proposed may be employed in applications of the conventional force-based design method using modal response spectrum analysis or in displacement-based design procedures such as the N2 method. In this study, such artifice was validated using one-storey shear buildings composed of elements with elastoplastic behaviour. However, such models can only provide insight of the global response of actual multi-storey buildings under earthquake loading as the behaviour of the latter is more complex due to factors such as the difference in yielding progression of structural components between one storey and multi-storey buildings and the contribution of higher modes to seismic response. For this reason, an investigation regarding the use of the artifice proposed for the design of multi-storey shear wall buildings is currently underway.

Acknowledgements Saúl López acknowledges DGAPA-UNAM for the sponsorship of the research project PAPIIT-IA104519 "Formulation and validation of a displacement-based seismic design procedure for buildings considering the effects of in-plan torsion". Daniel Pancardo acknowledges the National Council of Science and Technology (CONACYT) for his Master studies scholarship. Mario De Stefano and Valerio Alecci also acknowledge the financial support of the Italian Ministry of the Education, University and Research (MIUR) through the Project PRIN 2015 MICHe (Mitigating the Impacts of natural hazards on Cultural Heritage sites, structures and artefacts). The authors also thank the student Iván Garduño of FES Acatlán for his contribution to some of the analyses and results shown in this paper.

References

1. Fajfar P, Marusic D, Perus I (2005) Torsional effects in the pushover-based seismic analysis of buildings. J. Earth. Eng. 9(6):831–854
2. De Stefano M, Pintucchi B (2010) Predicting torsion-induced lateral displacements for pushover analysis: Influence of torsional system characteristics. Earthq Eng Struct Dyn 39:1369–1394
3. CEN (2004) Eurocode 8: design of structures for earthquake resistance-Part 1: general rules, seismic actions and rules for buildings. European Commitee for Standariza-tion, Brussels
4. Anagnostopoulos SA, Kyrkos MT, Stathopoulos KG (2015) Earthquake induced torsion in buildings: critical review and state of the art. Earthq Struct 8(2):305–377
5. Myslimaj B, Tso WK (2002) A strength distribution criterion for minimizing torsional response of asymmetric wall-type systems. Earthq Eng Struct Dyn 31(1):99–120
6. Iervolino I, Maddaloni G, Cosenza E (2008) Eurocode 8 compliant real records sets for seismic analysis of structures. J Struct Eng 12(1):54–90
7. McKenna F, Fenves GL, Filippou FC (2016) Open system for earthquake engineering simulations. University of California, Berkeley, Pacific Earthquake Engineering Research Center, Berkeley, CA
8. The Mathworks (2019) MATLAB and deep learning toolbox release 2019b. Natick, Massachusetss, The MathWorks Inc., Natick, MA